

Copyright
by
Jaclyn A. Kaiser
2019

**The Dissertation Committee for Jaclyn A. Kaiser Certifies that this is the approved
version of the following dissertation:**

**Characterization of Candidate Mutations for Use in a Live Attenuated
West Nile Virus Vaccine**

Committee:

Alan D.T. Barrett, PhD, Supervisor

David W.C. Beasley, PhD

Alexander N. Freiberg, PhD

Laura D. Kramer, PhD

Tian Wang, PhD

**Characterization of Candidate Mutations for Use in a Live Attenuated
West Nile Virus Vaccine**

by

Jaclyn A. Kaiser, B.S.

Dissertation

Presented to the Faculty of the Graduate School of
The University of Texas Medical Branch
in Partial Fulfillment
of the Requirements
for the Degree of

Doctor of Philosophy

**The University of Texas Medical Branch
November 20, 2019**

Dedication

This dissertation is dedicated to my husband, Michael, who has selflessly accompanied me on this journey.

Acknowledgements

First and foremost, I must acknowledge my supervisor, Alan Barrett. Alan has been an excellent support of my work life and home life, and this keeps me motivated and dedicated to pursuing my goals in science. Alan is always encouraging. He encouraged me to travel to Paris for a conference, a trip I will never forget. He encouraged me to be fearless during my PhD work, even when life was drastically changing because I was having a baby. He encouraged me to believe in myself and the quality of my work, resulting in several publications from my PhD studies. Alan's positive attitude is very helpful during the ups and downs of research, and I am grateful that I have spent the last 5+ years in his lab.

Next, I would like to acknowledge all of our current lab members. Li Li is a wonderful, motherly figure to have around the lab, always willing to lend a helping hand and a supportive smile. Vanessa Sarathy is an encyclopedia of scientific knowledge, and she has provided invaluable technical support when I need to try out new experiments, while also providing insight on how to become a better scientist. Ashley Strother, Kassy Carpio, and Clairissa Hansen each provide a great energy for our lab environment. I must extend a huge thank you to Emily Davis. Emily has made this marathon of a degree so much more enjoyable for me. She commiserates with me when I need to gripe, she is both intelligent and humble, she is always happy to help me with absolutely anything, and she is simply an incredible presence to be around.

Previous lab members Melissa Whiteman and Daniele Swetnam each were essential to my training as well. Melissa taught me how to work with the WNV infectious clone, a skill that is central to my project. Daniele taught me about NGS analysis, which proved to be essential to understanding my different mutants.

Thank you to my committee members Tina Wang, Laura Kramer, Alex Freiberg, and David Beasley. Their insight at my committee meetings always boosted my motivation and helped me stay on the right track toward graduation. They are a great group of scientists and it has been a pleasure to get to know each of them better during this process.

Thank you to Terry Juelich and Sasha Azar, who helped me irradiate virus samples and run them on a BioPlex machine. Thank you to Pei-Yong Shi who provided me an NS4B monoclonal antibody that is better for WNV than those commercially available. Thank you to the UTMB NGS core, especially Steve Widen for assisting with data analysis. Thank you to the Optical Microscopy Core, especially Maxim Ivannikov for training me and patiently answering my questions. Thank you to Dr. Lynn Soong for supporting my work with her T32 training grant, and for always being helpful in her role as my program director.

Finally, thank you to my family, who have always supported and encouraged me. My parents helped me move to Galveston in 2014, which was quite an adventure since we were travelling from West Virginia with three cats in our car. Thank you to all three of my siblings. We are each very different, but are united in our family and our support of one another's uniqueness. Thank you to my husband, Michael, who has accompanied me here to Galveston, and has made my time here something I will treasure. He has selflessly been here for me, and the comfort he provides has allowed me to continue to grow and develop with confidence. Finally, my daughter Hazel doesn't yet know how big of a role she has played, but having her in my life brings both a great joy and a motivation to be the best possible version of myself.

Characterization of Candidate Mutations for Use in a Live Attenuated West Nile Virus Vaccine

Publication No. _____

Jaclyn Abbey Kaiser, PhD

The University of Texas Medical Branch, 2019

Supervisor: Alan D.T. Barrett

West Nile virus (WNV) is a mosquito-borne flavivirus that causes neurological disease and fatalities annually in the United States and Europe, but no human WNV vaccines have been licensed. Studies of WNV vaccine candidates and of vaccines for related flaviviruses indicate that a live attenuated vaccine based on the full-length WNV genome will likely induce the most robust protective immune response compared to other vaccination strategies. This dissertation describes investigation of potentially attenuating mutations in WNV to aid in candidate vaccine development. Single gene mutations were investigated in the envelope (E), NS4B, and NS5 proteins. Additionally, multigenic mutants were investigated that combined mutations in the NS1 protein with mutations in the E or NS4B proteins, as a vaccine with multigenic mutations should have fewer chances of reversion to virulence. The E mutation investigated, E138K, did not have a mouse attenuated phenotype, and virulence was associated with reversion to wild-type genotype. Of seven NS4B mutations investigated, only P54A and P54G mutants were significantly attenuated in mice. While the P54G mutant was genotypically stable, P54A was capable of reversion. In the NS5 protein, two single mutants were studied independently (K61A and E218A) and in combination as a double mutant. The NS5 single mutants were

attenuated in mice, however, the double mutant had reduced attenuation associated with reversion at both mutated residues. For the multigenic mutants, strongly attenuating NS1 glycosylation site mutations (NS1_{mut}) were combined with NS4B-C102S, NS4B-W103Y, or E-E138K. Although NS4B-C102S and NS4B-W103Y mutations did not independently attenuate WNV mouse virulence, the multigenic mutants retained the attenuated phenotype of the NS1_{mut}. In comparison, the NS1_{mut}+E-E138K mutant was not attenuated, and instead, the genotype showed evidence of reversion. Overall, NS4B-P54G and NS5-K61A mutations were the most strongly attenuated and stable mutations investigated, and thus, they should be considered during WNV vaccine development. Additionally, the NS1_{mut} glycosylation site mutations should be stabilized with additional amino acid substitutions to continue to use this mutant in vaccine design. Overall, this dissertation describes the attenuating phenotype and stability of mutations in diverse regions of the WNV genome and provides insight into WNV rational vaccine development strategies.

TABLE OF CONTENTS

List of Tables	xii
List of Figures	xv
List of Abbreviations	xx
Chapter 1 – Introduction	22
1.1 History of West Nile virus	22
1.1.1 Global distribution of West Nile virus	22
1.1.2 WNV disease incidence in the US and Europe.....	23
1.1.3 Genetic lineages of WNV	24
1.2 WNV Transmission and Replication	26
1.2.1 WNV Transmission	26
1.2.2 WNV Replication Cycle	27
1.2.2.1 Structural proteins.....	28
1.2.2.2 Nonstructural proteins.....	29
1.2.2.3 5' and 3' Untranslated Regions	31
1.3 WNV Pathogenesis and Immune Response.....	31
1.3.1 WNV Pathogenesis	31
1.3.2 Immune Response to WNV Infection.....	32
1.4 Licensed flavivirus vaccines.....	34
1.4.1 Licensed flavivirus vaccines for human use	34
1.4.2 Licensed WNV vaccines for veterinary use.....	35
1.5 Biological properties of an ideal human WNV vaccine	36
1.6 Clinical trials of WNV vaccine candidates.....	40
1.7 The need for additional WNV vaccine candidates	41
1.8 Attenuating mutations in WNV	42
1.8.1 Attenuating mutations in WNV prM protein	43
1.8.2 Attenuating mutations in WNV E protein	43
1.8.3 Attenuating mutations in WNV NS1 protein.....	45
1.8.4 Attenuating mutations in WNV NS2A protein.....	45
1.8.5 Attenuating mutations in WNV NS3 protein.....	46

1.8.6 Attenuating mutations in WNV NS4A protein.....	47
1.8.7 Attenuating mutations in WNV NS4B protein.....	47
1.8.8 Attenuating mutations in WNV NS5 protein.....	48
1.9 Specific Aims.....	49
Chapter 2 - Materials and Methods.....	58
2.1 Cell culture.....	58
2.2 Recovery of recombinant WNV	58
2.3 Virus passaging.....	59
2.4 Virus titration.....	60
2.5 Temperature sensitivity assays	61
2.6 Multiplication kinetics	61
2.7 Cytokine quantification.....	62
2.8 Mouse neuroinvasion studies.....	62
2.9 Isolation of virus from mouse brain.....	63
2.10 Plaque reduction neutralization tests (PRNT)	63
2.11 RNA extraction	64
2.12 Sample preparation for sanger sequencing	64
2.13 Sequence alignments.....	64
2.14 Next-generation sequencing (NGS) analysis.....	65
2.15 Fluorescence microscopy.....	65
2.16 Molecular rendering.....	66
2.17 Statistical analysis.....	67
Chapter 3 - Mutation of the Japanese encephalitis virus SA14-14-2 vaccine-specific envelope residue E138K	69
3.1 Abstract.....	69
3.2 Introduction.....	70
3.3 Results.....	71
3.3.1 Generation of E-E138K mutant and consensus sequencing	71
3.3.2 Mouse virulence.....	72
3.3.3 Temperature sensitivity in Vero cells	73
3.3.4 Multiplication kinetics in Vero cells and A549 cells.....	73

3.3.5 A549 cell cytokine response	73
3.3.6 Deep sequencing analysis of virus quasispecies	74
3.4 Discussion.....	75
Chapter 4 - Mutation of the highly conserved flavivirus NS5 methyltransferase catalytic tetrad.....	94
4.1 Abstract.....	94
4.2 Introduction.....	94
4.3 Results.....	96
4.3.1 Generation of NS5 methyltransferase mutants and consensus sequencing	96
4.3.2 Mouse virulence.....	96
4.3.3 Temperature sensitivity in Vero cells	97
4.3.4 Multiplication kinetics in Vero cells and A549 cells.....	98
4.3.5 A549 cell cytokine response	99
4.3.6 Next-generation sequencing analysis of virus quasispecies	100
4.4 Discussion.....	101
Chapter 5 - Mutation of flavivirus conserved residues in NS4B	125
5.1 Abstract.....	125
5.2 Introduction.....	126
5.3 Results.....	128
5.3.1 Generation of NS4B mutants and consensus sequencing	128
5.3.1.1 Reevaluation of NS4B-P38G and NS4B-C102S mutants .	128
5.3.1.2 Generation of new NS4B mutants	129
5.3.2 Mouse virulence.....	130
5.3.3 Temperature sensitivity in Vero cells	132
5.3.4 Multiplication kinetics in Vero cells and A549 cells.....	133
5.3.5 A549 cell cytokine response	133
5.3.6 Analysis of virus quasispecies using NGS.....	134
5.3.6.1 Single nucleotide variants (SNVs).....	135
5.3.6.2 Shannon entropy	138
5.3.7 Intracellular localization of NS4B and NS1	139
5.4 Discussion.....	140

Chapter 6 - Combining mutations in multiple WNV genes.....	167
6.1. Abstract.....	167
6.2 Introduction.....	168
6.3 Results.....	172
6.3.1 Generation of multigenic mutants.....	172
6.3.2 Mouse virulence.....	172
6.3.3 Temperature sensitivity in Vero cells	174
6.3.4 Multiplication kinetics in Vero and A549 cells	175
6.3.5 A549 cell cytokine response	175
6.3.6 Intracellular staining of NS1 and NS4B	177
6.3.7 Analysis of virus quasispecies using NGS.....	179
6.3.7.1 Analysis of single nucleotide variants (SNVs).....	179
6.3.7.2 Shannon entropy analysis	182
6.4 Discussion.....	183
Chapter 7 – Final Discussion	212
7.1 NS4B protein	213
7.2 NS5 protein.....	215
7.3 E protein.....	216
7.4 Multigenic mutants	217
7.5 Phenotypic comparison of attenuated mutants in different viral genes	220
7.6 Future directions	221
References.....	224
Curriculum Vitae	242

List of Tables

Table 1.1:	Summary of WNV human vaccine candidates that have been studied in clinical trials.....	52
Table 1.2:	Attenuating mutations previously studied in WNV infectious clones.	53
Table 1.3:	Genetic lineages of WNV have diverse geographic distributions and virulence phenotypes	54
Table 2.1:	Primers utilized for WNV NY99ic site-directed mutagenesis.....	68
Table 3.1:	The E-E138K mutant did not have an attenuated phenotype <i>in vivo</i> ...	82
Table 3.2:	The E-E138K mutant does not have a temperature sensitive phenotype in Vero cells.....	83
Table 3.3:	Summary of all single nucleotide variants $\geq 1\%$ of viral RNA populations of NY99ic and the E-E138K mutant in unpassaged (P0) virus stocks	84
Table 4.1:	NY99 infectious clone and WNV strain 3356 infectious clone have genotypic differences.....	110
Table 4.2:	The NS5 double mutant has a temperature sensitive phenotype in Vero cells, but single mutants do not.....	111
Table 4.3:	The NS5 single mutants are attenuated in mice, but the double mutant is virulent.....	112

Table 4.4:	Mouse brain-derived virus had reversion of NS5-K61A/E218A double mutation	113
Table 4.5:	Summary of single nucleotide variants $\geq 1\%$ of viral RNA populations for Vero cell passage one (P1) stocks of NY99ic and each NS5 mutant	114
Table 4.6:	Evidence of reversion of the NS5-K61A/E218A mutant increases after Vero cell passage	117
Table 5.1:	Consensus genotypes, plaque phenotypes, temperature sensitivity, and mouse attenuation of NS4B mutants	147
Table 5.2:	New and old stocks of the NS4B P38G and C102S mutants exhibit distinct single nucleotide variants.....	148
Table 5.3:	New NS4B mutants exhibit distinct single nucleotide variants.....	150
Table 6.1:	Consensus genotypes, plaque phenotypes, and mouse attenuation of new multigenic mutants compared to the parental single gene mutants	190
Table 6.2:	Outbred mice inoculated with the NS1 _{mut} +NS4B-W103Y mutant develop neutralizing antibodies by 35 dpi	191
Table 6.3:	The NS1 _{mut} and NS1+NS4B mutants are significantly temperature sensitive in plaque-forming assays	192
Table 6.4:	The NS1 _{mut} and NS1+NS4B mutants exhibit temperature sensitive phenotypes in focus-forming assays	193

Table 6.5:	The P0 stocks of single gene and multigenic mutants each had distinct SNVs detected $\geq 1\%$ frequency	194
Table 6.6:	The NS1 _{mut} +NS4B-W103Y and NS1 _{mut} +E-E138K mutants maintain high frequency SNVs after a single passage in Vero cells	198
Table 7.1:	Overview of <i>in vitro</i> and <i>in vivo</i> characteristics of WNV mutants.....	223

List of Figures

Figure 1.1: Annual West Nile neurological disease cases (WNND) and deaths reported to the US CDC.....	55
Figure 1.2: Annual WNV case number and countries reporting confirmed WNV infection to the European CDC.....	56
Figure 1.3: WNV genome organization	57
Figure 3.1: Amino acid alignment of JEV and WNV lineages reveals that residue E138 is highly conserved.....	85
Figure 3.2: Multiplication kinetics of NY99ic and the E-E138K mutant are similar in Vero and A549 cells at a moi of 0.1	86
Figure 3.3: Extracellular cytokine responses are similar in E-E138K infected cells compared to NY99ic infected cells.....	87
Figure 3.4: Single nucleotide variant profiles of the unpassaged (P0) virus stocks differ between NY99ic and the E-E138K mutant.....	88
Figure 3.5: The E-E138K mutant had SNVs clustered in the E protein and one encoded reversion at residue 138.....	89
Figure 3.6: The E-E138K mutant had higher Shannon entropy across the genome than NY99ic.....	90
Figure 3.7: Reversion of E-E138K increases in frequency after Vero cell passage, but does not yield a consensus sequence change.....	91

Figure 3.8: Alignment of WNV and JEV E protein structural motifs reveals amino acid differences between the viruses	92
Figure 3.9: Location in the WNV E protein monomer of residues associated with the electrostatic gap in the E protein dimer of neurotropic flavivirus	93
Figure 4.1: The structure of WNV NS5 methyltransferase domain.....	118
Figure 4.2: Multiplication kinetics of NS5 mutants are different than those of NY99ic in Vero and A549 cells.....	119
Figure 4.3: Each NS5 mutant induced different cytokine patterns in A549 cells ..	120
Figure 4.4: Single nucleotide variant profiles are different for the different NS5 mutants.....	121
Figure 4.5: The NS5-K61A/E218A mutant had few SNVs $\geq 1\%$ frequency, but still showed evidence of reversion.....	122
Figure 4.6: There are higher peaks of Shannon entropy for the NS5 single mutants compared to the double mutant and to NY99ic	123
Figure 4.7: WNV and DENV NS5 methyltransferase have an amino acid difference in GTP-binding domain residue NS5-152	124
Figure 5.1: Amino acid alignment of the N-terminal portion of NS4B of representative mosquito-borne and tick-borne flaviviruses.....	154
Figure 5.2: Location of different amino acid residues described in this study within the predicted structure of NS4B.....	155

Figure 5.3: The NS4B-P54 mutants exhibited a trend toward higher neutralizing antibody titers than the NS4B-C102S (+E-D114A/V139M) mutant...	156
Figure 5.4: All new NS4B mutants can multiply to high titers in both Vero and A549 cells	157
Figure 5.5: Attenuated WNV NS4B mutants exhibit two different patterns of cytokine induction.....	158
Figure 5.6: SNV Profiles of all NS4B mutants	159
Figure 5.7: New and old stocks of P38G and C102S mutants have different SNV genotypes	160
Figure 5.8: New NS4B mutants each have unique SNV genotypes	161
Figure 5.9: The NS4B-P54A mutation is capable of reversion.....	162
Figure 5.10: Shannon entropy of the new P38G and C102S mutants is significantly higher than that of the historical stocks	163
Figure 5.11: Shannon entropy demonstrates unique genotype diversity for each new NS4B mutant.....	164
Figure 5.12: The WNV P54G mutant had reduced NS4B accumulation and NS1-NS4B colocalization in infected cells one day post infection	165
Figure 5.13: Attenuated WNV NS4B-P54G mutant exhibited lower levels of both NS4B and NS1 two days post infection.....	166
Figure 6.1: The structure of the WNV NS1 dimer reveals three distinct domains	200

Figure 6.2: Focus size of the NS1 _{mut} and NS1+NS4B mutants is reduced at 41°C compared to 37°C	201
Figure 6.3: The NS1 _{mut} and NS1+NS4B mutants had strongly reduced multiplication kinetics in A549 cells	202
Figure 6.4: The NS1+NS4B mutants induced cytokines similar to the NS1 _{mut} , but the NS1+E mutant had a unique phenotype of cytokine induction in A549 cells	203
Figure 6.5: The NS1 _{mut} +NS4B-W103Y mutant had reduced accumulation and colocalization of NS1 and NS4B one day post infection.....	204
Figure 6.6: The attenuated NS1 _{mut} +NS4B-W103Y mutant and NY99ic had similar staining of NS1 and NS4B proteins two days post infection.....	205
Figure 6.7: SNV profiles of single gene and multigenic mutants	206
Figure 6.8: The multigenic NS1 _{mut} +NS4B-W103Y mutant had higher SNV frequency than the single gene NS1 _{mut} or NS4B-W103Y mutants.....	207
Figure 6.9: The E-E138K mutation reduced stability of the NS1 _{mut} glycosylation site mutations.....	208
Figure 6.10: The attenuated NS1 _{mut} +NS4B-W103Y and virulent NS1 _{mut} +E-E138K mutants had higher peaks of Shannon entropy than the parental single gene mutants	209
Figure 6.11: NS4B residues oriented toward the ER lumen may be involved in interaction with NS1	210

Figure 6.12: Diverse regions of the E protein are associated with mutation in the context of NS1 glycosylation site mutations	211
---	-----

List of Abbreviations

AST	average survival time
BBB	blood brain barrier
CCL	chemokine ligand
CCR	chemokine receptor
CMC	carboxymethylcellulose
CNS	central nervous system
CPE	cytopathic effect
CXCL	chemokine ligand
DC	dendritic cell
DENV	dengue virus
dpi	days post infection
FBS	fetal bovine serum
FFU	focus-forming units
FGF	fibroblast growth factor
G-CSF	granulocyte colony-stimulating factor
GM-CSF	granulocyte-macrophage colony-stimulating factor
GMT	geometric mean titer
hpi	hours post infection
IC	infectious clone
IFN	interferon
IL	interleukin
IP	interferon gamma-induced protein
IRF	interferon response factor
ISG	interferon stimulated gene
JEV	Japanese encephalitis virus
MAVS	mitochondrial antiviral signaling protein
MCP	monocyte chemoattractant protein
MDA5	melanoma differentiation associated protein 5
MEM	minimum essential media
MIAF	mouse immune ascites fluid
MIP	macrophage inflammatory protein
mL	mililiter
moi	multiplicity of infection
MTase	methyltransferase
MVEV	Murray Valley encephalitis virus
n.d.	not done
NS	nonstructural
NTPase	nucleotide triphosphatase
NY99ic	New York 1999 infectious clone
OAS	oligoadenylate synthase
PBS	phosphate-buffered saline
PCC	Pearson's correlation coefficient
PDGF	platelet-derived growth factor

PFU	plaque-forming units
PRNT	plaque reduction neutralization test
PRR	pattern recognition receptor
RANTES	regulated on activation normal T cell expressed and secreted
RLR	RIG-I-like receptor
RNAi	RNA interference
RdRp	RNA-dependent-RNA-polymerase
RIG-I	retinoic acid-inducible gene I
RTPase	RNA triphosphatase
r.t.	room temperature
RT-PCR	reverse transcription polymerase chain reaction
RVP	reporter virus particle
SD	standard deviation
SLEV	Saint Louis encephalitis virus
ssRNA	single stranded RNA
TBS	tris-buffered saline
TLR	toll-like receptor
TNF	tumor necrosis factor
U	units
US	United States
VEGF	vascular endothelial growth factor
WNND	West Nile neuroinvasive disease
WNV	West Nile virus
WT	wild-type
YFV	yellow fever virus
ZIKV	Zika virus

Chapter 1 – Introduction

1.1 HISTORY OF WEST NILE VIRUS

1.1.1 Global distribution of West Nile virus

West Nile virus (WNV) is a member of the family Flaviviridae and the genus *Flavivirus*, which consists of >70 viruses that are mostly arthropod-borne (arboviruses) (Lindenbach et al., 2007). The majority of flaviviruses are mosquito-borne, while some are tick-borne, and some have no known vector (Lindenbach et al., 2007). WNV is mosquito-borne and is related to other medically relevant flaviviruses including dengue (DENV), yellow fever (YFV), Zika (ZIKV), and Japanese encephalitis (JEV) (Kuno et al., 1998). Genetically and serologically it is a member of the JEV group that includes Murray Valley encephalitis (MVEV), Saint Louis encephalitis (SLEV), Yaounde, Cacipacore, and Usutu viruses, along with JEV and WNV (Schweitzer et al., 2009). Of these, Yaounde virus has not been associated with human disease (Williams et al., 2012), and Cacipacore and Usutu viruses infrequently cause symptomatic infection in humans (Batista et al., 2011; Clé et al., 2019; de Figueiredo et al., 2017). However, Usutu virus has been associated with significant bird mortality in Europe and there is concern over the possibility of increased human outbreaks (Roesch et al., 2019). The related viruses MVEV, SLEV, JEV, and WNV each have been more notably associated with human disease outbreaks. MVEV is endemic in Australia and SLEV is endemic in the US, and both have been responsible for relatively small annual human outbreaks (typically <20 cases per year) (CDC, 2019a; Knox et al., 2012). JEV is endemic throughout many countries in Asia, and even though many cases are prevented by vaccination, it is still estimated to cause approximately 68,000 clinical cases annually (WHO,

2019). Of the JEV group viruses, WNV has the largest geographic distribution. First isolated in Africa in 1937, WNV is now broadly distributed throughout Africa, the Middle East, Europe, western Russia, southwestern Asia, Australia, and the Americas (Chancey et al., 2015; Petersen et al., 2013; Smithburn et al., 1940). Until the 1990s, WNV was only associated with sporadic cases of febrile illness and very few reports of neuroinvasive disease (Mann et al., 2013). Outbreaks of WNV disease grew in magnitude throughout the 1990s in several parts of the world including Africa, the Middle East, and Europe (Mann et al., 2013). An epidemic in Romania in 1996 was the first to be notably associated with neurological disease (Tsai et al., 1998). In 1999, WNV emerged into eastern North America via New York (NY) state (Nash et al., 2001). The origin of the NY outbreak is not known, but phylogenetic analysis has indicated the closest known relative to the NY99 strain could be an isolate from a dead goose in Israel in 1998 (Lanciotti et al., 1999, 2002), or alternatively, both the NY99 strain and the Israel 1998 strain may have been derived independently from spread of WNV out of Africa (May et al., 2011). Although there were only 62 confirmed cases in 1999 and 21 confirmed cases in 2000, WNV was detected in birds or mosquito pools as far south as North Carolina by the end of 2000 (Roehrig, 2013). Throughout 2001, WNV was detected in most states on the eastern side of the US (Roehrig, 2013). By 2004, WNV was detected in all 48 contiguous US states, and by 2006, detection was also reported in Canada, Mexico, and South America (Mann et al., 2013).

1.1.2 WNV disease incidence in the US and Europe

Human WNV infections can be categorized into a typical infectious disease iceberg, in which the majority (80%) of WNV cases are asymptomatic, and approximately one in five cases develop WN fever, a flu-like illness (CDC, 2018a). Approximately one in every 150 cases progresses to

potentially fatal WN neurological disease (WNND), which can manifest as either encephalitis, meningitis, or acute flaccid paralysis (CDC, 2018a). Approximately 10% of WNND cases have been fatal (CDC, 2019b). Notably, WNV physical and/or cognitive sequelae can persist for more than a year after acute infection (Klee et al., 2004).

Since its emergence into the US, WNV has been responsible for annual neurological disease and fatalities (**Fig. 1.1**). Although WNV was first detected in the US in 1999, the first large outbreak occurred in 2002 with 2946 WNND cases and 284 deaths (**Fig. 1.1**) (CDC, 2019b). Another large outbreak occurred in 2003 resulting in 2866 WNND cases and 264 deaths (**Fig. 1.1**) (CDC, 2019b). Following 2003, reporting of non-WNND cases was not required, so the extent of WN fever is unknown. Nonetheless, between 2004-2019 the CDC received reports of 386-2873 annual cases of WNND causing 32-286 annual fatalities, including another large outbreak in 2012 that was centered in Texas (CDC, 2019b) (**Fig. 1.1**). Importantly, WNV is also endemic in parts of Europe, and 2018 marked the largest recorded WNV European outbreak in history with >2,000 reported cases and 181 deaths in 15 European countries (**Fig. 1.2**) (Barrett, 2018). Although Europe experienced a significant increase in WNV cases in 2018, the number of countries reporting WNV disease was similar to previous years, supporting that WNV can reemerge in regions of endemicity (**Fig. 1.2**).

1.1.3 Genetic lineages of WNV

There are nine putative genetic lineages of WNV that have diverse geographic origins and virulence phenotypes (summarized in **Table 1.3**) (Fall et al., 2017). Lineage 1 is widely distributed across the world and is the primary clade associated with neurological disease outbreaks, including those that have occurred in the US (Fall et al., 2017). Lineage 2 was historically considered less

pathogenic than Lineage 1 and was primarily associated with circulation in Africa, but since 2004 it has been associated with several severe neurological disease epidemics in both South Africa and Europe (Fall et al., 2017). WNV Lineage 3, also known as Rabensburg virus, has been isolated in mosquito pools in the Czech Republic, but it has not been associated with human disease cases and it did not infect birds in experimental inoculation of house sparrows and chickens (Aliota et al., 2012). Similarly, Lineages 4 and 5 have not been associated with human disease and have only been isolated from mosquito pools in Russia and India, respectively (Fall et al., 2017; Vázquez et al., 2010). Notably, Lineage 5 WNV is sometimes categorized as a distinct clade within the Lineage 1 group (Fall et al., 2017). A putative Lineage 6 strain was identified in mosquito pools in Spain, but it has not been associated with human disease (Vázquez et al., 2010). Lineage 7 WNV, also known as Koutango virus, was isolated from ticks and rats in Africa, and thus stands out as WNV is not commonly associated with ticks (Fall et al., 2014; Hall et al., 2001). Although Koutango virus has not been associated with any natural human infections, there has been one reported laboratory exposure, and experimental infection of outbred mice demonstrated a strong degree of neuroinvasion, similar to that of the NY99 strain (Fall et al., 2017; Pérez-Ramírez et al., 2017; Prow et al., 2014). A putative 8th Lineage was isolated in Senegal in 1992, but no additional isolates have been reported (Fall et al., 2014). Similarly, a putative 9th Lineage was isolated from mosquitoes in Austria in 2013, but no additional isolates have been reported and it is not clear if this virus represents a distinct Lineage or a clade within Lineage 4 (Pachler et al., 2014).

Most research into WNV involves Lineages 1 and 2, as the remaining lineages currently have limited geographic distribution and are not strongly associated with human disease epidemics. While Lineage 1 WNV has been most strongly associated with human disease, this group can be divided into three sublineages that have differing virulence phenotypes. Lineage 1a includes

isolates from the US, Europe, the Middle East, Russia, and Africa and is associated with disease outbreaks in each of these regions (May et al., 2011). Alternatively, Lineage 1b includes the Australian Kunjin virus, which is rarely associated with human disease, and Lineage 1c (also known as Lineage 5) has only been isolated from mosquitoes in India (Hall et al., 2001; May et al., 2011). In sum, WNV Lineage 1a is uniquely associated with higher disease burden and wider geographic expansion than other Lineages of WNV.

1.2 WNV TRANSMISSION AND REPLICATION

1.2.1 WNV Transmission

The primary WNV transmission cycle occurs between *Culex spp.* mosquitoes and wild birds. Humans and other large mammals (i.e. horses) are dead end hosts of WNV as they can become infected but do not develop high enough viremia to transfer the virus to a mosquito taking a blood meal. The primary season for WNV transmission is between Summer and Fall, corresponding to peak mosquito season (CDC, 2018b). The United States has seen WNV infection in many species including 66 mosquito species and over 300 species of birds (CDC, 2016, 2018c). WNV has been naturally or experimentally detected in many other animals including horses, bats, cats, dogs, squirrels, chipmunks, and alligators, demonstrating an expansive host range (Austgen et al., 2004; Blitvich, 2008; Davis et al., 2005; Jacobson et al., 2005; Padgett et al., 2007; Platt et al., 2007). While some animals showed little or no signs of neurological disease from WNV infection (e.g. bats), others are susceptible to severe neurological symptoms and fatality (e.g. horses) (Blitvich, 2008; Davis et al., 2005).

WNV is the most common mosquito-borne disease in the United States (CDC, 2018b), and the periodic pattern of large outbreaks of WNV in the US (**Fig 1.1**) is typical of mosquito-borne

viruses (Rosenberg et al., 2018). Therefore, it can be anticipated that there will continue to be annual WNND cases along with large outbreaks that are difficult to predict as they depend on a multitude of environmental factors including temperature, precipitation, relative humidity, and landscape, as well as any other factors that may impact mosquito distribution, bird migration patterns, or urban development (Brown et al., 2008; Hess et al., 2018; Marcantonio et al., 2015; Paz and Semenza, 2013).

Although most cases of WNV are associated with mosquito transmission, there have been rare incidences of alternative modes of transmission. Specifically, WNV can be transmitted via infected blood or organ donations, consequently, all blood donations in the US are now screened for WNV (CDC, 2018b). Additionally, there have been several cases of WNV in newborns that implicated possible mother-child transmission during pregnancy, and WNV has been detected in the breast milk of nursing mothers (CDC, 2018b). Finally, there has been one reported laboratory-acquired case of WNV disease in which the infected individual had no known history of a mosquito bite (Campbell et al., 2002). While these alternative modes of transmission are fairly rare compared to mosquito transmission, the potential for severe disease cannot be ruled out.

1.2.2 WNV Replication Cycle

WNV has an enveloped, icosahedral virion that is approximately 50 nm in diameter (Lindenbach et al., 2007). Cell surface receptors for WNV have not been definitively described, but several host proteins have been implicated to bind WNV, including glycosaminoglycans, DC-SIGN, DC-SIGNR, and integrins (Brinton, 2013). Upon attachment to host cells, WNV is transferred into the cell via receptor-mediated endocytosis (Brinton, 2013). Fusion with the endosome results in the release of the viral genome into the cytoplasm. The virus replicates and

assembles on the endoplasmic reticulum (ER) membrane and immature virions are trafficked through the Golgi where they undergo maturation prior to exocytosis into the extracellular space.

The WNV genome is comprised of single-stranded, positive-sense RNA that is 11,029 bases long and encodes a single polyprotein that is co- and post-translationally cleaved into ten viral proteins: the structural proteins capsid (C), pre-membrane (prM), envelope (E), as well as the nonstructural (NS) proteins NS1, NS2A, NS2B, NS3, NS4A, NS4B, and NS5 (**Fig. 1.3**).

1.2.2.1 STRUCTURAL PROTEINS

The first protein encoded in the WNV genome is the highly basic C protein. C forms a dimer, and interactions with RNA can induce the C protein to form nucleocapsid structures to encapsulate the viral genome (Lindenbach et al., 2007).

The second structural protein is the prM protein, which contains one N-linked glycosylation site in the N-terminal domain and acts as a scaffold to ensure proper E protein assembly. Specifically, E protein endosomal fusion is initiated by acidic pH, therefore, the prM protein protects E on newly assembled virions from undergoing improper folding in acidic regions of the secretory pathway (Lindenbach et al., 2007). Virion maturation occurs in the Golgi as prM is cleaved by host furin proteases (or similar enzymes) (Lindenbach et al., 2007). Maturation causes the release of pr from the mature M protein and induces the formation of E protein homodimers (Lindenbach et al., 2007). Notably, immature virions are generally not considered infectious (Lindenbach et al., 2007), except in some cases of prM antibody opsonization (Colpitts et al., 2011).

The third structural protein is the E protein, which coats the majority of the WNV virion and is responsible for host cell attachment and fusion to the endosomal membrane (Lindenbach et al.,

2007). Many, but not all, strains of WNV have a single N-linked glycosylation site at residue E-154 (Hanna et al., 2005). The E protein ectodomain consisting of approximately 80% of the N-terminal domain of the protein has three distinct domains: DI forms a β -barrel that is essential to the structure of DII and DIII, DII harbors the highly conserved fusion loop (amino acids 98-110) required for endosomal fusion, and DIII has the putative receptor-binding domain and is the primary target of potent neutralizing antibodies (Kanai et al., 2006; Lindenbach et al., 2007; Nybakken et al., 2006). The remaining 100 amino acids on the C-terminal of the E protein act as a transmembrane anchor for the virion, and during endosomal fusion this C-terminal region structurally shifts towards the fusion loop to facilitate the release of viral RNA (Kanai et al., 2006).

1.2.2.2 NONSTRUCTURAL PROTEINS

The seven NS proteins form the replication complex on the ER membrane. Specifically, the NS1 protein is translocated into the ER lumen whereas NS2A, NS2B, NS4A, and NS4B are membrane-associated proteins and NS3 and NS5 have enzymatic activity.

The NS1 protein is a hydrophilic glycoprotein, and WNV NS1 has three conserved N-linked glycosylation sites (residues NS1-130/175/207). NS1 exists as a dimer in the ER lumen during viral replication, and is also found on the cell surface as a dimer and secreted into the extracellular space as a hexamer (Akey et al., 2015b). Intracellular NS1 can antagonize IFN- β production (Zhang et al., 2017), and secreted NS1 can antagonize complement activation by sequestering components of complement (Brinton, 2013). High levels of secreted NS1 are associated with severe disease during DENV infection, (Rastogi et al., 2016). NS1 is capable of interacting with prM, E, NS2A, NS4A, and NS4B at various times during virus replication (Lindenbach et al., 2007; Lindenbach and Rice, 1999; Scaturro et al., 2015; Youn et al., 2012).

The four small hydrophobic NS proteins, NS2A, NS2B, NS4A, and NS4B, all associate with the ER membrane, but each has unique functions during viral replication. NS2A is involved in virus assembly (Kummerer and Rice, 2002), antagonizing IFN-I induction (Liu et al., 2006) and it may induce apoptotic cell death (Melian et al., 2013), while NS2B acts as a cofactor for NS3 serine protease activity (Chappell et al., 2008). NS4A has a signal sequence referred to as the 2K peptide that helps NS4B translocate properly into the ER lumen, and it can also regulate NS3 helicase activity (Shiryaev et al., 2009). Flavivirus NS4A and NS4B antagonize IFN-I signaling (Mun et al., 2005), and studies using DENV have demonstrated that NS4B can interact with NS3 and assist the viral helicase in dissociating from ssRNA (Umareddy et al., 2006). NS4B has also been associated with suppression of stress granule formation, activation of the unfolded protein response, and RNA interference (RNAi) in various flaviviruses (Zmurko et al., 2015). Each of these hydrophobic NS proteins likely have additional functions during flavivirus replication and pathogenesis that have yet to be defined.

The NS3 protein encodes three enzymatic domains including a N-terminal serine protease, and a C-terminal RNA helicase and RNA triphosphatase, all of which are essential to viral replication (Lindenbach et al., 2007). As mentioned previously, NS2B acts as a cofactor for NS3 serine protease activity, and this protease is responsible for cleaving several junctions in the viral polyprotein including NS2A/NS2B, NS2B/NS3, NS3/NS4A, and NS4B/NS5 (Lindenbach et al., 2007). The protease also generates the C-terminal end of C and NS4A proteins and can target internal cleavage sites in NS2A and NS3 (Lindenbach et al., 2007). The RNA helicase helps to unwind the viral RNA, and the RNA triphosphatase (RTPase) activity dephosphorylates the 5' end of the genome prior to RNA capping (Lindenbach et al., 2007). Besides its enzymatic activity, NS3 is also implicated in inducing apoptosis (Lindenbach et al., 2007).

The NS5 protein also encodes enzymatic activity essential to replication including an N-terminal methyltransferase (MTase) and a C-terminal RNA-dependent-RNA-polymerase (RdRp) (Lindenbach et al., 2007). The MTase is responsible for capping the 5' end of the viral RNA with a Type 1 cap structure (Zhou et al., 2007), whereas the RdRp synthesizes new strands of the viral RNA genome (Lindenbach et al., 2007). NS5 can stimulate the nucleotide triphosphatase (NTPase) and RTPase activities of NS3, and although it localizes to the ER for viral replication, NS5 also localizes to the nucleus (Lindenbach et al., 2007). Furthermore, NS5 is able to antagonize IFN-I signaling (Laurent-rolle et al., 2010).

1.2.2.3 5' AND 3' UNTRANSLATED REGIONS

The WNV genome also includes 5' and 3' untranslated regions (UTRs). The 5' UTR is 96 nucleotides long and is modified with a type 1 cap structure by the NS5 MTase (Brinton, 2013). The 3' UTR is 635 nucleotides in length and has no poly-A tail, but it incorporates secondary structures that are important to replication and translation of viral RNA (Brinton, 2013). Additionally, the 3' and 5' UTRs interact as cyclization of the genome is required for RNA replication (Brinton, 2013).

1.3 WNV PATHOGENESIS AND IMMUNE RESPONSE

1.3.1 WNV Pathogenesis

WNV is thought to first replicate in Langerhans dendritic cells (DCs) in the skin at the site of inoculation (Byrne et al., 2001). Infected DCs migrate to draining lymph nodes where the virus continues to replicate, resulting in viremia and migration to peripheral tissues (Samuel and

Diamond, 2006). In animal models, after approximately one week, WNV is cleared from the periphery and migrates to the CNS where it can infect neuronal tissue in various regions of the brain (Samuel and Diamond, 2006). It is not clear exactly how WNV crosses the blood brain barrier (BBB), though there are several hypotheses including (1) TNF- α mediated compromise of the BBB, (2) hematogenous dissemination, (3) retrograde axonal transport, and (4) transport from olfactory neurons (Fredericksen, 2014; Samuel and Diamond, 2006). Since higher viremia is often correlated with CNS invasion in animal models, it is likely that hematogenous spread is at least in part responsible for WNND (Fredericksen, 2014; Samuel and Diamond, 2006). While survival from WNV is typically associated with virus clearance in animal models and humans, there is evidence of WNV persistence and continued pathology in neuronal and renal tissues in humans years after acute infection (Garcia et al., 2015).

1.3.2 Immune Response to WNV Infection

WNV is detected inside infected cells by pattern recognition receptors (PRRs) including retinoic acid-inducible gene I (RIG-I) and melanoma differentiation associated protein 5 (MDA5) (Fredericksen et al., 2008). These PRRs signal through the adaptor mitochondrial antiviral signaling protein (MAVS) (Suthar et al., 2010). MAVS activates interferon response factor 3 (IRF-3), which induces many interferon-stimulated genes (ISGs) (Fredericksen et al., 2004, 2008; Fredericksen and Gale, 2006). IFN as well as pro-inflammatory cytokines, chemokines, and antiviral genes all play a role in control of WNV infection and spread. Although multiple flavivirus proteins are capable of antagonizing components of the IFN-I pathway, the presence of IFN- α and/or IFN- β during early infection is essential to reduce viremia and rapid disease progression (Samuel and Diamond, 2005). Another pathway that is essential to WNV control in humans

involves OAS/RNase L. 2'5' oligoadenylate synthase (OAS) is an enzyme in the pathway to RNase L activation and subsequent degradation of viral RNA (Yakub et al., 2005). A single nucleotide polymorphism (SNP) in the human OAS gene is associated with increased susceptibility to severe WNND (Bigham et al., 2011; Yakub et al., 2005). Another risk factor for enhanced WNV disease of humans is chemokine receptor 5 (CCR5) deficiency. Although the exact mechanism of CCR5 control of WNV is not known, one consideration is that CCR5 deficiency was associated with decreased leukocyte trafficking in the CNS of mice (Glass et al., 2005). Other chemokine receptors that have been associated with protection from WNND in mouse models include CCR2 and CXCR3 (Lim et al., 2011; Zhang et al., 2008). Although deficient chemokine signaling can be a WNV risk factor limiting leukocyte migration to the CNS, it is notable that inflammatory responses in the CNS tissues have also been linked to increased disease severity in other studies (Getts et al., 2012; Kumar et al., 2010). Another critical component of the innate immune response to WNV includes CD3⁺ T cells ($\gamma\delta$ T cells), which lack conventional major histocompatibility (MHC) restriction and can rapidly mount antiviral responses and reduce WN viral load and dissemination by secretion of IFN- γ (Wang et al., 2003a).

In terms of adaptive immunity, studies of animal models suggest that B cells and both IgM and IgG antibodies are critical in the control of viral dissemination during WNV infection (Diamond et al., 2003a, 2003b; Roehrig et al., 2006). CD4⁺ and CD8⁺ T cells are important in controlling and eliminating the virus from the host and contribute to long-lasting protective immunity in part by promoting strong antibody responses (Shrestha et al., 2006a; Sitati and Diamond, 2006; Wang et al., 2003b). Potent neutralizing antibody responses are the most established correlate of protection against WNV disease based on studies thus far in animal models and WNV candidate vaccine clinical trials (discussed below).

1.4 LICENSED FLAVIVIRUS VACCINES

1.4.1 Licensed flavivirus vaccines for human use

While no human vaccine has been licensed for WNV, there are effective live, attenuated vaccines available for the related mosquito-borne viruses YFV, DENV, and JEV. Inactivated vaccines are also licensed for JEV and the tick-borne flaviviruses tick-borne encephalitis (TBEV) and Kyasanur forest disease (KFDV). The YFV live, attenuated vaccine strain 17D was empirically derived by serial passage and incorporates 20 amino acid substitutions that differentiate the vaccine from the parental strain (Beck and Barrett, 2015). YFV 17D induces strong, typically life-long immunity with only one dose and has been associated with very few adverse events in the 82 years since its development (Martins et al., 2015). In 2016, the first DENV vaccine was licensed as a tetravalent vaccine to protect against the four serotypes of DENV. The DENV vaccine (Dengvaxia™) is a chimeric live, attenuated vaccine that incorporates the YFV 17D genome substituting the prM/E genes of DENV-1-4 (Guirakhoo et al., 2004). The chimeric use of 17D, referred to as ChimeriVax technology, has been explored for use in development of multiple different flavivirus vaccines, including JEV (Imojev™). Although Dengvaxia™ has moderate efficacy after administration of three doses (0, 6, and 12 months), there are concerns over safety in vaccinees who are DENV seronegative at the time of immunization, and alternative candidate recombinant live, attenuated DENV vaccines are in clinical evaluation (Beth et al., 2015; Clapham and Wills, 2018). Finally, WNV and JEV are closely related both serologically and genetically, and licensed vaccines for JEV could be considered the most relevant to WNV vaccine development. There are multiple licensed JEV vaccines, including a live, attenuated vaccine strain SA14-14-2, formalin-inactivated JEV (using multiple virus strains), and the chimeric IMOJEV™ vaccine combining the YFV 17D nonstructural genes with the prM/E genes from SA14-14-2 (Chen

et al., 2015). JE SA14-14-2 was empirically derived by serial passage in primary hamster kidney cells and harbors seventeen vaccine-specific amino acid differences from the parental strain SA14 (Ni et al., 1995; Yu, 2010). SA14-14-2 has an excellent safety profile and can induce protective immunity for years following a single primary dose (Ginsburg et al., 2017). Some countries administer two booster doses of SA14-14-2, while others recommend only a single dose (WHO). Likewise, the chimeric IMOJEV™ vaccine is also safe and effective when administered with just a single dose, though pediatric boosters are recommended (Chokephaibulkit et al., 2016). The inactivated Vero-cell-derived JEV vaccines also have an excellent safety profile but require two primary doses as well as a recommended booster dose (Chen et al., 2015; WHO). In sum, flavivirus vaccines are licensed for five flaviviruses, three of which are mosquito-borne. Since there are multiple vaccines licensed against JEV, and since JEV and WNV share significant sequence homology (approximately 75% homology in coding sequence) (Tanaka et al., 1991), it is rational that a human WNV vaccine can also be developed.

1.4.2 Licensed WNV vaccines for veterinary use

WNV is not only pathogenic in humans, but it is also a significant veterinary pathogen that has been associated with severe neurological disease and death in horses, wild mammalian and avian species, and a variety of animals found in zoological gardens. Several veterinary vaccines are commercially available and their properties may help to inform work on human vaccine development. Currently there are four WNV veterinary vaccines on the market: three that comprise whole inactivated virus (WN Innovator™, Vetera™ WNV, and Prestige® WNV) and one that is a live chimeric virus combining the WNV prM/E into a canarypox backbone (Recombitek™ Equine WNV) (El Garch et al., 2008; Health, 2019; Ng et al., 2003; Vetera WNV). Although

WNV veterinary vaccines are protective in horses (Angenvoort et al., 2013; Gardner et al., 2007; Schuler et al., 2004), all four require two primary doses and an annual booster. Of note, although Recombitek™ WNV is a live virus, there is no evidence that canarypox-based vaccines are capable of replication in mammals (Plotkin et al., 1995), so canarypox vaccines do not elicit as strong immunity as many replicating live, attenuated vaccines.

1.5 BIOLOGICAL PROPERTIES OF AN IDEAL HUMAN WNV VACCINE

There are several properties that could be used to define an optimum human WNV vaccine candidate. Although WND has been reported in children and younger adults, WNV primarily causes severe disease in the elderly. Based on the prevalence of severe disease in older adults as well as mathematical modeling of cost effectiveness (Shankar et al., 2017), the target population for WNV vaccination would likely be the elderly (e.g. individuals aged ≥ 50). It is important that all licensed vaccines induce an immune response, however, robust and long-lasting protective immunity is especially critical for vaccination of the elderly, as older age is associated with immunosenescence and a reduction of responsiveness to vaccination (Amanna, 2013; Weinberger, 2012). There is a strong body of work from investigations in mice and humans indicating that WNV-specific neutralizing antibodies are the most reliable correlate of protection for flavivirus infections (Hombach et al., 2005; Markoff, 2000), and thus they are the primary measurement of vaccine efficacy. Besides neutralizing antibodies, there is a strong body of work indicating that WNV-specific T cells are also important components of protective immunity using mice and humans. Multiple groups have demonstrated that CD8⁺ T cells are needed to clear WNV infection in mice and are associated with enhanced protection after vaccination of mice with candidate WNV vaccines (Brien et al., 2009; Engle and Diamond, 2003; Shrestha et al., 2008; Shrestha and

Diamond, 2004; Uhrlaub et al., 2011). Alternatively, a recent study using a collaborative cross mouse model found that reduced regulatory T cells in the periphery and CD8⁺ T cells in the brain may be associated with protection from WNV neurological disease (Graham et al., 2019). Although a balanced T cell response seems to be an essential component of WNV protective immunity in mice, additional studies are needed to determine if the same is true in humans, including identification of specific peptide targets associated with immunity in order to use them as a correlate of protection. However, it has been shown that a Chimerivax-WNV vaccine candidate induced WNV E protein-specific CD8⁺ T cell responses up to one year post vaccination in a clinical trial (Smith et al., 2011). Since neutralizing antibody titers are used by the World Health Organization (WHO) as a correlate of protection for JEV (Hombach et al., 2005), this will likely be the measurement for a WNV vaccine correlate of protection. It should be noted, however, that the definition of a correlate of protection is an immune marker (e.g. neutralizing antibodies) that is statistically associated with vaccine-induced protection, and this is different from a surrogate of protection which is defined as an attribute on the direct causal pathway to vaccine-induced protection (WHO, 2013). Currently, surrogates of WNV protection are not known, and prior to either vaccine efficacy studies in humans (i.e. a study undertaken under ideal clinical trial conditions) or vaccine effectiveness studies (i.e. a clinical study undertaken under field conditions), it is difficult to draw further conclusions on what the appropriate correlate(s) of protection may be.

As a point of comparison for flavivirus vaccine efficacy, a single dose of the JE SA14-14-2 live, attenuated vaccine is capable of inducing neutralizing antibodies in children for at least five years (Ginsburg et al., 2017; Sohn et al., 2008). SA14-14-2 is commonly administered to children as young as 8 months old in countries across Asia. Children typically have underdeveloped

immune responses and thus require multiple doses of most vaccines, so the degree of protection described is significant. Furthermore, the YFV 17D vaccine is capable of inducing life-long protective immunity with a single dose in individuals 9 months and older (CDC, 2019c). These vaccines suggest that long-lived protective immunity can be induced by a live vaccine. Examination of the inactivated JE and TBE vaccines shows that intermediate levels of immunity can also be achieved using these vaccine platforms, however, multiple primary doses plus boosters are typically necessary. For instance, inactivated JE vaccines require two primary doses and a booster after 1-2 years, whereas inactivated TBEV vaccines require three primary doses and boosters every three to five years in order to maintain protection (Aerssens et al., 2016; Dubischar-Kastner et al., 2010).

Besides immunogenicity, another important characteristic of a WNV vaccine is safety. It is critical that the risk of reversion of a candidate live attenuated WNV vaccine is very low, especially considering that the vaccine needs to be safe for use in older populations with weakened immune responses. Correspondingly, the safest vaccination strategies utilize inactivated virus, non-replicating virus or subunit protein/DNA/RNA viral components as the risk of reversion in these platforms is very low. Unfortunately, increased safety is often correlated with reduced efficacy as non-replicating vaccines require multiple doses to induce a protective immune response. Although live attenuated vaccines have the highest risk of adverse events, it is possible to develop safe live vaccines as has been demonstrated for YF, JE, measles, and varicella zoster viruses, for example. For JE SA14-14-2 which is most closely related to WNV, no serious adverse events or deaths have been directly associated with vaccination even though over 300 million doses have been distributed (Ginsburg et al., 2017). An additional consideration for the safety of a live, attenuated WNV vaccine is the importance of reduced mosquito competence to prevent circulation of the vaccine

strain in nature which could result in unexpected alterations to the vaccine phenotype. Although JE SA14-14-2 does not decrease mosquito infection rates compared to the parental SA14 strain, vaccine isolated from mosquitoes was not virulent in mice and did not have any amino acid mutations following sequential passage between a mosquito vector and pig reservoir (Liu et al., 2019; Yu, 2010). Moreover, YFV 17D and the chimeric JE vaccine Imojev™ each have strongly reduced infection rates in both *Aedes* and *Culex spp.* mosquitoes, respectively (Bhatt et al., 2000; Danet et al., 2019).

Marketing of a new vaccine is an expensive endeavor, so it is also important that a WNV vaccine be cost effective. The cost of direct and indirect medical care of individuals hospitalized for WNV in the United States was estimated to be on average \$56 million dollars per year (Staples et al., 2014), demonstrating the substantial economic impact that WNV continues to cause. Using mathematical modeling, it has been suggested that a vaccination program in the United States targeting adults ≥ 50 years old would be more cost effective than a universal vaccination program (Shankar et al., 2017). In particular, the 60-year-cohort had a mean cost per neuroinvasive disease case prevented of \$664,000. However, the model used couldn't take into account a specific vaccine cost, vaccine efficacy, or duration of protection, but they did report that, not surprisingly, a single dose vaccination would be more cost effective than vaccines requiring multiple doses (Shankar et al., 2017).

In sum, a WNV vaccine ideally should induce robust long-term protective immunity with only a single dose, and if a live vaccine is developed it should show no evidence of reversion and have a loss of mosquito competence.

1.6 CLINICAL TRIALS OF WNV VACCINE CANDIDATES

Several WNV vaccine candidates have progressed into clinical evaluation including (1) plasmid DNA expressing WNV prM/E (Ledgerwood et al., 2011; Martin et al., 2007), (2) recombinant WNV E protein (Coller et al.), (3) hydrogen peroxide-inactivated WNV (Woods et al., 2019), (4) formalin-inactivated WNV (Barrett et al., 2017), (5) chimeric live attenuated WN/DEN4Δ30 (Durbin et al., 2013; Pierce et al., 2017), and (6) chimeric live attenuated ChimeriVax-WN02 (Biedenbender et al., 2011; Dayan et al., 2012; Monath et al., 2006). A summary of the vaccine characteristics can be found in **Table 1.1**. Notably, for the DNA and subunit E protein platforms three primary doses were required to elicit neutralizing antibodies in the majority of subjects (Ledgerwood et al., 2011; Martin et al., 2007). Furthermore, the hydrogen peroxide inactivated vaccine administered in two doses only elicited neutralizing antibody titers in 31% of the cohort (Woods et al., 2019). While a formalin inactivated vaccine candidate elicited neutralizing antibodies in all participants, it required two primary doses plus a booster dose after six months (Barrett et al., 2017). Alternatively, the chimeric, live attenuated WN/DEN4Δ30 and ChimeriVax-WN02 vaccines were more immunogenic. WN/DEN4Δ30 combined the WNV prM/E with DENV-4 nonstructural genes incorporating a 30 nucleotide deletion in the 3' UTR (Pletnev et al., 2006). Importantly, in a cohort of older adults (ages 50-65) who are more susceptible to severe WNV, 95% seroconverted after a single dose of WN/DEN4Δ30 (Pierce et al., 2017). ChimeriVax-WN02 combined WNV prM/E with the YFV 17D vaccine nonstructural genes. This is a second generation ChimeriVax-WN vaccine that includes three mutations in the E protein to enhance attenuation of this vaccine candidate (discussed more in next section and in Chapter 3) (Arroyo et al., 2004). For ChimeriVax-WN02, all age groups tested, including individuals ≥65, exhibited >90% seroconversion after receiving a single dose of vaccine

(Biedenkemper et al., 2011; Dayan et al., 2012; Monath et al., 2006). Of note, differences in experimental design for quantification of neutralizing antibodies between the vaccine studies make it difficult to directly compare immunogenicity between the vaccine candidates. Regardless of this discrepancy, the two live, attenuated vaccine candidates appear to be the most immunogenic of the six candidates tested in humans, and moreover, neither of the live, attenuated strains were associated with any severe adverse events in the older cohorts tested.

1.7 THE NEED FOR ADDITIONAL WNV VACCINE CANDIDATES

Although there are at least two WNV vaccine candidates that have been safe and effective in studies thus far, it remains important to develop alternative candidates. One consideration is in regards to the safety concerns about Dengvaxia™. As discussed previously, Dengvaxia™ utilizes DENV structural genes and YFV 17D NS genes, but this vaccine has been associated with enhanced DENV disease in individuals who are seronegative at the time of vaccination. It is now thought that one reason this vaccine is not sufficiently protective is because the lack of DENV NS genes results in suboptimal T cell and neutralizing antibody responses to DENV NS1 (Halstead, 2018). Since T cell epitopes for WNV are known to be widely distributed in prM, E, NS2B, NS3, NS4B, and NS5 proteins (Brien et al., 2007; Lanteri et al., 2008; McMurtrey et al., 2008; Purtha et al., 2007), there is concern that the two live, attenuated candidates tested thus far are each chimeric viruses and may not provide as potent of protection as a full-length WNV vaccine could. Furthermore, the first generation of the ChimeriVax-WN02 vaccine candidate, was previously licensed as a veterinary vaccine, PreveNile. This vaccine was licensed for veterinary use in 2006 but was recalled in 2010 due to reports of serious adverse events in horses including neurological disease and death (American Veterinary Medical Association, 2010). Although the second

generation of this vaccine includes three site-directed mutations in the E protein to enhance attenuation, it is a concern that the vaccine backbone was not sufficiently safe in horses and may be subject to reversion to WT virulence. Overall, based on inadequate safety and efficacy of some other chimeric flavivirus vaccines, an ideal live, attenuated WNV vaccine would likely be comprised of the complete WNV genome.

1.8 ATTENUATING MUTATIONS IN WNV

Since an optimal WNV vaccine would have mutations in multiple genes to protect from reversion to a virulent phenotype, it is important to identify virulence determinants in diverse regions of the genome that may be targeted for mutagenesis. Multiple groups have identified WNV attenuating mutations by either genotypic analysis of naturally attenuated WNV isolates or by site-directed mutagenesis of amino acid residues predicted to be virulence determinants. For instance, of six mouse and avian attenuated WNV isolates collected in Texas in 2003, three harbored a NS4B-E249G mutation (Brault et al., 2011; Davis et al., 2004, 2007). Other mutations that were conserved amongst more than one of the attenuated isolates include prM-N4D, NS5-A804V, and several sites in the 3' UTR (Davis et al., 2004). Importantly, none of these mutations alone conferred complete attenuation, but rather, each strain harbored a unique combination of mutations in NS4B, prM, NS5, and/or the 3' UTR, i.e., attenuation was due to a combination of multigenic mutations (Davis et al., 2007). Beyond analysis of natural isolates, other work has utilized infectious clone technology to investigate mutations in WNV prM, E, NS1, NS2A, NS3, NS4A, NS4B, and NS5 proteins (**summarized in Table 1.2**).

1.8.1 Attenuating mutations in WNV prM protein

WNV prM protein has a single N-linked glycosylation site present at amino acids 15-17 (i.e., not present in the mature M protein), and ablation of this glycosylation motif alters virus particle release and infectivity (Hanna et al., 2005). Using WNV reporter virus particles (RVPs) capable of a single round of infection, a decrease in the quantity of viral RNA by real-time PCR was observed when cells were infected with a prM-N15Q mutant and compared to wild-type WNV (Hanna et al., 2005). Besides mutation of the glycosylation site, another group found that mutation of prM-K31T or prM-K31V caused delayed multiplication and reduced infectivity in cell culture compared to WT WNV (Calvert et al., 2012). Although the prM mutations investigated in past studies each had attenuating properties *in vitro*, it has not been reported whether or not they attenuate WNV in animal or mosquito models.

1.8.2 Attenuating mutations in WNV E protein

Mutation of the single glycosylation site present in the WNV E protein (E-154) has been associated with attenuation. While some natural isolates of WNV do not harbor the E glycosylation site, this site is present in most highly pathogenic strains responsible for human outbreaks (Hanna et al., 2005). In WNV RVPs, E glycosylated WNV replicated to approximately 10-fold higher titer than non-glycosylated strains in cell culture (Hanna et al., 2005). Furthermore, E-N154S mutation attenuated neuroinvasion (i.p. LD₅₀ = 126-200 PFU for the mutant compared to 0.1-1.3 for WT) and mildly attenuated neurovirulence (i.c. LD₅₀ = 1.1-125 PFU for the mutant compared to 0.3 for WT) in outbred mice (Beasley et al., 2005; Whiteman et al., 2010). Considering that some natural, attenuated strains of WNV are already lacking E glycosylation, ablation of this glycosylation motif may be a stable, attenuating component of a WNV vaccine.

Another E mutation that was attenuating to WNV is E-T198F. Mutation of this residue caused increased susceptibility to a neutralizing antibody and attenuated the virus in C57Bl/6J mice in that only 2/15 mice died from 10^2 FFU s.c. as opposed to 13/15 mice inoculated with WT (Goo et al., 2017). The E-T198F mutation was found to alter structural flexibility of the E protein that is important for virion stability (Goo et al., 2017).

Another attenuating E mutation that was chosen for investigation was based on the JE SA14-14-2 live, attenuated vaccine. SA14-14-2 has an E-L107F mutation (Gromowski et al., 2015), and the wild-type leucine residue is conserved in WNV. Studies of E-L107F in WNV determined that this mutation attenuated neuroinvasion in outbred mice (i.p. $LD_{50} > 1000$ PFU) but did not significantly attenuate neurovirulence (i.c. $LD_{50} = 3.1$ PFU) (Zhang et al., 2006). Although E-L107F mutation was attenuating, there was some evidence of reversion to wild-type in virus isolated from brains of mice that succumbed to infection (Zhang et al., 2006). E-L107F along with E-A316V and E-K440R mutations were each included in the second-generation ChimeriVax-WN02 since the first generation ChimeriVax-WN retained low level neurovirulence in horses (Arroyo et al., 2004). Of six E mutations tested in ChimeriVax-WN (L107F, E138K, Y176V, K280M, A316V, K440R), the three selected had the most profound effect on attenuation of neurovirulence in outbred mice (Arroyo et al., 2004). These studies in the ChimeriVax-WN platform could be informative for development of alternative live, attenuated WNV vaccine candidates. However, it is notable that E-L107F was capable of reversion as a vaccine will need the attenuating determinants to be stable.

1.8.3 Attenuating mutations in WNV NS1 protein

In addition to mutation of the WNV structural genes, mutation of NS genes has also been a useful tool for identification of potential residues to target for vaccine mutagenesis. Simultaneous mutation of three glycosylation motifs in WNV NS1 strongly attenuated mouse neuroinvasion (i.p. $LD_{50} > 10^6$ PFU) and neurovirulence (i.c. $LD_{50} = 800$ PFU) in an outbred mouse model (Whiteman et al., 2011). Ablation of the glycosylation motifs with alanine substitution (NS1-N130A/N175A/N207A) yielded mouse attenuation, but there was evidence that the first glycosylation site could revert (Whiteman et al., 2010, 2011). When all three amino acids in the first motif were mutated (NS1-NNT130QQA/N175A/N207A), the resulting virus was stable in cell culture and in mice (Whiteman et al., 2011). Moreover, 50 PFU of the mutant could protect half of mice from a lethal challenge of WT (Whiteman et al., 2011) and this NS1 mutant had decreased vector competence compared to WT (Van Slyke et al., 2013). The glycosylation site mutations caused reduced secretion of NS1 compared to WT, and instead NS1 accumulated in the ER (Whiteman et al., 2015), providing a potential mechanism of attenuation. Overall, this NS1 mutant has several properties that are desirable for a WNV vaccine candidate including strong attenuation, protection from challenge, and reduced vector competence.

1.8.4 Attenuating mutations in WNV NS2A protein

In the NS2A protein, an A30P mutation was found to ablate the protein's ability to antagonize IFN- β (Liu et al., 2006). The WNV NS2A-A30P mutant accumulated approximately 7-8-fold more IFN- β mRNA compared to WT in cell culture (Liu et al., 2006). This mutation also attenuated WNV in outbred mice as the i.p. LD_{50} was $> 10^5$ PFU and the i.c. $LD_{50} = 30$ PFU (Liu et al., 2006). Furthermore, 10^4 PFU of the NS2A-A30P mutant protected all mice from a lethal

WT challenge (Liu et al., 2006). Notably, this study was using a naturally attenuated WNV Kunjin strain as the backbone for mutagenesis (Liu et al., 2006). When another group investigated NS2A-A30P in the virulent TX02 strain of WNV, the attenuating properties were not as strong (i.p. LD₅₀ = 4.2 PFU in outbred mice) (Rossi et al., 2007). Besides A30P, this group also investigated mutation of NS2A-D73H and NS2A-M108K, both of which attenuated WNV neuroinvasion (i.p. LD₅₀ >1000 PFU) and induced neutralizing antibodies (Rossi et al., 2007). One mouse died from infection with NS2A-D73H due to reversion, but there was no lethality associated with NS2A-M108K (Rossi et al., 2007). These two NS2A mutations are associated with cell culture adaptation, and although their mechanism of attenuation is not known, they may be good candidates for inclusion in a WNV vaccine.

1.8.5 Attenuating mutations in WNV NS3 protein

Mutations that alter the enzymatic properties of NS3 have been investigated in WNV. Specifically, deletion of residue NS3-D483 (NS3Δ483) in the RNA helicase domain attenuated WNV in C3H/HeN mice as only 1/8 mice died from s.c. inoculation with 10⁵ PFU of the mutant, but 8/8 mice died from 10 PFU of WT (Ebel et al., 2011). In cell culture, NS3Δ483 was 10-fold more sensitive to inhibition by IFN-β compared to WT, and in mice the mutant had reduced viremia, lower organ virus titers, and reduced spread into the central nervous system (CNS) (Ebel et al., 2011), making it an attractive candidate for WNV vaccine development.

1.8.6 Attenuating mutations in WNV NS4A protein

While attenuating mutations in the NS4A protein have not been assessed directly in WNV, one group has utilized soluble protein constructs to investigate NS4A mutations that may be useful in vaccine development. NS4A is a cofactor of NS3 RNA helicase activity, therefore, protein constructs of soluble NS3_{HEL} and NS3_{HEL}-NS4A were generated (Shiryaev et al., 2009). Using *in vitro* measurements of ATPase activity, the experiments demonstrated that NS3_{HEL} alone had approximately five-fold more ATPase activity when compared to the NS3_{HEL}-NS4A construct (Shiryaev et al., 2009). Since it has been previously shown that *in vitro* ATP is required in mM concentrations for NS3 RNA helicase activity, it was hypothesized that the ATP-saving function of the soluble portion of NS4A acts as a cofactor to sustain NS3 helicase activity *in vivo* under lower concentrations of ATP (Shiryaev et al., 2009). When they changed three negatively charged NS4A amino acids (Glu, Glu, Asp) at residues 46, 47, and 50 to positively charged lysine residues, the NS3_{HEL}-NS4A construct no longer exhibited low ATPase activity and instead it behaved as the NS3_{HEL} fragment and exhibited a high rate of ATP degradation (Shiryaev et al., 2009). If viable in full-length WNV, these mutations could attenuate the virus by altering replication efficiency.

1.8.7 Attenuating mutations in WNV NS4B protein

As mentioned previously, a NS4B-E249G mutation was associated with attenuation of natural WNV isolates, but this mutation was not solely responsible for the attenuated phenotype. NS4B-E249G has also been engineered in a WNV infectious clone. When administered with 10³ PFU by the s.c. route, the NS4B-E249G mutant was attenuated in C3H/HeN mice as only 4/8 mice died from the mutant as opposed to 8/8 that died from WT (Puig-Basagoiti et al., 2007). The

surviving mice were all protected from a lethal challenge dose of WNV, indicating that the E249G mutant is immunogenic (Puig-Basagoiti et al., 2007).

Another group screened at least 15 different mutations in NS4B and identified two mutations that were strongly attenuating: P38G and C102S (Wicker et al., 2006, 2012). Both of the mutants were highly attenuated for neuroinvasion (i.p. LD₅₀ > 10,000 PFU) and less than 1 PFU of each mutant was able to protect half of mice from a lethal challenge of WT (Wicker et al., 2006, 2012). The P38G mutant was not attenuated for neurovirulence (Wicker et al., 2012); however, the C102S mutation provided significant neurovirulence attenuation (i.c. LD₅₀ > 1,000 PFU) (Wicker et al., 2006). Interestingly, the P38G mutation caused compensating mutations at NS4B-T116I and NS3-N480H, but when tested independently these compensating mutations were not attenuating but instead provide stability of the P38G mutation, as virus could not be recovered with the P38G mutation alone (Wicker et al., 2012). Surprisingly, the NS4B-P38G and C102S mutants had enhanced vector competence compared to WT, demonstrating that these mutations alone are not optimal for vaccine development (Van Slyke et al., 2013). However, the strong degree of protection conferred by these mutants could be beneficial in a WNV candidate vaccine if combined with other mutations that could reduce mosquito competence.

1.8.8 Attenuating mutations in WNV NS5 protein

Another NS gene that has been investigated using mutagenesis is NS5. Four mutations in WNV NS5 that attenuate methyltransferase activity (K61A, D146A, K182A, and E218A) have been previously studied (Daffis et al., 2011; Zhou et al., 2007). While NS5-D146A is not a viable mutation in WNV, the other three mutations each demonstrated attenuation. Specifically, NS5-K61A and NS5-K182A mutants each caused no lethality in C3H/HeN mice when inoculated s.c.

with 10^5 PFU whereas WT was lethal in 5/8 mice with 10 PFU (Zhou et al., 2007). Additionally, a NS5-E218A mutant caused no lethality in BALB/c mice when inoculated s.c. or i.c. with 10^5 PFU, but 10 PFU of WT inoculated s.c. or i.c. caused 25% or 100% lethality, respectively (Daffis et al., 2011). Each of these mutants demonstrated strong attenuation, and although they were not tested in a more susceptible mouse model (i.e. outbred mice), the reported attenuation could be useful in vaccine development.

1.9 SPECIFIC AIMS

While attenuating mutations in multiple WNV genes have been identified, none of the previously studied single gene mutants are sufficiently attenuated and protective to proceed with vaccine development. For example, several of the mutations described above were not stable, some had enhanced mosquito competence, and some may not be viable as they have never been investigated in full-length WNV. Importantly, a WNV vaccine should have independently attenuating mutations in more than one viral gene so that the vaccine strain is not likely to revert to a virulent phenotype. To aid in vaccine development, this dissertation has utilized mutagenesis to (1) investigate new potentially attenuating mutations in WNV, (2) continue investigation of several attenuating mutations that have been previously identified, and (3) generate multigenic mutants that harbor mutations in more than one viral gene. The overall goal is to identify multiple independently attenuating mutations in WNV that can ultimately be combined to yield a stable, attenuated vaccine strain that induces a protective immune response. The hypothesis is that targeted mutations in WNV E, NS4B, and NS5 genes will be stable, attenuating, and protective, and that multigenic mutants utilizing a NS1 glycosylation mutant as the backbone will have an

increased attenuated phenotype compared to single gene mutants. These studies are divided into four specific aims:

Specific Aim 1: Investigate JEV vaccine-specific envelope E138K mutation for attenuation of WNV

Hypothesis: E-E138K mutation in WNV will confer mouse attenuation and induce protective immunity.

Rationale: JEV and WNV are closely related flaviviruses. While the JE SA14-14-2 live vaccine has 17 amino acid substitutions compared to the parental strain, there is a robust body of literature demonstrating that E-E138K mutation alone confers strong attenuation of mouse neuroinvasion and neurovirulence. Since residue E-E138 is conserved between JEV and WNV, it is proposed that this mutation could also attenuate WNV.

Specific Aim 2: Investigate NS5-K61A and NS5-E218A methyltransferase mutants for attenuation of WNV when expressed alone and when combined.

Hypothesis: Single NS5-K61A and NS5-E218A mutants will have an attenuated phenotype, and when combined, the double mutant NS5-K61A/E218A will have enhanced attenuation compared to the single mutants.

Rationale: Both NS5-K61A and NS5-E218A have been previously investigated by other groups, but these studies will utilize a different infectious clone and a different mouse model than previous work. Moreover, in DENV, double mutation of NS5-K61A/E217A (or E216A) has been proposed as a tetravalent vaccine candidate, but the double mutant has never been investigated in WNV and may be a good candidate for WNV vaccine development.

Specific Aim 3: Generate new NS4B mutants with an increased attenuated phenotype compared to NS4B-P38G and NS4B-C102S.

Hypothesis: New NS4B mutants will be stable and have an increased attenuated phenotype compared to previous NS4B mutants.

Rationale: Since previous studies have shown that point mutations in NS4B can confer significant attenuation, new mutations with increased attenuating properties would likely be good candidates for use in a WNV vaccine. Based on an alignment of different flaviviruses, conserved NS4B residues were targeted for mutagenesis so that the findings may be applicable to other mosquito-borne flaviviruses.

Specific Aim 4: Generate and characterize the attenuated phenotype of multigenic mutants based on the NS1 glycosylation mutant backbone.

Hypothesis: Combined NS1+E and NS1+NS4B mutants will be viable and have an increased attenuated phenotype compared to E, NS4B, and NS1 mutants alone.

Rationale: Previous studies have described characterization of WNV NS1 and NS4B mutants independently, but each had insufficient attenuation of neurovirulence, and importantly a vaccine strain should also have mutations in multiple viral genes. Additionally, previous work in the related JEV has demonstrated that E mutations are critical to the attenuation of a JE live, attenuated vaccine. To increase attenuation *and* generate viruses with multigenic mutations using the NS1 glycosylation site mutant as a backbone, it is proposed to combine mutations in at least two viral genes that have been shown to be capable of harboring attenuating mutations.

Table 1.1: Summary of WNV human vaccine candidates that have been studied in clinical trials

Vaccine	Developer	Vaccine type	WNV Strain	Clinical trial (onset)	Clinical trial number	Dose and route	Dosing series
¹ VRC 302	NIAID Vaccine Research Center	prM/E DNA with ¹ CMV or ² CMV/R promoter	NY99	Phase I (2006)	¹ NCT00106769	4 mg i.m.	Three doses four weeks apart
² VRC 303					² NCT00300417		
WN-80E	Hawaii Biotech	Recombinant, truncated E protein	NY99	Phase I (2008)	NCT00707642	5, 15, or 50 µg i.m.	Three doses four weeks apart
WN/DEN4Δ30	NIAID Division of Intramural Research	Chimeric, live virus with WNV prM/E and DENV-4 nonstructural genes with a 30 nt deletion	NY99	Phase I (2004) Phase I (2007) Phase I (2014)	NCT00094718 NCT00537147 NCT02186626	10 ³ , 10 ⁴ , or 10 ⁵ PFU s.c.	*One or two doses
HydroVax-001	Najit Technologies	Hydrogen peroxide-inactivated whole virus	Kunjin	Phase I (2015)	NCT02337868	1 or 4 µg i.m.	Two doses four weeks apart
Formalin-inactivated WNV	Nanotherapeutics Inc.	Formalin-inactivated whole virus	NY99	Phase I/II	none	1.25, 2.5, 5.0, or 10.0 µg i.m.	Two doses 21 days apart plus booster dose on day 180
ChimeriVax-WN02	Sanofi Pasteur	Chimeric, live virus with WNV prM/E and YFV 17D nonstructural genes with three site-directed mutations in the E protein	NY99	Phase I Phase II (2005) Phase II (2008)	none NCT00442169 NCT00746798	10 ³ , 10 ⁴ , or 10 ⁵ PFU s.c.	One dose

¹ Corresponds to the study NCT00106769 using the CMV promoter² Corresponds to the study NCT00300417 using the modified CMV/R promoter

* Although WN/DEN4Δ30 was tested in a two-dose regimen, one dose was found to provide better neutralizing antibody responses in older adults

NIAID = National Institute of Allergy and Infectious Diseases, CMV = cytomegalovirus, nt = nucleotide, i.m. = intramuscular, s.c. = subcutaneous

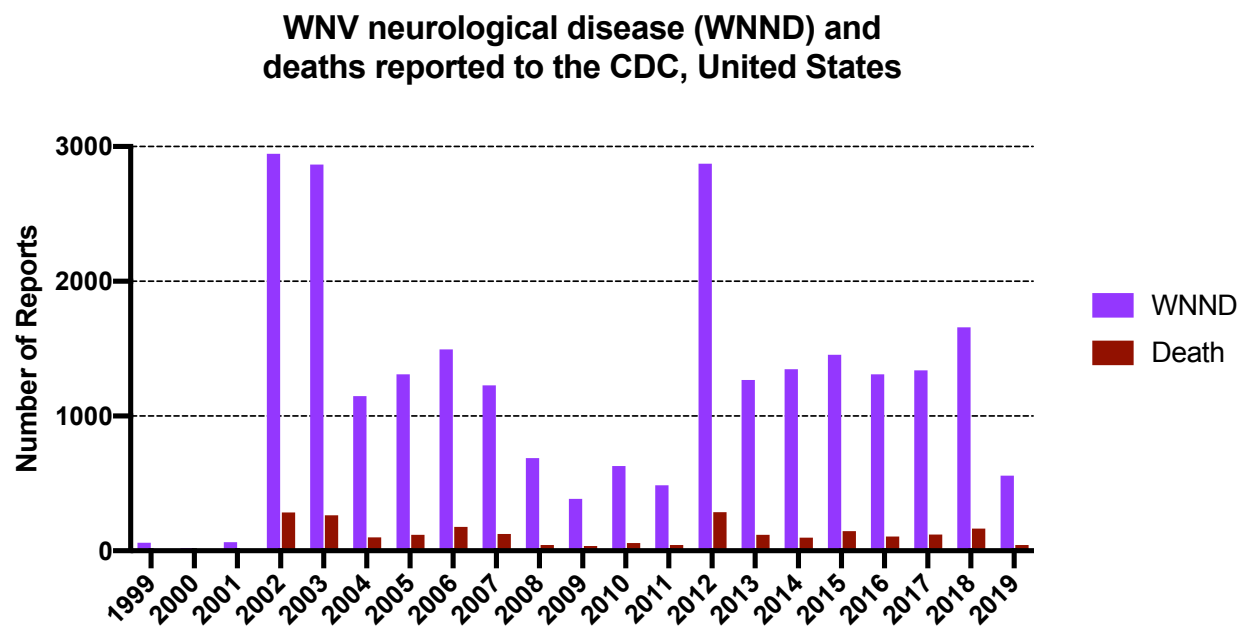
Table 1.2: Attenuating mutations previously studied in WNV infectious clones

Viral Protein	Viral Protein Position	Parental Amino Acid	Mutant Amino Acid	Attenuated Phenotype
prM	15	N	Q	Decreased reporter virus particle RNA (Hanna et al., 2005)
	31	K	T/V	Delayed multiplication/reduced infectivity (Calvert et al., 2012)
E	107	L	F	Reduced outbred mouse neuroinvasion (Arroyo et al., 2004; Zhang et al., 2006)
	154	N	S	Reduced outbred mouse neuroinvasion/neurovirulence (Beasley et al., 2005; Whiteman et al., 2010)
	198	T	F	Reduced inbred mouse neuroinvasion (Goo et al., 2017)
	316	A	V	Reduced neurovirulence of candidate chimeric vaccine (Arroyo et al., 2004)
	440	K	R	Reduced neurovirulence of candidate chimeric vaccine (Arroyo et al., 2004)
NS1	130-132/175/207	NNT/N/N	QQA/A/A	Reduced outbred mouse neuroinvasion/neurovirulence and mosquito competence (Whiteman et al., 2011)
NS2A	30	A	P	Reduced outbred mouse neuroinvasion (Liu et al., 2006; Rossi et al., 2007)
	73	D	H	Reduced outbred mouse neuroinvasion (Rossi et al., 2007)
	108	M	K	Reduced outbred mouse neuroinvasion (Rossi et al., 2007)
NS3	483	D	deletion	Reduced inbred mouse neuroinvasion (Ebel et al., 2011)
NS4A	46/47/50	E/E/D	K/K/K	Caused rapid use of ATP by soluble NS3 protein helicase domain (Shiryaev et al., 2009)
NS4B	38	P	G	Reduced outbred mouse neuroinvasion (Wicker et al., 2012)
	102	C	S	Reduced outbred mouse neuroinvasion/neurovirulence (Wicker et al., 2006)
	249	E	G	Reduced inbred mouse neuroinvasion (Puig-Basagoiti et al., 2007)
NS5	61	K	A	Reduced inbred mouse neuroinvasion (Zhou et al., 2007)
	182	K	A	Reduced inbred mouse neuroinvasion (Zhou et al., 2007)
	218	E	A	Reduced inbred mouse neuroinvasion/neurovirulence (Daffis et al., 2011)

Table 1.3: Genetic lineages of WNV have diverse geographic distributions and virulence phenotypes

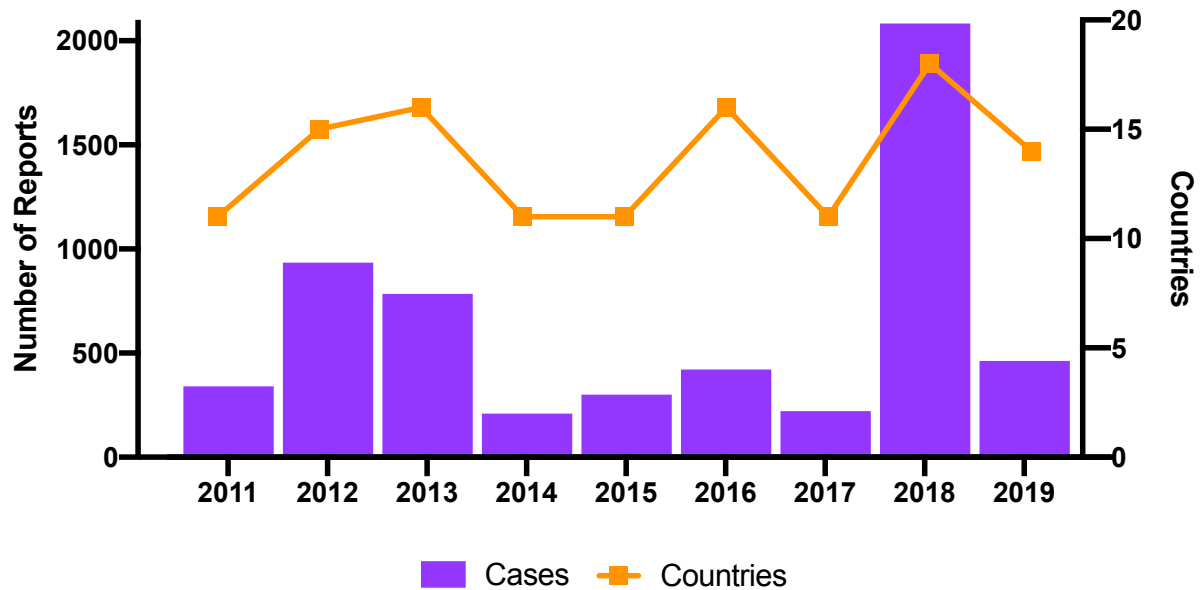
Lineage	Location(s) Isolated	Species Isolated	Associated with WNND outbreaks?
1a	America, Europe, Africa, Middle East, Russia	Mosquitoes, birds, horses, humans, other mammals	yes
1b (Kunjin)	Australia	Mosquitoes, birds, horses, humans	no
1c/5	India	Mosquitoes	no
2	Africa, Europe	Mosquitoes, birds, horses, humans	yes
3 (Rabensburg)	Czech Republic	Mosquitoes	no
4	Russia	Mosquitoes	no
5/1c	India	Mosquitoes	no
6	Spain	Mosquitoes	no
7 (Koutango)	Africa	Ticks, rats	no
8	Africa	Mosquitoes	no
9/4b	Austria	Mosquitoes	no

Figure 1.1: Annual West Nile neurological disease cases (WNND) and deaths reported to the US CDC



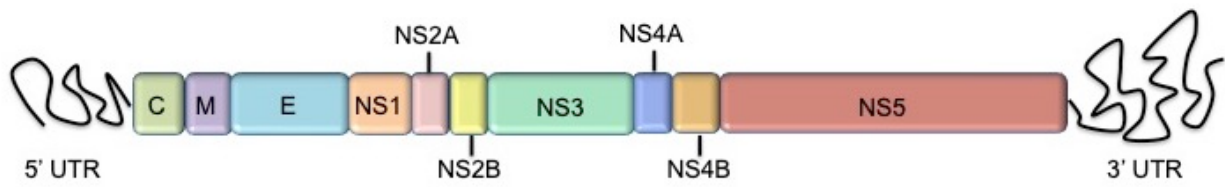
Data from 2019 is accurate as of November 18, 2019 at which time there have been 557 WNND cases and 44 deaths (CDC, 2019b).

Figure 1.2: Annual WNV case number and countries reporting confirmed WNV infection to the European CDC



Data from 2019 is accurate as of November 18, 2019 at which time there have been 462 confirmed cases across 14 countries (ECDC, 2019).

Figure 1.3: WNV genome organization



C=capsid, M=membrane, E=envelope, NS=nonstructural, UTR=untranslated region

Chapter 2 - Materials and Methods

2.1 CELL CULTURE

Vero African Green Monkey kidney cells (ATCC CCL-81) and A549 human alveolar epithelial cells (ATCC CCL-185) were grown at 37°C with 5% CO₂ in minimum essential media (MEM) supplemented with 100 U/mL penicillin, 100 ug/mL streptomycin, 2 mM L-glutamine, 0.1 mM non-essential amino acids, and 8% fetal bovine serum (FBS).

2.2 RECOVERY OF RECOMBINANT WNV

Recombinant viruses were generated using a WNV infectious clone based on strain NY99-flamingo 382-99 (hereafter referred to as NY99ic) (Beasley et al., 2005; Whiteman et al., 2010; Wicker et al., 2006, 2012; Zhang et al., 2006). The NY99ic is comprised of two plasmids, one containing the 5' UTR and the virus structural genes, and a second containing the NS genes through the 3' UTR. Quikchange II XL Site-Directed Mutagenesis Kit (Agilent) was utilized to generate all mutants. In mutants that harbored more than one targeted mutation, sequential mutagenesis was utilized to add secondary mutations into plasmids that already had one mutation of interest. The mutagenesis primers were ordered from Eurofins as high purity salt-free primers for mutation of WNV residues E-E138K, NS5-K61A, NS5-E218A, NS4B-P38G, NS4B-P54A, NS4B-P54G, NS4B-L56A, NS4B-C102S, and NS4B-W103Y. Each primer sequence is listed in **Table 2.1**. After mutagenesis, plasmids were transformed into MC1061 competent *E. Coli* cells and grown in 200 mL Luria broth (LB) with 100 ug/mL ampicillin. After growth for 14-16 hours, bacteria were pelleted and suspended in glucose-tris-EDTA buffer. Cells were lysed using 0.2 M

NaOH/1% SDS, and lysis was neutralized using 3 M KOAc. After isopropanol precipitation, the plasmid was treated with RNase A for 60 minutes, then purified using phenol:chloroform:isoamyl alcohol. The purified plasmid was ethanol precipitated, then desalted and concentrated using the QiaQuick PCR purification kit (Qiagen). Three μg of the 5' plasmid and six μg of the 3' plasmid were digested for two hours at 37°C with *NgoMIV* and *XbaI*, and then plasmids were ligated by incubating with T4 DNA ligase at 4°C overnight. The ligase was inactivated at 70°C for ten minutes and then linearized with *XbaI* for two hours at 37°C. Phenol:chloroform extraction was utilized to purify the linearized plasmid, and the DNA was precipitated at -20°C overnight using ethanol and 3M pH 5.2 NaOAc. After drying the purified DNA, *in vitro* transcription was completed using the Ampliscribe T7 High Yield Transcription Kit (Lucigen). After approximately three hours, the transcription reaction was added to 3.4×10^6 Vero cells in 500 μL PBS and electroporated with two pulses at 1.5 kV, 25 μF , ∞ ohms using a Gene Pulser electroporator (Bio-Rad). Cells were grown in MEM media (prepared as described in section 2.1) at 37°C with 5% CO₂ until cytopathic effect (CPE) became apparent. Viruses were rescued in Vero cells between 3-5 days post transfection and stocks were stored at -80°C. Viruses were passaged once in Vero cells to generate the stocks utilized for *in vitro* and *in vivo* experiments described in this dissertation unless otherwise specified.

2.3 VIRUS PASSAGING

Viruses were passaged in Vero cells by washing cells with PBS and then adding virus at a multiplicity of infection (moi) of approximately 0.1. Infected flasks were incubated for 30 minutes at room temperature. After virus adsorption, MEM media (as described in section 2.1) with 2%

FBS was added (hereafter referred to as MEM maintenance media). Flasks were incubated at 37°C with 5% CO₂ until CPE was apparent, at which time cell supernatant was isolated. Since CPE was utilized to determine the time of harvest and different viruses caused CPE at different times, the time to harvest varied between 2-4 dpi. Cell debris were pelleted by centrifugation at 2000 RPM for 5 minutes, and the supernatants were aliquoted and stored at -80°C.

2.4 VIRUS TITRATION

Infectivity titers were measured using plaque titration in 6-well cell culture dishes that were 90% confluent with Vero cells. Cells were washed with phosphate-buffered saline (PBS) and then ten-fold serial dilutions (10^{-1} - 10^{-6}) of each virus were incubated on the cell monolayers for 30 minutes at room temperature (r.t.) with rocking every 5 minutes. Following incubation, cells were overlaid with 4 mL of MEM maintenance media containing 1% agarose. Plates were incubated at 37°C for two days, and then an additional 2 mL of overlay containing 2% neutral red (Sigma) was added to each well. Plates were monitored for two days (3 and 4 days post infection [dpi]) as plaques formed, and infectivity titers were calculated based upon the reciprocal dilution of plaque-forming unit (PFU) containing wells. Plaque size was defined by the phenotype on 3 and 4 dpi, where small plaques were ≤ 2 mm, medium plaques were >2 - <4 mm, and large plaques were ≥ 4 mm. For several viruses described in Chapter 6, overlays were completed 4 dpi and plates were read 5 dpi in order to allow plaque size to grow larger.

Several viruses were also titrated using focus-forming assays in 6-well cell culture dishes that were 90% confluent with Vero cells. Cells were washed with PBS and then ten-fold serial dilutions (10^{-1} - 10^{-6}) of each virus were incubated on the cell monolayers for 30 minutes with rocking every 5 minutes. Following incubation, cells were overlaid with 4 mL of MEM

maintenance media containing 0.8% carboxymethylcellulose (CMC). Three dpi, the CMC overlay was removed and cells were fixed with 1:1 acetone:methanol solution at -20°C overnight. Fixative was removed and cells were dried prior to adding 2 mL PBS with 1% FBS blocking buffer for 30 minutes. The blocking buffer was removed, and each well was incubated for one hour with 300 uL of WNV mouse immune ascites fluid (MIAF) diluted 1:5000 in blocking buffer. Cells were washed twice with PBS prior to incubating for one hour with 300 uL of goat anti-mouse-HRP antibody diluted 1:1000 in blocking buffer. Cells were again washed twice with PBS prior to incubating for one hour with neutravidin-HRP diluted 1:1000 in blocking buffer. After washing the cells twice more with PBS, foci were developed using 3,3'-diaminobenzidine staining (Pierce Cat. No. 34002) by incubating wells with 300 uL of stain for approximately 5 minutes. After development, plates were thoroughly washed with water prior to counting focus-forming units (FFU), and infectivity titers were calculated based upon the reciprocal dilution of focus-containing wells.

2.5 TEMPERATURE SENSITIVITY ASSAYS

Infectivity titers of viruses were determined in duplicate with plaque assays and/or focus assays (as described in section 2.4) at both 37°C and 41°C.

2.6 MULTIPLICATION KINETICS

Duplicate flasks of Vero cells and A549 cells were grown to approximately 80-90% confluence, washed with PBS, and infected with a moi of 0.1. After incubating the virus with the cells for 30 minutes at room temperature, cells were washed twice with PBS before adding MEM

maintenance media and incubating at 37°C with 5% CO₂ for four days. At 0, 24, 36, 48, 72, and 84/96 hours post infection (hpi), two aliquots were collected from each flask, centrifuged at 2,000 RPM for 5 minutes, and supernatants were stored at -80°C until titration for infectivity using plaque assays as described above.

2.7 CYTOKINE QUANTIFICATION

A549 cells grown in 6-well plates were infected with a moi of 0.1 of each mutant or PBS, which was used as a mock infection. At 36 hpi, supernatants were collected from each well as described for multiplication kinetics experiments above. Samples of each supernatant were gamma irradiated using 5 megarads to remove infectivity, and cytokines were then measured using the Bio-Plex Pro Human Cytokine 27-Plex Assay (Bio-Rad) and a Bio-Plex custom assay for human IFN- α 2 and IFN- β . Bio-Plex assays were performed according to the manufacturer's guidelines. Cytokine levels of NY99ic were compared to each mutant and to mock-infected cells by using a Kruskal-Wallis test with Dunn's multiple comparisons.

2.8 MOUSE NEUROINVASION STUDIES

Groups of 4 week-old female Swiss Webster outbred mice (Taconic Farms, Germantown, NY) were utilized to evaluate attenuation of neuroinvasion. Mice were inoculated by the intraperitoneal (i.p.) route with an inoculum of 500 PFU, and mice that survived through 35 days post-infection (dpi) were challenged with a 10,000 PFU i.p. dose of NY99ic. An additional group of mice was also inoculated i.p. with undiluted virus if the mutant was attenuated using the 500 PFU inoculum. Virus inocula were back-titrated to ensure that the appropriate dose was tested.

All animal experiments complied with the National Institutes of Health guide for the care and use of laboratory animals and were approved by the Institutional Animal Care and Use Committee of the University of Texas Medical Branch. Specifically, mice were humanely euthanized if they exhibited any of the following clinical signs of fatal WNND: >20% weight loss, hind limb paralysis, paralysis of all four legs, no movement when gently stimulated, or unable to reach food/water.

2.9 ISOLATION OF VIRUS FROM MOUSE BRAIN

For some mutants, brains were harvested from mice that succumbed to the 500 PFU inoculum. The brains were frozen at -80°C until homogenization. Approximately half of each brain was homogenized with 30 cycles/second for two minutes in 500 uL of MEM with 2% FBS using the Qiagen TissueLyser II. Homogenates were immediately placed on ice prior to centrifugation at 4°C at a speed of 10,000 RPM for 10 minutes. The supernatants were collected and immediately titrated using plaque assays prior to storage at -80°C.

2.10 PLAQUE REDUCTION NEUTRALIZATION TESTS (PRNT)

For several groups of mice, whole blood was collected 35 dpi and centrifuged at 2,000 RPM for 15 minutes to separate serum, which was aliquoted and stored at -80°C. Prior to analysis, serum samples were incubated at 56°C for 30 minutes to inactivate complement. Serum was then diluted using two-fold serial dilutions and incubated with a known quantity of NY99ic for 30 minutes at 37°C (final serum dilutions were 1:20-1:10,240). Following incubation, serum-virus mixtures were added to 6-well plates of Vero cells and incubated for 30 minutes at room

temperature. Plates were overlaid with agarose overlays and monitored for plaque production as described in section 2.4. The PRNT₅₀ titer represents the serum dilution for which the number of NY99ic PFU was reduced by 50% compared to a virus control well.

2.11 RNA EXTRACTION

RNA was extracted from Vero cell culture supernatant or from mouse brain homogenate using the QiaAmp Viral RNA Kit (Qiagen) according to the manufacturer's instructions. RNA was stored at -80°C.

2.12 SAMPLE PREPARATION FOR SANGER SEQUENCING

RNA from cell culture supernatant or mouse brain homogenate was amplified using RT-PCR with the Titan One Tube RT-PCR System (Roche Cat. No. 11855476001) according to the manufacturer's protocol. Primers used were specific to the viral gene of interest, and PCR products were purified using the QiaQuick PCR Purification Kit (Qiagen) prior to Sanger sequencing.

2.13 SEQUENCE ALIGNMENTS

Nucleotide and protein sequences of interest were downloaded in fasta format from GenBank and aligned using Clustal Omega online alignment program.

2.14 NEXT-GENERATION SEQUENCING (NGS) ANALYSIS

RNA extractions were sequenced as paired-end reads on the Illumina NextSeq 550 platform, and Trimmomatic (Bolger et al., 2014) was utilized to remove adapters and any sequences with a quality score below 30. The trimmed reads were aligned to a NY99ic reference sequence using Bowtie2 with the very sensitive local parameter. All reads were sorted based on genome position and coordinate position using SAMtools v. 1.3, and PCR duplicates were marked and removed using Picard Tools v. 1.119 (Broad Institute) with the optical duplicate pixel distance set to 0. Depth of coverage was determined using SAMtools. LoFreq software was utilized to measure single nucleotide variants in the viral RNA populations, and variants that had a significant strand bias ($p < 0.001$ with chi-square test or Fishers exact test) were not included in the analysis (Wilm et al., 2012). To measure the absolute diversity at each nucleotide position, Shannon entropy was calculated (Collins et al., 2018; Nishijima et al., 2012) using the formula

$$S_n = - \frac{\sum_{i=1}^n f_i(\ln f_i)}{N}$$

where n is the number of possible nucleotides identified, f_i is the observed frequency of a variant, and N is the total number of clones analyzed. Mean genomic entropy for mutants was compared using a Mann Whitney test.

2.15 FLUORESCENCE MICROSCOPY

Vero cells were infected with a moi of 0.1 of NY99ic, mutant WNV, or PBS as a mock infection. After 24 or 48 hpi, cells were seeded onto Teflon-coated microscope slides (Polysciences Cat. No. 18357-1). Cells were placed in the 37°C incubator for approximately five hours to adhere and then they were fixed with a 1:1 acetone:methanol solution. Slides were stored

at -20°C until immunostaining. Prior to staining, slides were incubated in 5% normal goat serum/3% bovine serum albumin blocking buffer for 1 hour at r.t.. Slides were washed twice with tris-buffered saline (TBS) then incubated with primary antibody for two hours at r.t. DENV NS4B monoclonal antibody 44-4-7 (kindly provided by Dr. Pei-Yong Shi, UTMB) and a WNV NS1 polyclonal antibody (Genetex Cat. No. 132053) were diluted 1:500 to generate working stocks. Slides were washed twice with TBS prior to incubation with secondary antibodies (Invitrogen Cat. No. A-11001 and A-11011) for 1 hour at r.t. After washing three times with TBS, slides were incubated with 7 µg/mL DAPI for 5 minutes, and then washed again four times with TBS. Slides were mounted with Vectashield (Vector Laboratories Cat. No. H-1000) and stored at 4°C overnight. Slides were imaged with a Zeiss LSM 880 confocal microscope using a 1.4 numerical aperture 63x oil immersion lens. Using ImageJ software, background fluorescence was subtracted uniformly from each image and mean fluorescence intensities and Pearson's correlation coefficients were calculated by drawing regions of interest around infected cells.

2.16 MOLECULAR RENDERING

Pymol was utilized to model the WNV E protein (PDB 2hg0), the NS5 methyltransferase domain of WNV (PDB 2OY0) and DENV-2 (PDB 2P3Q), as well as the WNV NS1 protein (PDB 4o6d).

2.17 STATISTICAL ANALYSIS

ANOVA, Kruskal-Wallis tests, Mann Whitney tests, measurements of standard deviation, and survival analyses were each performed using GraphPad Prism version 8.0. Standard error of the mean was calculated in Microsoft Excel.

Table 2.1: Primers utilized for WNV NY99ic site-directed mutagenesis

Mutant	Primer 1	Primer 2
E-E138K	catggacaaaaatggccacctgtacttgatattctctttcaag	cttgaaagagaatatcaagtacaaggtggccattttgtccatg
NS5-K61A	gaccagccatctcagtgctgctgtgccctagagac	gtctctaggggcacagcagcactgagatggctggtc
NS5-E218A	actcacccaatacatcgctgctggaattccg	cggaattccacgcacgcgatgtattgggtgagt
NS4B-P38G	gaccaggctgtgccccctcaagtccaaaag	cttttgacttgaggggggcaacagcctggtc
NS4B-P54A	acaacagcggtcctcactgccctgctaaagcatttgatc	gatcaaatgctttagcagggcagtgaggaccgctgttgt
NS4B-P54G	tgctttagcagtcagtgaggaccgctgtgtgcaca	tgtgacaacagcggtcctcactggactgctaaagca
NS4B-L56A	gacgtgatcaaatgctttgccagtgagtgaggaccgc	gcggtcctcactccactggcaaagcatttgatcacgtc
NS4B-C102S	cctgctagcagccggatcctggggacaagtcaccc	gggtgacttgccccaggatccggctgctagcagg
NS4B-W103Y	gctagcagccggatgctatggacaagtcaccctc	gagggtgacttgccatagcatccggctgctagc

Chapter 3 - Mutation of the Japanese encephalitis virus SA14-14-2 vaccine-specific envelope residue E138K

3.1 ABSTRACT

Although there are no licensed human vaccines for WNV, multiple vaccines against JEV have been approved for use in humans, including the live attenuated vaccine SA14-14-2. Investigations into determinants of attenuation of JE SA14-14-2 demonstrated that envelope (E) protein mutation E138K was crucial to the attenuation of mouse virulence. Since WNV is closely related to JEV, in this chapter it was investigated whether or not the E-E138K mutation would be beneficial to be included in a candidate live attenuated WNV vaccine. Rather than conferring a mouse attenuated phenotype, the WNV E-E138K mutant reverted and retained a wild-type mouse virulence phenotype. Next-generation sequencing analysis demonstrated that, although the consensus sequence of the mutant had the E-E138K mutation, there was increased variation in the E protein, including a single nucleotide variant (SNV) revertant to the wild-type glutamic acid residue. Modeling of the E protein and analysis of SNVs showed that reversion was likely due to inability of critical E protein residues to be compatible electrostatically. Therefore, this mutation may not be reliable for inclusion in candidate live attenuated vaccines in related flaviviruses, such as WNV, and care must be taken in translation of attenuating mutations from one virus to another virus, even if they are closely related.

3.2 INTRODUCTION

While there are many mosquito-borne flaviviruses of public health significance including DENV, YFV, and ZIKV viruses transmitted by *Aedes aegypti*, WNV clusters serologically and phylogenetically with JEV (Petersen et al., 2013). WNV and JEV are both neurotropic flaviviruses that can cause potentially fatal disease in humans and are transmitted by *Culex spp* mosquitoes. The most widely used JEV vaccine utilizes the live, attenuated strain, SA14-14-2, and multiple groups have investigated the genetic determinants of attenuation of SA14-14-2. While there are vaccine-associated mutations spanning both the structural and ns protein genes of the virus, six mutations in the envelope (E) protein (L107F, E138K, I176V, T177A, Q264H, K279M) were found to be indispensable to the attenuated phenotype (Gromowski et al., 2015; Yang et al., 2014).

Of the SA14-14-2 vaccine-specific E protein mutations, E138K stands out in the literature for its robust contribution to the attenuation of the mouse neuroinvasive and neurovirulent phenotypes of JEV. Substitution of E138K in a wild-type JEV IC strongly reduced the mouse neuroinvasive and neurovirulent phenotypes (Zhao et al., 2005). A single site reversion of K138E in a JE SA14-14-2 IC most profoundly increased neurovirulence compared to reversion of other vaccine-specific E protein residues (Yang et al., 2017). Genomic sequencing of historical vaccine derivatives also supports that E138K is important for vaccine attenuation, as all attenuated derivatives of SA14-14-2 harbor this substitution (Ni et al., 1994). In sum, E-E138K seems to be critical for the attenuated phenotype of JE SA14-14-2. A sequence alignment of the E genes of wild-type strains of JEV and WNV showed that the glutamic acid residue at 138 is conserved between

JEV and WNV strains (**Fig. 3.1**). The E-E138K mutation has been investigated in cell culture adapted WNV, an IC based on a lineage 2 WNV isolate, and a chimeric WNV/YFV 17D virus, and the mutation was found to increase attenuation to different degrees in each virus backbone (Arroyo et al., 2004; Lee et al., 2004; Yamshchikov et al., 2016, 2017). Since E-E138K had not previously been studied by rational mutation of the virulent lineage 1 NY99 infectious clone (NY99ic), the phenotype of this mutant was investigated in detail. It was hypothesized that the E-E138K mutation in WNV NY99ic would attenuate mouse neuroinvasion and neurovirulence and be beneficial for inclusion in a candidate live attenuated WNV vaccine; however, this was not found to be correct. Rather, the virulent mouse phenotype of WNV NY99ic was retained. Analysis of E protein structural modeling and single nucleotide variants provided a plausible explanation for the reversion to wild-type phenotype.

3.3 RESULTS

3.3.1 Generation of E-E138K mutant and consensus sequencing

The WNV E-E138K mutant was recovered from transfected Vero cells with the engineered E-E138K mutation plus a single synonymous C1077U nucleotide mutation from NY99ic, but no additional mutations were present in the consensus sequence of the genome. The virus had an infectivity titer of $8.5 \log_{10}$ PFU/mL.

3.3.2 Mouse virulence

The neuroinvasive phenotype of the WNV E-E138K mutant was compared to NY99ic in groups of five NIH Swiss Webster outbred mice inoculated by the intraperitoneal (i.p.) route. All mice inoculated with 500 PFU of NY99ic had a lethal infection and succumbed between 8-12 days post infection (dpi) (**Table 3.1**). Surprisingly, the 500 PFU inoculum of the E-E138K mutant was also completely lethal and all mice died between 7-11 dpi (**Table 3.1**). The experiment was repeated and the results were confirmed (10/10 mice succumbed in total). A further five mice inoculated with a high dose of undiluted virus (82 million PFU) of the E-E138K mutant died more quickly (5-6 dpi) than the mice inoculated with 500 PFU ($p = 0.009$) (**Table 3.1**). In conclusion, the E-E138K mutation in WNV did not confer significant attenuation of mouse neuroinvasion, but instead it retained the virulent phenotype of NY99ic.

Virus was harvested from the brains of five mice that succumbed to the 500 PFU inoculum of the E-E138K mutant on either 8 or 10 dpi. One mouse that succumbed on 8 dpi had a mean virus titer in the brain of $8.7 \log_{10}$ PFU/g, and four mice that succumbed on 10 dpi had mean viral titers of 4.9, 5.6, 7.1, and $8.7 \log_{10}$ PFU/g, respectively. Sequencing of the E gene of viral RNA from brain homogenates demonstrated that the E-E138K mutation reverted to the wild-type glutamic acid residue in all five mice.

3.3.3 Temperature sensitivity in Vero cells

The mutant multiplied to a high infectivity titer comparable to that of NY99ic ($> 8 \log_{10}$ PFU/mL), and neither NY99ic nor the E-E138K mutant had a temperature sensitive (TS) phenotype at 41°C (**Table 3.2**).

3.3.4 Multiplication kinetics in Vero cells and A549 cells

Multiplication kinetics in Vero and A549 cells were compared to investigate differences in both interferon-I (IFN-I) deficient and IFN-I competent cell lines, respectively. In Vero cells, the E-E138K mutant multiplied to titers approximately 10-fold lower than NY99ic between 24-96 hpi; however, both viruses multiplied to high titers (**Fig. 3.2a**). In A549 cells, the two viruses had nearly identical multiplication kinetics, suggesting the E-E138K mutant does not have increased sensitivity to IFN-I at the time points measured (**Fig. 3.2b**).

3.3.5 A549 cell cytokine response

Supernatants from infected A549 cells isolated at 36 hpi were used to measure a total of 29 cytokines/chemokines using a BioPlex Pro 27-plex human cytokine assay and a custom BioPlex 2-plex IFN- α and IFN- β assay. Three cytokines in the multiplex were undetectable in all samples (IL-10, IL-15, PDGF-bb), which could be a limitation of cytokine signaling in A549 cells or of the specific time point investigated. Twenty-four cytokines, chemokines, and growth factors were not differentially induced between the two

viruses, and the only cytokines with a statistical difference were IL-5 and VEGF (**Fig. 3.3**). For IL-5, the E-E138K mutant caused approximately 7-fold less production than NY99ic ($p=0.02$), and for VEGF the E-E138K mutant caused approximately 1.5-fold increased production ($p=0.02$) (**Fig. 3.3**).

3.3.6 Deep sequencing analysis of virus quasispecies

To further investigate the stability of the WNV E-E138K mutant, the quasispecies diversity of the unpassaged (P0) cell culture stocks (i.e. the virus obtained post transfection of Vero cells) of NY99ic and the E-E138K mutant were compared using next-generation sequencing (NGS). Following deep sequencing of the entire genome, both NY99ic and the E-E138K mutant had a high depth of coverage averaging 6,868 and 6,983 reads, respectively. Since the coverage was comparable between the two viruses, SNVs were measured without down sampling to a lower average coverage. Overall, 154 SNVs were detected in NY99ic, and they all had a frequency $<1\%$ (**Fig. 3.4**). Ninety-eight SNVs were detected in the E-E138K mutant quasispecies, and although there were fewer SNVs than in NY99ic, some SNVs in the E-E138K mutant population were present at a higher frequency (0.1% - 14.2%) (**Fig. 3.4**). To investigate these differences in more detail, continued analysis was only undertaken on SNVs with a frequency of 1% or higher. This filtering reduced the number of SNVs in NY99ic to zero, while E-E138K had 30 subpopulations primarily located in the E protein gene (**Fig. 3.5, Table 3.3**). The most prominent SNV in the E-E138K mutant population had a frequency of 14.2% and encoded a reversion of E-K138E (**Fig. 3.5, Table 3.3**). There was no evidence of SNVs at E-138

in NY99ic. As an alternative measurement of diversity, Shannon entropy was calculated for NY99ic and the E-E138K mutant. The E-E138K mutant had more nucleotide diversity than NY99ic, and this was most evident in the E protein gene ($p < 0.0001$) (**Fig. 3.6**). After a single passage (P1) and five passages (P5) in Vero cells, the E-E138K mutation was retained in the consensus sequence, however, reversion was evident in the SNVs at 48% and 37% frequency, respectively (**Fig. 3.7**).

3.4 DISCUSSION

Based on robust literature describing the important role of the E-E138K mutation for the attenuation of the JEV live, attenuated vaccine SA14-14-2, it was hypothesized that the homologous mutation in WNV would confer an attenuated phenotype. The genome of the rescued WNV E-E138K mutant had one additional mutation at nucleotide 1077, but since this mutation did not encode an amino acid substitution, it was hypothesized that it would not significantly modify the virulence phenotype. *In vitro* characterization of the WNV E-E138K mutant suggested that the virus had a similar phenotype to the parental NY99ic. Specifically, TS assays, multiplication kinetics, and 36 hpi cytokine quantification did not identify strongly distinct phenotypic differences between the E-E138K mutant and the parental NY99ic. Studies describing the E-E138K mutation in JEV have reported that the mutant can multiply well in cell culture, but it results in 10-1000 fold reduction in titer in Vero cells compared to parental strains (Wang et al., 2017; Yamshchikov et al., 2016). Similarly, using the WNV lineage 1 NY99ic backbone, the E-E138K mutant had infectivity titers that were approximately 10-fold lower than the

parental viruses at each time point measured in Vero cells.

To test if the E-E138K mutation would confer attenuation in WNV, outbred Swiss Webster mice were utilized as a model as they are highly susceptible to WNV and the i.p. LD₅₀ for the parental NY99ic is between 0.1-10 PFU (Whiteman et al., 2010, 2011; Wicker et al., 2006, 2012). The E-E138K mutation was shown to attenuate JEV for both mouse neuroinvasion and neurovirulence in previous studies. For example, the E-E138K mutation in a JEVic was attenuated > 1000-fold from the parental virus for both neuroinvasion and neurovirulence in the BALB/c mouse model (Zhao et al., 2005). Furthermore, two studies of different JEV strains harboring the E-E138K mutation reported that the mutation conferred complete attenuation of neuroinvasion in inbred immunocompetent mice inoculated with either 100,000 PFU or 50 million PFU, while the parental strains were completely lethal (Liang et al., 2009; Wang et al., 2017). While there is robust literature studying the mouse attenuation phenotype of the E-E138K mutation in JEV, fewer studies have been undertaken with WNV. Serial passage in human adrenal gland epithelial SW13 cells of WNV New York 1999-flamingo 382-99 strain resulted in the E-E138K mutation and this was mildly attenuated 50-fold by the i.c. route and 200-fold by the i.p. route, however, it is not known if this virus had compensatory mutations in the ns genes that contributed to the virulence phenotype (Lee et al., 2004). Similarly, the E-E138K mutation decreased neurovirulence of a chimeric WNV vaccine candidate, Chimerivax-WNV, that combines the structural genes of WNV NY99 with the ns genes of the YFV 17D vaccine (Arroyo et al., 2004). An infectious DNA (iDNA) vaccine platform based on the lineage 2 WNV isolate W956 with an engineered E-E138K mutation was not lethal in outbred mice

when administered by intramuscular or intradermal routes with either 1 µg or 100 ng of iDNA, but the mutant iDNA retained virulence when inoculated by the i.c. route (Yamshchikov et al., 2016). Based on the potential for E-E138K to confer mouse attenuation in JEV and WNV, it was anticipated that the WNV NY99ic E-E138K mutant would have at least partial attenuation of neuroinvasion, therefore, both a relatively low dose (500 PFU) and a high dose (82 million PFU) were tested by the i.p. route. Surprisingly, all mice succumbed to infection by the i.p. route, therefore, virus was not administered by the i.c. route. It is possible that the WNV E-E138K mutant is very mildly attenuated as demonstrated for SW13 cell passaged WNV (Lee et al., 2004), but low level attenuation would not be ideal for live, attenuated vaccine development; thus, lower doses were not evaluated.

One explanation for the virulence of the WNV E-E138K mutant is that the mutation is not stable. Multiple studies have reported that E-E138K is a stable mutation when JEV is passaged in cell culture (Liu et al., 2018; Ni et al., 1994; Yang et al., 2014), however, in JEV and in the WNV iDNA platform, the mutation was capable of reversion after passage in mouse brain (Yamshchikov et al., 2017; Yang et al., 2014; Zhao et al., 2005). Previous studies utilized Sanger sequencing that provides only a consensus sequence, while NGS allows for more detailed analysis of nucleotide diversity. Measurement of nucleotide diversity with Shannon entropy and measurement of significant SNVs revealed that the WNV E-E138K mutant had a high frequency of mutations concentrated in the region of the E protein gene. Although the E-E138K mutation was stable in the consensus sequence, there was evidence of a relatively large (14.2%) SNV encoding reversion of K138E in the

unpassaged virus. Due to the similarity between glutamic acid (GAA/GAG) and lysine (AAA/AAG), only the first nucleotide in the codon can be changed to induce the desired mutation at E-138. Thus, mutation of the first nucleotide (and not the third variable base) suggests that the virus is undergoing selection for the revertant subpopulation. The E-E138K mutation is associated with cell culture adaptation of glycosaminoglycan (GAG) binding in both JEV and WNV (Lee et al., 2004; Wang et al., 2017; Zhao et al., 2005), therefore, it is not surprising that reversion of E-K138E was not evident in the consensus sequences of Vero-passaged P1 and P5 stocks of the mutant. However, the evidence of reversion in the SNVs of the unpassaged P0 stock as well as the P1 and P5 stocks of the WNV E-E138K mutant demonstrates that the virus is capable of rapidly selecting for the parental amino acid. Additionally, the P1 virus was used for the mouse studies and was found to revert *in vivo* regardless of the absence of a consensus sequence change.

Although there has been evidence of E-K138E reversion in JEV, it is a relatively infrequent outcome as the mutation typically remains stable and induces attenuation of JEV mouse neuroinvasion and neurovirulence (Yang et al., 2014; Zhao et al., 2005). Insights into the location of E-E138K on the structure of the WNV E protein compared to that of the JEV E protein may help to explain why the mutation is poorly tolerated in WNV and does not attenuate the virus. Structural studies of JEV demonstrated that when the E monomers form a dimer on the viral surface, the dimer has unique “holes” between monomers that are specific to the encephalitic flaviviruses, while hemorrhagic flaviviruses like DENV have more interactions between monomers and thus have less prominent holes (Wang et al., 2017). The study postulates that the E dimer hole is functionally important

for virus entry into the nervous system (Wang et al., 2017). E-138 is one of nine E protein electrostatic residues responsible for this unique hole along with D28, R44, K136, K166, E243, E244, E273, and K279 (Wang et al., 2017). The encephalitic hole in JEV is the result of five amino acid motifs responsible for the positioning of the nine electrostatic amino acids listed above, and JEV and WNV differ at 19 of 77 amino acids within the five motifs (Wang et al., 2017) (**Fig. 3.8**). Therefore, the position of E-E138 in WNV may not be identical to the position in JEV, ultimately allowing mutation of this electrostatic residue to be better tolerated in JEV than WNV. Interestingly, lineage 1 and 2 WNV have identical amino acids in the five motifs with the exception of motif 3 (**Fig. 3.8**). Motif 3 harbors electrostatic E residues 136, 138, and 166, and therefore the differences in attenuation between WNV lineage 1 and 2 could in part explain why the lineage 2 virus used in other studies can more stably harbor the E-E138K mutation (Yamshchikov et al., 2016, 2017). The NGS data showed that mutation of E-E138K in WNV not only caused reversion of K138E in a SNV, but five other SNVs are prevalent in structurally neighboring residues, including K136Q, R166T, R166S, K280E, and K280Q (K280 in WNV is homologous to K279 in JEV) (**Table 3.3, Fig. 3.9**). Thus, three of the nine electrostatic residues responsible for the hole in the JEV E protein have evidence of mutation when E-E138K is mutated in WNV. Investigation of E-E138K in the WNV iDNA vaccine platform found that loss of positive charge at E-166 by mutation of R166I or R166S stabilized the gain of positive charge resulting from the E-E138K mutation and thus prevented reversion to virulence at E-138 (Yamshchikov et al., 2017). Notably, each of the five SNVs that structurally neighbor E-138 are associated with a loss of positive charge by mutation of

either lysine or arginine, supporting the hypothesis that the virus is trying to compensate for the lysine at E-138. It is possible that fixation of an amino acid that is not positively charged at E-136, E-166, or E-280 would stabilize the E-E138K mutation and prevent reversion to virulence.

In summary, the E-E138K mutation does not confer attenuation in WNV even though it is strongly attenuating for mouse neuroinvasion and neurovirulence of JEV. In JEV, it has been demonstrated that E-E138K will infrequently revert if the virus is passaged in mouse brain, however, the mutation is stable when passaged in cell culture (Yang et al., 2014; Zhao et al., 2005). This chapter has found that E-E138K is not stable in WNV and begins to revert upon rescue of the transfected virus prior to passage. The E-E138K mutation was considered for the candidate chimeric WNV/YFV 17D vaccine, ChimeriVax-WN02. The first generation of this vaccine platform, ChimeriVax-WN01, retained low level neurovirulence in mice and was associated with several severe adverse events after its licensure for veterinary use (Arroyo et al., 2004; Brandler and Tangy, 2013). To improve the safety of ChimeriVax-WNV, it was proposed to include several JEV SA14-14-2 E protein mutations that are important for attenuation of mouse neurovirulence and presumably human virulence (Arroyo et al., 2004). Although E-E138K did decrease mouse neurovirulence of ChimeriVax-WNV, the mutations E-L107F, E-A316V, and E-K440R were ultimately selected for further development of ChimeriVax-WN02 as they caused more profound neurovirulence attenuation than E-E138K in outbred ICR mice (Arroyo et al., 2004). The data demonstrating that E-E138K mutation is not stable in WNV is consistent with this study that the residues E-107, E-316, and E-440 would be better targets

for mutagenesis of ChimeriVax-WN02 since these residues are not structurally neighboring E-138. Although E-E138K is an important determinant of attenuation for the live vaccine JE SA14-14-2, the equivalent mutation in WNV does not confer significant attenuation, but instead it increases variation of the viral E protein and would not be a safe mutation to include in a candidate WNV vaccine.

Table 3.1: The E-E138K mutant did not have an attenuated phenotype *in vivo*

Virus (Inoculum)	# Mice survived/total	Average Survival Time (days) \pm SD
NY99ic (500 PFU)	0/10	9.0 \pm 1.3
E138K (500 PFU)	0/10	9.4 \pm 1.3
E138K (8.2x10⁷ PFU)	0/5	**5.4 \pm 0.5

Groups of five 4 week-old Swiss Webster outbred mice were inoculated by the intraperitoneal (i.p.) route. Significance was tested using a Kruskal-Wallis test with Dunn's multiple comparisons to compare mutant survival time to NY99ic survival time. ** p = 0.009

Table 3.2: The E-E138K mutant does not have a temperature sensitive phenotype in Vero cells

	37°	41°	Delta	One-Way ANOVA
NY99ic	8.2	8.0	0.2	ns (p = 0.43)
E138K	8.5	8.4	0.1	ns (p = 0.97)

Infectious titers are listed as Log₁₀ PFU/mL. For NY99ic, five replicates were averaged at each temperature, and two replicates were averaged per temperature for the E-E138K mutant. Temperature sensitivity significance was measured using a one-way ANOVA with Bonferroni's correction.

Table 3.3: Summary of all single nucleotide variants $\geq 1\%$ of viral RNA populations of NY99ic and the E-E138K mutant in unpassaged (P0) virus stocks

	Nucleotide Position	Major Nucleotide	Minor Nucleotide	Viral Protein Position	Major Residue	Minor Residue	Frequency (%)
E138K	88	A	G	5' UTR	-	-	2.1
	767	A	U	prM-101	E	V	2.6
	939	A	G	prM-158	L	L	1.5
	1044	A	G	E-26	E	E	1.9
	1077	U	C	E-37	D	D	3.7
	1079	A	G	E-38	K	R	1.8
	1105	A	G	E-47	N	D	4.1
	1216	A	G	E-84	K	E	1.7
	1372	A	C	E-136	K	Q	3.0
	1378	A	G	E-138	K	E	14.2
	1380	G	A	E-138	K	K	6.2
	1463	G	C	E-166	R	T	1.9
	1464	A	U	E-166	R	S	1.7
	1501	A	G	E-179	K	E	4.8
	1701	A	C	E-245	P	P	1.8
	1795	A	G	E-277	N	D	1.3
	1804	A	G	E-280	K	E	1.9
	1804	A	C	E-280	K	Q	2.7
	1826	A	G	E-287	K	R	1.6
	1832	G	A	E-289	R	K	1.2
	1894	A	C	E-310	K	Q	1.9
	2066	C	U	E-367	A	V	2.6
	2229	A	G	E-421	L	L	1.2
	7395	A	C	NS4B-160	P	P	1.1
	7977	A	G	NS5-99	E	E	1.1
	8119	A	C	NS5-147	I	L	1.1
	8849	A	G	NS5-390	E	G	2.2
	9934	A	U	NS5-752	N	Y	1.6
	10888	U	A	3' UR	-	-	1.1
	10906	A	G	3' UTR	-	-	1.4

Amino acid residues highlighted in blue are non-synonymous substitutions.

Figure 3.1: Amino acid alignment of JEV and WNV lineages reveals that residue E138 is highly conserved

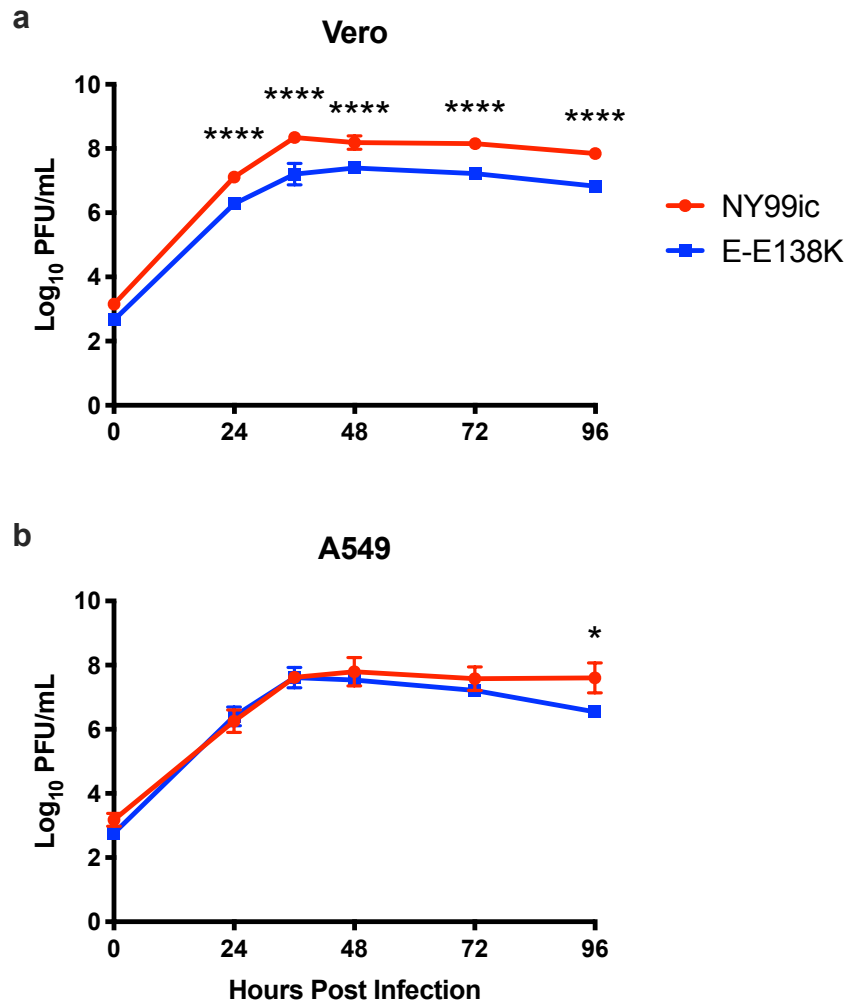
```

JE_LIN1      GRMIQPENIKYEVGIFVHGTTTSENHGNYSAQVGASQAAKFTVTPNAPSITLKLGDYGEV
JE_LIN2      GRTIQPENIKYEVGIFVHGTTTSENHGNYSAQVGASQAAKFTVTPNAPSITLKLGDYGEV
JE_LIN3      GRTIQPENIKYEVGIFVHGTTTSENHGNYSAQVGASQAAKFTVTPNAPSITLKLGDYGEV
JE_LIN4      GKTIQPENIKYEVGIFVHGTTTSENHGNYTAQIGASQAAKFTITPNAPSITLKLGDYGEV
JE_LIN5      GKIIQPENIKYEVGIFVHGTTTSENHGNYTAQIGASQAAKFTITPNAPSITLKLGDYGEV
WN_LIN1a     GRTILKENIKYEVAIFVHGPTTVESHGNYSTQVGATQAGRFSITPAAPSYTLKLGEYGEV
WN_LIN1b     GRTILKENIKYEVAIFVHGPTTVESHGNYFTQTGAAQAGRFSITPAAPSYTLKLGEYGEV
WN_LIN2      GWIIQKENIKYEVAIFVHGPTTVESHGK----IGATQAGRFSITPSAPSYTLKLGEYGEV
WN_LIN3      GWIIQKENIKYEVAIFVHGPTTVDSHGNYSTQMGATQAGRFTVSPSAPTYTMKLGEYGEV
WN_LIN4      GLTIQRENVKYEVAVSVHGPTTVDTHT--MSAQNAAVQAGRFSVSPAAPHTLTLGLDYGEV
WN_LIN5      GRTILKENIKYEVAIFVHGPTTVESHGDYSTQQGATQAGRFSITPAAPSYTLKLGEYGEV
WN_LIN7      GKIIQKENIKYEVSIFVHGPTTVESHGNYFTQRTATQAGTISVSPSAPSTLKLGDYGEV
WN_LIN8      GRTILKENIKYEVAIFVHGPTNVESHGNYSMQTGATQAGRFSVSPAAPSYTLKLGEYGEV
WN_LIN9      GLTIQRENVKYEVAAFVHGPTTVDTHTSNLSAQSAAVQAGRFSVSPAAPSHLTLGLDYGEV

```

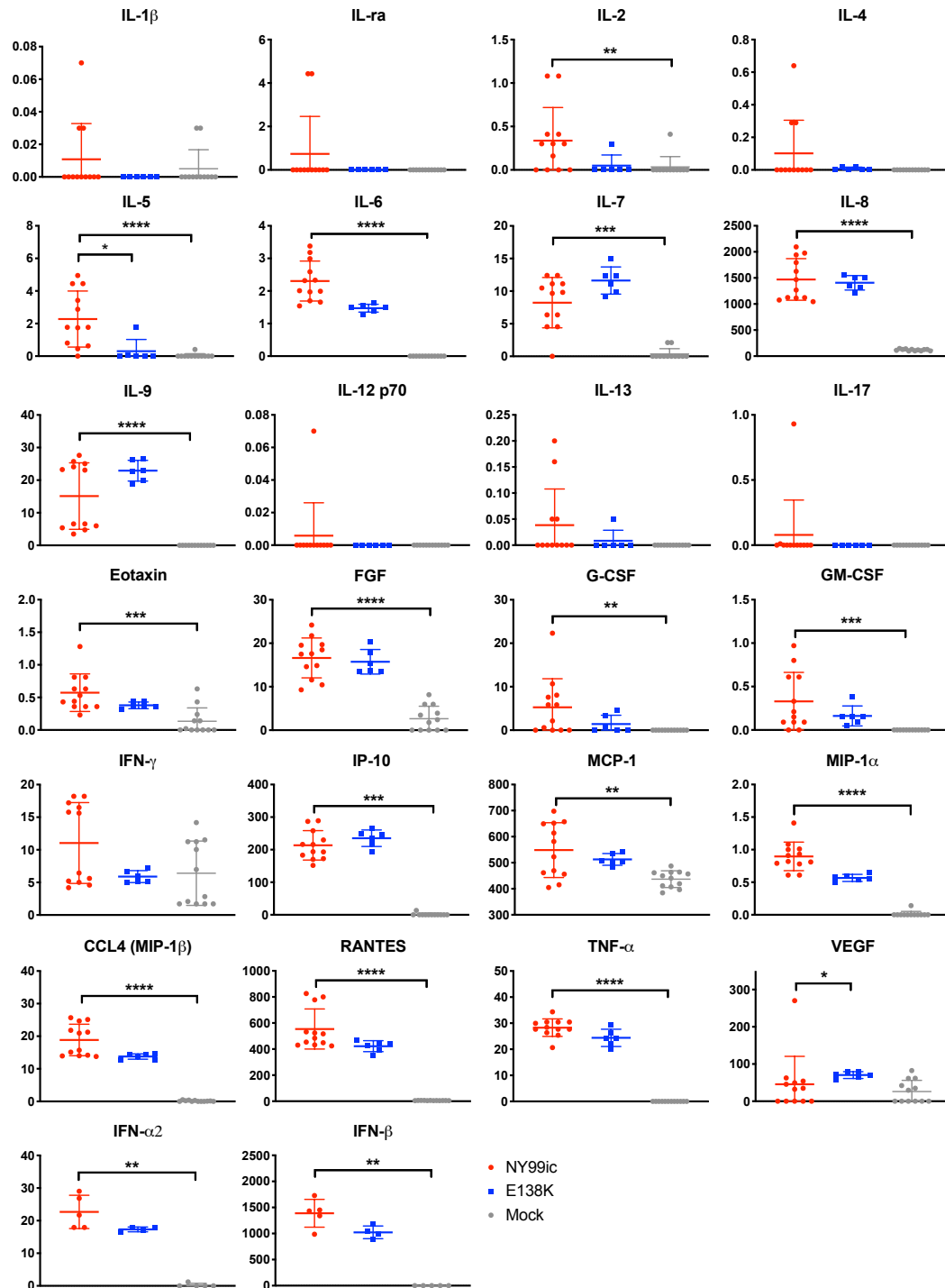
All JEV and WNV lineages are represented, except for putative WNV lineage 6, for which there is only a short gene fragment of the NS5 protein available (Acc. No. GU047875). Residue E-E138 is highlighted in yellow with **bold** text. The accession numbers are as follows: JE_LIN1: BAB20816.1, JE_LIN2: AAF73859.1, JE_LIN3: ANV81277.1, JE_LIN4: AAP39942.1, JE_LIN5: AEK75355.1, WN_LIN1a: AAF20092.2, WN_LIN1b: BAA00176.1, WN_LIN2: NP_776014.1, WN_LIN3: AAW81711.1, WN_LIN4: AAP22088.1, WN_LIN5: ADM88864.1, WN_LIN7: ABW76844.2, WN_LIN8: ATN45391.1, WN_LIN9: AII00962.1.

Figure 3.2: Multiplication kinetics of NY99ic and the E-E138K mutant are similar in Vero and A549 cells at a moi of 0.1



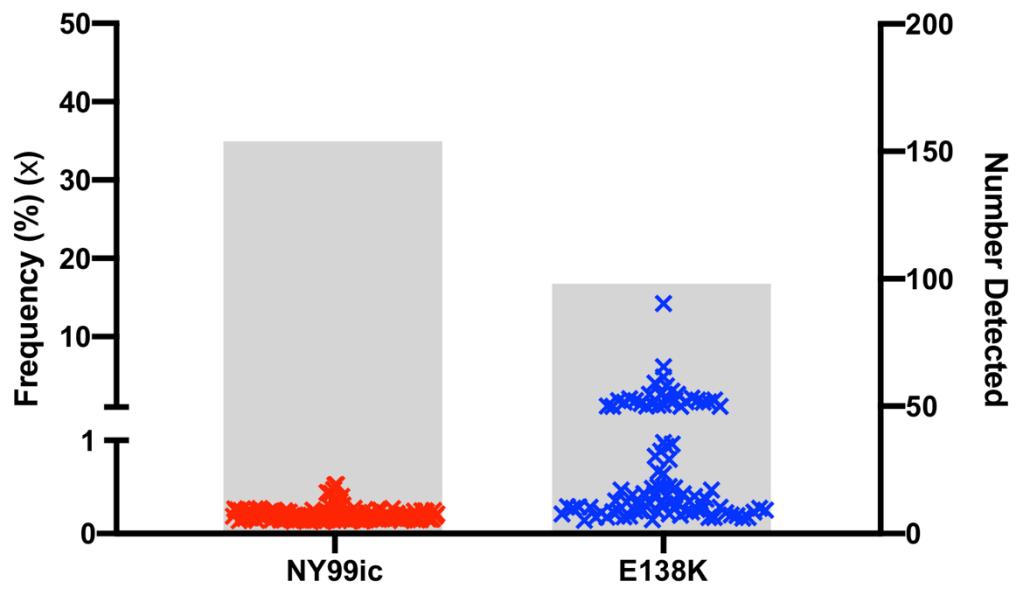
Error bars represent the standard deviation of two titrations of two biological replicates (four titrations in total). Significance was tested using an ANOVA with Bonferroni correction. * $p=0.02$, **** $p<0.0001$.

Figure 3.3: Extracellular cytokine responses are similar in E-E138K infected cells compared to NY99ic infected cells



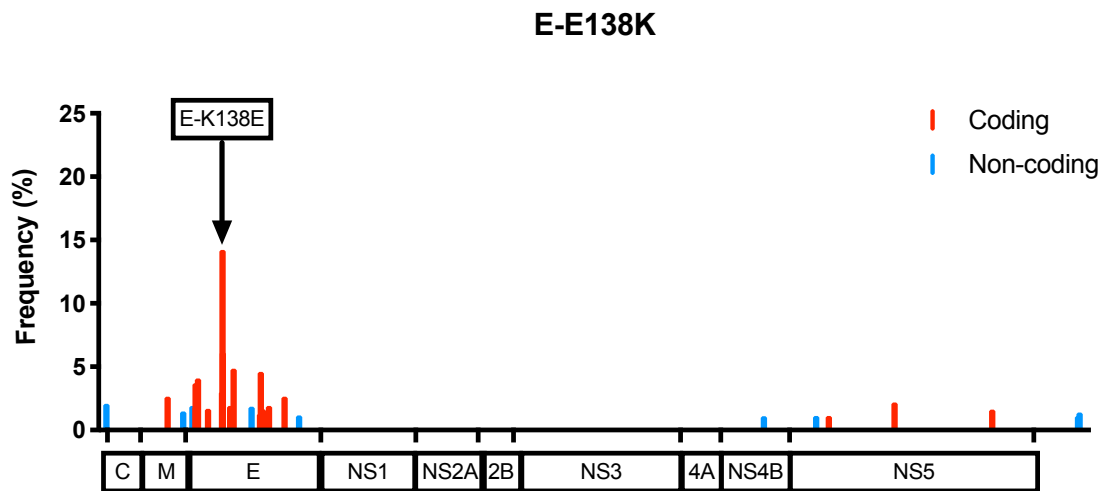
Cytokines were measured in pg/mL in A549 cell supernatant at 36 hpi. Error bars represent the standard deviation for twelve replicates (NY99ic) or six replicates (E-E138K). *p<0.05, **p<0.01, ***p<0.001, ****p<0.0001 in Kruskal-Wallis test with Dunn's multiple comparisons.

Figure 3.4: Single nucleotide variant profiles of the unpassaged (P0) virus stocks differ between NY99ic and the E-E138K mutant.



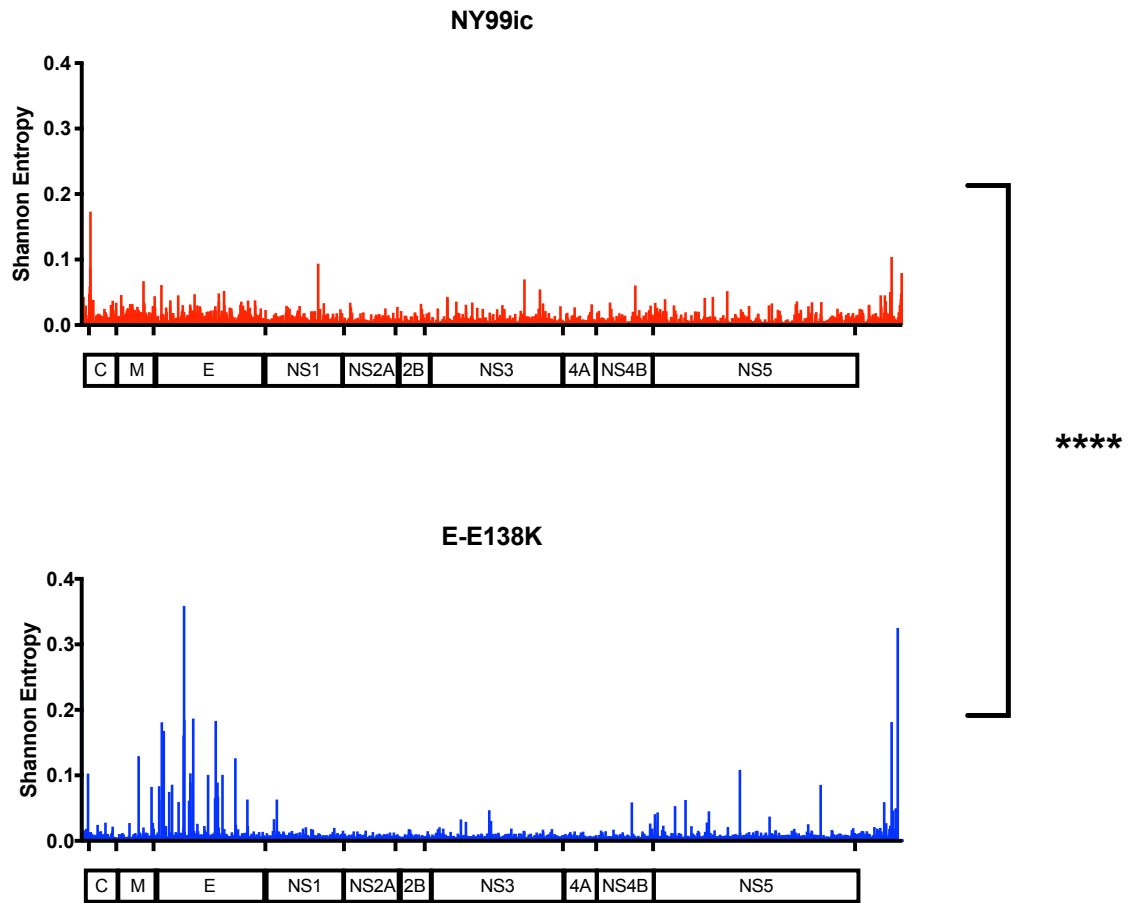
Each 'x' represents the frequency of a variant, and the grey bars display the total number of variants detected.

Figure 3.5: The E-E138K mutant had SNVs clustered in the E protein and one encoded reversion at residue 138



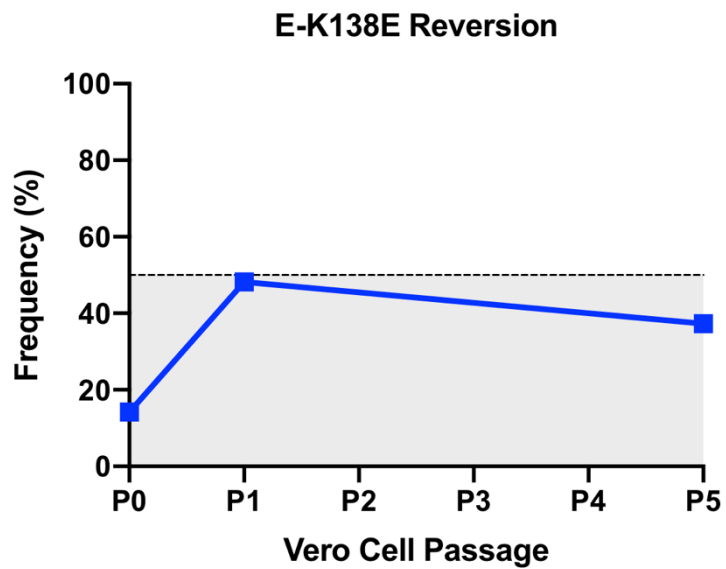
The SNVs $\geq 1\%$ frequency in the P0 stock of the E-E138K mutant are plotted at their corresponding positions in the genome.

Figure 3.6: The E-E138K mutant had higher Shannon entropy across the genome than NY99ic



Shannon entropy was compared in the P0 stocks of each virus. A Mann Whitney test was used to compare the entropy of the entire genome for NY99ic and the E-E138K mutant. **** $p < 0.0001$

Figure 3.7: Reversion of E-E138K increases in frequency after Vero cell passage, but does not yield a consensus sequence change



Vero cell P0, P1, and P5 stocks of the E-E138K mutant were sequenced with NGS for SNV analysis.

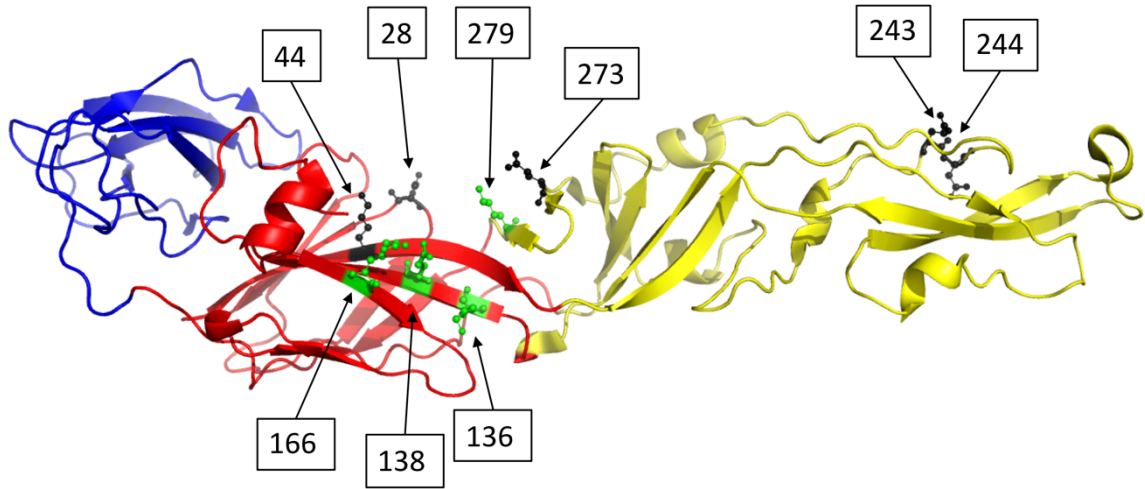
Figure 3.8: Alignment of WNV and JEV E protein structural motifs reveals amino acid differences between the viruses

	28	44	136	138	166
JEV	GDS	R MINIE	K YEVGIFVHGTTTSENHGNYS	AQVGASQA	A KFT
WNV1	GDS	K MMNME	K YEVAIFVHGPTTVESHGNYSTQVGATQAG	RFS	
WNV2	GDS	K MMNME	K YEVA-FVHGPTTVESHGK----	IGATQAG	RFS
		* * *	*	* * *	* * *
	M1	M2	M3		

	243	273	279
JEV	EF E EAHATKQS	V V EYSS-SV K LTSGHLKCRLKMDK	
WNV1	EF E EPHATKQS	P V EFSSNTV K LTSGHLKCRVKMEK	
WNV2	EF E EPHATKQS	P V EFSSNTV K LTSGHLKCRVKMEK	
	*	* * *	* *
	M4	M5	

Amino acid sequences of JEV strain SA14 (accession no. ANV81277.1), WNV lineage 1 (WNV1) strain NY99 (accession no. AAF20092.2), and WNV lineage 2 (WNV2) strain W956 (accession no. NP_041724.2) were aligned. The five motifs responsible for the hole between envelope protein dimers are denoted as M1-M5 (Wang et al., 2017). Amino acids in **bold** are the nine charged residues that directly cause the hole, and amino acids that are denoted with an asterisk are residues that are different between WNV1 (used in this study) and JEV.

Figure 3.9: Location in the WNV E protein monomer of residues associated with the electrostatic gap in the E protein dimer of neurotropic flavivirus



The WNV E protein monomer is modelled with domain I (DI) colored in red, DII in yellow, and DIII in blue. The nine electrostatic residues that cause a gap between E protein monomers after dimerization are indicated (Wang et al., 2017). Residues shown in green (136, 138, 166, and 279) were associated with SNVs in the E-E138K mutant described in this chapter. The residues shown in black (28, 44, 243, 244, and 273) had no evidence of mutation during NGS analysis of the E-E138K mutant.

Chapter 4 - Mutation of the highly conserved flavivirus NS5 methyltransferase catalytic tetrad

4.1 ABSTRACT

Several WNV genes have been targeted for mutagenesis in attempts to generate live attenuated vaccine candidates, including the non-structural protein NS5. Specifically, mutation of WNV NS5-K61A or NS5-E218A in the catalytic tetrad of the methyltransferase decreases enzyme activity of the NS5 protein and correspondingly attenuates the virus in mice. In this chapter, NS5-K61A, NS5-E218A, and a double mutant encoding both mutations (NS5-K61A/E218A) were compared both *in vitro* and *in vivo*. Each single mutant was strongly attenuated in highly susceptible outbred mice, whereas the double mutant unexpectedly was not attenuated. Sequencing analysis demonstrated that the double mutant was capable of reversion at both residues NS5-61 and NS5-218, whereas the genotypes of the single mutants were more stable. Overall, either NS5-K61A or NS5-E218A methyltransferase mutations could be potential mutations to include in a candidate live WNV vaccine; however, combining both NS5-K61A and NS5-E218A mutations in the catalytic tetrad of the methyltransferase was not tolerated.

4.2 INTRODUCTION

The NS5 protein is the largest NS protein and includes an N-terminal methyltransferase (MTase) and a C-terminal RNA-dependent-RNA-polymerase (Klema et

al., 2015). Previous studies of WNV, JEV, YFV, and DENV have reported that the flavivirus NS5 MTase has conserved function and sequentially catalyzes N-7 methylation followed by 2'OH methylation to generate a type 1 cap on the 5' end of the viral RNA (Daffis et al., 2011; Li et al., 2013; Zhou et al., 2007; Zust et al., 2013; Züst et al., 2017). Importantly, a K-D-K-E catalytic tetrad (NS5-K61-D146-K182-E218) is conserved in all flaviviruses, and therefore, data on one flavivirus should be applicable to others. The K-D-K-E tetrad (**Fig. 4.1**) catalyzes 2'O methylation, and mutation of any one of the four residues in the tetrad completely ablates 2'O methylation and strongly attenuates flaviviruses (Daffis et al., 2011; Li et al., 2013; Zhou et al., 2007; Zust et al., 2013; Züst et al., 2017). For example, an infectious clone based on WNV strain 3356 harboring single site substitutions of either NS5-K61A or NS5-K182A was not lethal in C3H mice inoculated subcutaneously (s.c.) with 10⁵ PFU (Zhou et al., 2007). Additionally, a WNV strain 3356 clone with a NS5-E218A mutation was not lethal in C57Bl/6 mice when 10⁵ PFU was inoculated by either s.c. or intracranial (i.c.) routes (Daffis et al., 2011). The strong degree of attenuation conferred by mutating the K-D-K-E tetrad provides a promising target for rational flavivirus vaccine design. One group has proposed to use MTase mutants as a tetravalent DENV vaccine candidate. Specifically, a combination of the four DENV serotypes with double mutations of K61A/E217A (or E216A depending on the DENV serotype) inoculated in AG129 mice by the i.p. route reduced viremia compared to wild-type and elicited virus-specific neutralizing antibodies and T-cell responses (Züst et al., 2017). Additionally, DENV-2 with an E217A mutation has strongly reduced vector competence in *Aedes aegypti* mosquitoes (Zust et al., 2013).

In sum, studies in DENV as well as WNV support the use of NS5 MTase mutants in vaccine design. To further characterize WNV MTase mutants in an alternative infectious clone backbone based on strain NY99 (**Table 4.1**) using a highly susceptible outbred mouse model, mutation of two single amino acid residues, NS5-K61A and NS5-E218A, as well as double mutation of both amino acids NS5-K61A/E218A was undertaken. While the single site mutants had an attenuated phenotype, surprisingly, the double mutant had a virulent phenotype.

4.3 RESULTS

4.3.1 Generation of NS5 methyltransferase mutants and consensus sequencing

Single site mutants NS5-K61A and NS5-E218A and the double mutant NS5-K61A/E218A were recovered with no compensatory mutations identified in the genomic consensus sequences, and each had a similar infectivity titer compared to NY99ic (**Table 4.2**).

4.3.2 Mouse virulence

Studies in highly susceptible NIH Swiss Webster outbred mice were undertaken to investigate the mouse neuroinvasive phenotype following i.p. inoculation of virus. NY99ic was strongly neuroinvasive and caused lethality in all mice between 8-12 days post infection (dpi) with an inoculum of 500 PFU, whereas, both NS5-K61A and NS5-E218A mutations were strongly attenuated for neuroinvasiveness, as all mice survived a relatively

low inoculum of 500 PFU as well as a high inoculum of 290,000 PFU and 380,000 PFU, respectively (**Table 4.3**). Although both single mutants were attenuated, the NS5-K61A/E218A double mutant was less attenuated. Three of ten mice survived from the 500 PFU inoculum of NS5-K61A/E218A, and three of five mice survived from a very high inoculum of >40,000,000 PFU (**Table 4.3**). Mice that survived 500 PFU of each mutant were also protected from a lethal 10,000 PFU NY99ic i.p. challenge, demonstrating induction of a protective immune response (**Table 4.3**). The mice that succumbed to infection with the double mutant exhibited clinical symptoms including paralysis, slow movement, and dehydration, whereas all mice that survived did not exhibit signs of WNND. Overall, the double mutant did demonstrate mild attenuation of neuroinvasion and longer average survival time compared to NY99ic, however, it was less attenuated than each of the single mutants and the virulence of the double mutant was not dose-dependent.

Virus was harvested from the brains of four mice that succumbed to the 500 PFU inoculum of the NS5-K61A/E218A mutant. Three of the mouse brains had viral infectivity titers $> 4 \log_{10}$ PFU/g, while one of the brains had an infectivity titer $> 8 \log_{10}$ PFU/g (**Table 4.4**). Sanger sequencing of the NS5 MTase domain verified that each virus reverted to the wild-type amino acid residues NS5-A61K/A218E (**Table 4.4**).

4.3.3 Temperature sensitivity in Vero cells

Infectivity titers were measured at both 37°C and 41°C to determine if a temperature sensitive (TS) phenotype would correlate with mouse attenuated phenotypes. NY99ic had a similar infectivity titer at both 37°C and 41°C. Similarly, NS5-K61A and

NS5-E218A mutations did not cause a significant reduction in infectivity titer at 41°C, whereas, the double mutant NS5-K61A/E218A had a significant reduction of 1.1 log₁₀ PFU at 41°C compared to 37°C, demonstrating that the combination of the two mutations together induced a TS phenotype (**Table 4.2**).

4.3.4 Multiplication kinetics in Vero cells and A549 cells

Multiplication kinetics of the three mutants were compared to the NY99ic parent in both Vero (IFN-I deficient) and A549 (IFN-I competent) cell lines.

In Vero cells, all three mutants had reduced multiplication kinetics compared to NY99ic from 24-96 hpi, with the most significant differences occurring between 24-36 hpi (**Fig. 4.2a**). The NS5-K61A and NS5-E218A mutants had the largest decrease in multiplication kinetics at 24 hpi, at which time each had > 100-fold reduction in titer compared to NY99ic (**Fig. 4.2a**). At 24 hpi, the NS5-K61A/E218A double mutant had a phenotype more closely resembling wild-type than the NS5 single mutants, but at 36 hpi, all three NS5 mutants had > 10-fold reduction in titer compared to NY99ic (**Fig. 4.2a**).

In A549 cells, the mutants most closely resembled NY99ic at 24 hpi, however, each mutant had notably reduced kinetics compared to the parent strain between 36-96 hpi (**Fig. 4.2b**). After reaching peak titers by 36 hpi, the infectivity kinetics for each virus remained relatively constant throughout the remainder of the time points measured. While both NS5-E218A and NS5-K61A/E218A had approximately 10-fold lower infectivity titers than NY99ic between 36-96 hpi, the NS5-K61A mutant had a 100-fold reduction in titer compared to NY99ic (**Fig. 4.2b**).

4.3.5 A549 cell cytokine response

Cytokine and chemokine production was measured in cell culture supernatant of human A549 cells at 36 hpi as this was the time point with maximum infectivity production with minimal cytopathic effect evident. A total of 29 cytokines and chemokines were measured with a BioPlex Pro human 27-plex cytokine assay and a custom IFN- α /IFN- β human cytokine assay. Three cytokines (IL-10, IL-15, and PDGF-bb) were not detected in any of the samples tested, which may be a limitation of A549 cells or of the specific time point analyzed. Nineteen cytokines and chemokines had no statistical difference in the quantities induced when comparing each of the mutants to NY99ic, while seven (IL-5, IL-6, IL-9, G-CSF, CXCL10, CCL5, and VEGF) had differential induction amongst the viruses tested (**Fig. 4.3**). The pro-inflammatory cytokine IL-6 had significantly decreased production from NS5-E218A infected cells compared to NY99ic, however, neither NS5-K61A nor NS5-K61A/E218A mutation modified the IL-6 pro-inflammatory response compared to NY99ic (**Fig. 4.3**). NS5-E218A also was the only mutant to significantly decrease the production of IL-5, although all three mutants show a trend of lower IL-5 levels compared to NY99ic (**Fig. 4.3**). The double mutant induced a significant increase in IL-9, G-CSF, CXCL10, and CCL5 whereas neither of the single mutants caused a significant change from NY99ic (**Fig. 4.3**). Both single mutants caused significantly increased production of the growth factor VEGF, but the double mutant did not induce a significant change (**Fig. 4.3**). In sum, all three NS5 mutants altered inflammatory cytokine or chemokine production, however, each mutant had a unique cytokine/chemokine profile.

4.3.6 Next-generation sequencing analysis of virus quasispecies

To further investigate the instability of the genotype of the NS5-K61A/E218A mutant, next-generation sequencing (NGS) analysis was undertaken on the Vero cell P0, P1, and P5 virus stocks. Since the P1 virus stocks were used in the mouse studies, these viruses were the focus of the quasispecies analysis. Average sequencing coverage was found to be similar and ranged between 7,589-7,796 for NY99ic and the NS5-K61A, NS5-E218A, and NS5-K61A/E218A mutants. Therefore, each sequencing file was analyzed for single nucleotide variants (SNVs) without downsampling. As expected for RNA viruses, many SNV subpopulations were detected in each virus (**Fig. 4.4**). In order to narrow the analysis to SNVs that were most prominent, only SNVs that comprised 1% or greater of the total RNA population were investigated. NY99ic had eleven SNVs detected above 1%, whereas, the NS5-K61A mutant had 34, the NS5-E218A mutant had 21, and the NS5 double mutant had nine (**Fig. 4.5, Table 4.5**). Although the NS5-K61A/E218A double mutant had only nine significant SNVs, three of these encoded reversions of A61K and A218E (**Table 4.5**). Specifically, SNVs at nucleotides 7861 and 7862 were encoded simultaneously (observed on Tablet software), and taken together these two nucleotide changes caused reversion from alanine to lysine at amino acid 61. The SNV observed at nucleotide 8333 encoded reversion from alanine to glutamic acid at amino acid 218. There was no evidence of any modification to the two catalytic tetrad residues that were not mutated, NS5-D146 and NS5-K182. Upon rescue of the double mutant, the P0 stock of the virus had A61K and A218E reversions in 3.3% and 2.8% of the viral RNA population, respectively (**Table 4.6**). After a single passage (P1) in Vero cells, the A61K reversion

had increased to 5.0% of the viral RNA population, while the A218E reversion had increased to 4.1% (**Tables 4.5 and 4.6**). After five passages in Vero cells (P5), the NS5-K61A/E218A double mutant did not revert to a wild-type consensus sequence, but 41% of the viral RNA population encoded reversion at residue NS5-61 and 47.6% encoded reversion at residue NS5-218, suggesting that further passage may yield reversion in the consensus sequence (**Table 4.6**). In comparison, both NS5-K61A and NS5-E218A single mutants had no SNVs of >1% frequency that encoded reversion in P0, P1, or P5 stocks (**Table 4.6**). Although SNVs as low as 0.1% could be detected, the P5 NS5-K61A mutant had no evidence of reversion even at very low levels. Alternatively, the P5 NS5-E218A mutant had a SNV encoding A218E reversion in 0.2% of the viral RNA population. Shannon entropy was also calculated on P1 stocks of each virus as an alternative measurement of diversity for each mutant as has been described in previous reports (Beck et al., 2014; Collins et al., 2018), and the results reflected the patterns displayed in the SNV frequencies shown in **Table 4.5**. Specifically, NY99ic and the NS5-K61A/E218A mutant had low levels of entropy across the genome, and the NS5-K61A and NS5-E218A mutants had higher peaks of entropy across the genome (**Fig. 4.6**).

4.4 DISCUSSION

WNV NS5-K61A and NS5-E218A mutants have previously been characterized in a IC based on WT WNV strain 3356 isolated from New York in 2000 (Daffis et al., 2011; Zhou et al., 2007). The mutants generated for this study utilized a different WNV strain backbone based off of a similar strain of WNV from New York in 1999 (NY99ic),

however, there are 27 nucleotide differences and seven amino acid substitutions between the two clones, including a valine to alanine substitution in the MTase domain of NS5 (**Table 4.1**) (Beasley et al., 2005; Shi et al., 2002). In addition, double mutation in the NS5 MTase catalytic tetrad has previously been proposed as a vaccine candidate for the four DENV serotypes, however, the homologous mutations had not been investigated in WNV prior to this study. Therefore, this chapter describes the characterization of NS5-K61A and NS5-E218A mutations in an alternative model to that which was used by other groups, while simultaneously reporting the first investigation of combined NS5-K61A/E218A mutations in WNV.

Consistent with published data using inbred mice (Daffis et al., 2011; Zhou et al., 2007), NS5-K61A or NS5-E218A mutation caused no lethality in outbred mice when inoculated peripherally with $\geq 100,000$ PFU (**Table 4.3**). Significantly, relatively low 500 PFU doses of NS5-K61A and NS5-E218A mutants both induced productive immune responses capable of protecting mice from lethal WNV challenge (**Table 4.3**). As our previous work with attenuated WNV NS1 and NS4B mutants found a correlation between low viremia and attenuated neuroinvasion (Whiteman et al., 2011; Wicker et al., 2006, 2012), it is possible that the NS5 MTase mutants do not replicate to high viremia and thus cannot invade the central nervous system. This speculation is in agreement with the observation that the MTase mutants are sensitive to the antiviral effects of IFIT proteins (Daffis et al., 2011)

Previous studies reported that double mutation of NS5-K61A/E217A (or E216A) in the KDE tetrad was attenuating for the four DENV serotypes (Züst et al., 2017), but

surprisingly, in WNV the double mutation caused a reduction of attenuation compared to mutation of either NS5-K61A or NS5-E218A alone. It was hypothesized that the double mutant had reduced attenuation *in vivo* due to the instability of the combined MTase mutations, and this was confirmed by Sanger sequencing of mouse-brain derived viruses. NGS analysis of the NS5-K61A/E218A mutant that was used to inoculate mice revealed SNV subpopulations that encoded reversions of both mutations. Importantly, the reversion of NS5-A61K required the first two nucleotides in the codon to change (AAA to GCA), indicating the strong selective pressure on the virus to restore the wild-type genotype and methyltransferase activity. To make the NS5-E218A mutation, only one nucleotide in the codon could be changed (GAG to GCG) due to the codon similarity between glutamic acid and alanine; therefore, the A218E reversion only required a single nucleotide substitution. Although the P1 stocks of the single mutants that were used in the mouse studies had more SNVs > 1% detected across the genome, none encoded reversion. NS5-K61A had no SNVs in the MTase domain at all (NS5 amino acids 1-267), while NS5-E218A only had one SNV in the MTase at amino acid 30, which is not structurally neighboring the MTase catalytic tetrad. While the double mutant had few SNVs detected overall, three out of nine encoded reversion. Although the NGS reads were not long enough to show whether or not the A61K and A218E reversions were encoded on the same sequencing contigs, it is hypothesized that the reversions occurred simultaneously since the virus would be expected to have an attenuated phenotype if either of the mutations remained. Interestingly, for all four DENV serotypes, double mutation of NS5-K61A/E217A (or E216A) was stable in the consensus sequences after five passages in Vero cells (Fink et al., 2014; Züst et al., 2017),

and the consensus genome was also stable in WNV after five passages of the mutant in Vero cells; however, there was >40% reversion to wild-type evident in the SNVs indicating the consensus sequence may revert upon continued passage. The P5 stock of the NS5-K61A mutant had no evidence of reversion, but the P5 stock of NS5-E218A had a small 0.2% SNV encoding reversion. The small A218E SNV in the P5 NS5-E218A mutant could potentially decrease the attenuation of this mutant, but it is unclear how high SNV frequency has to be to impact pathogenicity.

During investigation of SNVs, a NS5-T728I variant stood out for its high frequency (43.1%) in the P1 virus stock of the attenuated NS5-E218A mutant (**Table 4.5**). NS5-728 resides in the interface between the thumb and palm domain, so it is possible that the SNV at this residue alters ssRNA access to the RdRp catalytic site (Malet et al., 2007). This could potentially attribute to the increased multiplication kinetics of the NS5-E218A mutant compared to the NS5-K61A mutant, but additional studies are needed to better understand how the NS5-T728I mutation may influence the WNV phenotype. Of note, the P5 virus stock of the NS5-E218A mutant retained this SNV in 41% of viral RNA, so the frequency remained fairly constant following five cell culture passages.

Along with investigation of SNVs, Shannon entropy was also calculated for NY99ic and each NS5 mutant as an alternative method to compare quasispecies diversity. In studies of YFV, it has been demonstrated that the live, attenuated 17D vaccine strain has low Shannon entropy that is associated with the attenuated phenotype, as the parental, virulent Asibi strain has higher entropy (Beck et al., 2014). Interestingly, the same correlation was not observed for WNV NY99ic and the NS5 methyltransferase mutants.

Conversely, NY99ic and the virulent NS5-K61A/E218A double mutant had relatively low entropy compared to the attenuated NS5-K61A and NS5-E218A single mutants. Since the consensus sequences of the NS5 single mutants were stable through P5, the higher entropy observed in P1 stocks did not seem to indicate that the mutations of interest were unstable. It is possible that the correlation of low entropy and attenuation seen in YFV may not be the same in all flaviviruses, especially considering the relatively low entropy observed in the virulent NY99ic quasispecies.

Despite conserved amino acids and functions of the KDKE catalytic tetrads, differences in the DENV and WNV MTase could allow double mutation in the MTase catalytic tetrad to be stable in DENV but not in WNV. Structural studies have identified the GTP-binding domain required for MTase function in DENV, and one of the key amino acids, proline at NS5-152, is a serine in WNV (**Fig. 4.7**) (Egloff et al., 2002). It is possible that DENV and WNV have a different affinity for GTP-binding that permits stability of double mutations in the DENV MTase, but not in WNV (Egloff et al., 2002), however, GTP-binding affinities of WNV and DENV NS5 proteins have not been compared.

None of the prior studies of flavivirus NS5 MTase mutants investigated *in vitro* TS at 41°C compared to 37°C. Interestingly, the attenuated NS5-K61A and NS5-E218A single mutants were not significantly TS, while the virulent NS5-K61A/E218A double mutant was TS with >10-fold reduction in titer at 41°C compared to 37°C. It is possible that TS does not correspond with mouse attenuation for NS5 MTase mutants. Alternatively, TS phenotypes could suggest that the double mutant would be more strongly

attenuated than either of the single mutants if double mutation in the WNV NS5 MTase catalytic tetrad was stable and not susceptible to reversion to wild-type sequence.

The MTase single mutants were similar to those previously studied in that the largest reductions in multiplication kinetics in Vero cells compared to wild-type were between 24-36 hpi, but in contrast to other studies (Zhou et al., 2007), the NS5-K61A and NS5-E218A mutants had similar kinetics to one another (**Fig. 4.2a**). In DENV-2, NS5-K61A/E217A mutations caused approximately 10-fold reduction in Vero cell multiplication kinetics from 24-120 hpi compared to wild-type, and the DENV-2 double mutant had lower infectivity titers at 48 hpi compared to either of the single mutants (Zust et al., 2013). In WNV, double mutation in the MTase domain did not decrease multiplication kinetics compared to either of the single mutants, and at 24 hpi the double mutant had an infectivity titer that was higher than either of the single mutants and was approaching that of NY99ic (**Fig. 4.2a**). Therefore, Vero cell multiplication kinetics indicated that the NS5-K61A/E218A had a different phenotype than that which was observed for DENV-2 and for the WNV MTase single mutants. However, this different phenotype may be contributed by the 4-5% wild-type reversion of the double mutant P1 seed that outcompetes the double mutant virus replication during multiplication at a MOI of 0.1.

In previous studies, WNV and DENV MTase mutants were found to have increased sensitivity to the antiviral activity of IFN-I induced IFIT proteins compared to wild-type WNV, but they induced equivalent levels of IFN- β (Daffis et al., 2011; Zust et al., 2013). Although IFN- α and IFN- β levels were not statistically different when comparing the

WNV NS5 mutants to NY99ic, it is notable that the NS5-K61A/E218A mutant exhibited a trend toward increased IFN-I production (**Fig. 4.3**). The NS5-K61A mutant had the greatest reduction in A549 cell multiplication kinetics (**Fig. 4.2b**), indicating that this mutant may be more sensitive to IFN-I signaling than NS5-E218A or NS5-K61A/E218A. Despite differences in viral titer, both single mutants increased levels of VEGF compared to NY99ic, but only NS5-E218A caused significant reductions in IL-5 and IL-6. IL-5 has not been widely studied during WNV infection, but its primary roles in immunity are to facilitate eosinophil and B cell proliferation (NCBI, 2019). It is not clear what role VEGF might play during WNV infection. Increased VEGF is associated with severe disease in humans infected with DENV or other viruses that utilize angiogenesis to increase infectivity (Alkharsah, 2018), but it is possible that this blood vessel growth factor has a different impact during hemorrhagic DENV infection compared to neurotropic WNV. Reduction of IL-6 induced by NS5-E218A could be a protective response, considering high levels of inflammatory cytokines could increase WNV neuroinvasion (Kumar et al., 2010; Wang et al., 2004). The NS5-K61A/E218A double mutant induced significantly more IL-9, G-CSF, CXCL10, and CCL5 compared to NY99ic. All three NS5 mutants exhibited a trend toward mildly increased IL-9, which often functions to dampen inflammation (Goswami and Kaplan, 2011). While G-CSF is not often studied in the context of WNV infection, it can function as a neuronal ligand to reduce apoptosis (Schneider et al., 2005), indicating that it could contribute to protective immunity against WNV neurological disease. Likewise, both CXCL10 and CCL5 are important chemokines for WNV control in mice (Glass et al., 2005; Klein et al., 2005; Qian et al., 2015; Zhang et al., 2008), and

genetic deficiency of the CCL5 receptor, CCR5, is a risk factor for symptomatic WNV disease in humans (Glass et al., 2006; Lim et al., 2008). Considering that NS5 can antagonize innate immunity by many different mechanisms depending on the specific amino acid sequences of NS5 found in different flaviviruses (Best, 2017), it is not surprising that mutation of different amino acids would have unique effects on the immune response. Although the NS5-K61A/E218A mutant induced potentially protective cytokines/chemokines in a human cell line, this phenotype did not correlate with attenuation in the outbred mouse model. As described for the TS phenotypes, it is possible that the double mutant could induce a protective immune response leading to viral attenuation if the mutations were stable and could not revert to wild-type sequence.

In sum, this chapter describes the first genotypic and phenotypic characterization of double mutation of the NS5 MTase catalytic tetrad in WNV. Although *in vitro* studies of the NS5-K61A/E218A mutant suggested the mutations could be attenuating, the virus was more virulent than either of the MTase single mutants tested. Characterization of the NS5-K61A and NS5-E218A single mutants was also completed to verify published results using an alternative model while also expanding on the published work. Even though the NS5-K61A/E218A mutant did not have the attenuated phenotype expected, the independent mutations NS5-K61A and NS5-E218A were strongly attenuating and protective as was reported in previous studies using a different infectious clone and alternative animal models. Sequencing analysis of each mutant used in the mouse studies indicated that mutation of a single amino acid in WNV NS5 MTase catalytic tetrad was stable, whereas, double mutation of both amino acids simultaneously gave rise to reversion.

Since the single site NS5-K61A and NS5-E218A mutations were stable and attenuated *in vivo*, they remain good candidates to consider for rational WNV vaccine development. Considering that the P5 stock of NS5-E218A had a very low frequency SNV (0.2%) encoding reversion of A218E, NS5-K61A appears to be a more stable mutation and thus may be a safer choice for inclusion in a candidate vaccine. Since a live WNV vaccine would need multiple attenuating mutations, NS5-K61A should be characterized in the context of additional independently attenuating mutations in other viral genes.

Table 4.1: NY99 infectious clone and WNV strain 3356 infectious clone have genotypic differences

Nucleotide Position	WNV NY99 Clone Nucleotide	WNV 3356 Clone Nucleotide	Viral Protein Position	WNV NY99 Clone Residue	WNV 3356 Clone Residue
625	C	U	prM-54	P	S
1428	U	C	E-154	N	N
1599	C	U	E-211	F	F
1855	C	U	E-297	L	L
1974	C	U	E-336	C	C
2321	C	U	E-452	S	L
2562	G	A	NS1-31	R	R
3707	U	C	NS2A-61	V	A
3840	U	C	NS2A-105	I	I
3880	U	C	NS2A-119	Y	H
4195	G	A	NS2A-224	A	T
4257	A	G	NS2B-12	L	L
4922	G	A	NS3-104	R	K
5865	C	U	NS3-418	F	F
7015	U	C	NS4B-34	L	L
7029	U	G	NS4B-38	P	P
7797	G	A	NS5-39	A	A
7826	U	C	NS5-49	V	A
8811	U	C	NS5-377	N	N
8859	C	A	NS5-393	P	P
8862	A	G	NS5-394	R	R
8880	A	G	NS5-400	E	E
8958	A	G	NS5-426	E	E
9123	C	U	NS5-481	L	L
9660	C	U	NS5-660	L	L
10613	C	U	3' UTR	-	-
10851	A	G	3' UTR	-	-

Amino acid residues in blue text indicate non-synonymous substitutions.

Table 4.2: The NS5 double mutant has a temperature sensitive phenotype in Vero cells, but single mutants do not

	37°	41°	Delta	One-Way ANOVA
NY99ic	8.2	8.0	0.2	ns (p = 0.68)
K61A	7.3	7.1	0.2	ns (p > 0.99)
E218A	7.3	6.9	0.4	ns (p > 0.99)
K61A/E218A	8.5	7.4	1.1	* p = 0.03

Infectious titers are listed as Log₁₀ PFU/mL on 4 dpi. For NY99ic, five replicates were averaged at each temperature, and two replicates were averaged per temperature for the NS5 mutants. Temperature sensitivity significance was measured using a one-way ANOVA with Bonferroni's correction.

Table 4.3: The NS5 single mutants are attenuated in mice, but the double mutant is virulent

Virus	# survived 500 PFU	AST (days) ± SD	# protected 10⁴ PFU NY99ic challenge	Undiluted Inoculum (PFU)	# survived undiluted inoculum
NY99ic	0/10	9.0 ± 1.3	n.d.	n.d.	n.d.
K61A	5/5	>35	5/5	2.9x10 ⁵	5/5
E218A	5/5	>35	5/5	3.8x10 ⁵	5/5
K61A/E218A	3/10	[#] *11.1 ± 1.7	2/2	4.2x10 ⁷	3/5

Groups of five 4 week-old NIH Swiss Webster outbred mice were inoculated by the intraperitoneal (i.p.) route. Significance was tested using a Mann Whitney test to compare mutant survival time to NY99ic survival time. * p=0.02, [#]calculated from mice that died, n.d. = not done, AST = average survival time, SD = standard deviation

Table 4.4: Mouse brain-derived virus had reversion of NS5-K61A/E218A double mutation

	Time of death (dpi)	Viral titer in brain (log₁₀ PFU/gram)	Consensus sequence at nucleotide 7861 (NS5-61) [amino acid]	Consensus sequence at nucleotide 8333 (NS5-218) [amino acid]
Input Virus	-	-	GCA [A]	GCG [A]
Mouse 1	8	8.7	AAA [K]	GAG [E]
Mouse 2	10	4.9	AAA [K]	GAG [E]
Mouse 3	12	4.9	AAA [K]	GAG [E]
Mouse 4	12	4.4	AAA [K]	GAG [E]

Brains were harvested from mice that died from the 500 PFU intraperitoneal inoculation of the NS5-K61A/E218A mutant.

Table 4.5: Summary of single nucleotide variants $\geq 1\%$ of viral RNA populations for Vero cell passage one (P1) stocks of NY99ic and each NS5 mutant

	Nucleotide Position	Major Nucleotide	Minor Nucleotide	Viral Protein Position	Major Residue	Minor Residue	Frequency (%)
NY99ic	103	A	G	C-3	K	E	2.1
	106	A	G	C-4	K	E	2.0
	532	A	U	prM-23	I	F	1.7
	653	A	C	prM-63	E	A	1.1
	981	A	G	E-5	G	G	1.9
	1072	A	G	E-36	K	E	1.7
	1588	A	U	E-208	T	S	1.5
	2135	A	G	E-390	E	G	1.4
	5952	A	U	NS3-447	P	P	1.0
	7981	A	C	NS5-101	R	R	1.4
	9278	A	U	NS5-533	Y	F	1.2
K61A	106	A	C	C-4	K	Q	6.6
	306	A	G	C-70	R	R	4.6
	307	G	A	C-71	G	S	4.7
	388	C	A	C-98	R	R	8.6
	489	G	A	prM-8	G	G	6.9
	492	G	A	prM-9	K	K	3.6
	507	A	G	prM-14	V	V	16.1
	756	G	A	prM-97	Q	Q	14.2
	768	A	G	prM-101	E	E	1.5
	788	A	G	prM-108	K	R	13.1
	1415	A	G	E-150	E	G	2.2
	2184	A	G	E-406	K	K	6.3
	2798	A	G	NS1-110	K	R	5.0
	3337	A	G	NS1-290	S	G	2.9
	4387	A	G	NS2B-57	T	A	1.9
	4540	A	G	NS2B-108	S	G	7.5
	4740	A	G	NS3-43	E	E	1.9
	4862	A	G	NS3-84	K	R	2.2
	5925	A	G	NS3-438	G	G	1.6
	6106	A	C	NS3-499	I	L	6.1
	6197	A	G	NS3-529	E	G	3.0
	6295	A	G	NS3-562	R	G	1.0
	7015	U	C	NS4B-34	L	L	16.9

	7578	A	G	NS4B-221	T	T	1.4
	8815	A	G	NS5-379	T	A	18.5
	8947	A	U	NS5-423	S	C	4.4
	9092	A	G	NS5-471	K	R	3.8
	9570	A	G	NS5-630	G	G	3.8
	9766	A	G	NS5-696	I	V	7.3
	9936	C	A	NS5-752	N	K	4.7
	10417	A	G	3' UTR	-	-	8.4
	10807	A	G	3' UTR	-	-	12.0
	10814	A	U	3' UTR	-	-	1.6
	10888	U	A	3' UTR	-	-	1.2
E218A	353	A	G	C-86	K	R	2.5
	555	A	G	prM-30	G	G	2.4
	557	A	G	prM-31	K	R	2.4
	1303	A	G	E-113	I	V	3.1
	1525	A	G	E-187	T	A	5.2
	1531	G	A	E-189	D	N	3.5
	1996	G	A	E-344	A	T	13.2
	2148	U	C	E-394	N	N	2.3
	2176	A	G	E-404	I	V	3.2
	4479	C	G	NS2B-87	L	L	3.4
	4686	C	U	NS3-25	I	I	3.6
	4976	A	G	NS3-122	E	G	11.8
	5684	A	G	NS3-358	K	R	6.9
	5713	A	G	NS3-368	M	V	2.1
	7427	A	G	NS4B-171	K	R	2.3
	7557	A	G	NS4B-214	A	A	4.8
	7768	G	A	NS5-30	E	K	5.0
	9160	C	U	NS5-494	L	F	1.3
	9855	U	C	NS5-725	D	D	1.1
	9863	C	U	NS5-728	T	I	43.1
	10814	A	U	3' UTR	-	-	1.8
K61A/E218A	285	A	G	C-63	R	R	1.6
	763	G	C	prM-100	G	R	1.4
	5166	G	A	NS3-185	R	R	1.0
	6686	A	C	NS4A-73	Q	P	1.6
	7657	A	U	NS4B-248	M	L	1.6
	7861	G	A	NS5-61	*A	*K	5.0

7862	C	A	NS5-61			
8333	C	A	NS5-218	A	E	4.1
10814	A	U	3' UTR	-	-	1.2

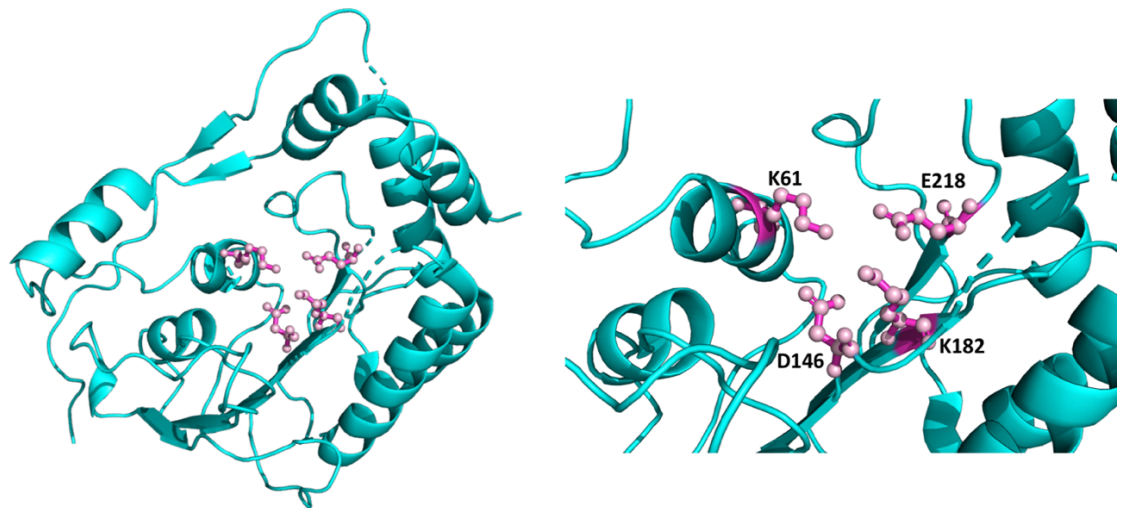
Amino acid residues highlighted in blue are non-synonymous substitutions. *SNVs at nucleotide 7861 and 7862 were encoded simultaneously

Table 4.6: Evidence of reversion of the NS5-K61A/E218A mutant increases after Vero cell passage

Virus	P0	P1	P5
K61A	< 0.1%	< 0.1%	< 0.1%
E218A	< 0.1%	< 0.1%	0.2%
K61A/E218A	3.3% / 2.8%	5.0% / 4.1%	41% / 47%

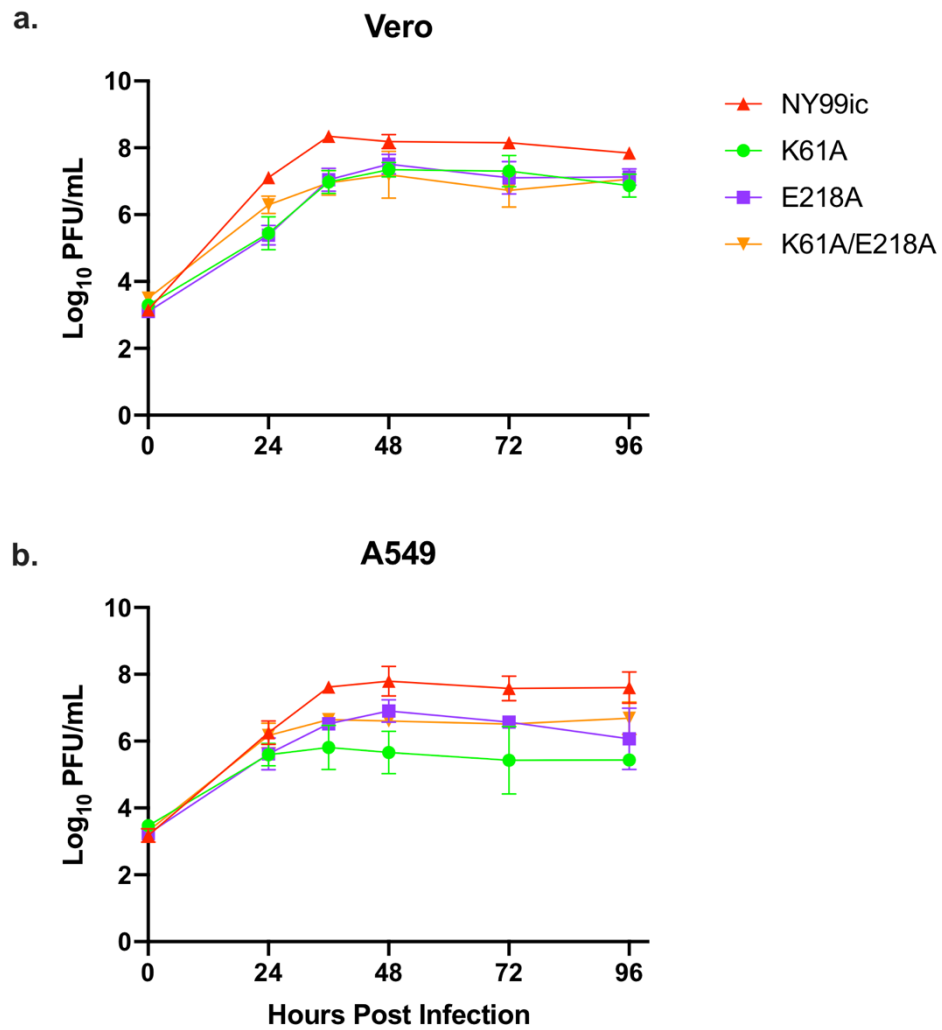
The frequency of reversion in single nucleotide variants (SNVs) of cell culture stocks of each NS5 mutant are listed. The limit of SNV detection for the LoFreq analysis was 0.1%. P0, P1, P5 = Vero cell passage 0, 1, or 5

Figure 4.1: The structure of WNV NS5 methyltransferase domain.



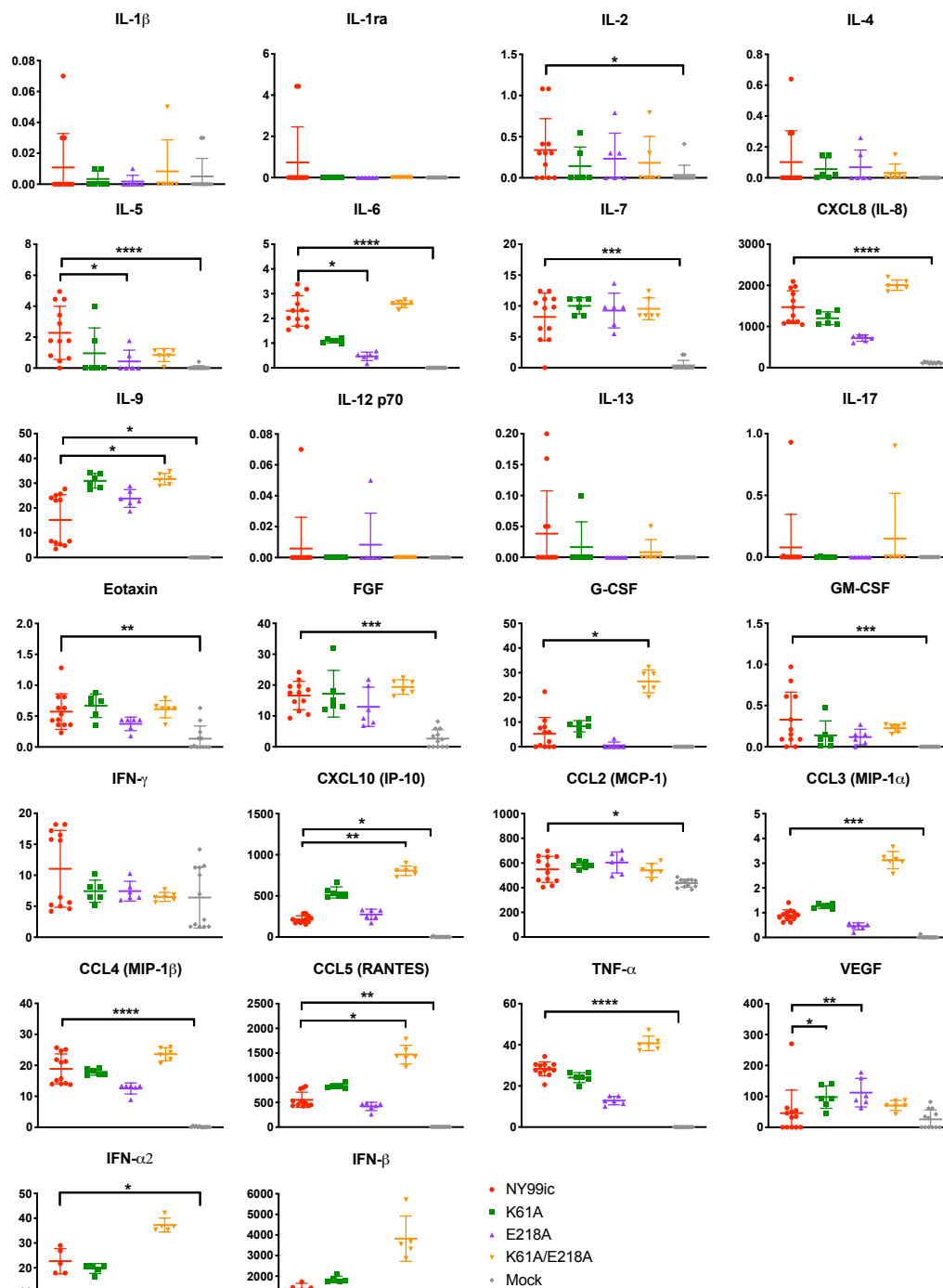
Amino acids displayed in pink represent the K61-D146-K182-E218 methyltransferase catalytic tetrad.

Figure 4.2: Multiplication kinetics of NS5 mutants are different than those of NY99ic in Vero and A549 cells



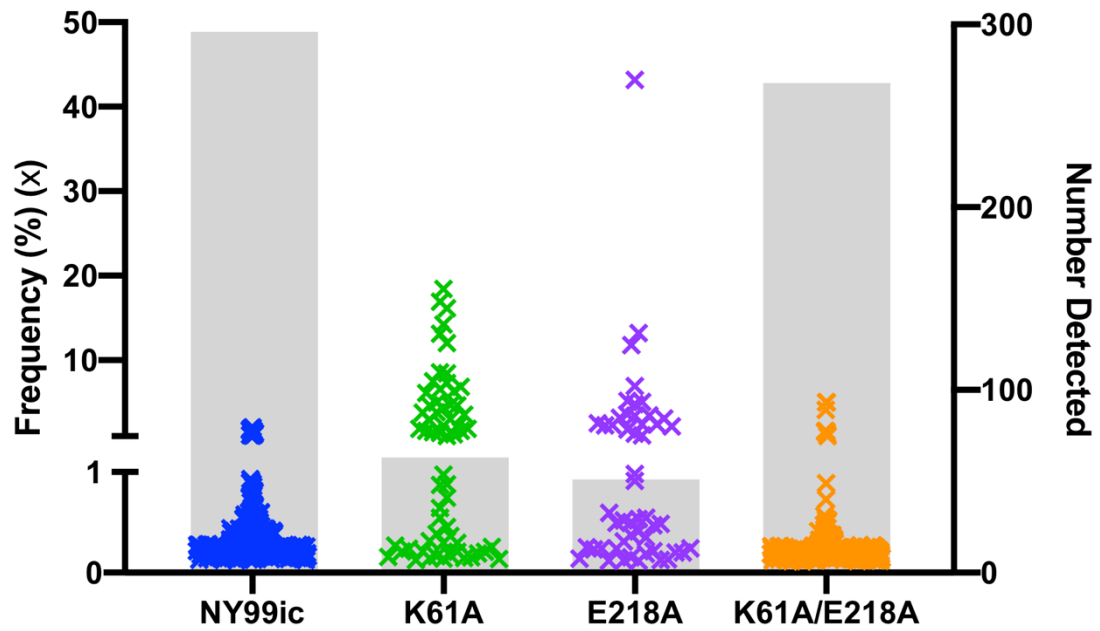
Cells were infected with a moi= 0.1 of virus.

Figure 4.3: Each NS5 mutant induced different cytokine patterns in A549 cells



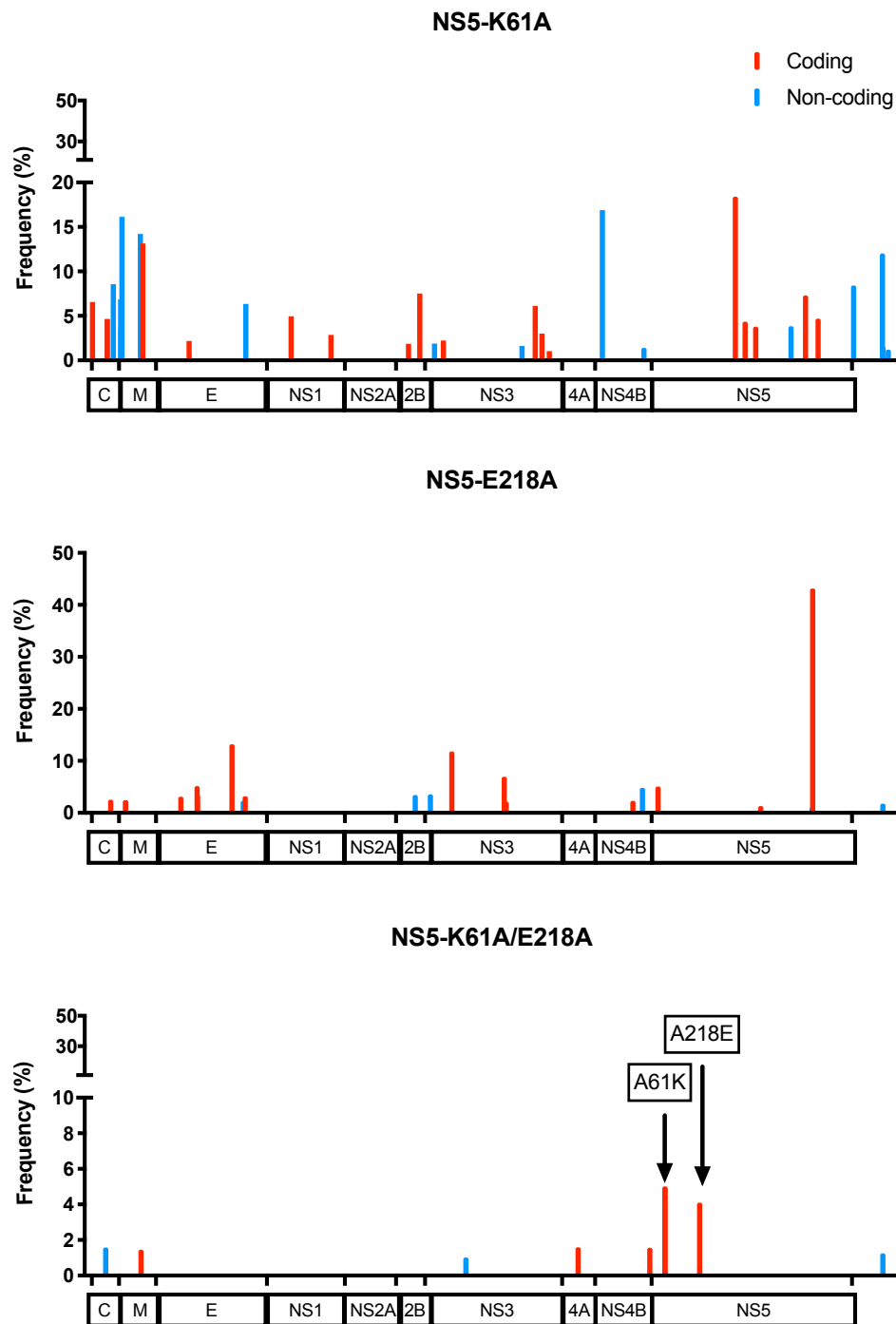
Cytokines were measured at 36 hpi in pg/mL in A549 cell supernatant after infection with a moi=0.1 of each virus. Twelve replicates were tested for NY99ic and mock-infected cells, and six replicates were tested for the three NS5 mutants. *p<0.05, **p<0.01, ***p<0.001 ****p<0.0001 in Kruskal-Wallis test with Dunn's multiple comparisons.

Figure 4.4: Single nucleotide variant profiles are different for the different NS5 mutants



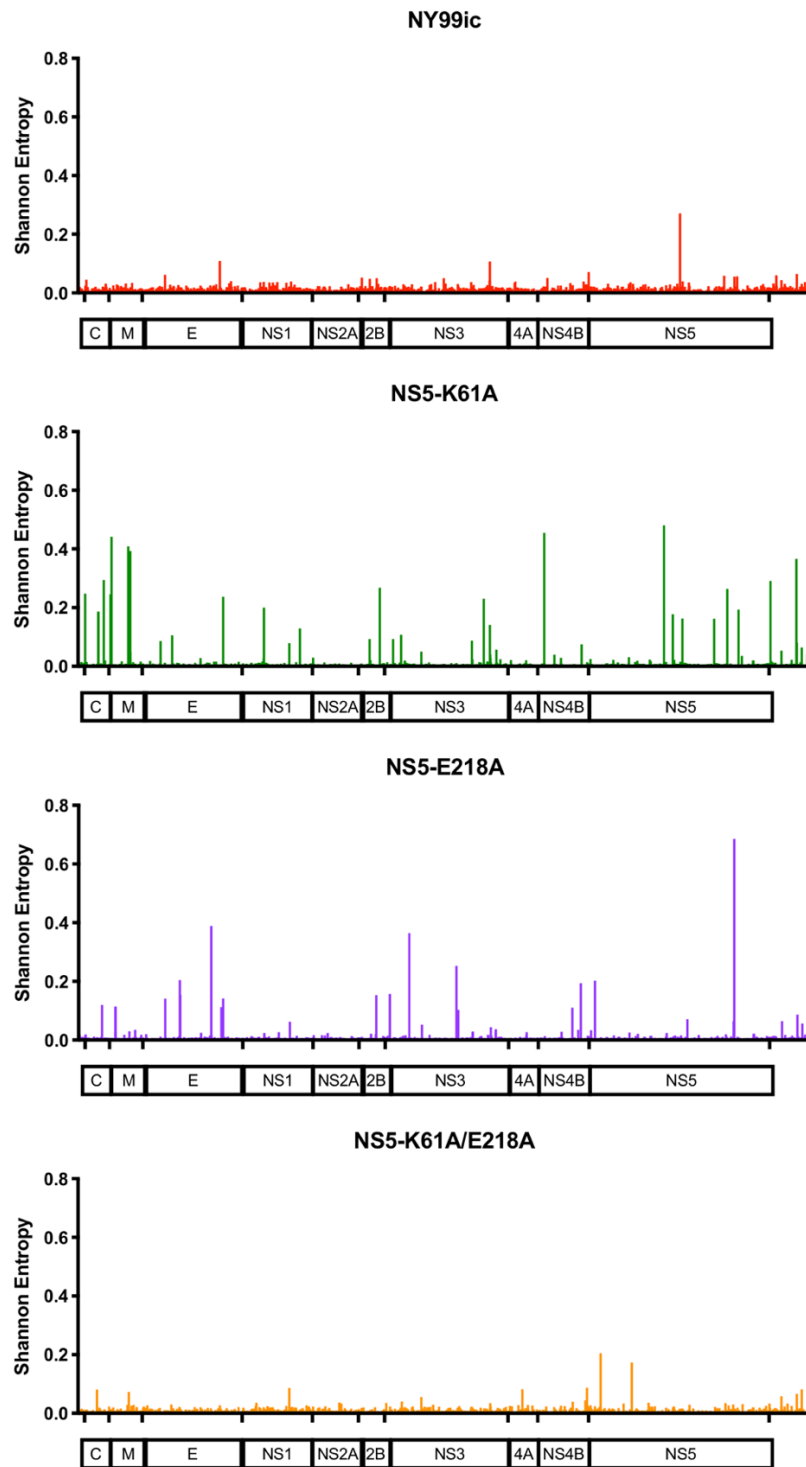
Each 'x' represents the frequency of a SNV, and the grey bars display the total number of SNVs detected. SNVs displayed were identified in the Vero cell passage one (P1) stock of each virus.

Figure 4.5: The NS5-K61A/E218A mutant had few SNVs $\geq 1\%$ frequency, but still showed evidence of reversion



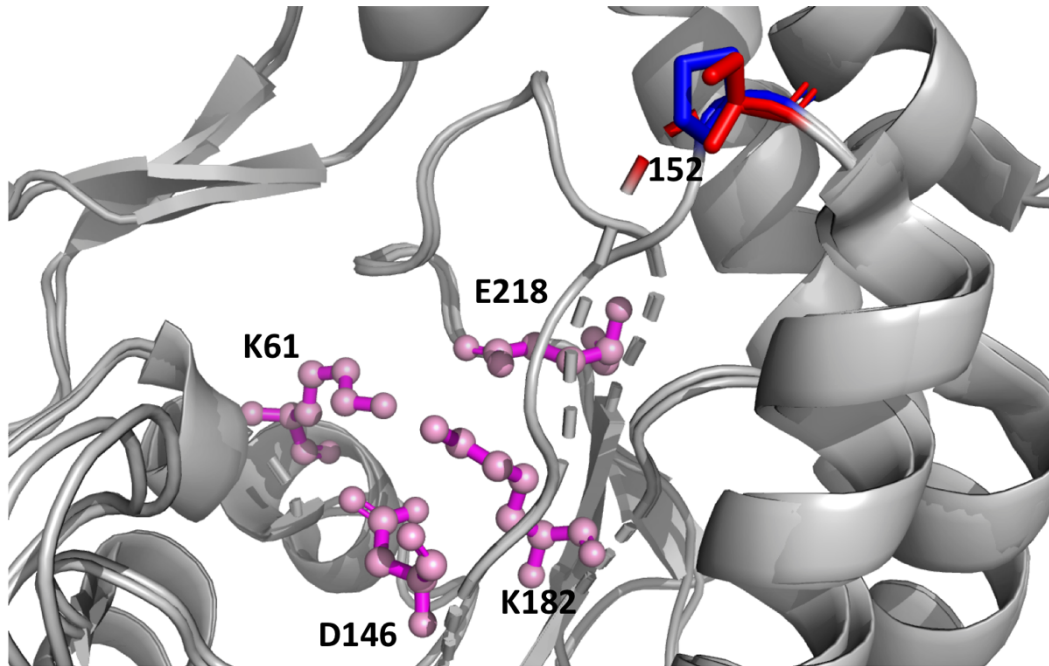
The SNVs $\geq 1\%$ frequency in the Vero cell P1 stocks of each virus are displayed in their corresponding genome position.

Figure 4.6: There are higher peaks of Shannon entropy for the NS5 single mutants compared to the double mutant and to NY99ic



Shannon entropy was measured in the Vero cell passage one (P1) stock of each virus.

Figure 4.7: WNV and DENV NS5 methyltransferase have an amino acid difference in GTP-binding domain residue NS5-152



The catalytic tetrad is shown in magenta. Proline152 in DENV is shown in blue, while Serine152 in WNV is shown in red. Figure based on findings from published data (Egloff et al., 2002).

Chapter 5 - Mutation of flavivirus conserved residues in NS4B

5.1 ABSTRACT

West Nile virus (WNV) non-structural protein NS4B is a hydrophobic transmembrane protein that is important for viral replication and host immune antagonism. Using reverse genetics, this chapter evaluated the role of conserved NS4B residues P38, P54, L56, C102, and W103 in attenuation both *in vitro* and *in vivo*. The NS4B mutants L56A, C102S, W103Y, and C102S/W103Y did not confer an attenuated phenotype, but instead had phenotypes similar to wild-type WNV. Although it was previously published that NS4B-C102S conferred significant attenuation, this chapter suggests that the attenuation was instead due to two compensatory envelope protein mutations that the historical C102S virus stocks harbored and that C102S alone does not encode an attenuated phenotype. Previous characterization of a P38G mutant found that the virus was strongly attenuated in mice but required two compensatory mutations: NS3-N480H and NS4B-T116I. In this chapter, a P38G mutant without NS3-N480H was characterized and it retained an attenuated phenotype, but to a lesser degree than what was previously observed indicating that all three residues are required for attenuation. Importantly, a new virulence determinant of WNV was identified at NS4B residue P54, as both P54A and P54G mutations strongly attenuated mouse neuroinvasion >100,000-fold compared to NY99ic. While P54A mutation was not stable, P54G mutation was, and thus NS4B-P54G mutation may be a good candidate for inclusion in a WNV live, attenuated vaccine.

5.2 INTRODUCTION

The flavivirus NS4B is a predominantly hydrophobic transmembrane protein that localizes in the perinuclear region of virus-infected cells and traverses the ER membrane (Zmurko et al., 2015). Detailed nuclear magnetic resonance (NMR) studies of dengue virus 2 (DENV-2) and DENV-3 NS4B structures indicate that this protein has five transmembrane domains as well as several regions that reside within the ER lumen and a series of amino acids that reside in the cytoplasm (Li et al., 2015, 2016). Although structural studies have not been reported for WNV NS4B, it is predicted that the structure is conserved amongst members of the flavivirus genus. NS4B is known to exist as both a monomer and dimer (Zou et al., 2014), and it interacts with other viral proteins including NS1, NS2B, NS3, and NS4A at various times during the replication cycle (Youn et al., 2012; Yu et al., 2013; Zou et al., 2015a, 2015b). During replication, NS4B is found closely associated to all NS proteins and to double-stranded RNA, indicating it plays a role in the replication complex (Kaufusi et al., 2014). Along with a function in viral replication, several roles of NS4B in host innate immune antagonism have been identified. For instance, DENV, yellow fever virus (YFV), and WNV NS4B are able to antagonize type-1 interferon signaling by inhibiting STAT1 and STAT2 phosphorylation and thus inhibiting downstream induction of interferon-stimulated genes (ISGs) (Mun et al., 2005; Wang et al., 2005). Studies of the four serotypes of DENV have found that NS4B can inhibit host RNA interference (RNAi) by inhibiting Dicer activity (Kakumani et al., 2013), but it is not yet known if WNV NS4B functions similarly.

NS4B has proven to be capable of harboring a number of amino acids whose mutation can have varying impacts on virus viability, virulence, and attenuation. Specifically, there have been reports of NS4B mutations that confer an attenuated phenotype identified in DENV-2 and DENV-4 NS4B (Grant et al., 2011; Orozco et al., 2012; Pletnev et al., 2002), as well as YFV (Dunster et al., 1999). Additionally, the YFV 17D and the Japanese encephalitis virus (JEV) SA14-14-2 live, attenuated vaccines have two and one NS4B mutation(s), respectively, that may be important to vaccine attenuation (Gromowski et al., 2015; Hahn et al., 1987). In terms of WNV, several NS4B mutations that confer attenuation in mice were previously identified, including P38G, C102S, and E249G, although compensatory mutations appear to contribute to the attenuated phenotypes (Davis et al., 2004; Wicker et al., 2006, 2012). Considering that small changes to NS4B can have a substantial impact on the phenotype of WNV, mutation of NS4B may be an important component of candidate live, attenuated WNV vaccine development. To further understand the importance of conserved NS4B residues while also evaluating specific mutations for their ability to confer attenuation, this chapter characterizes several mutations in WNV NS4B for changes in cell culture and mouse attenuation phenotypes. Importantly, this chapter describes new WNV NS4B-P54 mutants that are strongly attenuated.

5.3 RESULTS

5.3.1 Generation of NS4B mutants and consensus sequencing

5.3.1.1 REEVALUATION OF NS4B-P38G AND NS4B-C102S MUTANTS

Previous work characterized two attenuated NS4B mutants, C102S and P38G (Wicker et al., 2006, 2012), but notably Sanger sequencing showed that the P38G mutant harbored two additional mutations in the consensus sequence: NS3-N480H and NS4B-T116I (Wicker et al., 2012). The two mutants were regenerated and next-generation sequencing (NGS) showed that the new P38G virus only had the NS4B-T116I compensatory change, and not the NS3-N480H mutation in the genomic consensus sequence (**Table 5.1**) nor as a SNV in the virus population (see NGS section 5.3.6 below for details). NGS of the old virus stock confirmed that the NS3-N480H and NS4B-T116I mutations were both present in the consensus sequence, showing that the new and old stocks were genotypically different. Analysis of historical stocks by NGS revealed that the original rescued C102S mutant had two additional consensus changes in the envelope protein at E-D114A and E-V139M, however, the newly rescued C102S virus had no compensatory mutations nor SNVs at E-D114A and E-V139M (see NGS section 5.3.6 below for details). For this chapter, the two new mutants harboring NS4B-C102S only and NS4B-P38G (+NS4B-T116I) were characterized to identify the specific roles that these residues play in attenuation.

5.3.1.2 GENERATION OF NEW NS4B MUTANTS

Given the surprising results obtained for NS4B-C102S and NS4B-P38G by NGS, it was decided to identify additional attenuating mutations in NS4B. As with previous studies, new residues targeted for mutation were shared between different mosquito-borne flaviviruses in order to correlate results obtained from WNV to other flaviviruses. Accordingly, residues P54, L56, and W103 in NS4B were targeted for mutation based on their homology in multiple flaviviruses. P54 is very strongly conserved amongst both mosquito and tick-borne flaviviruses, while L56 and W103 have a moderate level of conservation amongst mosquito-borne flaviviruses (**Fig. 5.1**). Besides conservation in the flavivirus genus, the specified amino acid residues were selected due to their putative location in the NS4B protein, thus providing a means of investigation of different regions of NS4B for attenuating mutations. Specifically, P38 is in the NS4B N-terminal domain, P54 and L56 are in the first transmembrane domain, and C102 and W103 are on the ER lumen side of the membrane (**Fig. 5.2**).

The genotypes of all new NS4B mutants are shown in **Table 5.1**. In total, five new NS4B mutants were generated, including P54A, P54G, L56A, W103Y, and a double mutant combining C102S/W103Y. The genomic consensus sequence of each virus was verified using NGS, and none of the new mutants had any compensatory consensus mutations upon rescue. After a single passage in Vero cells, only the L56A mutant had an additional consensus sequence mutation at residue NS1-T108S. All viruses had similar infectivity titers, and only NY99ic and L56A produced large plaques while the remainder of the mutants produced medium-sized plaques (**Table 5.1**).

5.3.2 Mouse virulence

Using 4 week-old female Swiss Webster outbred mice, each of the new mutants was tested at a relatively low dose using i.p. inoculation of 500 PFU and then any mutant that was attenuated at the low dose was also tested at a high dose by the i.p. route where the virus was administered undiluted (undiluted doses listed in **Table 5.1**).

With the 500 PFU dose, 100% (10/10) mice died from inoculation with NY99ic while, as expected, all (5/5) mice survived inoculation with the old P38G (+ NS3-N480H/NS4B-T116I) or C102S (+ E-D114A/V139M) viruses (**Table 5.1**). Only 20% (1/5) of mice died from inoculation with the new P38G (+ NS4B-T116I) mutant, while the new mutant harboring only a C102S mutation was 100% (5/5) lethal (**Table 5.1**). Since the results differed from what was observed in the past, the experiment with C102S was repeated with a larger group to verify the results. Ten additional mice were inoculated with the new C102S mutant and all succumbed to infection, indicating that the attenuated phenotype observed from this mutant in previous studies was likely due to the contributions of the E protein mutations it harbored.

The new L56A, W103Y, and C102S/W103Y mutants were lethal in 100% (5/5) of mice with the 500 PFU inoculum, and no additional *in vivo* studies were carried out with these mutants (**Table 5.1**). Of note, both the P0 stock of the L56A mutant and the P1 stock that had the NS1-T108S consensus sequence change were 100% lethal using the 500 PFU inoculum. In comparison, all (5/5) mice inoculated with 500 PFU of either P54A or P54G survived infection (**Table 5.1**). Furthermore, all surviving mice were challenged with 10,000 PFU of NY99ic at 36 dpi, and all challenged mice survived (**Table 5.1**); therefore,

mutation of P38G, P54A, and P54G conferred an attenuated phenotype and infection with those attenuated viruses also induced protective immunity.

To investigate the attenuated phenotype further, groups of mice were inoculated with undiluted virus: 13 million PFU of P38G (+ NS4B-T116I), while P54A was tested at both 350,000 and 54 million PFU doses, and P54G was tested at both 520,000 and 15 million PFU doses. P38G (+ NS3-N480H/NS4B-T116I) and C102S (+ E-D114A/V139M) were also tested as attenuated controls using inocula of 1.2 million and 1.3 million PFU, respectively.

For the old P38G (+ NS3-N480H/NS4B-T116I) and C102S (+ E-D114A/V139M) mutants, 100% (5/5) of mice survived the undiluted inoculum, as expected (**Table 5.1**). Alternatively, for the new P38G (+NS4B-T116I) mutant lacking the NS3-N480H mutation, 20% (1/5) of mice succumbed to infection with the undiluted inoculum (**Table 5.1**). Both the P54A and P54G mutants caused no lethality (5/5 mice) following inoculation with >300,000 PFU (**Table 5.1**), so higher doses of each of these mutants were also investigated. All (5/5) mice survived a 54 million PFU dose of the P54A mutant, while 50% (5/10) of mice survived a 15 million PFU dose of the P54G mutant (**Table 5.1**).

Serum samples from groups of five mice infected with the C102S (+E-D114A/V139M), P54A, and P54G mutants were collected on 36 dpi and used to measure neutralizing antibodies with PRNT₅₀ assays. For the C102S (+E-D114A/V139M) and P54A mutants, serum was tested from mice inoculated with both the 500 PFU dose and the undiluted inocula. For the P54G mutant, serum was only collected from mice inoculated with the high dose. All samples tested had detectable neutralizing antibodies with a titer

>1:20, which was the limit of detection. The C102S (+E-D114A/V139M) mutant had the lowest neutralizing antibodies of the three groups tested with geometric mean titers (GMTs) of $1:70 \pm 29$ and $1:184 \pm 106$ for the low and high doses, respectively (**Fig. 5.3**). The P54A mutant had a GMT of $1:320 \pm 109$ for the low dose and $1:1280 \pm 873$ for the high dose (**Fig. 5.3**). Finally, the P54G mutant had a GMT of $1:279 \pm 88$ for the high dose (**Fig. 5.3**). In sum, the P54A mutant and to a lesser extent the P54G mutant exhibited a trend toward higher neutralizing antibody titers than the C102S (+E-D114A/V139M) mutant. The variability in the standard error of the GMT values was not unexpected as the experiments used outbred mice.

5.3.3 Temperature sensitivity in Vero cells

To investigate temperature sensitive (TS) phenotypes, each virus was titrated at both 37°C and 41°C, including the previously studied P38G (+ NS3-N480H/ NS4B-T116I) and C102S (+E-D114A/V139M) mutants. In agreement with previous studies, the C102S (+E-D114A/V139M) mutant was not able to form plaques at 41°C and thus was strongly TS (**Table 5.1**). Significantly, the new mutant harboring C102S with no extra mutations had no TS phenotype (**Table 5.1**). Consistent with previous studies, the P38G (+NS3-N480H/NS4B-T116I) mutant had a TS phenotype (1.2 log₁₀ reduction) (p <0.0001), and similarly, the new P38G (+NS4B-T116I) mutant was also significantly TS (0.7 log₁₀ reduction) (p = 0.0001) (**Table 5.1**).

The new P54, L56, W103, and C102/W103 mutants were also tested for a TS phenotype. While the mutants P54G, L56A, W103Y, and C102S/W103Y did not exhibit

significant reduction of infectivity titer at 41°C, P54A was the only new NS4B mutant that was significantly TS (1 log₁₀ reduction) (p <0.0001) (**Table 5.1**).

5.3.4 Multiplication kinetics in Vero cells and A549 cells

Multiplication kinetics of each new virus were compared to those of parental NY99ic using a MOI of 0.1 in both Vero (Type I Interferon [IFN-I] deficient) and A549 cells (IFN-I competent). In both cell lines, most of the mutants had similar multiplication kinetics to those of NY99ic (**Fig. 5.4**). The P54A mutant had the most significantly reduced kinetics compared to NY99ic in Vero cells. Specifically, the P54A mutant grew to titers >100-fold lower than those of NY99ic at early time points, but by two dpi, the mutant and NY99ic exhibited similar infectivity titers (**Fig. 5.4A**). In A549 cells, both P54A and P38G (+ NS4B-T116I) multiplied to titers >10-fold below those of NY99ic at all time points between 1-4 dpi (**Fig. 5.4B**). Despite the observed differences from NY99ic, all NS4B mutants were able to multiply in each cell line to relatively high titers >6 log₁₀ PFU/mL.

5.3.5 A549 cell cytokine response

Using a BioPlex Pro 27-plex human cytokine assay and a custom IFN- α /IFN- β assay, 29 cytokines were measured in A549 cell culture supernatant at 36 hpi with each mutant, NY99ic, or PBS as a mock infection. Two cytokines (IL-10 and IL-15) were not detected at all, but the remaining 27 cytokines were detected to varying degrees.

Several patterns in the cytokine profiles of virulent and attenuated NS4B mutants were detected. Specifically, each of the NS4B mutants that had a virulent phenotype in mice (L56A, C102S, W103Y, C102S/W103Y) induced cytokine responses that were very similar to NY99ic (**Fig. 5.5**). In terms of the attenuated mutants, two distinct cytokine patterns were observed. Cells infected with the mutants P38G (+NS4B-T116I), P38G (+NS3-N480H/NS4B-T116I), and C102S (+E-D114A/V139M) each induced overall higher cytokine and chemokine responses than NY99ic (**Fig 5.5**). Specifically, P38G (+NS3-N480H/NS4B-T116I) caused the most significantly increased induction of many of the pro-inflammatory cytokines measured, which was consistent with previous studies (Welte et al., 2011; Xie et al., 2015). The related P38G (+NS4B-T116I) retained the ability to induce strong cytokine responses, but quantities were slightly reduced in the absence of the NS3-N480H mutation. In comparison, both attenuated P54A and P54G mutants consistently induced relatively low cytokine responses that were typically similar to those in mock-infected cells and lower than those of NY99ic (**Fig. 5.5**). The only cytokine for which all attenuated mutants had a similar trend that was distinct from the virulent viruses was IFN- β , where each of the attenuated viruses caused lower production.

5.3.6 Analysis of virus quasispecies using NGS

To investigate the stability of each NS4B mutation, quasispecies diversity was analyzed using SNV detection and Shannon entropy calculation in the cell culture stocks of each virus. For the majority of the new mutants, viruses that were passaged once in Vero cells (P1) were analyzed since these were the stocks utilized in the mouse studies.

For the NS4B-L56A mutant, the P0 and P1 stocks are described since the P1 stock acquired a NS1-T108S consensus change that was not present in P0. For the NS4B-C102S/W103Y mutant, P0 data was analyzed as deep sequencing of this mutant was not completed on the P1 stock. Finally, P4 and P2 stocks of the P38G (+NS3-N480H/NS4B-T116I) and C102S (+E-D114A/V139M) mutants, respectively, were analyzed as the current stocks were generated via passaging of historical stocks. Each of these stocks had similar depths of coverage of sequencing reads with the average coverage ranging from 7217-7796, therefore, stocks were analyzed without down sampling.

5.3.6.1 SINGLE NUCLEOTIDE VARIANTS (SNVs)

The total number and frequency of SNVs identified varied between the different viruses, and there was no obvious pattern to correlate SNV number or frequency with attenuation (**Figure 5.6**). For instance, several virulent or attenuated strains had many (>300) detectable SNVs (NY99ic, C102S, C102S/W103Y, P38G [+NS3-N480H/NS4B-T116I]), whereas others had evidence of notably high frequency SNVs (L56A, P54A) (**Fig. 5.6**). Although SNVs as low as 0.1% frequency were detected, continued analysis was completed on SNVs $\geq 1\%$ to focus on the variants of the greatest significance.

Comparison of the new and old stocks of the P38G mutant demonstrated that the new P38G (+NS4B-T116I) mutant had 11 SNVs $\geq 1\%$ frequency compared to the old P38G (+NS3-N480H/NS4B-T116I) mutant which only had three (**Table 5.2, Fig. 5.7**). Neither of the P38G mutants had any SNVs at residues NS4B-38, NS4B-116, or NS3-480, indicating that the observed consensus sequence changes were stable. The new (virulent)

stock of the C102S mutant had 39 SNVs $\geq 1\%$ frequency, whereas the old (attenuated) C102S (+E-D114A/V139M) mutant only had four, none of which were coding (**Table 5.2, Fig. 5.7**). Additionally, the new C102S mutant had no evidence of SNVs at residues E-D114 or E-V139, which are mutated in the consensus sequence of the old stocks. No SNVs were shared amongst the two C102S mutants, but the two P38G mutants each harbored a NS4B-M177L variant (**Table 5.2**).

Comparison of the SNVs of the new NS4B mutants demonstrated that there were no SNVs that were shared amongst all of the mutants and none that appeared associated with attenuated or virulent phenotypes of the mutants. The C102S/W103Y mutant had a similar genotype to that of NY99ic in that both had >300 total variants but only two or one SNV(s), respectively, were $\geq 1\%$ frequency (**Table 5.3, Figs. 5.6 and 5.8**). Four out of 15 SNVs $>1\%$ in the P0 stock of the L56A mutant had $>20\%$ frequency, including a NS1-T108S mutation present in 43.8% of the population (**Table 5.3, Fig. 5.8**). Upon passage, the P1 stock had 12 SNVs $>1\%$ frequency, four of which had a frequency $>20\%$. Additionally, in the P1 virus the NS1-T108S mutation increased in frequency and was a consensus sequence change where 51.4% of the population harbored this additional mutation. Although there was no evidence of reversion at residue NS4B-56, the accumulation of a consensus sequence change and other high frequency variants indicated the genotype was not stable. The virulent W103Y mutant had 55 SNVs ranging from 1.0-6.5% frequency, but there was no evidence of reversion at residue NS4B-103 (**Table 5.3, Fig. 5.8**). Most SNVs detected in the P54G mutant quasispecies were approximately 1% frequency with only 10% (3/30) that were $>5\%$ frequency in the population, and none were

detected in the NS4B gene (**Table 5.3, Fig. 5.8**). In comparison, of 20 SNVs $\geq 1\%$ frequency in the P54A mutant quasispecies, 50% (10/20) had a frequency $>10\%$ and nine were clustered in the NS4B gene (**Table 5.3, Fig. 5.8**). The nine nucleotide changes in NS4B encoded seven amino acid substitutions, including one that exhibited reversion of NS4B-A54P in 13.0% of the population (**Table 5.3, Fig. 5.9A**).

To further investigate the stability of the P54A mutation, Vero cell P0 and P5 stocks were sequenced and variants were analyzed. The P0 stock of the P54A mutant (the virus rescued directly after transfection) had slightly lower average sequencing coverage than the other mutants analyzed (6165 compared to >7216), but regardless, the P0 stock had a similar genotype to the P1 stock. Specifically, no extra coding consensus sequence changes were identified throughout the genome and of 20 SNVs $>1\%$ frequency, one encoded reversion in 18.0% of the population (**Figure 5.9B**). In comparison, the P5 stock had 16 SNVs $>1\%$ frequency and had undergone consensus sequence reversion and harbored both NS4B-A54P and NS4B-D90G consensus genome mutations (**Figure 5.9B**). It is notable that during serial passage of the P54A mutant, the viral titer did not significantly change, but the plaque phenotype changed from medium-sized (P0 and P1) to mixed medium and large sized plaques (P5). Based on the instability of the P54A mutation, P0 and P5 stocks of the P54G mutant were also analyzed. The P0 stock had an average coverage depth of only 1729, which was significantly lower sequencing coverage depth than the other viruses analyzed. Therefore, the SNV results of this stock may be biased since there were fewer viral reads. With this limitation in mind, the P0 stock of the P54G mutant was similar to the P1 stock in that it harbored 34 SNVs $>1\%$ frequency, none of which were in NS4B.

The P5 stock of the P54G mutant had 18 SNVs >1% frequency, and although six were in NS4B, there was no evidence of reversion of the P54G mutation and there were no additional consensus sequence changes. Consistent with the sequencing results, the viral titer and the medium-size plaque phenotype remained constant during five serial passages of the P54G mutant.

5.3.6.2 SHANNON ENTROPY

As an alternative method of quasispecies analysis, absolute nucleotide diversity at each position in the genome was also measured using Shannon entropy. Comparison of the new and old stocks of the P38G and C102S mutants demonstrated that the new mutants both have significantly higher Shannon entropy compared to the old stocks ($p=0.003$ and $p<0.0001$, respectively) (**Fig. 5.10**). Shannon entropy of the new NS4B mutants showed that each new mutant had distinct quasispecies diversity. NY99ic had relatively low entropy across the entire genome, indicating it is likely stable in Vero cells, and the C102S/W103Y mutant displayed similar patterns (**Fig. 5.11**). The P54A and L56A mutants both had unique high spikes of entropy (**Fig. 5.11**), similar to the unique high frequency SNV genotypes these two mutants displayed (**Fig. 5.8**). Both P54G and W103Y mutants had higher peaks of entropy than those observed in the NY99ic quasispecies, however, they did not incorporate high diversity peaks relative to P54A and L56A mutants (**Fig. 5.11**). Overall, the Shannon entropy results are in agreement with the SNV results and support that the different mutations investigated each uniquely alter the viral diversity.

5.3.7 Intracellular localization of NS4B and NS1

Since the P54G mutant was strongly attenuated in mice and had a stable genotype after cell culture passage, confocal microscopy was used to further investigate the mechanism of attenuation for this single site mutant. Virus-infected Vero cells were stained for both NS4B and NS1 since it is known that these two viral proteins interact (Youn et al., 2012). Furthermore, an attenuated NS1 glycosylation site mutant (NS1-NNT130QQA/N175A/N207A; hereafter termed NS1_{mut}) that was used for NS1 immunostaining in previous studies (Whiteman et al., 2015) was used as an attenuated control virus. One day post infection, the P54G mutant had fewer virus-infected cells than NY99ic (**Fig. 5.12A**), which was expected based on the differences in infectivity titers (**Fig. 5.4A**). Cells infected with the P54G mutant, however, had significantly lower levels of NS4B ($p = 0.0002$), but had similar staining of NS1 compared to NY99ic (**Fig. 5.12B**). Consistent with previous studies, the attenuated WNV NS1_{mut} had lower levels of NS1 ($p = 0.006$), but the staining of NS4B was similar to that in NY99ic infected cells (**Fig. 5.12B**). Pearson's correlation coefficient (PCC) was also calculated to compare colocalization of NS1 and NS4B in infected cells. For PCC, a value of 0 indicates no colocalization, whereas a value of 1 indicates perfect colocalization. At one dpi, all infected cells exhibited some degree of colocalization of NS1-NS4B, but both the NS4B-P54G mutant and the NS1_{mut} had significantly less colocalization compared to NY99ic ($p = 0.004$ and $p = 0.01$, respectively) (**Fig. 5.12C**).

At two dpi, the P54G mutant still exhibited lower levels of NS4B compared to NY99ic ($p = 0.03$), however, there were also significantly lower levels of NS1 staining (p

= 0.03) (**Figs. 5.13A and 5.13B**). The NS1_{mut} attenuated control had similar levels of NS4B as NY99ic, and in agreement with previous studies demonstrating that this mutant had a block of NS1 transport out of the ER (Whiteman et al., 2015), there was stronger NS1 staining compared to NY99ic ($p = 0.02$) (**Fig. 5.13A and 5.13B**). At 48 hpi, NY99ic and the NS1_{mut} had strong colocalization of NS1-NS4B, but the P54G mutant still exhibited a significant reduction in colocalization ($p = 0.009$) (**Fig. 5.13C**).

5.4 DISCUSSION

Previous studies reported that the P38G mutant could only be rescued with the compensatory NS3-N480H and NS4B-T116I mutations (Wicker et al., 2012), however, the current studies showed that the NS3-N480H mutation is not necessary for viability of the P38G mutant. Compared to the old P38G (+NS3-N480H/NS4B-T116I) mutant, the new P38G (+NS4B-T116I) mutant exhibited less attenuation of mouse neuroinvasion. Considering that the new P38G (+NS4B-T116I) mutant was lethal in 1/5 mice at both the low and high inoculum, the neuroinvasive phenotype was not dose-dependent. It has been shown that DENV2 NS4B interacts with NS3 and can impact its enzymatic helicase activity, and specifically, NS4B-P104L mutation (**Fig. 5.2**) can disrupt the NS4B-NS3 interaction (Umareddy et al., 2006; Zou et al., 2015a). It is possible that the NS3-N480H mutation in WNV adds additional factor(s) to the mechanism of attenuation that independently contribute to the attenuated phenotype conferred by NS4B-P38G. The NS3-N480H mutation alone in WNV was not found to have attenuating properties (Wicker et al., 2012), therefore, it seems that NS4B-P38G and NS3-N480H may have a synergistic

effect on attenuation. This is supported by comparison of cytokine responses between the two P38G mutants, as each mutant induced strong cytokines and chemokines, but the P38G (+NS3-N480H/NS4B-T116I) mutant induced more robust innate immune responses. Notably, previous studies have demonstrated that the P38G (+NS3-N480H/NS4B-T116I) mutant induced stronger pro-inflammatory cytokines than NY99 in dendritic cells, THP-1 cells, THP-1 macrophages, and C57Bl/6 mice (Welte et al., 2011; Xie et al., 2015), so the findings in A549 cells support published data and indicate that induction of a robust immune response may contribute to the mechanism of attenuation for the WNV P38G mutants. One similarity of the old and new stocks of the P38G mutant was that they each harbored NS4B-M177L mutations in the SNVs (**Table 5.2**). Residue NS4B-177 is in the fourth transmembrane domain of NS4B and is structurally distant from NS4B-38, which is in the ER lumen preceding the first transmembrane domain (**Fig. 5.2**). Considering that NS4B-T116I is in the third transmembrane domain but seems to be required for viability of the P38G mutant (**Fig. 5.2**), it is rational that distant amino acid residues can impact the stability of the NS4B protein. Though the mechanisms behind the synergistic effects of distant amino acids in NS4B are not known, one consideration is that the mutations of interest could impact NS4B dimer formation (Zou et al., 2014).

Although it was previously reported that a WNV NS4B-C102S mutation could confer a strong degree of attenuation in mice, the current studies determined that the stock virus used in past studies had two additional mutations: E-D114A and E-V139M. In previous reports the incomplete viral genome was verified using Sanger sequencing (Wicker et al., 2006), but 15 years later robust NGS technologies can be utilized that allow

investigation of the genome in greater detail. It has now been determined that mutation of NS4B-C102S alone (without the envelope protein mutations) does not induce notable phenotypic changes from NY99ic. Additionally, the new NS4B-C102S mutant had no evidence of E-D114A or E-V139M mutations in the consensus sequence or in the SNVs, so it is unlikely that these E protein mutations directly compensate for mutation of C102S. In sum, mutation of the conserved C102 residue does not alter the virulence of WNV, but instead, the E protein mutations D114A and V139M are likely responsible, at least in part, for the substantial attenuation observed in previous studies. Characterization of the phenotypes of E-D114A and E-V139M mutations alone warrants further study. In particular, E-114 is adjacent to the conserved flavivirus fusion loop (E protein amino acids 98-110) and may contribute to the attenuated phenotype, but this would need further investigation using additional mutants generated by reverse genetics.

Several novel amino acid mutations in NS4B were also characterized for their ability to alter the phenotype of WNV. Based on the NMR structure of DENV NS4B (Li et al., 2015, 2016), the putative location of each of the amino acid residues of interest can be determined, and thus mutation in different domains of NS4B can be evaluated (**Fig. 5.2**). It was hypothesized that the region where C102/W103 reside on the interface between the lumen and membrane of the ER (see **Fig. 5.2**) may be susceptible to harboring attenuating mutations because of the implicit attenuating properties of the C102S mutation, however, neither C102S nor W103Y mutations conferred attenuation of mouse neuroinvasion and thus this region within the ER lumen appears unlikely to be an ideal site for incorporation of attenuating mutations. Although P54 and L56 are both located in the first

transmembrane domain of NS4B (**Fig. 5.2**), the L56A mutant maintained a similar phenotype to that of NY99ic while both P54A and P54G mutants conferred significant mouse attenuation. Notably, L56 in WNV is homologous to L52 in DENV, and a L52F mutation conferred increased virulence in DENV2 by decreasing viral RNA synthesis, whereas a leucine at this residue was associated with attenuation (Grant et al., 2011). Therefore, it is rational that mutating L56 in WNV will not strongly decrease virulence if this leucine has a conserved function in WNV and DENV to reduce viral RNA synthesis. In terms of the P54 mutants, proline residues can be key to protein structure, specifically in alpha helices (Li et al., 2016), therefore, it is possible that mutation of P54 alters the structure and thus the function of NS4B. This hypothesis is supported by the immunostaining of virus-infected cells at 24 hpi demonstrating that cells infected with the P54G mutant do not accumulate NS4B as rapidly as NY99ic-infected cells even though NS1 staining was comparable. Furthermore, the reduction in colocalization of NS1 and NS4B in cells infected with the P54G mutant could indicate that there is less interaction between these two viral proteins, which may inhibit the function of the replication complex, but further investigation is required. While the possibility that the P54G mutation altered binding of the monoclonal antibody used for staining cannot be ruled out, this is considered unlikely since mab 44-4-7 binds to NS4B amino acid residues 141-147 that are in the cytoplasmic loop of NS4B and are not structurally neighboring any of the mutations investigated in this chapter (Li et al., 2016; Xie et al., 2014) (**Fig. 5.2**).

Interestingly, P54G was the only mutant in the panel for which temperature sensitivity did not correlate with *in vivo* attenuation (**Table 5.1**). Nonetheless, both P54A

and P54G had similar phenotypes to one another, including their low induction of cytokines and chemokines. It was surprising that both mutants had fairly low cytokine induction similar to mock-infected cells, as in mouse studies each was protective from a 10,000 PFU challenge and each induced stronger neutralizing antibody responses than the C102S (+E-D114A/V139M) mutant (**Table 5.1, Fig. 5.3**). In many viral infections, cytokine storm is associated with severe pathology, so it is possible low cytokine induction by the P54 mutants reduces disease severity. Based on the multiplication kinetics and the immunostaining, the P54G mutant does not replicate as well as NY99ic, so it is possible that the P54 mutants could have reduced viremia that correlates with a reduction in both neuroinvasion and cytokine induction. Additionally, it is possible that induction of cytokines by the P54 mutants may be stronger *in vivo* than what was observed in cell culture, but if this is the case then it would be a unique feature of these mutants as the P38G mutants induce strong innate immune responses both *in vitro* and *in vivo*. Of all 27 cytokines analyzed, IFN- β was the only one for which both P38 and P54 attenuated mutants induced lower levels than those induced by NY99ic. In THP-1 macrophages, the P38G (+NS3-N480H/NS4B-T116I) mutant induced slightly lower IFN- β than NY99 at one dpi, but by day four the mutant induced more IFN- β , albeit the differences were not statistically significant (Xie et al., 2015). It is possible that low levels of IFN- β at early time points during infection may be protective in some cell types by preventing detrimental inflammation, but further investigation is needed.

Although the P54A and P54G mutants had very similar phenotypes and the P54A mutant had the strongest degree of mouse attenuation, SNV analysis demonstrated that

P54A was not a stable mutation, while P54G was. This is not surprising since a single nucleotide substitution can revert alanine to proline, but two nucleotide changes are required to revert glycine to proline. Even though the P54A mutation did not rapidly revert in mouse experiments, the SNVs identified in the P1 cell culture stock exhibited instability of the genotype with many high frequency SNVs, especially in the NS4B gene. One of these, NS4B-D90G, was selected for during cell culture passage and encoded a consensus sequence change by P5. NS4B-90 is on the ER lumen side of the protein, and while the role of this residue during WNV infection is not known, it is possible that the loss of negative charge at this position helped to compensate for changes to NS4B induced by the P54A mutation. However, NS4B-D90G mutation was not evident in the quasispecies of the P54G mutant through P5. While the P54G mutation was stable in all studies undertaken thus far, further passaging in both cell culture and in animal models is warranted to investigate whether or not the observed accumulation of low frequency SNVs in structural and NS proteins would lead to reversion to virulence.

Overall, this chapter has both revisited mutations studied in the past while also characterizing several new NS4B mutations. Importantly, residue NS4B-P54 was identified as an important virulence determinant for WNV as mutation of both P54A and P54G caused significant attenuation and protection from challenge in mice. Since P54 is very strongly conserved amongst both mosquito and tick-borne flaviviruses, it is hypothesized that mutation of this residue in other flaviviruses could also induce an attenuated phenotype. Based on the strong degree of mouse attenuation and the stability

of the P54G mutation after serial cell culture passage, mutation of this residue may be a good candidate to include in a candidate live, attenuated WNV vaccine.

Table 5.1: Consensus genotypes, plaque phenotypes, temperature sensitivity, and mouse attenuation of NS4B mutants

NS4B mutant	Additional consensus mutations	Vero cell passage number	Plaque morphology	37°C titer	41°C titer	Δ titer	Survived 500 PFU i.p. (%)	°AST	Survived 10,000 PFU challenge	High dose (PFU/mouse)	Survived high dose (%)
NY99ic	-	1	large	8.2	8.1	0.1	0/10 (0)	9.0±1.3	n.d.	n.d.	n.d.
P38G	NS4B-T116I	1	medium	8.5	7.8	***0.7	4/5 (80)	13.0±0.0	4/4	1.3 x 10 ⁷	4/5 (80)
P38G	NS3-N480H NS4B-T116I	4	medium	8.4	7.2	****1.2	5/5 (100)	>35	5/5	1.2 x 10 ⁶	5/5 (100)
P54A	-	1	medium	8.3	7.3	***1.0	5/5 (100)	>35	5/5	3.5 x 10 ⁵ 5.4 x 10 ⁷	5/5 (100) 5/5 (100)
P54G	-	1	medium	8.2	8.0	0.2	5/5 (100)	>35	5/5	5.2 x 10 ⁵ 1.5 x 10 ⁷	5/5 (100) 5/10 (50)
L56A	-	0	large	7.7	n.d.	n.d.	0/5 (0)	9.6±2.6	n.d.	n.d.	n.d.
L56A	NS1-T108S	1	large	8.5	8.3	0.2	0/5 (0)	11.6±2.4	n.d.	n.d.	n.d.
C102S	-	1	medium	7.6	7.6	0.0	0/15 (0)	8.5±3.1	n.d.	n.d.	n.d.
C102S	E-D114A E-V139M	2	medium	7.8	< 1.7	#> 6.1	5/5 (100)	>35	5/5	1.3 x 10 ⁶	5/5 (100)
W103Y	-	1	medium	7.8	7.5	0.3	0/5 (0)	9.8±2.4	n.d.	n.d.	n.d.
C102S/W103Y	-	1	medium	8.5	8.4	0.1	0/5 (0)	9.4±2.1	n.d.	n.d.	n.d.

Two previously published mutants, NS4B-P38G (+ NS3-N480H/NS4B-T116I) and NS4B-C102S (+ E-D114A/V139M), were passaged once from historical stocks, titrated, sequenced, and used for current studies. All other viruses were rescued from transfection and passaged once in Vero cells for subsequent studies. The L56A mutant acquired an extra consensus sequence mutation after a single passage in Vero cells, therefore, the P0 mutant was also tested in mouse studies. Infectivity titers are listed as log₁₀ PFU/mL. Temperature sensitivity significance was measured using a one-way ANOVA with Bonferroni's correction. n.d. = not done. AST=average survival time. ***p < 0.001, ****p < 0.0001, # = statistics not completed because 41°C titer was below limit of detection (LOD<1.7 log₁₀ PFU/mL). °AST was calculated for mice that died from the 500 PFU dose. A Kruskal-Wallis test indicated that none of the mutant ASTs were statistically different than NY99ic.

Table 5.2: New and old stocks of the NS4B P38G and C102S mutants exhibit distinct single nucleotide variants

	Nucleotide Position	Major Nucleotide	Minor Nucleotide	Viral Protein Position	Major Residue	Minor Residue	Frequency (%)
NY99ic	2135	A	G	E-390	E	G	1.9
	2041	A	C	E-359	N	H	2.1
P38G (+ NS4B-T116I)	2983	A	C	NS1-172	R	R	1.3
	2998	A	G	NS1-177	T	A	1.2
	3290	A	U	NS1-274	E	V	9.0
	4998	C	U	NS3-129	D	D	2.9
	5218	A	C	NS3-203	R	R	1.0
	7444	A	C	NS4B-177	M	L	13.5
	9858	A	G	NS5-726	G	G	8.8
	10382	A	U	NS5-901	E	V	1.2
	10582	G	U	3' UTR	-	-	1.0
	10814	A	U	3' UTR	-	-	1.9
P38G (+ NS3-N480H/NS4B-T116I)	7244	U	C	NS4B-110	V	A	1.1
	7359	C	U	NS4B-148	N	N	1.0
	7444	A	C	NS4B-177	M	L	1.2
C102S	155	G	A	C-20	G	D	1.7
	156	A	U	C-20			1.7
	196	A	G	C-34	M	V	1.3
	217	A	G	C-41	K	E	2.7
	313	A	G	C-73	N	D	2.5
	364	A	G	C-90	T	A	1.5
	410	G	A	C-105	R	K	1.0
	459	A	G	C-121	V	V	1.6
	485	A	G	prM-7	Q	R	1.9
	490	A	G	prM-9			1.3
	491	A	C	prM-9	*K	*A	1.3
	527	A	C	prM-21	D	A	1.6
	757	A	G	prM-98	T	A	1.8
	804	C	G	prM-113	D	E	2.6
	1072	A	G	E-36	K	E	3.0

	1216	A	G	E-84	K	E	1.1
	1597	U	G	E-211	F	V	1.1
	1697	A	U	E-244	E	V	1.4
	1725	A	G	E-253	I	M	1.5
	2074	A	G	E-370	K	E	1.1
	3135	A	U	NS1-222	S	S	1.6
	3488	A	C	NS1-340	H	P	3.6
	4545	G	U	NS2B-109	A	A	4.0
	4573	G	U	NS2B-119	V	L	3.4
	4597	C	U	NS2B-127	*Q	*S	1.4
	4598	A	C	NS2B-127			1.4
	4925	A	U	NS3-105	N	I	1.6
	6090	A	G	NS3-493	R	R	1.3
	6282	A	C	NS3-557	S	S	3.1
	6358	A	G	NS3-583	I	V	1.5
	7000	A	C	NS4B-29	M	L	1.1
	7584	C	G	NS4B-223	A	A	1.3
	7689	A	U	NS5-3	A	A	1.2
	7842	A	G	NS5-54	P	P	1.2
	8781	A	G	NS5-367	E	E	1.0
	10405	A	G	3' UTR	-	-	1.0
	10426	A	G	3' UTR	-	-	1.4
	10429	A	C	3' UTR	-	-	1.1
	10518	A	U	3' UTR	-	-	3.3
C102S (+ E-D114A/V139M)	3841	U	C	NS2A-106	L	L	2.5
	7020	C	U	NS4B-35	D	D	1.0
	7104	U	C	NS4B-63	D	D	5.5
	10888	U	A	3' UTR	-	-	1.8

All SNVs ≥ 1 % frequency are listed. The P1 stocks of the new NS4B-P38G (+NS4B-T116I) and NS4B-C102S mutants were analyzed, whereas a P4 and P2 stock of the historical NS4B-P38G (+NS3-N480H/NS4B-T116I) and NS4B-C102S (+E-D114A/V139M) mutants were analyzed, respectively. SNVs that encoded amino acid changes are shown in blue, and SNVs in the NS4B protein are highlighted with a grey background. *two nucleotide changes occurred simultaneously, viewed on Tablet software

Table 5.3: New NS4B mutants exhibit distinct single nucleotide variants

	Nucleotide Position	Major Nucleotide	Minor Nucleotide	Viral Protein Position	Major Residue	Minor Residue	Frequency (%)
NY99ic	2135	A	G	E-390	E	G	1.9
	904	A	U	prM-147	S	S	7.3
P54A	1435	A	G	E-157	T	A	10.7
	6347	A	G	NS3-579	E	G	23.2
	7000	A	C	NS4B-29	M	L	6.9
	7075	G	C	NS4B-54	*A	*P	13.0
	7077	C	A	NS4B-54			12.7
	7184	A	G	NS4B-90	D	G	35.7
	7189	G	A	NS4B-92	G	R	29.5
	7223	G	A	NS4B-103	*W	*Y	14.6
	7224	G	U	NS4B-103			14.3
	7420	A	C	NS4B-169	M	L	5.9
	7627	C	G	NS4B-238	L	V	7.1
	8973	A	C	NS5-431	P	P	10.6
	8973	A	U	NS5-431	P	P	6.9
	9956	U	G	NS5-759	L	R	9.6
	10342	A	C	NS5-888	M	L	8.0
	10440	A	G	3' UTR	-	-	23.6
	10464	A	G	3' UTR	-	-	2.5
	10582	G	U	3' UTR	-	-	1.4
	10814	A	U	3' UTR	-	-	1.9
P54G	117	G	A	C-7	G	G	1.2
	139	A	G	C-15	N	D	5.0
	155	G	A	C-20	G	E	7.3
	225	A	G	C-43	P	P	1.1
	320	A	G	C-75	Q	R	1.7
	330	G	A	C-78	M	I	1.4
	488	G	A	prM-8	*G	*E	2.0
	489	G	A	prM-8			1.3
	507	A	G	prM-14	V	V	1.1
	681	A	G	prM-72	S	S	1.9
	728	G	A	prM-88	R	K	3.6
	767	A	G	prM-101	E	G	1.2

	831	A	G	prM-122	V	V	2.1
	920	G	A	prM-152	R	K	1.5
	2346	A	G	E-460	I	M	1.1
	2624	A	G	NS1-52	E	G	1.1
	2788	A	G	NS1-107	T	A	1.8
	3440	A	G	NS1-324	Q	R	6.8
	3561	C	U	NS2A-12	G	G	3.0
	4113	A	G	NS2A-196	K	K	4.4
	4871	A	C	NS3-87	H	P	1.6
	4918	G	A	NS3-103	G	S	1.9
	5187	G	C	NS3-192	L	L	1.9
	5502	A	U	NS3-297	A	A	1.7
	5580	A	G	NS3-323	S	S	1.6
	6357	C	U	NS3-582	V	V	1.2
	6717	A	G	NS4A-83	G	G	4.4
	8179	A	G	NS5-167	A	G	1.1
	9681	A	G	NS5-667	G	G	1.2
	10888	U	A	3' UTR	-	-	1.2
L56A	103	A	G	C-3	K	E	2.9
	414	A	U	C-106	G	G	1.7
	417	A	G	C-107	G	G	1.8
	462	A	C	C-122	G	G	3.8
	1425	A	G	E-153	G	G	3.3
	1805	A	C	E-280	K	T	2.4
	2679	A	U	NS1-70	A	A	6.2
	2791	A	U	NS1-108	T	S	43.8
	3488	A	C	NS1-340	H	P	23.1
	6361	A	U	NS3-584	T	S	31.5
	6477	A	G	NS4A-3	I	M	2.9
	6567	A	C	NS4A-33	A	A	28.8
	8295	A	G	NS5-205	G	G	3.1
	9238	A	U	NS5-520	I	F	3.4
	10973	A	C	3' UTR	-	-	4.4
W103Y	358	C	A	C-88	L	I	1.2
	398	A	G	C-101	K	R	1.4
	715	A	U	prM-84	T	S	1.6
	722	A	G	prM-86	H	R	1.8
	840	A	G	prM-125	E	E	2.5

1454	A	G	E-163	Q	R	1.2
1459	G	A	E-165	G	R	2.3
1810	A	G	E-282	T	A	1.3
2009	A	G	E-348	D	G	1.2
2147	A	G	E-394	N	S	1.1
2485	A	C	NS1-6	I	L	1.9
2618	A	G	NS1-50	H	R	6.0
2712	G	A	NS1-81	E	E	3.6
2766	A	G	NS1-99	S	S	1.8
2773	A	G	NS1-102	K	E	2.8
3016	A	G	NS1-183	I	V	1.5
3205	A	U	NS1-246	T	S	3.3
3270	A	G	NS1-267	P	P	1.2
3279	A	G	NS1-270	E	E	3.1
3345	A	G	NS1-292	G	G	1.7
3391	A	G	NS1-308	I	V	4.6
3532	G	A	NS2A-3	A	T	1.2
3651	A	G	NS2A-42	L	L	1.0
3872	U	C	NS2A-116	M	T	1.3
3981	A	C	NS2A-152	S	S	5.8
4171	A	U	NS2A-216	M	L	6.5
4275	A	G	NS2B-19	G	G	4.4
4699	C	U	NS3-30	L	L	1.5
4970	A	G	NS3-120	E	G	2.3
5254	A	G	NS3-215	R	G	2.3
5352	A	G	NS3-247	A	A	5.0
5548	A	G	NS3-313	I	V	1.6
5670	A	U	NS3-353	T	T	1.1
5946	A	C	NS3-445	G	G	1.1
5971	A	G	NS3-454	S	G	3.6
6087	A	G	NS3-492	A	A	1.2
7058	C	U	NS4B-48	T	I	3.1
7777	A	C	NS5-33	I	L	1.8
7777	A	G	NS5-33	I	V	5.3
7814	A	G	NS5-45	K	R	1.8
7994	A	G	NS5-105	K	R	2.0
8136	A	G	NS5-152	S	S	1.2
8484	A	U	NS5-268	G	G	1.2

	8487	A	G	NS5-269	K	K	2.5
	8790	A	G	NS5-370	E	E	1.1
	8811	C	U	NS5-377	N	N	1.6
	9054	A	G	NS5-458	G	G	1.0
	9358	G	A	NS5-560	D	N	2.0
	9681	A	C	NS5-667	G	G	3.1
	9721	A	C	NS5-681	T	P	1.0
	9985	C	A	NS5-769	L	I	4.4
	10491	A	G	3' UTR	-	-	2.3
	10614	U	A	3' UTR	-	-	1.2
	10788	A	G	3' UTR	-	-	1.5
	10832	A	G	3' UTR	-	-	1.1
C102S/W103Y	106	A	G	C-4	K	E	1.8
	3930	A	C	NS2A-135	S	S	1.0

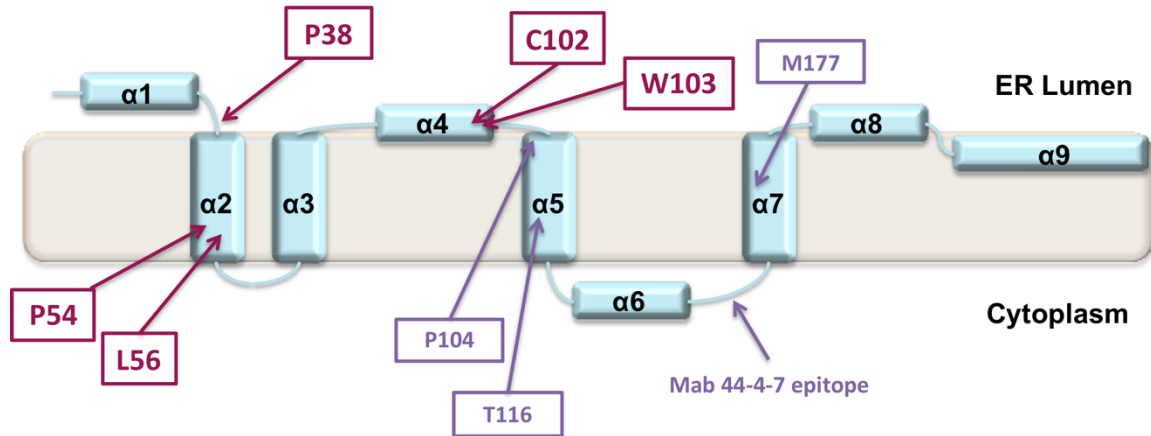
All SNVs ≥ 1 % frequency are listed. All viruses analyzed were P1 Vero cell culture stocks, except for the L56A and C102S/W103Y mutants for which the P0 stocks were analyzed. SNVs that encoded amino acid changes are shown in blue, and SNVs in the NS4B protein are highlighted with a grey background. *two nucleotide changes occurred simultaneously, viewed on Tablet software

Figure 5.1: Amino acid alignment of the N-terminal portion of NS4B of representative mosquito-borne and tick-borne flaviviruses

Mosquito	WNV	NEMGWLDKTKSDISSLFGQRIEVKENFSM--GEFLDLR↓PATAWSLYAVTTAVLT↓P↓LKH	58
	KUNV	NEMGWLDKTKSDISGLFGQRIETKENFSI--GEFLDLR↓PATAWSLYAVTTAVLT↓P↓LKH	58
	JEV	NEYGMLEXTKADLKSMFGGKTQASGLTGL--PSMALDLR↓PATAWALYGGSTVVLTP↓LKH	58
	SLEV	NEMGLETKKSDIAKLFGSQPGMGFVRTTPWDISLDIK↓PATAWALYAAATMVMT↓PLIKH	60
	ZIKV	NELGWLERTKSDIAHLMGRKEEGT----TMGFSMDIDLRLASAWAIYAALTTLIT↓PAVQH	56
	DENV-1	NEMGLETTTKKDLGIGHVA-VENH----HHATMLDVDLX↓PASAWTLYAVATTIIT↓PMMRH	55
	DENV-2	NEMGFLEKTKKDLGLGSIT-TQ-Q----PESNILDIDLRLASAWTLYAVATTFVT↓PMLRH	54
	DENV-3	NEMGLETTTKRDLGMSKEP-G-VV----SSTSylvDVLH↓PASAWTLYAVATTVIT↓PMLRH	54
	DENV-4	NEMGLIEKTKTDFGFYQVK-----TETTILDVDLRLASAWTLYAVATTILT↓PMLRH	51
	YFV	NELGMLEKTKEDLFGKKNLIPSS----ASPWSWPDLDLKPAAWTVYVGIVTMLS↓PMLHH	56
Tick	POWV	NELGYLEQTKTDISGLFRREDQGG---MVWDAWNTNIDIQ↓PARSWGTYVLIVSLFT↓PYMLH	57
	TBEV	NEMGFLEKTKADLSTALWSEREPP---RPWSEWNTNIDIQ↓PARSWGTYVLIVSLFT↓PYMLH	57
	LGTV	NEMGLEKTKADLAALFARDQGET---VRWGEWNTNIDIQ↓PARSWGTYVLIVSLFT↓PYMLH	57
	OHFV	NEMGFLEKTKADLSAVLWSEREPP---RVWSEWNTNIDIQ↓PARSWGTYVLIVSLFT↓PYMLH	57
Mosquito	WNV	LITS DYINTSLTSIN VQASALFTLARGFPFVDVGVSALLLAAG↓C↓W↓GQVTLTVTVTAATLL	118
	KUNV	LITS DYITTS LTSIN VQASALFTLARGFPFVDVGVSALLLAAG↓C↓W↓GQVTLTVTVTSATLL	118
	JEV	LITSEYVTTSLASINSQAGSLFVLPFGVPFTDLDLTVGLVFLG↓C↓W↓GQITLTVTLTAMVLA	118
	SLEV	LITTQYVNFSLTAIASQAGVLLGLTNGMPFTAMDLSVPLLVLG↓C↓W↓NQMTLPSLAAAVMLL	120
	ZIKV	AVTTSYNNYSLMAMATQAGVLFMGKGMPFYAWDFGVPLLMG↓CYSQLTPLTLIVAIILL	116
	DENV-1	TIENTTANISLTAIANQAAILMGLDKGWPI SKMDIGVPLLALG↓CYSQVNPLTLIAAVLML	115
	DENV-2	SIENSSVNVSLTAIANQATVLMGLGKGWPLSKMDIGVPLLAIG↓CYSQVNPLTLTAALFLL	114
	DENV-3	TIENSTANVSLAAIANQAIVLMGLDKGWPI SKMDIGVPLLALG↓CYSQVNPLTLAAAVLLL	114
	DENV-4	TIENTSANLSLAAIANQAIVLMGLGKGWPLHRMDLGVPLLAMG↓CYSQVNPTTLIASVLM	111
	YFV	WIKVEYGNLSLSGIAQSASVLSFMDKGIPFMKNISVILLVSG↓WNSITVMPLLCGIGCA	116
Tick	POWV	QLQTKIQRLVNSSVAAGTQAMRDLGGGTPFFGVAGHVVALGVTSLVGATPTSLALGVALA	117
	TBEV	QLQTKIQRLVNSSVAAGTQAMRDLGGGTPFFGVAGHVMTLGVVSLIGATPTSLMVGVGLA	117
	LGTV	QLQTRIQRLVNSSVAAGTQAMRDLGGGTPFFGVAGHVVALGVTSLVGATPTSLILGVGLA	117
	OHFV	QLQTRIQRLVNSSVAAGTQAMRDLGGGTPFFGVAGHVLTGLGVVSLVGATPTSLVGVGLA	117

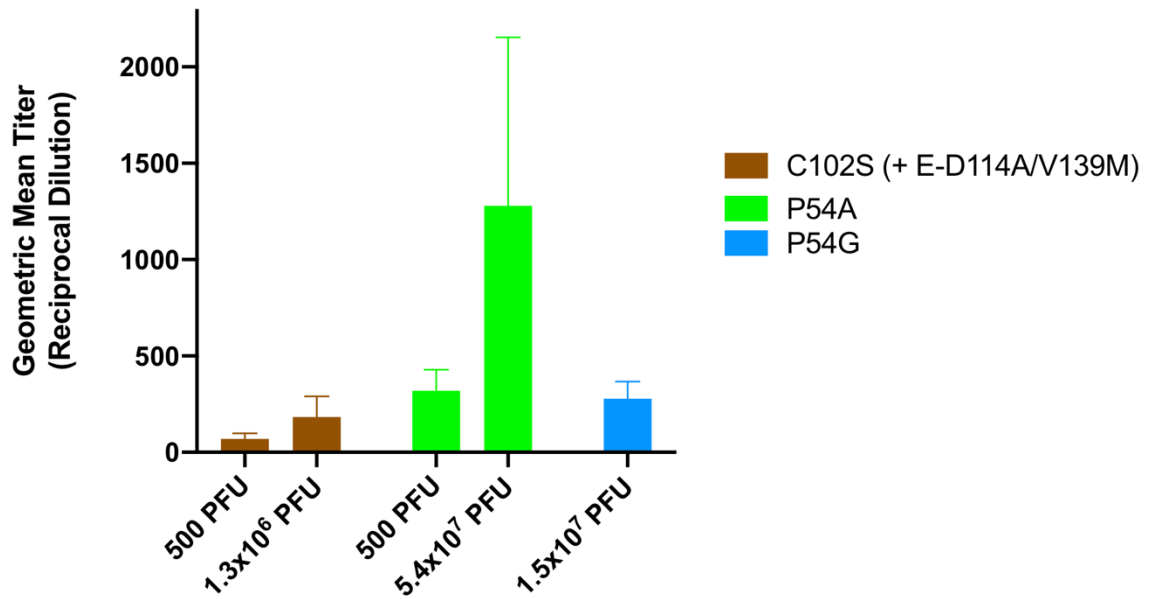
The highlighted residues in orange are the specific amino acids characterized by mutagenesis in this study and correspond to WNV NS4B P38, P54, L56, C102, and W103. The alignment was generated using Clustal Omega and virus abbreviations and Genbank accession numbers are as follows: WNV: West Nile virus (AAF20092.2); KUNV: Kunjin virus (BAA00176.1); JEV: Japanese encephalitis virus (ABQ52691.1); SLEV: Saint Louis encephalitis virus (ACT31738.1); ZIKV: zika virus (AMR39836.1); DENV-1: dengue virus 1 (AIU47321.1); DENV-2: dengue virus 2 (AAC59275.1); DENV-3: dengue virus 3 (ALS05358.1); DENV-4: dengue virus 4 (ALB78116.1); YFV: yellow fever virus (AHB63685.1); POWV: powassan virus (NP_620099.1); TBEV: tick-borne encephalitis virus (AAA86870.1); LGTV: langat virus (ACH42698.1); OFFV: Omsk hemorrhagic fever virus (NP_878909.1).

Figure 5.2: Location of different amino acid residues described in this study within the predicted structure of NS4B



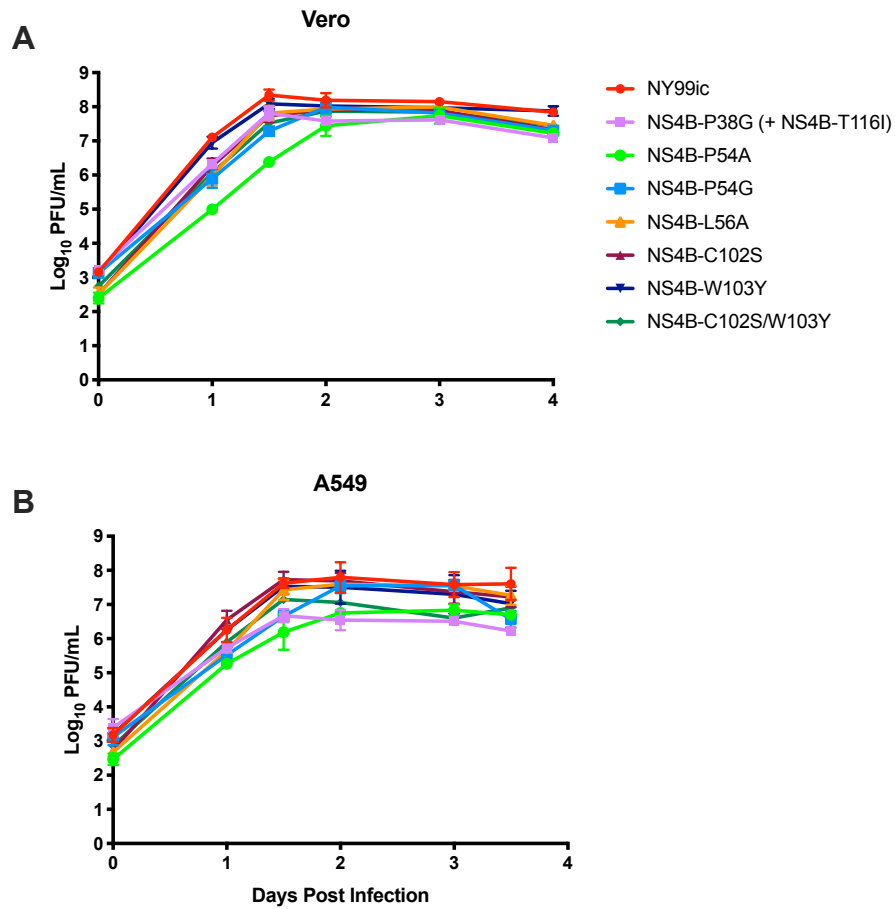
Each alpha helix is labeled as α1-α9 and locations are based on NMR studies of DENV NS4B. The amino acids mutated in this chapter are shown in magenta. Residue P38 is predicted to be within the ER lumen, nearing the first transmembrane domain. Residues P54 and L56 are both predicted to be within α2, which is the first transmembrane domain. Residues C102 and W103 are predicted to be near the C-terminal end of α4, which resides either very near or slightly within the ER membrane. Other NS4B regions of interest discussed in this chapter are shown in purple. A P104L mutation in DENV (located in α5) disrupted the interaction between NS3 and NS4B proteins (Umareddy et al., 2006). A T116I compensatory mutation (located in α5) is present in both new and old stocks of the P38G mutant. A M177L mutation (located in α7) is present in the SNVs of both new and old stocks of the P38G mutant. The epitope of the monoclonal antibody mab 44-4-7 (used for immunostaining) is indicated in purple and corresponds to amino acids 141-147 that are located in the cytoplasm (Xie et al., 2014).

Figure 5.3: The NS4B-P54 mutants exhibited a trend toward higher neutralizing antibody titers than the NS4B-C102S (+E-D114A/V139M) mutant



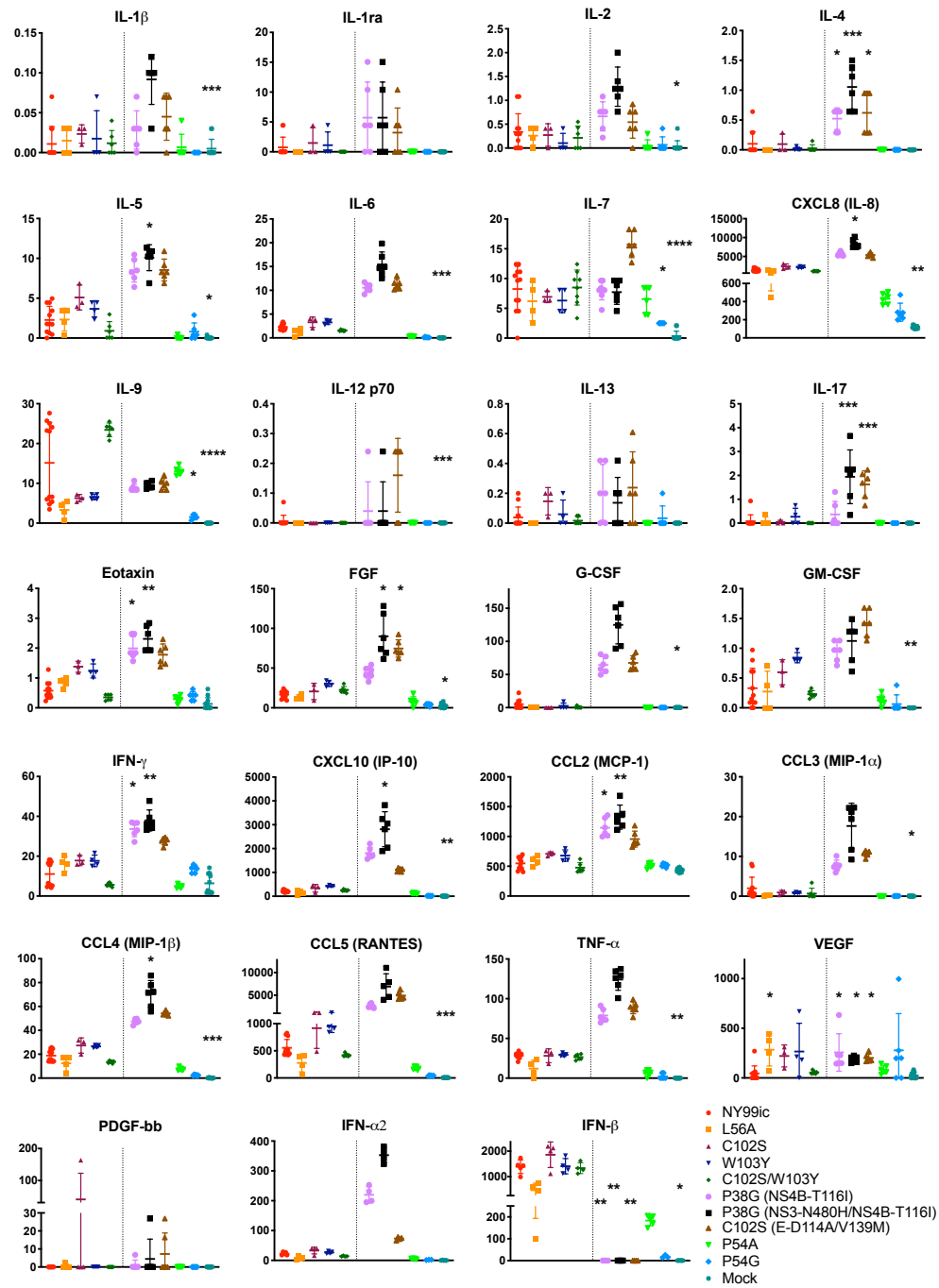
Outbred mouse serum was harvested on 36 dpi for PRNT₅₀ neutralizing antibody titration. Serum was collected from five mice in the following groups: C102S (+E-D114A/V139M) 500 PFU, C102S (+E-D114A/V139M) 1.3x10⁶ PFU, P54A 500 PFU, P54A 5.4x10⁷ PFU, and P54G 1.5x10⁷ PFU. Error bars represent the standard error of the mean.

Figure 5.4: All new NS4B mutants can multiply to high titers in both Vero and A549 cells



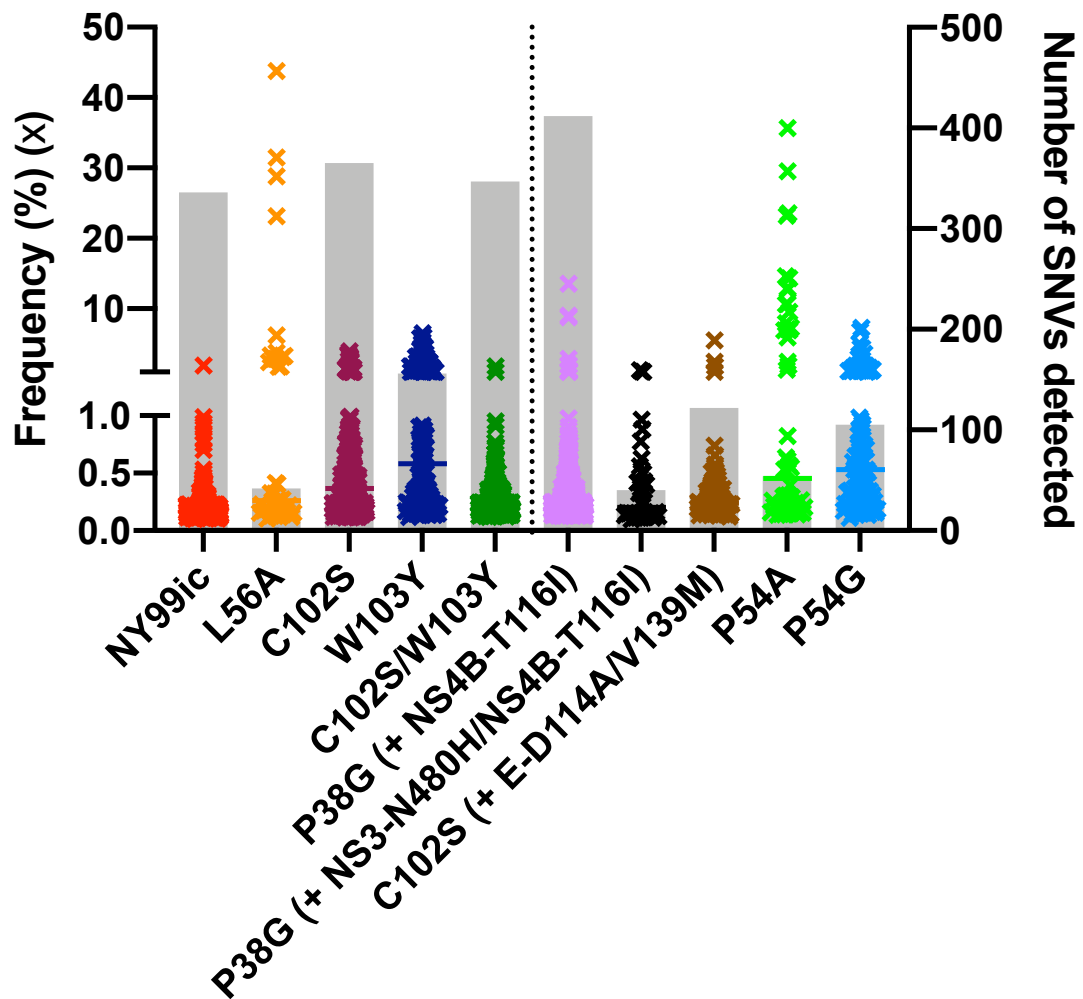
Cells were infected with a multiplicity of infection of 0.1 of each virus. Two biological replicates were infected and two samples from each flask were titrated at the time points indicated (four titrations total). n.d.= not done

Figure 5.5: Attenuated WNV NS4B mutants exhibit two different patterns of cytokine induction



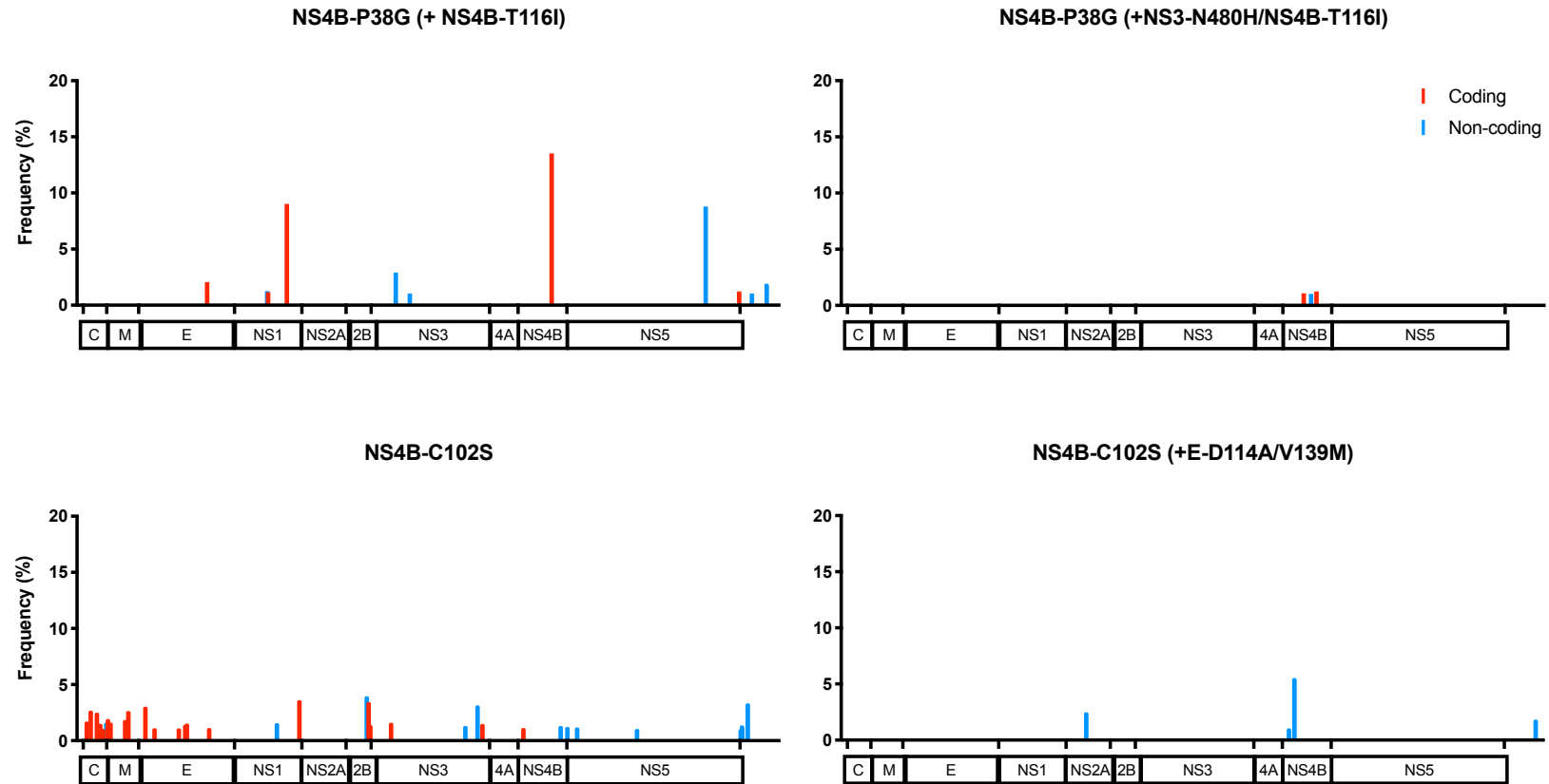
Cytokine levels produced by NS4B mutant infected cells were compared to NY99ic infected cells using a Kruskal-Wallis ANOVA with Dunn's post-hoc correction. Six replicates of each mutant and 12 replicates of NY99ic and mock were measured in pg/mL, except for IFN- α and IFN- β for which six replicates were tested for all viruses and controls. A dotted line is dividing cells infected with the virulent viruses (left) from the attenuated viruses and mock (right). *p<0.05, **p<0.01, ***p<0.001, ****p<0.0001

Figure 5.6: SNV Profiles of all NS4B mutants



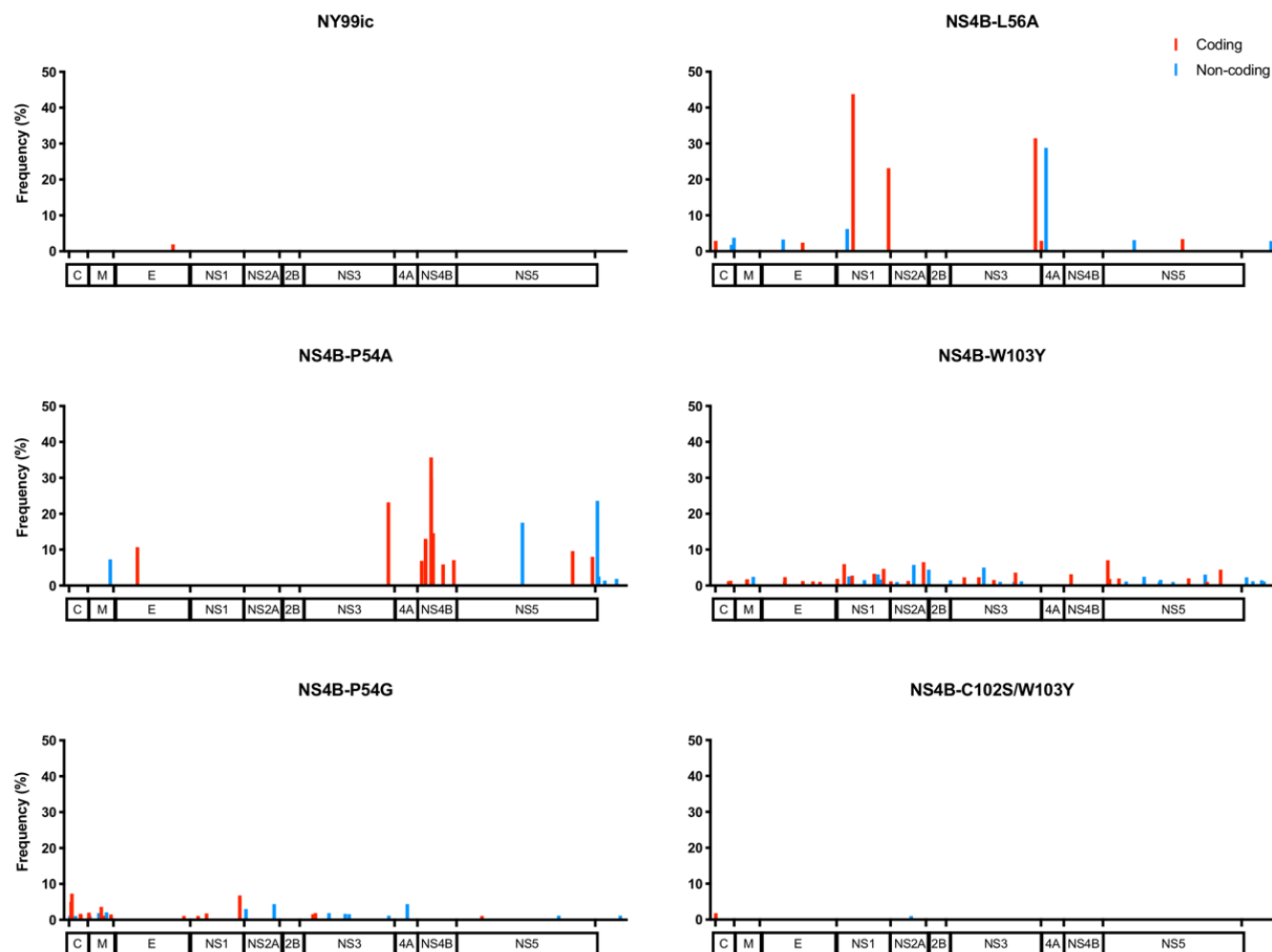
For each virus, the frequency of each SNV is indicated by an (x), and the grey bars in the background display the total number of SNVs detected. A dotted line is dividing the virulent viruses (left) from the attenuated viruses (right). Analysis was completed on the P1 Vero cell culture stocks of each mutant except for L56A and C102S/W103Y, for which analysis was done on the P0 stocks.

Figure 5.7: New and old stocks of P38G and C102S mutants have different SNV genotypes



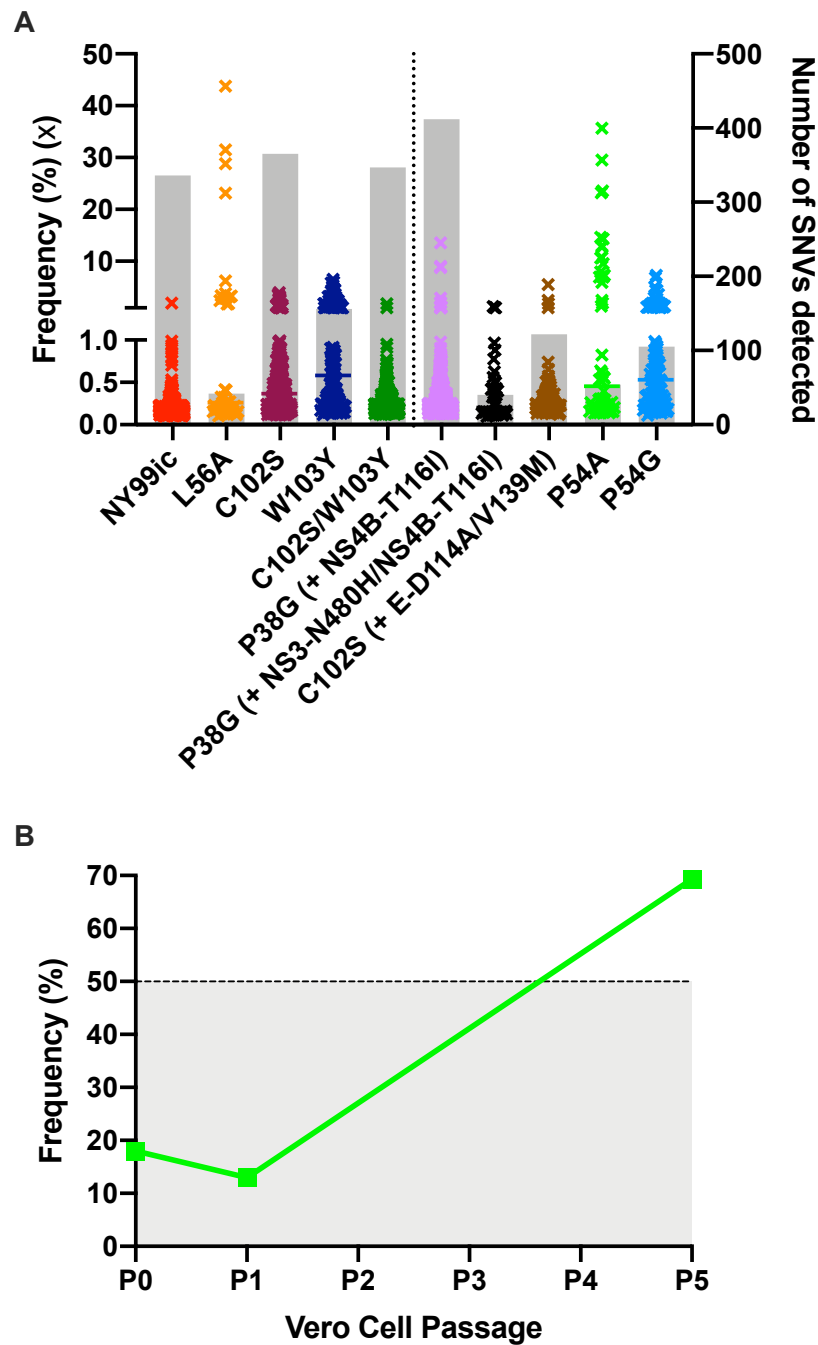
All SNVs $\geq 1\%$ frequency were plotted in the corresponding genome position. The P1 stocks of NS4B-P38G (+NS4B-T116I) and NS4B-C102S mutants were analyzed, whereas a P4 and P2 stock of the historical NS4B-P38G (+NS3-N480H/NS4B-T116I) and NS4B-C102S (+E-D114A/V139M) mutants were analyzed, respectively.

Figure 5.8: New NS4B mutants each have unique SNV genotypes



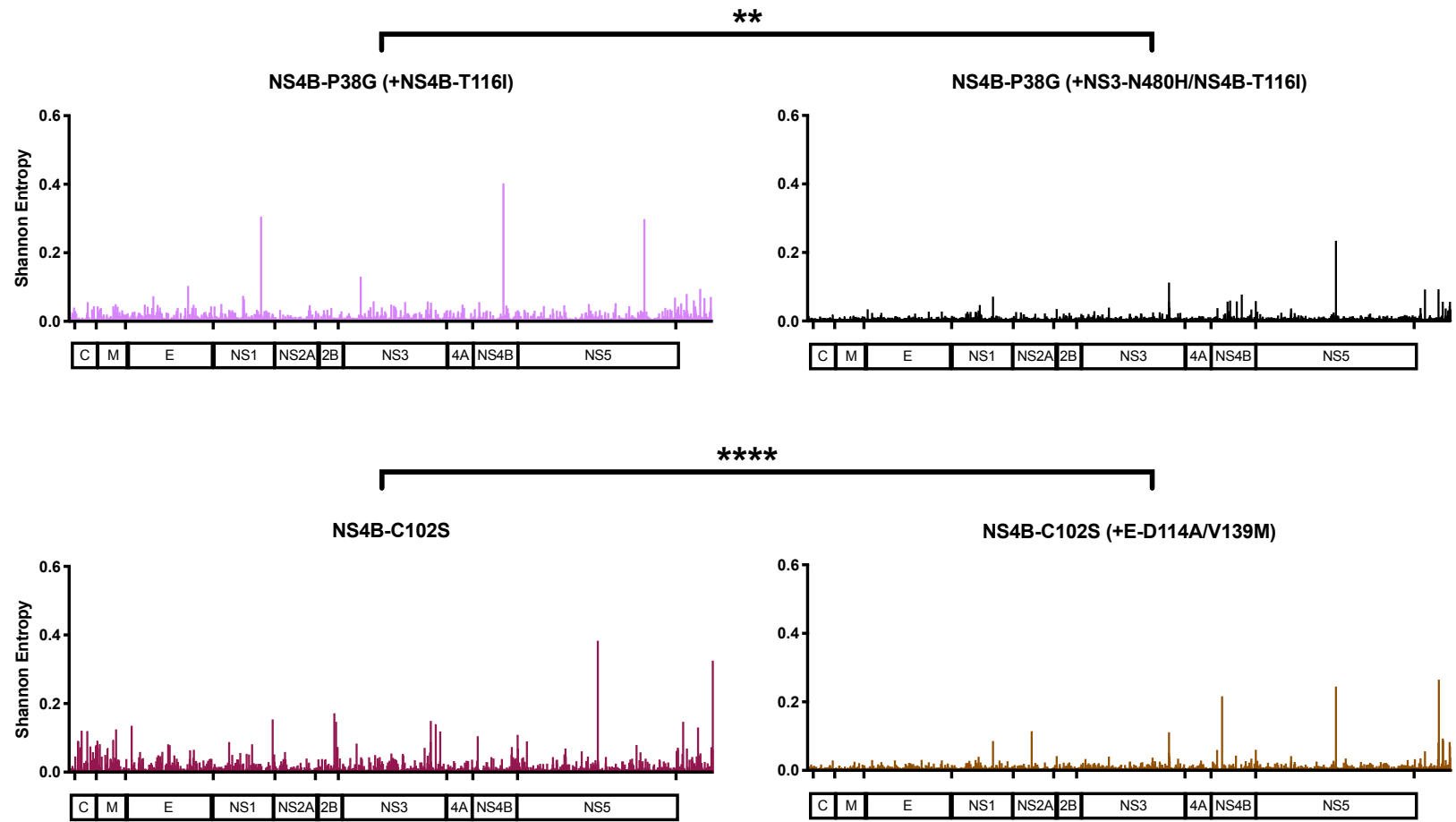
All SNVs $\geq 1\%$ frequency were plotted in the corresponding genome position. All viruses analyzed were P1 Vero cell culture stocks, except for the L56A and C102S/W103Y mutants, for which the P0 stocks were analyzed.

Figure 5.9: The NS4B-P54A mutation is capable of reversion



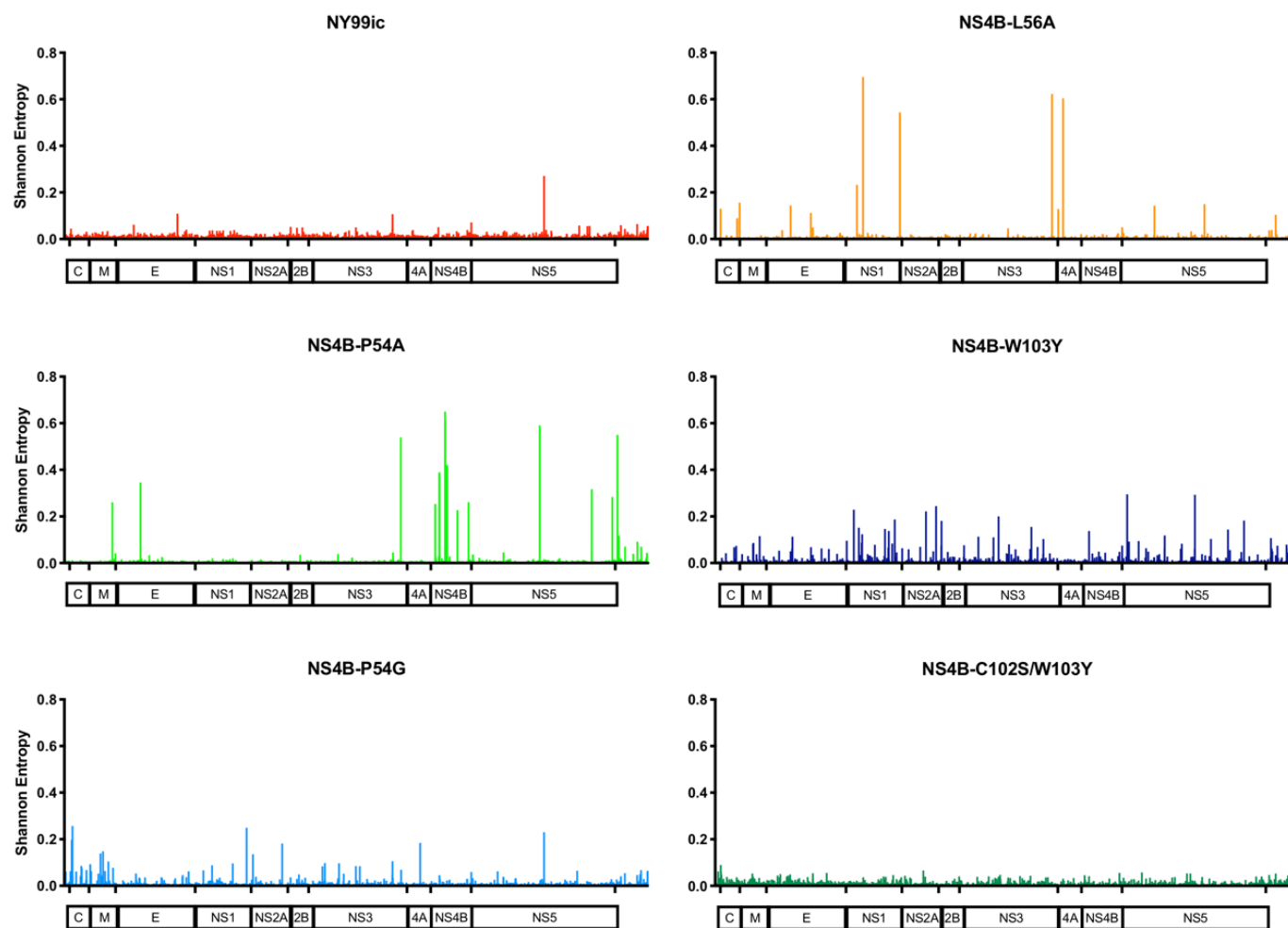
(A) All SNVs $\geq 1\%$ frequency in the NS4B gene of the P1 stock of the NS4B-P54A mutant are displayed. The amino acid mutations are indicated above each corresponding line. (B) Frequency of reversion of NS4B-A54P was measured in P0, P1, and P5 virus stocks of the P54A mutant. Points above the grey shading represent a genomic consensus sequence change.

Figure 5.10: Shannon entropy of the new P38G and C102S mutants is significantly higher than that of the historical stocks



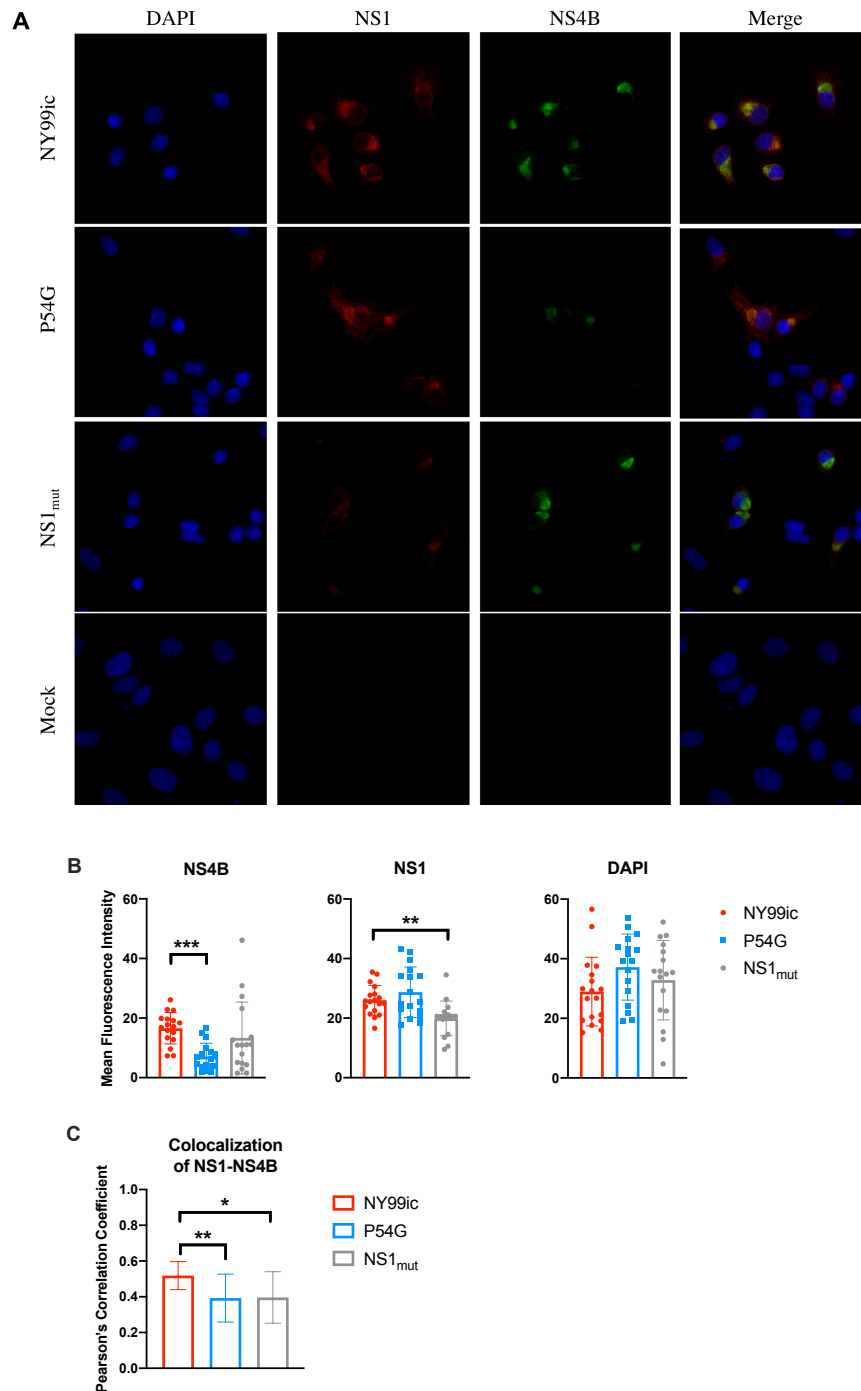
The P1 stocks of NS4B-P38G (+NS4B-T116I) and NS4B-C102S mutants were analyzed, whereas a P4 and P2 stock of the historical NS4B-P38G (+NS3-N480H/NS4B-T116I) and NS4B-C102S (+E-D114A/V139M) mutants were analyzed, respectively. Shannon entropy for the entire genome was compared between the two P38G mutants and the two C102S mutants using a Mann-Whitney test. ** $p=0.03$, **** $p<0.0001$

Figure 5.11: Shannon entropy demonstrates unique genotype diversity for each new NS4B mutant



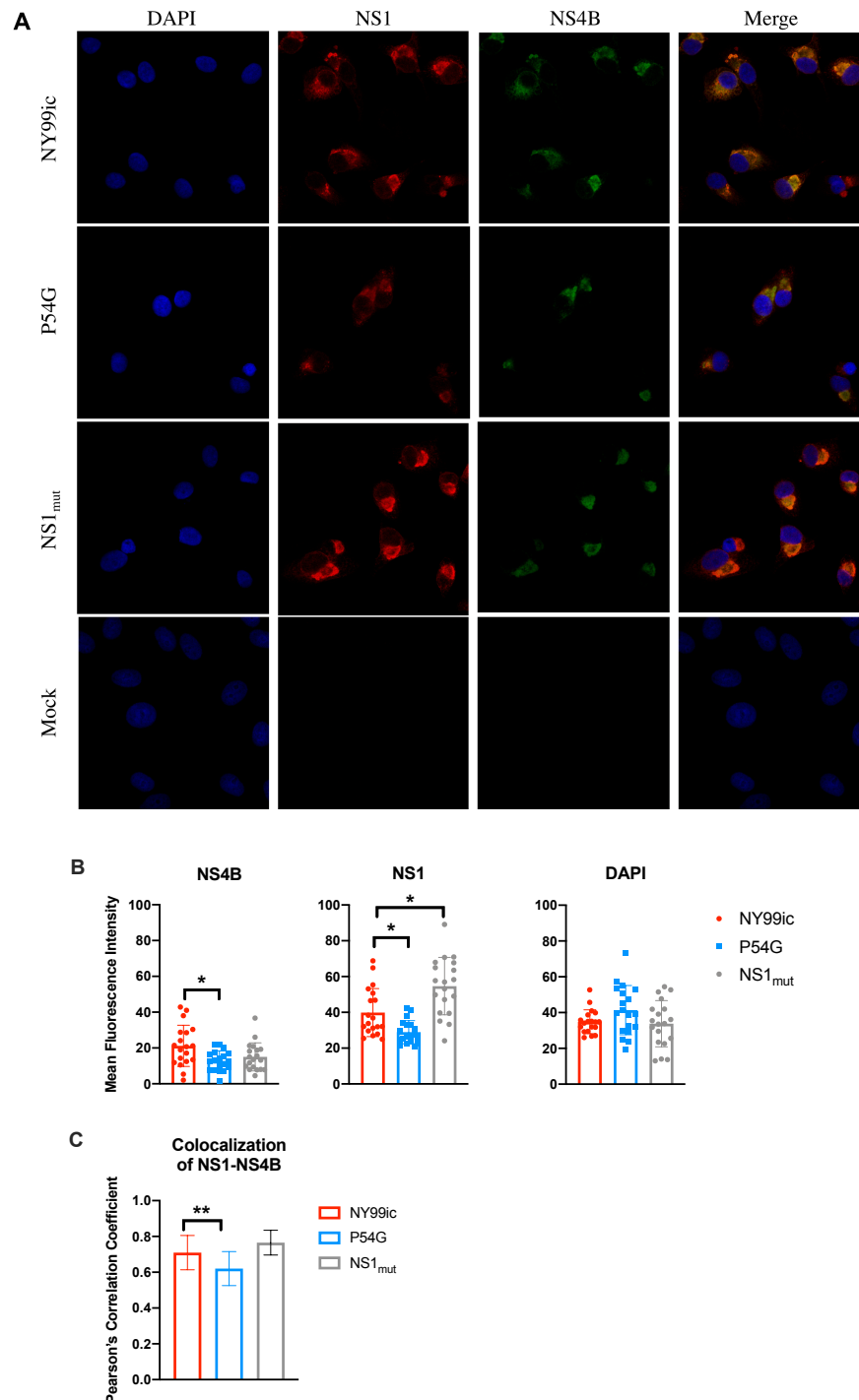
All viruses analyzed were P1 Vero cell culture stocks, except for the L56A and C102S/W103Y mutants for which the P0 stocks were analyzed.

Figure 5.12: The WNV P54G mutant had reduced NS4B accumulation and NS1-NS4B colocalization in infected cells one day post infection



Mean fluorescence intensity and Pearson's correlation coefficient were calculated on individual infected cells (n=18). Statistical differences were measured using a Kruskal-Wallis test with multiple comparisons to compare both mutants to NY99ic. *p<0.05, **p<0.01, *** p<0.001

Figure 5.13: Attenuated WNV NS4B-P54G mutant exhibited lower levels of both NS4B and NS1 two days post infection



Mean fluorescence intensity and Pearson's correlation coefficient were calculated on individual infected cells (n=19). Statistical differences were measured using a Kruskal-Wallis test with multiple comparisons to compare both mutants to NY99ic. * $p < 0.05$, ** $p < 0.1$

Chapter 6 - Combining mutations in multiple WNV genes

6.1. ABSTRACT

To make a safe WNV vaccine candidate, independently attenuating mutations across multiple viral genes should be combined so that reversion to virulence is unlikely. Past studies characterized a WNV NS1 glycosylation site mutant (NS1_{mut}) that had many of the features needed in a vaccine strain including attenuation in an animal model, induction of protective immunity, and loss of mosquito competence. This chapter describes the use of the NS1_{mut} as a backbone for a WNV vaccine by adding additional mutations in other viral genes. Specifically, NS4B-C102S, NS4B-W103Y, and E-E138K mutations were all predicted to independently attenuate WNV based on their conservation amongst flaviviruses and work undertaken in previous studies. Surprisingly, the NS4B and E protein mutations alone did not significantly attenuate the WNV mouse virulence phenotype, but each mutation had a unique impact on phenotype and genotype when inserted into the NS1_{mut} backbone. The NS1_{mut}+NS4B mutants maintained strong mouse attenuation similar to the parental NS1_{mut}, with the NS1_{mut}+NS4B-W103Y mutant displaying a trend toward increased attenuation. In comparison, the NS1_{mut}+E-E138K mutant had a loss of attenuation compared to the NS1_{mut}, and it had evidence of reversion of mutations in both the E and NS1 genes. Overall, the NS1_{mut} was a relatively stable backbone for addition of mutations in NS4B, but adding an E protein mutation caused a decrease in attenuation and genotypic stability.

6.2 INTRODUCTION

For a live, attenuated WNV vaccine to be safe, it must have a very low chance of reversion to WT virulence. For this reason, it is ideal that such a WNV vaccine harbors multiple attenuating mutations in more than one viral gene so that the overall attenuated phenotype is due to multigenic mutations that likely function by different mechanisms. The goal of this chapter was to generate and characterize multigenic mutants to determine if their overall attenuated phenotype was stronger than that of single gene mutants.

Previous studies characterized strongly attenuating mutations in the WNV NS1 protein. The NS1 protein is a unique viral protein in that, besides being localized to the ER replication complex, it is also found associated with cell membranes and secreted into the extracellular space (Akey et al., 2015a, 2015b). After translation, NS1 rapidly dimerizes and translocates into the ER lumen where it interacts with NS2A, NS4A, and NS4B transmembrane proteins (Lindenbach et al., 2007; Lindenbach and Rice, 1999; Youn et al., 2012). Dimerized NS1 is also the form typically associated with cell membranes, but secreted NS1 is most often hexameric (a trimer of dimers) (Akey et al., 2015b). Besides its essential role in viral replication, WNV NS1 is associated with antagonism of cytokine induction by suppressing activation of dsRNA sensors RIG-I and MDA5 (Zhang et al., 2017) and by inhibiting toll-like receptor 3 (TLR3) signal transduction (Wilson et al., 2008). Additionally, DENV NS1 interacts with E and impacts production of infectious viral particles, but the mechanism has yet to be determined (Scaturro et al., 2015). Extracellular NS1 can bind and antagonize components of the complement pathway (Conde et al., 2017). For DENV, extracellular NS1 is associated with production of cross-

reacting antibodies that target human proteins and are predicted to enhance disease progression (Falconar, 1997).

The crystal structure of dimeric WNV NS1 has been resolved, and three distinct domains have been identified (**Fig 6.1**). First, a β -roll domain (amino acids 1-29) is involved in dimerization and may play a role in complement antagonism and NS1-NS4B interaction (Akey et al., 2015b, 2015a; Youn et al., 2012). Second, a wing domain (amino acids 30-180) resembles the structure of RIG-I-like receptors (RLRs) (Akey et al., 2015b, 2015a). Third, an extended β -sheet, referred to as a β -ladder domain (amino acids 181-352), interferes with TLR3 antiviral signaling and may also be involved in complement antagonism (Akey et al., 2015b, 2015a; Wilson et al., 2008). Additionally, the β -ladder together with the wing domain resembles the structure of dsRNA-RLR complexes (Akey et al., 2015b, 2015a). The NS1 dimer has two distinct “faces”, an inner face and an outer face (**Fig. 6.1**). The inner face harbors the hydrophobic surface of the β -sheets and is membrane-associated (Akey et al., 2015b, 2015a). The outer face has less organized “spaghetti loop” structure and is exposed to the extracellular space (Akey et al., 2015b, 2015a). A low-resolution structure of DENV hexameric NS1 has also been determined using cryoelectron microscopy (Gutsche et al., 2011). Secreted, hexameric NS1 forms an open barrel-shaped structure with a hydrophobic central channel made up of the inner face of NS1 lined with lipid cargo that is predicted to derive from intracellular membranes (Gutsche et al., 2011).

The WNV NS1 protein harbors three N-linked glycosylation motifs at NS1 amino acids 130, 175, and 207, which are exposed on the outer face of the protein (**Fig. 6.1**) (Akey

et al., 2015b, 2015a; Whiteman et al., 2010). These motifs consist of three sequential amino acid residues including an asparagine followed by any amino acid followed by either serine or threonine (N-X-S/T). The first two glycosylation motifs are in the wing domain, with NS1-130NNT near the distal tip and NS1-175NTT in a connector domain joining the wing domain and the β -ladder. The third glycosylation motif at NS1-207NDT is in the β -ladder domain.

Mutations that simultaneously ablated the three WNV glycosylation motifs were strongly attenuating in an outbred mouse model. First, single amino acid mutations were investigated at all three motifs (NS1-N130A/N175A/N207A), and while the resulting mutant was attenuated, there was evidence of reversion at residue NS1-130 that was associated with increased mouse virulence (Whiteman et al., 2010). To stabilize the mutant, all three amino acids in the first glycosylation motif were mutated resulting in the genotype NS1-NNT130QQA/N175A/N207A (Whiteman et al., 2011), hereafter referred to as NS1_{mut}. The resulting NS1_{mut} had no evidence of reversion and was strongly attenuated for outbred mouse neuroinvasion (i.p. LD₅₀>10⁶ PFU) and neurovirulence (i.c. LD₅₀=800 PFU) (Whiteman et al., 2011). The NS1_{mut} was also protective as 50 PFU protected half of mice from a 100 LD₅₀ NY99 challenge (Whiteman et al., 2011). Additionally, the NS1_{mut} was attenuated in mosquitoes as it had reduced infectivity, dissemination, and transmission in *Cx. tarsalis* compared to NY99 (Van Slyke et al., 2013). Mechanistically, the NS1_{mut} had reduced secretion of NS1 compared to NY99, and instead the mutations caused the NS1 protein to accumulate in the ER, demonstrating a block of proper NS1 trafficking (Whiteman et al., 2015). In sum, the NS1_{mut} is a strong candidate

for a WNV vaccine as it was strongly attenuated in outbred mice, it generated a protective immune response, and it had decreased mosquito competence compared to WT WNV.

Importantly, to be used as a vaccine, the NS1_{mut} should ideally incorporate additional attenuating mutations in other viral genes to reduce the chance(s) of reversion to virulence. Previous studies evaluated an E glycosylation site mutation (E-N154S) in combination with the NS1_{mut}, however, the resulting multigenic mutant had lower i.p. LD₅₀ and i.c. LD₅₀ values (>1000 PFU and <100 PFU, respectively) compared to the NS1_{mut} alone (Whiteman et al., 2011). Besides the E-N154S mutation, no other mutations have been studied in the context of the NS1_{mut} backbone, therefore, this chapter describes investigation of three new multigenic mutants. One new mutant combined NS1_{mut}+NS4B-C102S since previous work indicated that NS4B-C102S mutation was attenuating to WNV (Wicker et al., 2006). Additionally, a NS1_{mut}+NS4B-W103Y mutant was investigated, as NS4B-W103Y was predicted to be an attenuating mutation based on its proximity to the NS4B-102 virulence determinant. Although NS4B-C102S and NS4B-W103Y did not confer attenuation of WNV (see Chapter 5), the NS1_{mut}+NS4B-C102S mutant was as attenuated as the NS1_{mut} alone, and furthermore, the NS1_{mut}+NS4B-W103Y mutant had increased attenuation compared to the NS1_{mut}. Finally, a NS1_{mut}+E-E138K mutant was characterized, as E-E138K is a key determinant of attenuation of the JEV live, attenuated vaccine SA14-14-2 (Yang et al., 2017; Zhao et al., 2005). The E-E138K mutation did not attenuate WNV in outbred mice (see Chapter 3), and moreover, this E mutation caused instability of the NS1_{mut} virus resulting in increased mouse virulence.

6.3 RESULTS

6.3.1 Generation of multigenic mutants

A new stock of the NS1_{mut} was rescued by reverse genetics, and it had the same genotype as that reported for the historical stocks (NS1-NNT130QQA/N175A/N207A) with no additional genomic consensus sequence changes. In agreement with previous studies, the NS1_{mut} had a small plaque phenotype (**Table 6.1**). As described in Chapters 3 and 5, the E-E138K, NS4B-C102S, and NS4B-W103Y mutants were each rescued with no extra coding consensus sequence changes, but the E-E138K mutant had a single non-coding nucleotide substitution (C1077U) in the consensus sequence. While the E-E138K mutant had a large plaque size, NS4B-C102S and NS4B-W103Y both had medium-sized plaques (**Table 6.1**).

The three multigenic mutants, NS1_{mut}+E-E138K, NS1_{mut}+NS4B-C102S, and NS1_{mut}+NS4B-W103Y, were each rescued with no additional genomic consensus sequence changes (**Table 6.1**). While the NS1_{mut}+E-E138K mutant had a mixed plaque size, both of the NS1+NS4B mutants had small plaque morphology (**Table 6.1**). All new mutants had similar infectivity titers ranging from 7.6-8.5 log₁₀ PFU/mL (**Table 6.1**).

6.3.2 Mouse virulence

Each new multigenic mutant was tested for attenuation of neuroinvasion by inoculating groups of outbred mice by the i.p. route with either 500 PFU or a high dose >10⁷ PFU. As described in Chapters 3 and 5, the E-E138K, NS4B-C102S, and NS4B-W103Y mutants were surprisingly not attenuated when the 500 PFU dose was administered

(**Table 6.1**). The new NS1_{mut}, as expected, had an attenuated phenotype similar to that reported in previous studies. Specifically, all mice (5/5) survived 500 PFU of the NS1_{mut} and the mice were all protected from a 10,000 PFU WT challenge administered 35 dpi (**Table 6.1**). Furthermore, when inoculated with 1.4×10^7 PFU of the NS1_{mut}, only 1/5 mice (20%) succumbed to the infection (**Table 6.1**). Both the NS1_{mut}+NS4B-C102S and NS1_{mut}+NS4B-W103Y mutants were also completely attenuated and protective at 500 PFU doses as 5/5 mice survived the initial infections and the subsequent challenge doses (**Table 6.1**). The NS1_{mut}+NS4B-C102S mutant had a similar phenotype to the NS1_{mut} in that only 1/5 (20%) mice died from a high dose of 1.3×10^7 PFU (**Table 6.1**). The NS1_{mut}+NS4B-W103Y mutant was very strongly attenuated and 100% of mice (5/5) survived from a high dose of 1.1×10^7 PFU. To confirm this result, ten more mice were inoculated with the high dose of the NS1_{mut}+NS4B-W103Y mutant and all survived (15 mice total) (**Table 6.1**). Unlike the NS1+NS4B mutants, the NS1_{mut}+E-E138K mutant demonstrated a loss of attenuation in that no (0/5) mice survived from the 500 PFU dose challenge and only 20% (1/5) of mice survived a high 1.7×10^7 PFU dose (**Table 6.1**).

Since the NS1_{mut}+NS4B-W103Y mutant had the strongest degree of mouse attenuation, serum was collected from five mice inoculated with the high 1.1×10^7 PFU dose to test for neutralizing antibodies using PRNT₅₀ assays. All five mice had detectable neutralizing antibodies, though the titer ranged from 1:160-1:2560 with a GMT of 557 and a standard error of the mean of ± 434 (**Table 6.2**). The high standard error was expected based on the variability observed in outbred mice.

6.3.3 Temperature sensitivity in Vero cells

Each mutant was tested for a TS phenotype by measuring infectivity titers using plaque assay at both 37°C and 41°C. Much like NY99ic, the E-E138K, NS4B-C102S, and NS4B-W103Y mutants did not have a significant difference of infectivity titer between the two temperatures (**Table 6.3**). For the NS1_{mut}, NS1_{mut}+NS4B-C102S, and NS1_{mut}+NS4B-W103Y mutants, plaques were smaller at 41°C than they were at 37°C; therefore, assays had to be incubated through day five (instead of day three when the plates for the remaining viruses were read) in order to allow the plaque sizes to grow large enough to be counted accurately. The NS1_{mut} and both NS1+NS4B mutants had significant TS phenotypes where each had >100-fold reduction in titer at 41°C compared to 37°C (**Table 6.3**). In comparison, the NS1_{mut}+E-E138K mutant did not have a TS phenotype, but instead it had similar infectivity titers at both temperatures (**Table 6.3**).

Since the NS1_{mut} and both NS1+NS4B mutants had unique small plaque phenotypes, additional TS assays were undertaken for these three mutants using focus forming assays to verify the results of the plaque assays. In both plaque and focus forming assays, NY99ic did not have a TS phenotype. For the NS1_{mut} and the NS1+NS4B mutants, the focus assay titers agreed with the plaque assays in that all three mutants had a significant reduction in titer at 41°C compared to 37°C (**Table 6.4**), however, the reduction in titer measured in the focus forming assays was less significant than that observed with the plaque assays (>1 log₁₀ reduction compared to >2 log₁₀). Similar to the plaque assays, the NS1_{mut} and the NS1+NS4B mutants each had smaller focus sizes at 41°C than at 37°C, whereas NY99ic had a similar focus size at both temperatures (**Fig. 6.2**). The NS1_{mut} and

the NS1_{mut}+NS4B-C102S mutant had similar focus sizes to one another, and the NS1_{mut}+NS4B-W103Y mutant had the smallest focus size of all mutants tested (**Fig. 6.2**).

6.3.4 Multiplication kinetics in Vero and A549 cells

To evaluate differences of the mutants in both IFN-I deficient and IFN-I competent cell lines, multiplication kinetics were measured in Vero and A549 cell lines, respectively. The single gene mutants and the multigenic mutants all had similar patterns of multiplication to NY99ic in Vero cells where infectivity titers peaked between 36-48 hpi and ranged from approximately 7-8 log₁₀ PFU/mL (**Fig 6.3a**). In A549 cells, the E-E138K, NS4B-C102S, and NS4B-W103Y mutants had very similar multiplication kinetics to those of NY99ic with peak titers of 7-8 log₁₀ PFU/mL at 36 hpi (**Fig 6.3b**). Alternatively, the NS1_{mut} and the two NS1+NS4B mutants had strongly reduced infectivity titers compared to NY99ic at all time points between 24-84 hpi (>1000-fold lower than NY99ic), with peak titers of approximately 4-5 log₁₀ PFU/mL at 36 hpi (**Fig 6.3b**). The NS1_{mut}+E-E138K did not have the strong attenuation of multiplication kinetics in A549 cells associated with the NS1_{mut}, although it did have infectivity titers approximately 10-fold lower than NY99ic between 36-84 hpi (**Fig 6.3b**).

6.3.5 A549 cell cytokine response

To measure differences in cytokine production between the single gene mutants and multigenic mutants, A549 cell supernatants were collected at 36 hpi and used in a

BioPlex Pro Human 27-Plex assay and a custom IFN- α and IFN- β 2-Plex assay. Of 29 total cytokines measured, IL-10 and IL-15 were not detected at all and the remaining 27 cytokines were detected to varying degrees in the virus-infected cell supernatants.

For nearly all of the cytokines detected (25/27), the single gene mutants NS4B-C102S, NS4B-W103Y, E-E138K and NS1_{mut} induced similar levels to those induced by NY99ic (**Fig. 6.4**). For IL-6, the NS1_{mut} induced significantly less than NY99ic ($p=0.03$) (**Fig. 6.4**), albeit, the NS1_{mut} had approximately 1000-fold lower titer than NY99ic, which may impact cytokine induction (**Fig. 6.3b**). For CXCL10, the NS4B-W103Y mutant induced significantly more than NY99ic ($p=0.04$) (**Fig. 6.4**).

In terms of the multigenic mutants, 21/27 of the cytokines detected had no significant difference from the levels produced by NY99ic. The NS1_{mut}+NS4B-C102S mutant induced significantly higher IFN- γ compared to NY99ic ($p=0.03$) (**Fig. 6.4**), which is notable considering that the mutant had approximately 1000-fold lower titer. The NS1_{mut} and NS1_{mut}+NS4B-W103Y mutants also induced more IFN- γ than NY99ic, however, the differences were not statistically significant (**Fig. 6.4**). The remaining five cytokines that were significantly different when comparing the multigenic mutants to NY99ic were all detected in NS1_{mut}+E-E138K mutant cell supernatant. Specifically, the NS1_{mut}+E-E138K mutant induced significantly higher levels of CXCL10 ($p=0.0005$), CCL4 ($p=0.02$), CCL5 ($p=0.0009$), VEGF ($p=0.02$), and PDGF-BB ($p=0.02$) compared to NY99ic (**Fig. 6.4**). Though differences in PDGF-BB were calculated, it was only detectable in 2/6 replicate samples of the NS1_{mut}+E-E138K mutant supernatant, so the results for this cytokine may not be reproducible. Several other cytokines were upregulated by the NS1_{mut}+E-E138K

mutant including IL-9, FGF, G-CSF, TNF- α , IFN- α 2, and IFN- β , but the differences were not statistically significant (**Fig. 6.4**). Overall, the NS1_{mut}+E-E138K mutant had a unique trend of increased induction of multifunctional cytokines and chemokines compared to NY99ic.

6.3.6 Intracellular staining of NS1 and NS4B

Since the NS1_{mut}+NS4B-W103Y mutant had the strongest mouse attenuation and also had a unique small plaque phenotype, additional studies were completed to better understand how this multigenic mutant differed from the single gene NS1_{mut} and NS4B-W103Y mutants. Localization and fluorescence intensities of NS1 and NS4B proteins were compared using fluorescence microscopy in Vero cells infected with NY99ic, the single gene NS1_{mut} and NS4B-W103Y mutants, the multigenic NS1_{mut}+NS4B-W103Y mutant, or PBS as a mock infection.

At 24 hpi, the NS1_{mut} and NS1_{mut}+NS4B-W103Y mutants had fewer infected cells than NY99ic and the NS4B-W103Y mutant (**Fig. 6.5a**), and this was not surprising based on the approximate 10-fold difference in viral titer at this time point (**Fig. 6.3a**). For all of the mutants, NS1 and NS4B were localized in the perinuclear region, but NS1 also had diffuse staining throughout the cell that was most apparent in NY99ic and NS4B-W103Y infected cells (**Fig. 6.5a**). To compare the staining of NS1 and NS4B, the mean fluorescence intensity was measured for both fluorophores in 17 infected cells from each group. Additionally, Pearson's correlation coefficient (PCC) was utilized to measure the degree of colocalization between NS1 and NS4B in each infected cell where 0 indicates no

colocalization and 1 indicates perfect colocalization. Both NY99ic and the NS4B-W103Y mutant had similar fluorescence of both NS1 and NS4B (**Fig. 6.5b**), and they had similar PCC values averaging at approximately 0.5 (**Fig. 6.5c**). The NS1_{mut} virus had significantly lower intensity of NS1 staining compared to NY99ic ($p=0.01$), but the staining of NS4B for the NS1_{mut} virus was not different than that observed in NY99ic-infected cells (**Fig. 6.5b**). The NS1_{mut} also had significantly reduced colocalization of NS1 and NS4B compared to NY99ic where the average PCC was approximately 0.4 ($p=0.04$) (**Fig. 6.5c**). The NS1_{mut}+NS4B-W103Y mutant had significantly reduced staining of both NS4B ($p<0.0001$) and NS1 ($p=0.001$) compared to NY99ic (**Fig. 6.5b**). Additionally, this multigenic mutant had reduced colocalization of NS1 and NS4B compared to NY99ic as the average PCC was <0.4 ($p=0.01$) (**Fig. 6.5c**). Overall, at 24 hpi, the NS1_{mut}+NS4B-W103Y mutant had a phenotype that was distinct from either of the single gene mutants.

The same analysis was completed on samples from 48 hpi, however, different patterns were observed (**Fig. 6.6a**). Specifically, the NS4B-W103Y mutant had significantly reduced staining of NS4B ($p=0.0004$) but not of NS1 (**Fig. 6.6b**). Additionally, this mutant had reduced colocalization of NS1 and NS4B with an average PCC of approximately 0.6 compared to 0.7 for both NY99ic and the NS4B-W103Y mutant ($p=0.009$) (**Fig. 6.6c**). The NS1_{mut} had significantly stronger staining of NS1 than NY99ic at 48 hpi ($p=0.0007$) (**Fig. 6.6b**), which was consistent with published observations that the NS1_{mut} does not properly secrete NS1 (Whiteman et al., 2015), however the NS4B staining was similar to that in NY99ic-infected cells and there was no difference in NS1/NS4B colocalization (**Fig. 6.6c**). Finally the NS1_{mut}+NS4B-W103Y mutant was not

statistically different from NY99ic at this time point for any of the parameters measured (**Figs. 6.6b and 6.6c**). In sum, the multigenic NS1_{mut}+NS4B-W103Y mutant had unique reductions in accumulation and colocalization of both NS1 and NS4B at 24 hpi, but these differences were no longer evident at 48 hpi.

6.3.7 Analysis of virus quasispecies using NGS

To determine if the multigenic mutations altered the viral quasispecies diversity compared to either NY99ic or the single gene mutants, NGS was utilized to interrogate the quasispecies population of Vero cell culture stocks of each mutant. Specifically, two methods were utilized including single nucleotide variant (SNV) analysis and Shannon entropy calculation. For all viruses, except for the NS4B-W103Y mutant, the P0 stock rescued directly after transfection was utilized for the sequencing analysis. For the NS4B-W103Y mutant, the Vero cell P1 stock was analyzed, as the P0 stock of this mutant was not sequenced using NGS because the consensus sequence of this mutant was confirmed only on the P1 stock that was tested in mouse studies. For the NS1_{mut}+NS4B-W103Y and NS1_{mut}+E-E138K mutants, data for the P1 stocks are also described to expand upon observations from the analysis of the P0 stocks.

6.3.7.1 ANALYSIS OF SINGLE NUCLEOTIDE VARIANTS (SNVs)

SNVs in each virus stock were measured using LoFreq, and the total number and frequency of SNVs detected are shown in **Fig. 6.7**. There was no apparent pattern

distinguishing the single gene mutants from the multigenic mutants nor was there a specific pattern of SNVs associated with an attenuated phenotype. Rather, each mutant had a distinct profile of SNVs. To focus on the most significant SNVs, only those that were present at $\geq 1\%$ frequency were analyzed in more detail (**Table 6.5**). NY99ic had no SNVs present at $\geq 1\%$ frequency, indicating that the WT clone was fairly stable in Vero cells (**Fig. 6.8**). Similarly, the virulent NS4B-C102S mutant had only two SNVs present $\geq 1\%$ frequency, one in NS2A (1.1%) and one in the 3' UTR (1.7%) (**Table 6.5, Fig. 6.8**). The virulent NS4B-W103Y mutant analyzed in this chapter was previously described in Chapter 5, and this mutant had 55 SNVs $\geq 1\%$ frequency that ranged from 1.0-6.5%, none of which encoded any changes at NS4B-103 (**Table 5.3, Fig. 6.8**). Additionally, the E-E138K virus stock analyzed in this chapter was previously described in Chapter 3, and this mutant had 30 SNVs $\geq 1\%$ frequency (**Table 3.3, Fig. 6.9**). These SNVs ranged from 1.1-14.2% frequency and 67% (20/30) were present in the E gene, with the highest frequency SNV encoding reversion of E-K138E (**Table 3.3, Fig. 6.9**). The NS1_{mut} had 48 SNVs detected $\geq 1\%$ frequency ranging from 1.0-3.4% (**Table 6.5, Fig. 6.8**). These were dispersed throughout the genome, and none encoded substitutions at any of the NS1 glycosylation motif mutations.

In terms of the multigenic mutants, the NS1_{mut}+NS4B-C102S had a similar genotype to the NS1_{mut}. Specifically, there were 37 SNVs $\geq 1\%$ frequency throughout the genome ranging from 1.1-6.3%, and none encoded reversion of the NS1 glycosylation motif mutations nor residue NS4B-102 (**Table 6.5, Fig. 6.8**). Although the NS1_{mut}+NS4B-W103Y mutant had a similar attenuated phenotype to the NS1_{mut} and NS1_{mut}+NS4B-

C102S mutants, it had a distinct SNV genotype. Specifically, the NS1_{mut}+NS4B-W103Y mutant had 20 SNVs $\geq 1\%$ frequency, but many were high frequency compared to the other mutants analyzed (**Table 6.5, Fig. 6.8**). The SNVs ranged from 1.1-23.1%, with three above 20% frequency (**Table 6.5, Fig. 6.8**). Two of the three highest frequency SNVs encoded an E-E150W mutation (20.1%), and the other was a non-coding nucleotide change in residue NS1-282 (23.1%) (**Table 6.5**). The P1 stock of this mutant was also investigated, and of 17 SNVs $\geq 1\%$ frequency, the E-E150W and NS1-282 SNVs were maintained at 16.8% and 19.7% frequency, respectively, plus the P1 virus had an additional non-coding high frequency SNV at residue NS5-92 (20.4%) that increased after passage (**Table 6.6**). Finally, the NS1_{mut}+E-E138K mutant also had notably high frequency SNVs with a total of 27 SNVs detected $\geq 1\%$ frequency and ranging from 1.0-47.5% (**Table 6.5, Fig. 6.9**). Of the 27 SNVs, 37% (10/27) were present in the E gene and 30% (8/27) were present in the NS1 gene (**Table 6.5**). Importantly, there was evidence of reversion of residue E-K138E (8.9%) as well as evidence of mutations at the NS1 glycosylation site residues (**Table 6.5**). The first glycosylation motif, NS1-NNT130QQA, had a SNV encoding NS1-Q131R mutation in 45.7% of the population (**Table 6.5**). This SNV did not restore glycosylation at the motif, but it mutated NS1-130QQA to NS1-130QRA. The second glycosylation motif, NS1-NTT175ATT, had SNVs that encoded reversion back to asparagine at residue NS1-175 in 22.7% of the population, restoring the WT genotype (**Table 6.5**). Similarly, the third glycosylation motif, NS1-NDT207ADT, had SNVs that encoded reversion of NS1-A207N in 30.6% of the population that restored the WT genotype (**Table 6.5**). To summarize, while SNVs in the first NS1 glycosylation motif

(NS1-130) did not restore the N-X-T glycosylation site, SNVs at both the second (NS1-175) and third (NS1-207) glycosylation motifs encoded reversion that restored the motifs by replacing the mutant alanine with the WT asparagine residues. In the P1 stock of the NS1_{mut}+E-E138K mutant, each of the SNV reversions were maintained at a high frequency (**Table 6.6**). Specifically, frequency of E-K138E reversion increased to 26.9% of the population (**Table 6.6**). NS1-QQA130QRA mutation decreased in frequency to 30% of the population in the P1 stock (**Table 6.6**). NS1-ATT175NTT reversion increased in frequency to 25.2%, and NS1-ADT207NDT reversion maintained 30.4% frequency of the population that was similar to that in the P0 stock (**Table 6.6**).

6.3.7.2 SHANNON ENTROPY ANALYSIS

To support the findings of the SNV analysis, Shannon entropy was used to measure absolute nucleotide heterogeneity as an alternative measurement of quasispecies diversity. The NY99ic and the virulent NS4B-C102S mutant each had relatively low Shannon entropy across the entire genome, supporting the hypothesis that these viruses were relatively stable in Vero cells (**Fig. 6.10**). Similar to the observed patterns of SNV frequency (**Fig. 6.8**), the virulent NS4B-W103Y mutant had higher entropy across the genome compared to NY99ic, but the increased diversity wasn't localized to any specific region of the genome (**Fig. 6.10**). The virulent E-E138K mutant, on the other hand, had increased entropy that was most prominent in the E gene (**Fig. 6.10**). Similarly, the virulent NS1_{mut}+E-E138K mutant had increased entropy, with the most apparent clusters of high nucleotide diversity in the E and NS1 genes specifically (**Fig. 6.10**).

For the attenuated mutants, the NS1_{mut} and NS1_{mut}+NS4B-C102S mutants had moderately increased Shannon entropy compared to NY99ic, with peaks of diversity dispersed across the genome (**Fig. 6.10**). While the attenuated NS1_{mut}+NS4B-W103Y mutant had relatively low entropy throughout most of the genome, there were high peaks of entropy that occurred in each viral gene except for C, NS4A, and NS4B (**Fig. 6.10**). The peaks of entropy in this mutant did not cluster in any specific region of the genome.

Overall, the Shannon entropy analysis was in agreement with the patterns observed in the SNV analysis (**Figs. 6.8-6.10**). Specifically, Shannon entropy correlated with SNV frequency for each mutant.

6.4 DISCUSSION

This chapter provided an important proof of concept: that mutations can be added into the NS1_{mut} backbone and generate a viable virus. Although the hypothesis that the NS4B-C102S, NS4B-W103Y, and E-E138K mutations would be independently attenuating to WNV was incorrect, investigation of these mutations in the context of the NS1_{mut} provided critical insight into the stability of the NS1_{mut} glycosylation site mutations as well as possible function(s) that these residues may have.

It was apparent in *in vitro* multiplication kinetics, TS assays, and cytokine quantification that both NS1_{mut}+NS4B mutants were both adopting an attenuated phenotype similar to that of the NS1_{mut}. Specifically, these mutants each had strongly reduced multiplication kinetics in A549 cells, were significantly TS, and induced a similar pattern of low IL-6/high IFN- γ production. Similarities were also observed *in vivo* as the

NS1_{mut}+NS4B mutants maintained the mouse attenuated phenotype associated with the NS1_{mut}. Additional studies are needed to elucidate the mechanism of restricted multiplication kinetics in A549 cells for these attenuated mutants, but since A549 cells are competent in IFN-I signaling and Vero cells are not, it is possible that the NS1_{mut} increases WNV susceptibility to the antiviral effects of IFN-I. While the levels of IFN-I (IFN- α 2 and IFN- β) produced were not statistically different between NY99ic and the NS1_{mut}/NS1_{mut}+NS4B mutants, there was a trend toward reduced IFN- β production by the attenuated mutants. Additionally, the three attenuated mutants induced relatively high levels of IFN- γ , indicating that type II interferon could play a role in the observed attenuated/protective phenotypes. Previous studies have demonstrated the essential role of IFN- γ in protection from WNV disease in mice (Shrestha et al., 2006b).

While the NS1_{mut}+NS4B mutants had several similarities to the NS1_{mut}, the NS1_{mut}+NS4B-W103Y mutant was unique in that its plaque/focus size was smaller than that of the NS1_{mut} and NS1_{mut}+NS4B-C102S mutants. Furthermore, the NS1_{mut}+NS4B-W103Y mutant exhibited a trend toward stronger mouse attenuation than the NS1_{mut}. To investigate how this multigenic mutant may be different than either of the single gene mutants, confocal microscopy was used to visualize patterns in NS1 and NS4B staining. The multigenic NS1_{mut}+NS4B-W103Y mutant had a unique phenotype where there was decreased fluorescence of both NS1 and NS4B compared to NY99ic at 24 hpi, but this phenotype was not observed for either of the single gene mutants. Since NS1 and NS4B interact, it is possible that the combination of mutations in NS1 and NS4B can act synergistically to enhance attenuation of WNV. The residues in NS4B that are responsible

for the interaction with NS1 have not been fully elucidated, but NS4B-F86 is one residue implicated to be involved (Youn et al., 2012). Like NS4B-86, NS4B-103 is oriented toward the ER lumen side of the NS4B protein, where the observed NS1-NS4B interaction is predicted to occur (**Fig. 6.11**). In the NS1 protein, the glycosylation sites are on the outer face of the protein that is oriented toward the ER lumen, while the inner face harboring the hydrophobic β -roll domain is associated with interaction with the ER membrane. Specifically, NS1-N10 and NS1-K11 residues are important for the interaction with NS4B (Youn et al., 2012), however, additional interacting residues in NS1 have not yet been identified. Based on the orientation of the glycosylation sites, it is hypothesized that these residues are not directly involved in the NS1-NS4B interaction. However, glycosylation may impact protein folding, and thus, ablation of the NS1 glycosylation sites could alter NS1 folding and interaction with NS4B. This hypothesis is supported by the observed decrease in NS1-NS4B colocalization in cells infected with the NS1_{mut} and NS1_{mut}+NS4B-W103Y mutants. It is possible that the NS1_{mut} has decreased interaction with NS4B and that the NS4B-W103Y mutation exacerbates this effect, however, additional studies are needed to address the NS1-NS4B interaction in detail.

In addition to having a unique plaque phenotype and enhanced *in vivo* attenuation, the NS1_{mut}+NS4B-W103Y mutant was also distinct from the NS1_{mut} and NS1_{mut}+NS4B-C102S mutants in that it had a unique quasispecies genotype with higher frequency variants and higher peaks of Shannon entropy. While there was no evidence of reversion of the mutated residues in NS1 or NS4B, the increased diversity could suggest that the mutant is not stable. Since the NS1_{mut}+NS4B-W103Y mutant seemed to be more strongly attenuated

than the NS1_{mut} alone, it is possible that the combination of mutations is causing increased quasispecies diversity to attempt to restore the parental phenotype. It is not clear why the NS4B-W103Y mutation had unique effects on the NS1_{mut}, but the neighboring mutation, NS4B-C102S, did not notably change the NS1_{mut} phenotype or genotype. WT strains of other flaviviruses including DENV and ZIKV already have a tyrosine at the homologous residue to WNV NS4B-103, and while tyrosine substitution at this residue did not attenuate mouse virulence of WNV using a 500 PFU dose, it did reduce the plaque size and uniquely reduce the staining of NS4B and the NS1-NS4B interaction compared to NY99ic at 48 hpi, indicating that it could mildly attenuate WNV. One consideration is that it has been shown that NS4B dimerizes in DENV infected cells (Zou et al., 2014), but since WT DENV strains already have a tyrosine at the residue homologous to WNV NS4B-103, it is unlikely that tyrosine mutation in WNV alters NS4B dimerization. Moreover, the cytoplasmic loop (amino acids 129-165) and C-terminal region (amino acids 166-248) of NS4B are associated with dimer formation, whereas the region containing NS4B-103 was not (Zou et al., 2014). Additional studies are warranted to better understand how NS4B-W103Y mutation impacts WNV both alone and in the context of the NS1_{mut} backbone.

Unlike the NS1+NS4B mutants, the NS1_{mut}+E-E138K mutant did not maintain the attenuated NS1_{mut} phenotype in *in vitro* nor *in vivo* studies. Based on the quasispecies analysis, it is hypothesized that this mutant did not exhibit mouse attenuation due to the evidence of reversion of mutations in both the E and NS1 genes. As described in Chapter 3, the E-E138K mutation is capable of reversion, and this correlated with a mouse virulence phenotype. However, it was surprising to find that the E-E138K mutation also induced

reversion at NS1 glycosylation site mutations that were otherwise stable (e.g. in the NS1_{mut} and NS1+NS4B mutants). One possibility is that the interaction between NS1 and E proteins was disrupted by the combination of mutations, resulting in an increase in quasispecies diversity. The exact function of NS1-E interaction is not known, however, it has been shown in DENV-2-infected cells that ablation of this interaction decreases production of infectious viral particles (Scaturro et al., 2015). The authors speculated that possible functions could include that either NS1 is important for viral particle formation, it may assist membrane budding, or it may facilitate conformational changes that are required for the envelopment of nucleocapsid (Scaturro et al., 2015). It is not known which residues in the E protein are important for interaction with NS1, but NS1-114 and NS1-115 in the distal tip of the wing domain (near the glycosylation motif at NS1-130-132) are implicated to be involved (Scaturro et al., 2015). On the other hand, NS1-180 is near the second glycosylation motif (NS1-175-177) in the connector region of the wing domain and β -ladder domains, but NS1-180 was not involved in the E-NS1 interaction (Scaturro et al., 2015). Finally, NS1-301, in the distal tip of the β -ladder was also not involved in NS1-E interaction (Scaturro et al., 2015). It is significant that a previous study evaluating the first generation of the NS1_{mut}, where only the first asparagine in each glycosylation motif was mutated with alanine substitution (NS1-N130A/N175A/N207A), reported that this mutant was unstable and that virus isolated from mice had reversion at residue NS1-130 that correlated with other consensus sequence changes in the E protein (E-M204V and E-E237G) (Whiteman et al., 2010, 2011). Additional findings in this chapter that pertain to the NS1-E interaction include that the NS1_{mut}+NS4B-W103Y mutant had a prominent E-

E150W SNV in 20.1% of the population. Furthermore, of all the SNVs $\geq 1\%$ in the NS1_{mut}+E-E138K mutant, the majority (67%) were in the E and NS1 proteins. The different E protein residues that have been associated with prominent changes in the context of the NS1 glycosylation site mutations (138, 150, 204, and 237) are in diverse regions of the E protein. Specifically, E-138 and E-150 are in DI of the E protein, while E-204 and E-237 are in DII (**Fig. 6.12**). Since none of these residues are structurally near one another in the E protein monomer, it is not clear if mutation of each of these residues impacts interaction with NS1, and whether or not they would impact interaction by the same mechanisms. While these findings support that the NS1_{mut} interferes with the interaction between NS1 and the E protein, additional studies are needed to understand if the NS1 glycosylation sites directly have an impact on the interaction with E, and additionally, if E-E138K mutation alters the interaction with NS1.

One important observation of the multigenic NS1_{mut}+E-E138K mutant was that mutation of all three amino acids in a glycosylation motif was more stable than single amino acid mutations. Specifically, glutamine substitution of NS1-NNT130QQA did not revert to WT and glycosylation was not restored at this site, whereas alanine substitution of only the first asparagine in the motifs at NS1-175 and NS1-207 was capable of reversion to WT. Even though this same instability was not observed in the other multigenic mutants, it provided evidence that the NS1_{mut} backbone could be further stabilized. Specifically, glutamine substitution of the second and third glycosylation motifs (so that each was mutated to QQA) could provide a more stable vaccine backbone that would be predicted to be less likely to revert to virulence.

Overall, although the NS4B-C102S, NS4B-W103Y, and E-E138K mutations engineered into the NS1_{mut} backbone were not independently attenuating, the multigenic mutants each provided insight into the phenotype and genotype of the NS1 glycosylation site mutations. The NS1_{mut} had a dominant phenotype and genotype when combined with the NS4B mutations, however, when combined with the E mutation there was a loss of attenuation and of genotypic stability. Importantly, the NS1_{mut} remains a good candidate for further WNV vaccine development, however, attenuating mutations in other viral genes should still be investigated in the context of the NS1_{mut} backbone, and additional mutation of the NS1 glycosylation sites should be undertaken to stabilize the mutations and prevent reversion to virulence.

Table 6.1: Consensus genotypes, plaque phenotypes, and mouse attenuation of new multigenic mutants compared to the parental single gene mutants

Mutant	Additional consensus mutations	Plaque size	Survived 500 PFU i.p. (%)	#AST	Survived 10,000 PFU challenge (%)	High dose (PFU)	Survived high dose (%)
NY99ic	-	large	0/10 (0)	9.0±1.3	n.d.	n.d.	n.d.
NS4B-C102S	-	medium	0/15 (0)	8.5±3.1	n.d.	n.d.	n.d.
NS4B-W103Y	-	medium	0/5 (0)	9.8±2.4	n.d.	n.d.	n.d.
E-E138K	C1077U (non-coding)	large	0/5 (0)	9.4±1.3	n.d.	8.2x10 ⁷	0/5 (0)
NS1-NNT130QQA/N175A/N207A (NS1 _{mut})	-	small	5/5 (100)	>35	5/5 (100)	1.4 x10 ⁷	4/5 (80)
NS1 _{mut} +NS4B-C102S	-	small	5/5 (100)	>35	5/5 (100)	1.3 x10 ⁷	4/5 (80)
NS1 _{mut} +NS4B-W103Y	-	small	5/5 (100)	>35	5/5 (100)	1.1 x10 ⁷	15/15 (100)
NS1 _{mut} +E-E138K	-	mixed	0/5 (0)	11.6±1.5	n.d.	1.7 x10 ⁷	1/5 (20)

Mutants were rescued in Vero cells and passaged once to make the stocks for mouse studies. Outbred mice were utilized to investigate attenuation of neuroinvasion. n.d.=not done. AST=average survival time. #ASTs were calculated for mice that died only. A Kruskal-Wallis test indicated that the ASTs of the mutants were not statistically different than NY99ic.

Table 6.2: Outbred mice inoculated with the NS1_{mut}+NS4B-W103Y mutant develop neutralizing antibodies by 35 dpi

	PRNT₅₀ titer
Mouse 1	2560
Mouse 2	640
Mouse 3	160
Mouse 4	320
Mouse 5	640

Serum was isolated 35 dpi from mice inoculated with 1.1×10^7 PFU of the mutant. PRNT₅₀ titers listed represent the reciprocal serum dilution

Table 6.3: The NS1_{mut} and NS1+NS4B mutants are significantly temperature sensitive in plaque-forming assays

Virus	37° C	41° C	Δ titer	ANOVA
NY99ic	7.2	7.0	0.2	ns
NS4B-C102S	7.6	7.6	0.0	ns
NS4B-W103Y	7.8	7.5	0.3	ns
E-E138K	8.5	8.4	0.1	ns
NS1 _{mut}	8.1	5.4	2.7	****
NS1 _{mut} +NS4B-C102S	8.1	5.4	2.7	****
NS1 _{mut} +NS4B-W103Y	8.3	6.0	2.3	****
NS1 _{mut} +E-E138K	7.6	7.3	0.3	ns

Infectivity titers are listed as log₁₀ PFU/mL and represent the average of two replicates at each temperature. Temperature sensitivity significance was measured using a one-way ANOVA with Bonferroni's correction for multiple comparisons. ns=not significant, ****p<0.0001

Table 6.4: The NS1_{mut} and NS1+NS4B mutants exhibit temperature sensitive phenotypes in focus-forming assays

Virus	37° C	41° C	Δ titer	ANOVA
NY99ic	7.2	7.0	0.2	ns
NS1 _{mut}	7.8	6.8	1.0	* p=0.01
NS1 _{mut} +NS4B-C102S	8.0	6.6	1.2	* p=0.002
NS1 _{mut} +NS4B-W103Y	7.5	6.7	0.8	* p=0.03

Infectivity titers are listed as log₁₀ PFU/mL and represent the average of two replicates at each temperature. Significance was tested using ANVOA with Bonferroni's correction for multiple comparisons. ns=not significant

Table 6.5: The P0 stocks of single gene and multigenic mutants each had distinct SNVs detected $\geq 1\%$ frequency

	Nucleotide Position	Major Nucleotide	Minor Nucleotide	Viral Protein Position	Major Residue	Minor Residue	Frequency (%)
C102S	3673	A	U	NS2A-50	T	S	1.1
	10888	U	A	3' UTR	-	-	1.7
NS1_{mut}	127	A	U	C-11	S	C	1.1
	418	A	G	C-108	K	E	1.3
	604	G	A	prM-47	D	N	1.2
	1120	A	U	E-52	N	Y	1.0
	1192	A	G	E-76	T	A	2.0
	1468	A	C	E-168	S	R	1.2
	1630	A	U	E-222	N	Y	2.7
	1653	A	G	E-229	G	G	1.8
	2062	A	C	E-366	T	P	1.2
	2112	A	U	E-382	S	S	3.2
	2134	G	A	E-390	*E	*N	2.2
	2136	A	C	E-390			2.2
	2262	A	U	E-432	G	G	2.7
	2322	A	G	E-452	S	S	1.6
	2433	A	C	E-489	G	G	3.4
	2534	A	C	NS1-22	H	P	2.0
	3480	A	U	NS1-337	P	P	2.8
	3570	C	G	NS2A-15	V	V	1.0
	4572	A	C	NS2B-118	S	S	1.7
	5025	A	U	NS3-138	P	P	2.6
	5070	A	U	NS3-153	G	G	1.1
	5254	A	C	NS3-215	R	R	2.7
	5363	A	G	NS3-251	E	G	2.7
	5547	A	U	NS3-312	A	A	1.7
	6048	G	A	NS3-479	T	T	1.0
	6783	C	G	NS4A-105	A	A	1.2
	7184	A	C	NS4B-90	D	A	1.4
	7212	A	C	NS4B-99	A	A	2.4
	7356	G	A	NS4B-147	K	K	2.4
	7470	A	U	NS4B-185	A	A	1.2
	7655	A	G	NS4B-247	N	S	1.4
	8025	A	C	NS5-115	L	L	2.5

NS1 _{mut} +NS4B-C102S	8119	A	C	NS5-147	I	L	1.5
	8583	A	C	NS5-301	P	P	1.2
	8849	A	G	NS5-390	E	G	2.6
	8953	A	C	NS5-425	R	R	1.2
	9100	A	C	NS5-474	R	R	1.5
	9195	A	C	NS5-505	S	S	1.9
	9601	A	C	NS5-641	T	P	2.1
	9754	G	C	NS5-692	V	L	1.4
	10068	A	C	NS5-796	G	G	1.9
	10117	G	A	NS5-813	D	N	1.4
	10120	A	C	NS5-814	M	L	1.0
	10212	A	C	NS5-844	S	S	1.6
	10320	A	U	NS5-880	G	G	1.8
	10399	A	U	3' UTR	-	-	1.1
	10633	A	U	3' UTR	-	-	2.5
	10705	A	C	3' UTR	-	-	1.7
	56	A	G	5' UTR	-	-	2.4
	106	A	G	C-4	K	E	6.1
	155	G	U	C-20	G	V	4.3
	360	A	U	C-88	L	L	1.8
	716	C	A	prM-84	T	K	1.3
	905	G	A	prM-147	S	N	2.3
	1179	A	G	E-71	K	K	1.5
	1426	A	G	E-154	N	D	1.8
	1784	A	G	E-273	E	G	1.3
	1804	A	G	E-280	K	E	1.5
	1943	A	G	E-326	E	G	1.4
	2135	A	G	E-390	E	G	3.6
	2946	A	U	NS1-159	G	G	2.4
	3337	A	G	NS1-290	S	G	1.3
	4122	A	U	NS2A-199	G	G	6.3
	4590	A	G	NS2B-124	I	M	1.4
	5118	A	G	NS3-169	E	E	1.2
	5251	A	G	NS3-214	N	D	2.2
	5309	C	A	NS3-233	A	D	4.0
	5522	A	G	NS3-304	K	R	3.2
	5559	A	G	NS3-316	T	T	1.7
	5830	A	G	NS3-407	I	V	1.5

	6004	A	G	NS3-465	N	D	1.1
	6282	A	G	NS3-557	S	S	2.5
	6450	C	U	NS3-613	D	D	1.6
	7000	A	U	NS4B-29	M	L	4.1
	7128	A	C	NS4B-71	S	S	4.0
	8197	C	U	NS5-173	H	Y	1.7
	8250	A	U	NS5-190	K	N	6.3
	8415	A	G	NS5-245	E	E	2.1
	9183	A	U	NS5-501	G	G	2.1
	9365	A	G	NS5-562	E	G	2.9
	9601	A	C	NS5-641	T	P	1.2
	10126	G	A	NS5-816	E	K	1.6
	10161	A	U	NS5-827	E	D	2.6
	10169	A	U	NS5-830	E	V	2.8
	10661	C	U	3' UTR	-	-	4.5
NS1 _{mut} +NS4B-W103Y	26	A	G	5' UTR	-	-	11.4
	127	A	G	C-11	S	G	1.5
	621	A	G	prM-52	E	E	5.9
	1072	A	G	E-36	K	E	13.2
	1414	G	U	E-150	*E	*W	20.1
	1415	A	G	E-150			20.2
	1552	A	U	E-196	I	F	3.9
	1894	A	C	E-310	K	Q	1.6
	1943	A	G	E-326	E	G	13.1
	2365	G	A	E-467	A	T	1.1
	2796	A	G	NS1-109	E	E	14.1
	3315	A	U	NS1-282	G	G	23.1
	4051	A	G	NS2A-176	I	V	4.4
	4504	A	G	NS2B-96	K	E	11.3
	5723	A	U	NS3-371	E	V	15.5
	5971	A	G	NS3-454	S	G	4.0
	7956	A	G	NS5-92	A	A	13.5
	8438	A	U	NS5-253	Q	L	15.7
	9516	A	G	NS5-612	L	L	12.8
	10440	A	G	3' UTR	-	-	5.6
NS1 _{mut} +E- E138K	879	A	U	prM-138	A	A	5.4
	969	C	G	E-1	F	L	1.1
	1131	G	C	E-55	E	D	6.6

1177	A	C	E-71	K	Q	3.6
1216	A	G	E-84	K	E	1.8
1350	A	U	E-128	R	S	1.0
1372	A	C	E-136	K	Q	11.7
1378	G	A	E-138	K	E	8.9
1445	G	A	E-160	G	E	2.7
1652	G	A	E-229	G	E	4.8
2261	G	A	E-432	G	E	1.0
2698	A	U	NS1-77	T	S	1.4
2861	A	G	NS1-131	Q	R	45.7
2865	C	G	NS1-132	A	A	47.5
2992	A	G	NS1-175	*A	*N	22.8
2993	A	C	NS1-175			22.7
3088	A	G	NS1-207	A	N	30.6
3089	A	C	NS1-207			31.0
3189	C	A	NS1-240	D	E	2.5
5887	A	G	NS3-426	S	G	1.0
5952	A	C	NS3-447	P	P	1.0
6462	A	G	NS3-617	G	G	1.1
6632	C	U	NS4A-55	A	V	10.8
6976	A	G	NS4B-21	I	V	4.6
8034	U	C	NS5-118	S	S	1.3
8407	A	C	NS5-243	R	R	1.6
10419	A	G	3' UTR	-	-	1.8

All SNVs ≥ 1 % frequency are listed. All viruses analyzed were P0 Vero cell culture stocks. SNVs for the NS4B-W103Y and E-E138K mutants are listed in Tables 5.3 and 3.3, respectively. SNVs that encoded amino acid changes are shown in blue. *two nucleotide changes occurred simultaneously, viewed on Tablet software

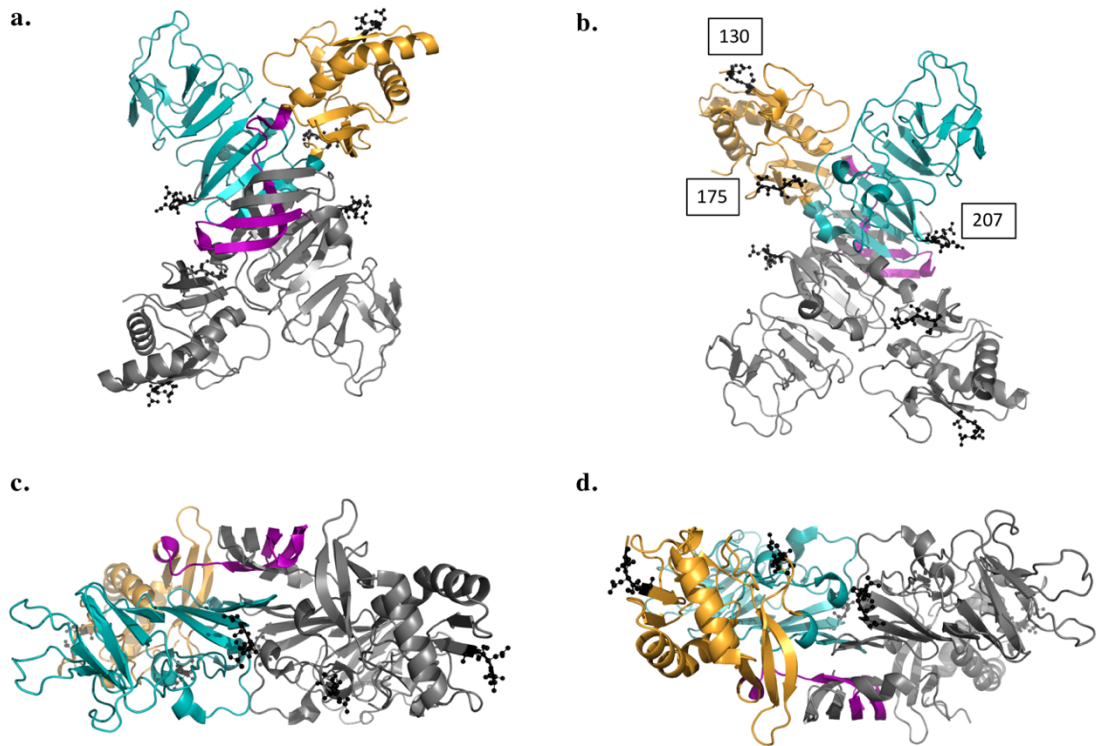
Table 6.6: The NS1_{mut}+NS4B-W103Y and NS1_{mut}+E-E138K mutants maintain high frequency SNVs after a single passage in Vero cells

	Nucleotide Position	Major Nucleotide	Minor Nucleotide	Viral Protein Position	Major Residue	Minor Residue	Frequency (%)
NS1 _{mut} +NS4B-W103Y	26	A	G	5' UTR	-	-	9.7
	621	A	G	prM-52	E	E	9.6
	1072	A	G	E-36	K	E	3.7
	1414	G	U	E-150	*E	*W	16.8
	1415	A	G	E-150			16.9
	1552	A	U	E-196	I	F	3.2
	1943	A	G	E-326	E	G	2.9
	2796	A	G	NS1-109	E	E	4.2
	3315	A	U	NS1-282	G	G	19.7
	4051	A	G	NS2A-176	I	V	4.4
	4504	A	G	NS2B-96	K	E	11.1
	5723	A	U	NS3-371	E	V	4.1
	5971	A	G	NS3-454	S	G	3.7
	7956	A	G	NS5-92	A	A	20.4
	8438	A	U	NS5-253	Q	L	4.4
	9516	A	G	NS5-612	L	L	3.7
	10440	A	G	3' UTR	-	-	10.2
NS1 _{mut} +E-E138K	879	A	U	prM-138	A	A	3.2
	1131	G	C	E-55	E	D	23.2
	1177	A	C	E-71	K	Q	4.0
	1372	A	C	E-136	K	Q	28.6
	1374	G	U	E-136	K	N	1.7
	1378	G	A	E-138	K	E	26.9
	1445	G	A	E-160	G	E	4.8
	1652	G	A	E-229	G	E	2.8
	1887	G	U	E-307	K	N	2.8
	2861	A	G	NS1-131	Q	R	35.0
	2865	C	G	NS1-132	A	A	36.6
	2992	A	G	NS1-175	*A	*N	25.2
	2993	A	C	NS1-175			25.3
	3088	A	G	NS1-207	A	N	30.4
	3089	A	C	NS1-207			30.7
	3189	C	A	NS1-240	D	E	1.1
	5952	A	C	NS3-447	P	P	1.2

6632	C	U	NS4A-55	A	V	27.7
6976	A	G	NS4B-21	I	V	4.6
8034	U	C	NS5-118	S	S	3.4
10814	A	U	3' UTR	-	-	1.4

All SNVs ≥ 1 % frequency are listed. Both viruses analyzed were P1 Vero cell culture stocks. SNVs that encoded amino acid changes are shown in blue. *two nucleotide changes occurred simultaneously, viewed on Tablet software

Figure 6.1: The structure of the WNV NS1 dimer reveals three distinct domains



The structure of the WNV NS1 dimer is displayed with one monomer colorized based on the three domains and the other monomer in grey. The magenta indicates the β -roll domain (amino acids 1-29), gold indicates the wing domain (amino acids 30-180), and cyan indicates the β -ladder domain (amino acids 181-352). NS1 has an inner face (a.) that associates with membranes and an outer face (b.) that is exposed to the extracellular space. The glycosylation motifs are shown in black and are denoted on the outer face with the corresponding amino acid residues 130, 175, and 207. The membrane-associated inner face is shown oriented to the top (c.) or bottom (d.) from a side view.

Figure 6.2: Focus size of the NS1_{mut} and NS1+NS4B mutants is reduced at 41°C compared to 37°C

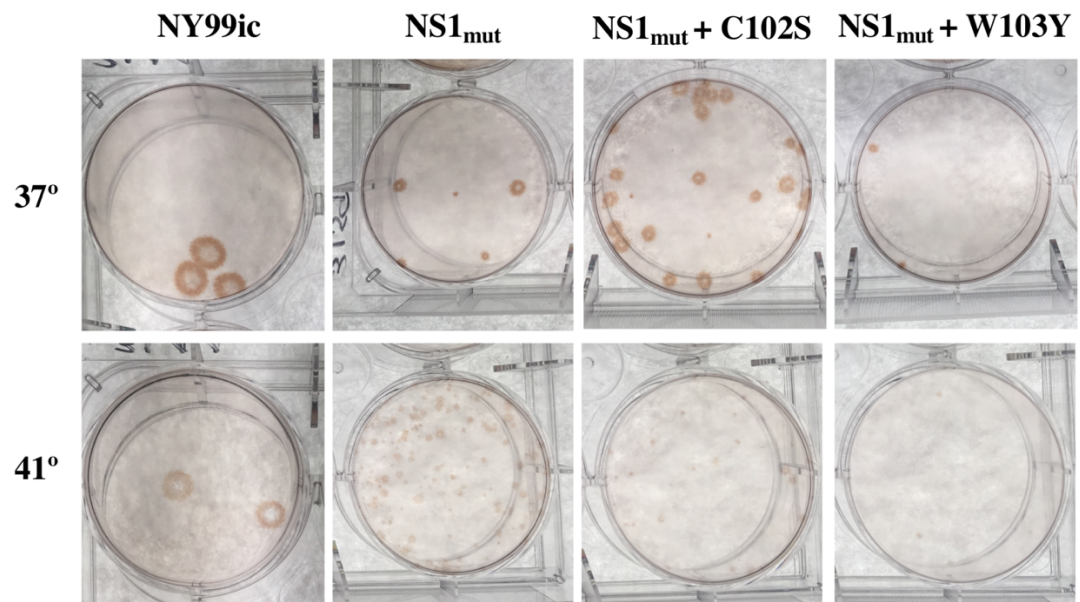
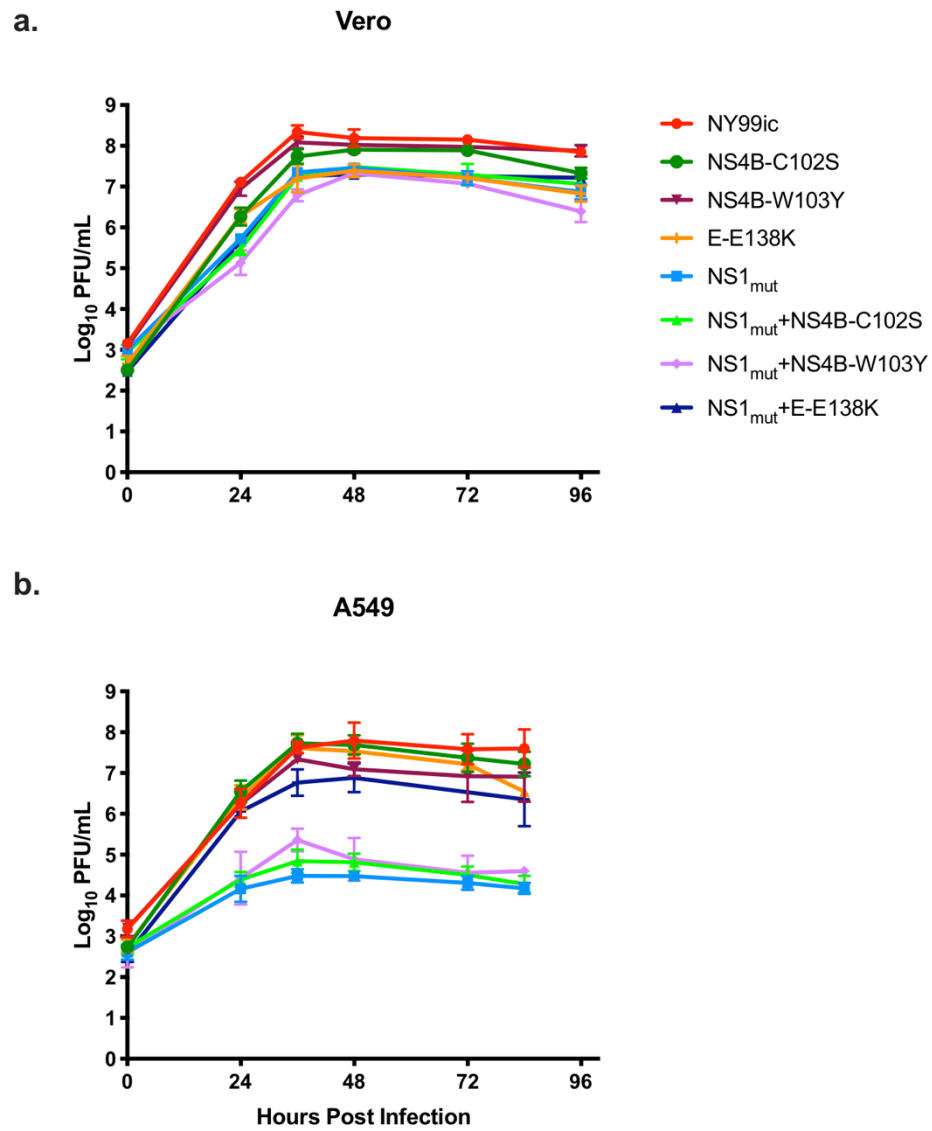
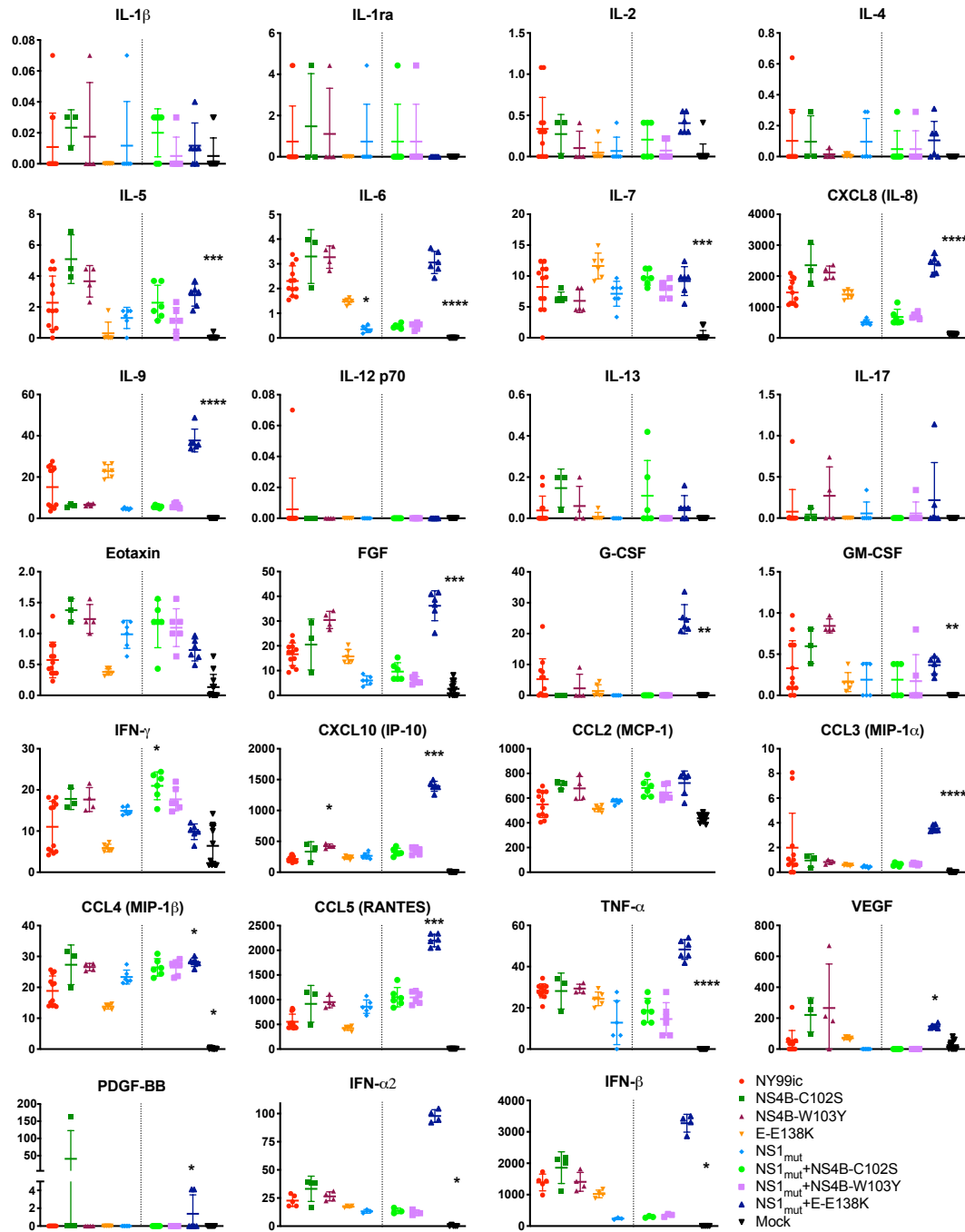


Figure 6.3: The NS1_{mut} and NS1+NS4B mutants had strongly reduced multiplication kinetics in A549 cells



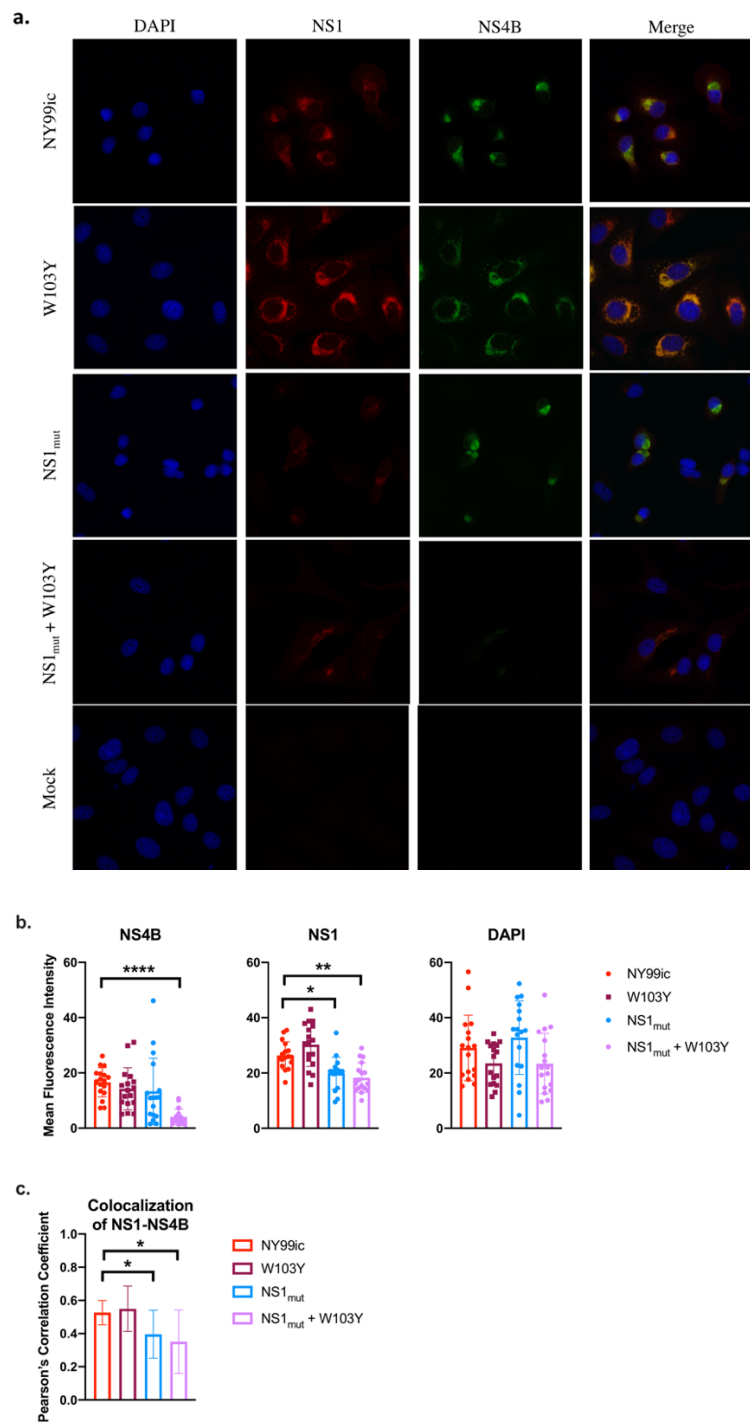
Cells were infected with a multiplicity of infection of 0.1 of each virus. Two biological replicates were infected and two samples from each flask were titrated at the time points indicated. n.d.= not done

Figure 6.4: The NS1+NS4B mutants induced cytokines similar to the NS1_{mut}, but the NS1+E mutant had a unique phenotype of cytokine induction in A549 cells



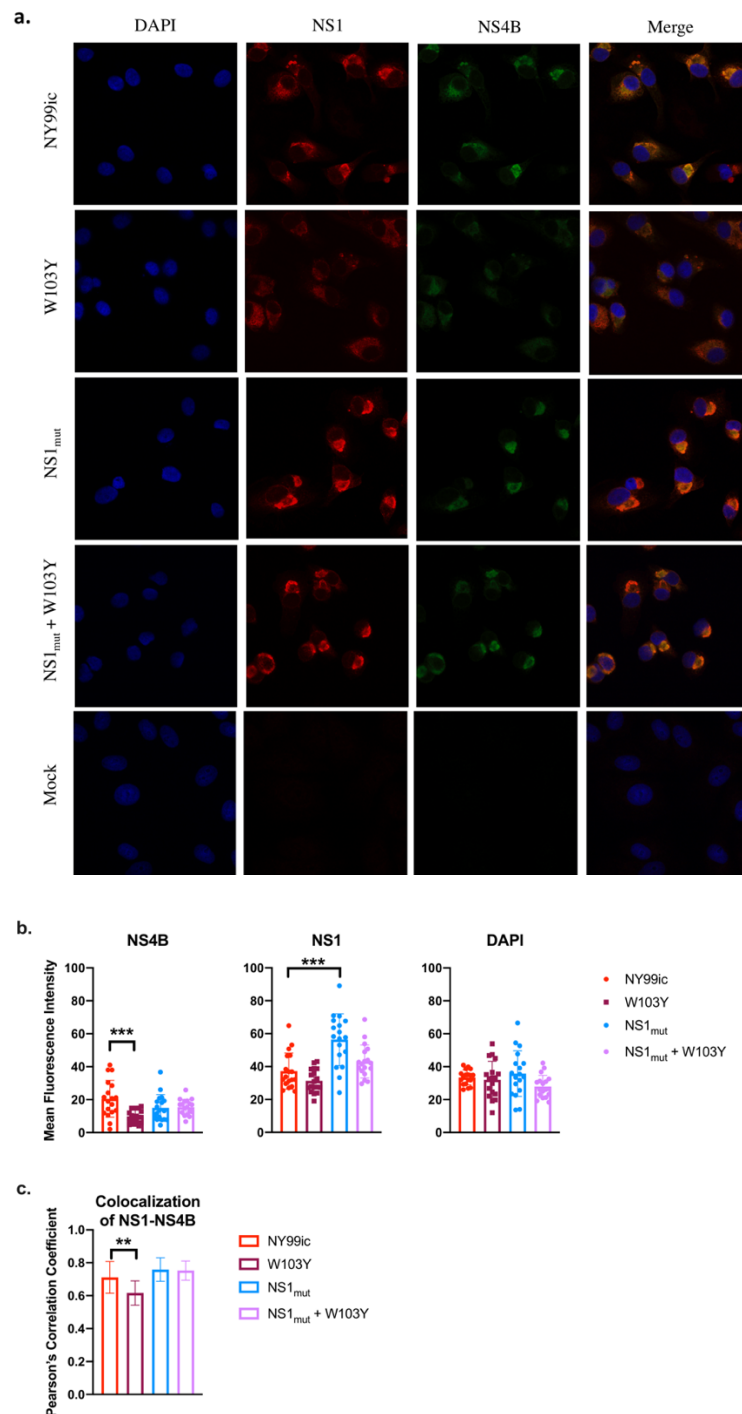
Cytokine levels produced by virus-infected cells were compared to NY99ic-infected cells using a Kruskal-Wallis ANOVA with Dunn's post-hoc correction. Six replicates of each mutant and 12 replicates of NY99ic and mock were measured in pg/mL, except for IFN- α and IFN- β for which six replicates were tested for all viruses and controls. A dotted line is dividing cells infected with the NY99ic and the single gene mutants (left) from the multigenic mutants and mock (right). *p<0.05, **p<0.01, ***p<0.001, ****p<0.0001

Figure 6.5: The NS1_{mut}+NS4B-W103Y mutant had reduced accumulation and colocalization of NS1 and NS4B one day post infection



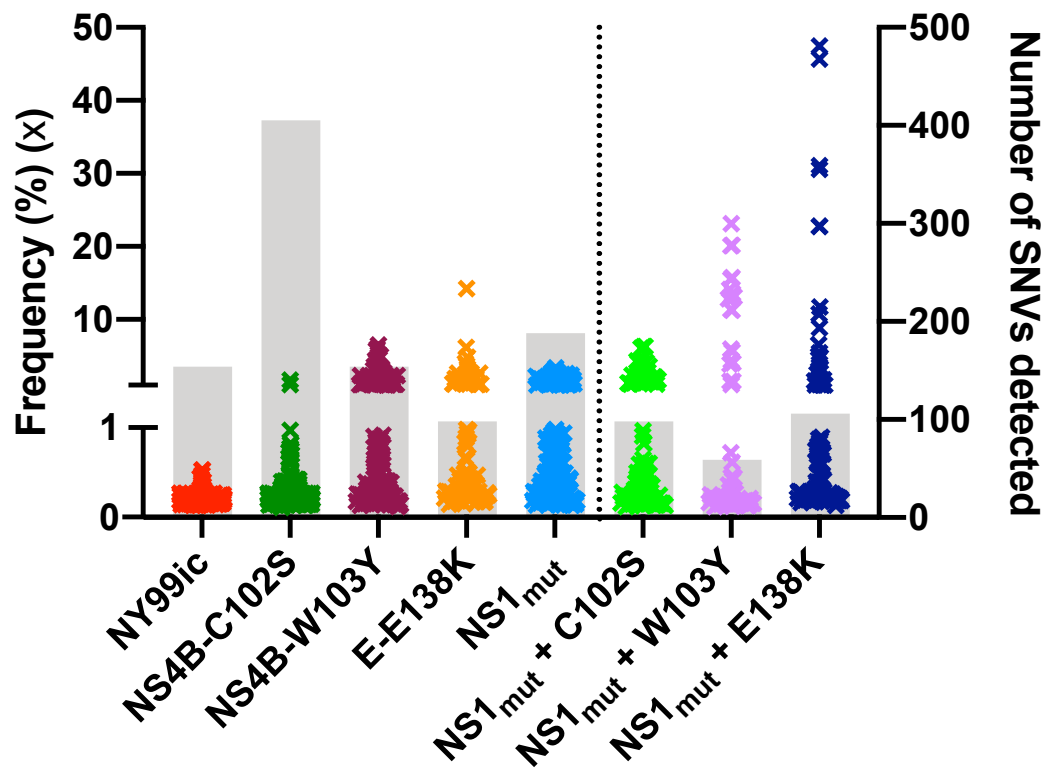
Mean fluorescence intensity and Pearson's correlation coefficient were calculated on individual infected cells (n=17). Statistical differences were measured using a Kruskal-Wallis test with multiple comparisons to compare both mutants to NY99ic. * $p < 0.05$, ** $p < 0.01$, **** $p < 0.0001$

Figure 6.6: The attenuated NS1_{mut}+NS4B-W103Y mutant and NY99ic had similar staining of NS1 and NS4B proteins two days post infection



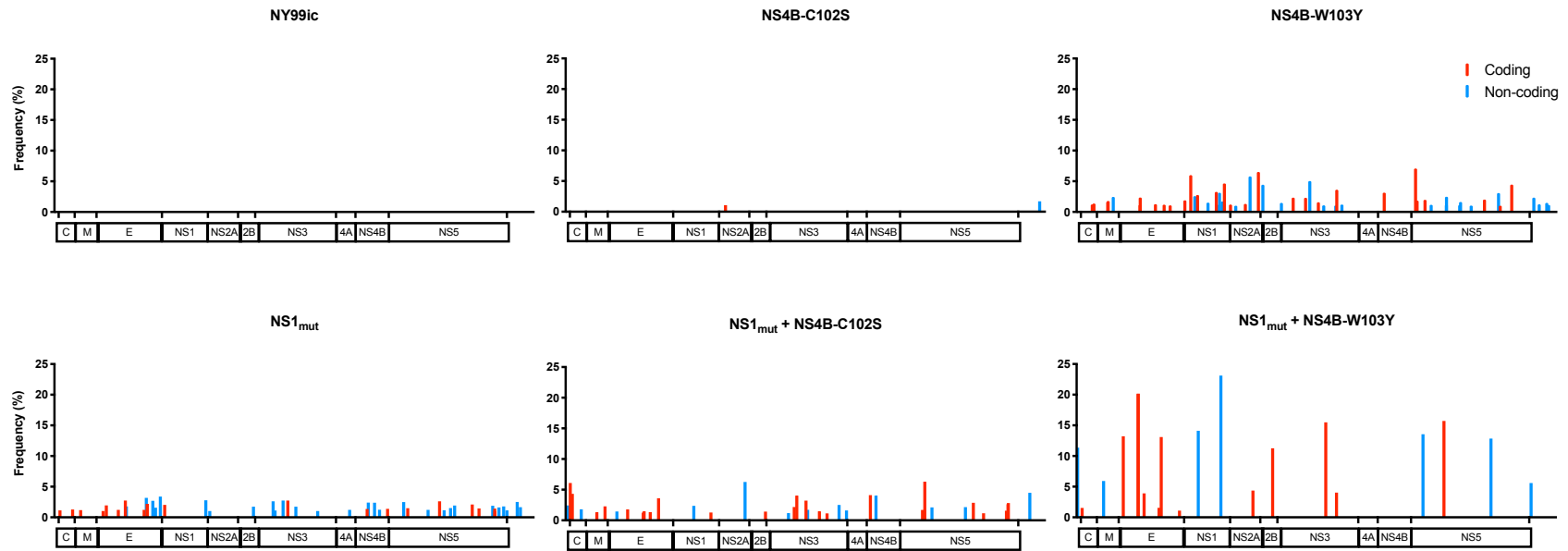
Mean fluorescence intensity and Pearson's correlation coefficient were calculated on individual infected cells (n=18). Statistical differences were measured using a Kruskal-Wallis test with multiple comparisons to compare both mutants to NY99ic. ** $p < 0.01$, *** $p < 0.001$

Figure 6.7: SNV profiles of single gene and multigenic mutants



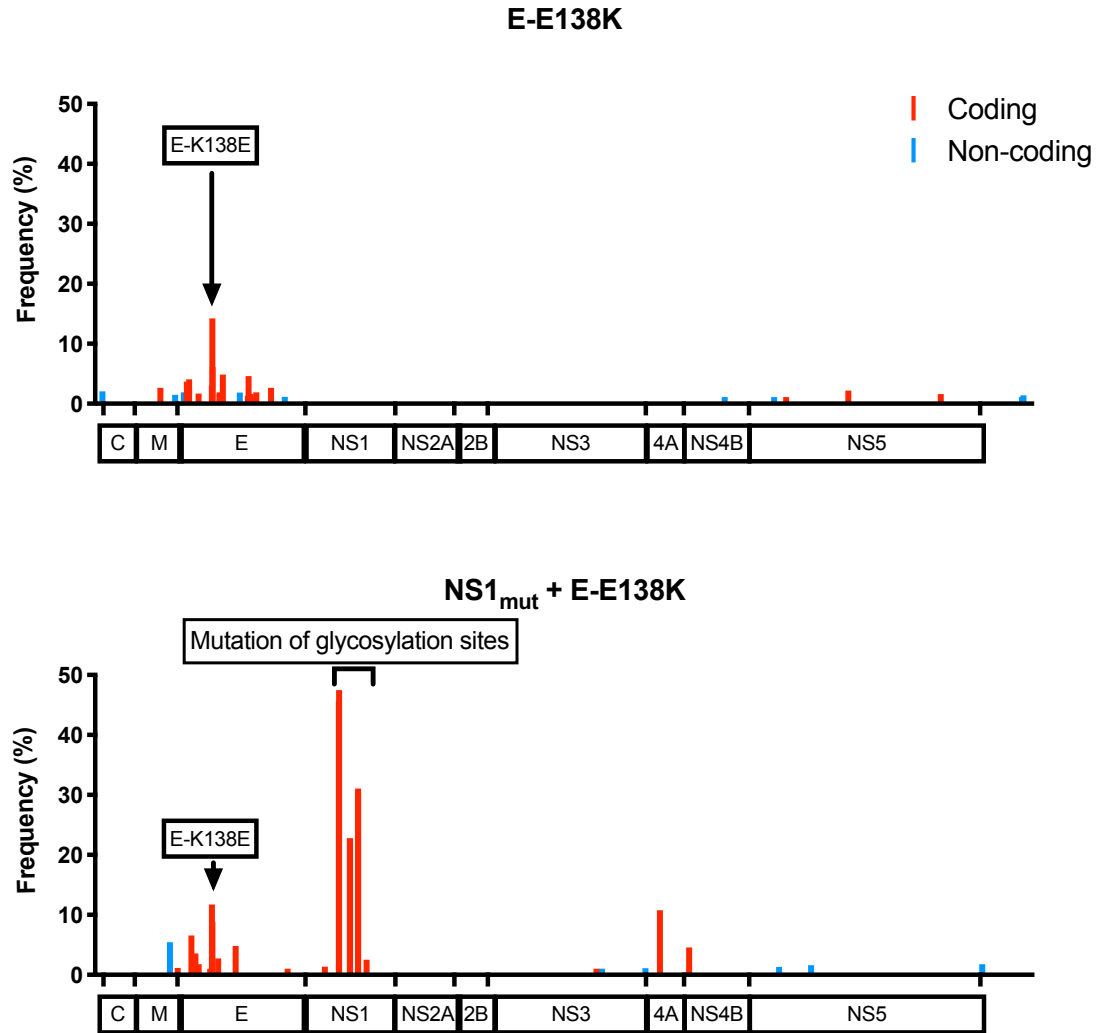
For each virus, the frequency of each SNV is indicated by an (x), and the grey bars in the background display the total number of SNVs detected. A dotted line is dividing NY99ic and the single gene mutants (left) from the attenuated mutants and mock (right). SNVs displayed were detected in the P0 Vero cell culture stocks of each mutant except for the NS4B-W103Y mutant, for which analysis was done on the P1 stock.

Figure 6.8: The multigenic NS1_{mut}+NS4B-W103Y mutant had higher SNV frequency than the single gene NS1_{mut} or NS4B-W103Y mutants



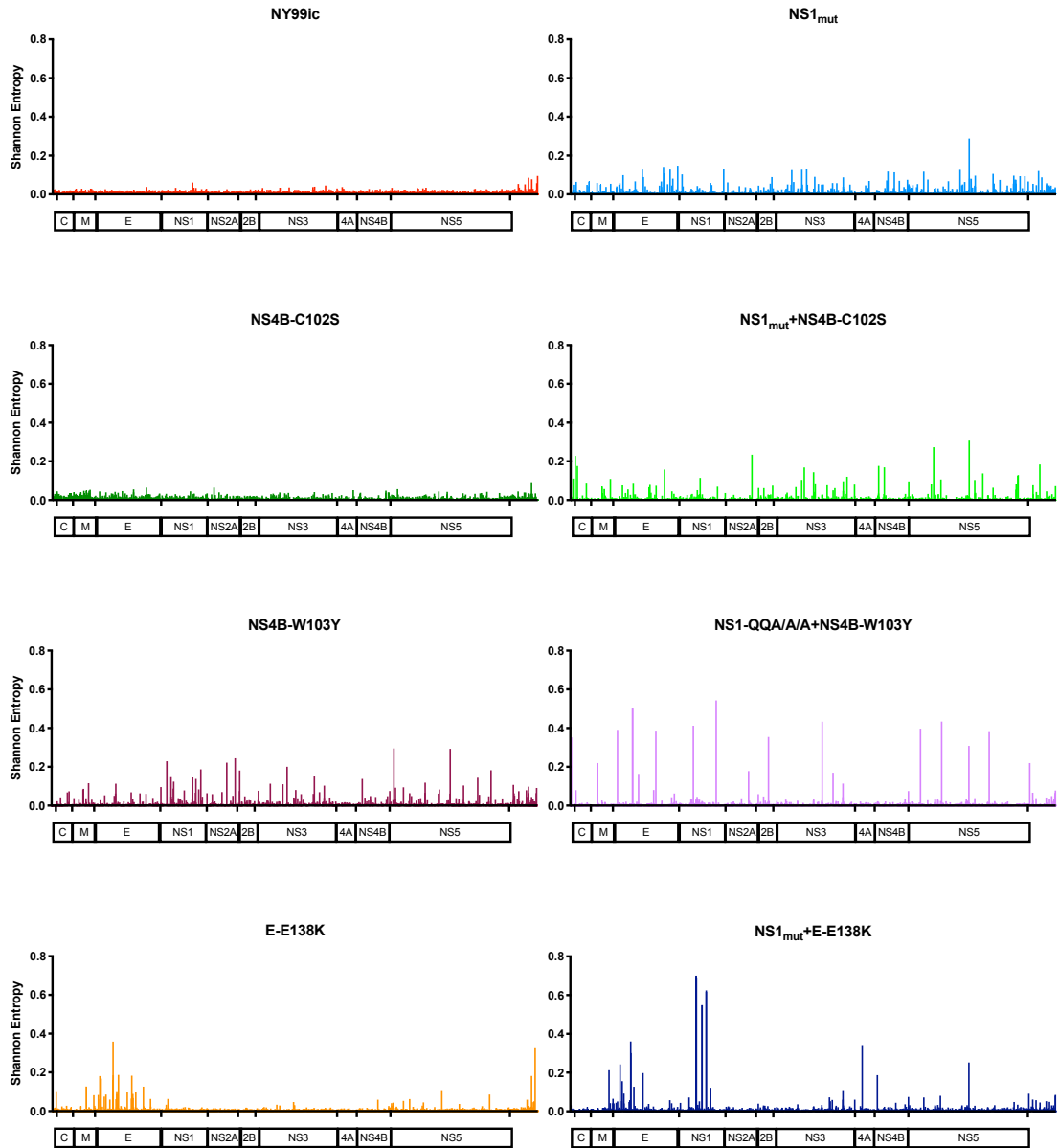
All SNVs $\geq 1\%$ frequency were plotted in the corresponding genome position. All viruses analyzed were P0 Vero cell culture stocks, except for the NS4B-W103Y mutant, for which the P1 stock was analyzed.

Figure 6.9: The E-E138K mutation reduced stability of the NS1_{mut} glycosylation site mutations



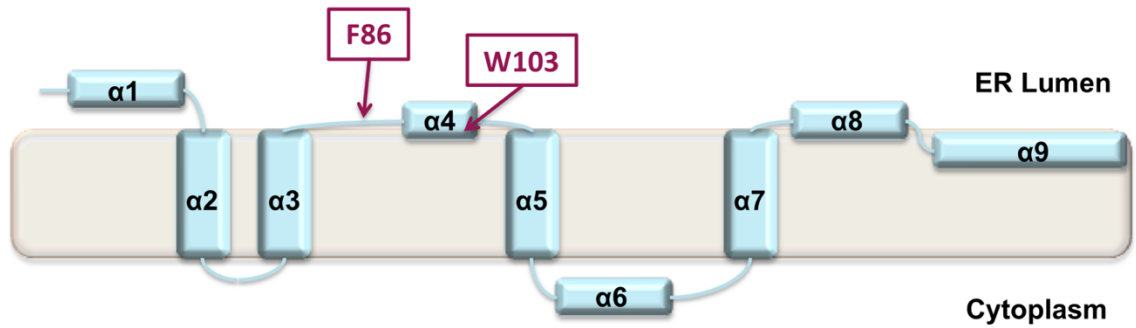
All SNVs $\geq 1\%$ frequency were plotted in the corresponding genome position. Both viruses analyzed were P0 Vero cell culture stocks.

Figure 6.10: The attenuated NS1_{mut}+NS4B-W103Y and virulent NS1_{mut}+E-E138K mutants had higher peaks of Shannon entropy than the parental single gene mutants



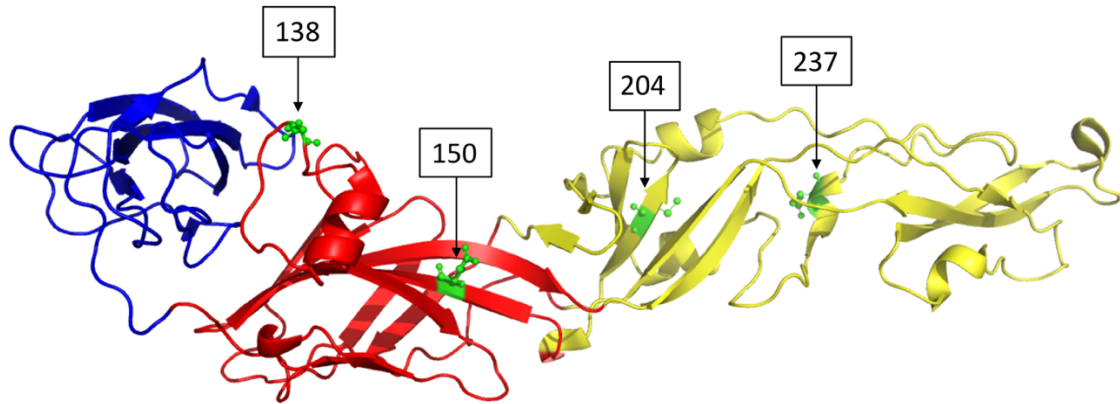
The P0 stock of each virus was used for Shannon entropy calculation, except for the NS4B-W103Y mutant, for which the P1 stock was analyzed.

Figure 6.11: NS4B residues oriented toward the ER lumen may be involved in interaction with NS1



The NMR structure of DENV-2 NS4B is modelled. The nine alpha-helices are listed as $\alpha 1$ - $\alpha 9$. Residue F86 in WNV is implicated to be involved in the NS1-NS4B interaction (Youn et al., 2012). Residue W103 was investigated in this chapter, and its role in NS1-NS4B interaction is not known. Both of these residues are positioned in a similar region of NS4B on the ER lumen side.

Figure 6.12: Diverse regions of the E protein are associated with mutation in the context of NS1 glycosylation site mutations



The E protein monomer of WNV is modelled with domain I (DI) colored in red, DII in yellow, and DIII in blue. E-138 was associated with reversion of the NS1_{mut} glycosylation site mutations. E-150 encoded a high frequency (>20%) SNV in the NS1_{mut}+NS4B-W103Y mutant. E-204 and E-237 were found in virus isolated from brains of mice that succumbed to the first generation NS1_{mut}, and these E protein mutations were associated with reversion of the NS1 glycosylation site mutations (Whiteman et al., 2011).

Chapter 7 – Final Discussion

WNV has been endemic in the US and Europe for at least 20 and 30 years, respectively, and it is essential that research and development of a WNV human vaccine continues to be pursued. Of six WNV vaccine candidates that have been studied in clinical trials, the two live attenuated strains exhibited the strongest immune induction. In order to develop a strongly immunogenic vaccine that is also cost effective (e.g. only requires a single dose), the live attenuated WNV vaccine platform is likely better than non-replicating vaccines (e.g. inactivated or subunit). The two live, attenuated WNV vaccines that have been tested in clinical trials thus far are both comprised of recombinant, chimeric viruses that only harbor the WNV prM and E genes but have NS genes from other flaviviruses (Biedenbender et al., 2011; Dayan et al., 2012; Durbin et al., 2013; Monath et al., 2006; Pierce et al., 2017). Importantly, chimeric flavivirus vaccines may not provide maximum protection, as antibody and T cell responses that are not specific to WNV can be generated to the NS genes of the vaccine, as has been observed for a chimeric DENV vaccine (Halstead, 2018). For these reasons, this dissertation aimed to utilize site-directed mutagenesis to identify attenuating mutations in WNV that could be included in a full-length candidate WNV vaccine. Specific goals of the dissertation were to investigate new potentially attenuating mutations in the WNV genome, to expand investigation of attenuating mutations that have been previously identified, and to generate multigenic mutants that harbor mutations in more than one viral gene. The overall goal was to identify multiple independently attenuating mutations in WNV that could ultimately be combined

to yield a live, attenuated vaccine that induces protective immunity. As described below, the utilization of a combination of genotypic and phenotypic markers provided critical insight to evaluate the overall attenuated phenotype of the viral genes that were mutated. Each mutant is summarized in **Table 7.1**.

The genes targeted for mutagenesis encode the NS4B, NS5, and E viral proteins. NS4B was targeted because previous studies reported that mutations in diverse regions of the NS4B protein could attenuate WNV (Davis et al., 2004; May et al., 2010; Wicker et al., 2006, 2012). Mutations in the NS5 MTase were targeted because there is a strong body of work suggesting that MTase catalytic tetrad mutations may be excellent candidates for flavivirus vaccine development (Daffis et al., 2011; Li et al., 2013; Zhou et al., 2007; Zust et al., 2013; Züst et al., 2017). The E protein was targeted because E protein mutations are important to the attenuation of the live, attenuated flavivirus vaccines JEV SA14-14-2 and YFV 17D (Gromowski et al., 2015; Hahn et al., 1987; Lee and Lobigs, 2008; Ryman et al., 1998; Wang et al., 2017; Yang et al., 2017), but to date, few E protein mutations have been investigated in WNV that are both strongly attenuating and stable (Goo et al., 2017; Whiteman et al., 2010; Zhang et al., 2006). Finally, the NS1_{mut} was chosen as a backbone for generation of multigenic mutants because the NS1 glycosylation site mutations have exhibited significant attenuation and stability in previous studies (Whiteman et al., 2011).

7.1 NS4B PROTEIN

Several flavivirus conserved residues in the NS4B protein were investigated that have not been previously studied in WNV. Specifically, NS4B-P54, NS4B-L56, and NS4B-W103 were mutated and the resulting mutants were characterized for an attenuated

phenotype, and mutation of P54 was strongly attenuating. Both P54A and P54G mutations significantly attenuated the WNV mouse virulence phenotype, and furthermore, each of these mutants induced protective immunity as measured by challenge studies and PRNT₅₀ assays. P54A mutation resulted in stronger mouse attenuation than P54G mutation, but it is not known why alanine substitution at this residue was more attenuating than glycine substitution. Proline residues are associated with breaking of α -helical structures (Kim and Kang, 1999), in agreement with the putative location of P54 near the end of a transmembrane α -helix (Li et al., 2016) (**Fig. 5.2**). Furthermore, proline has been associated with the α -helix ability to undergo rapid conformational changes, specifically when changing between hydrophobic and hydrophilic environments (Kumeta et al., 2017). Alanine is associated with stabilization of α -helical structures, whereas glycine is considered less stable (Scott et al., 2007), so it is possible that NS4B-P54A mutation stabilizes the first transmembrane α -helix and does not allow for sufficient flexibility of the protein.

NGS proved to be a powerful tool to help analyze attenuation. Although strongly attenuating, alanine substitution at residue NS4B-P54 was not stable and could revert after cell culture passage, whereas the glycine substitution was significantly attenuating and no evidence of reversion was detected. The NS4B-P54 residue is very strongly conserved amongst diverse groups of mosquito-borne and tick-borne flaviviruses (**Fig. 5.1**), and mutation of this residue could be an excellent component of a WNV live, attenuated vaccine as well as vaccines for related viruses. It is notable that previous studies of mouse attenuated NS4B mutants reported enhanced mosquito competence compared to WT (Van

Slyke et al., 2013). Therefore, before moving forward with a WNV vaccine including mutation of NS4B, it will be essential to verify that vector competence is reduced.

WNV NS4B-P38G and NS4B-C102S mutations were described in previous studies as strongly attenuating, however, these mutants both had extra compensatory mutations in the genomic consensus sequences (Wicker et al., 2006, 2012), with the C102S mutant harboring E-D114A and E-V139M mutations. A new NS4B-C102S mutant was rescued with no additional consensus sequence mutations, demonstrating that the E-D114A/V139M mutations were not required for viability of the NS4B-C102S mutant. The new rescue of this mutant had a phenotype similar to that of NY99ic (i.e. not attenuated). Therefore, either one or both of the E protein D114A or V139M mutations found in the old C102S mutant stocks likely conferred attenuation in WNV, and continued studies should investigate these E mutations alone and in combination as they may be useful in WNV vaccine development.

7.2 NS5 PROTEIN

Outside of NS4B, other mutations that have previously been found to attenuate WNV are in the NS5 MTase catalytic tetrad. Flavivirus 5' capping occurs by two sequential methylation steps: N-7 methylation and 2'O methylation. The MTase catalytic tetrad is comprised of four NS5 residues: K61-D146-K182-E218. All four of these residues are required for 2'O methylation, whereas, D146 is required for N-7 methylation, and thus NS5-D146 mutation is not viable in flaviviruses (Ray et al., 2006; Zhou et al., 2007). In this dissertation, the NS5-K61A and NS5-E218A mutations were confirmed to be strongly attenuating to WNV as they were tested in a highly susceptible outbred mouse

model. As with the NS4B mutants, NGS showed that mutation of NS5-K61A is the best target for continued vaccine development since it had no evidence of reversion through P5, whereas, the P5 stock of the NS5-E218A mutant acquired very low frequency reversion in SNVs. Moving forward it will be important to evaluate NS5-K61A mutation in the context of attenuating mutations in other viral genes to evaluate stability.

7.3 E PROTEIN

Another mutation, E-E138K, was previously studied in JEV and WNV, but its direct role in attenuation of WNV was not fully elucidated. It was established that E-E138K mutation conferred attenuation to the JEV SA14-14-2 live, attenuated vaccine, plus this mutation alone conferred attenuation to WT JE strains (Gromowski et al., 2015; Wang et al., 2017; Yang et al., 2017; Zhao et al., 2005). In WNV, the E-E138K mutation was associated with varying degrees of attenuation in cell culture adapted WNV, in a chimeric WNV vaccine candidate, and in an infectious DNA platform, but it was not investigated independently using site-directed mutagenesis (Arroyo et al., 2004; Lee et al., 2004; Yamshchikov et al., 2016). In the virulent NY99ic, the E-E138K mutation was not attenuating when tested at doses of 500 PFU, and NGS showed that virulence was associated with reversion to the WT genotype. Although JEV and WNV belong to the same serogroup and phylogenetic lineage, it is hypothesized that there are key differences in the structure of the E protein dimer that alter stability of the E-E138K mutation between the two viruses. Another mutation from the JEV SA14-14-2 vaccine, E-L107F, has been used in a candidate chimeric live, attenuated WNV vaccine along with E-A316V and E-K440R mutations (Arroyo et al., 2004). Studies of E-L107F in WNV reported evidence of

reversion to leucine at E-107 in the brains of mice that died from i.p. inoculation with an E-L107F/A316V/K440R triple mutant (Zhang et al., 2006), indicating that this JEV vaccine-specific mutation is also lacking stability in WNV. The findings that E-E138K and E-L107F mutations do not have conserved properties between JEV and WNV demonstrate that attenuating mutations in one flavivirus cannot necessarily be transferred to another flavivirus and retain safety and stability.

7.4 MULTIGENIC MUTANTS

Some flavivirus conserved residues retain attenuating properties across many members of the flavivirus genus, including the NS5 MTase mutations that are attenuating in WNV, DENV, and JEV (Daffis et al., 2011; Li et al., 2013; Zhou et al., 2007; Zust et al., 2013; Züst et al., 2017), and NS1 glycosylation site mutations that are attenuating to WNV, YFV, DENV, and ZIKV (Annamalai et al., 2019; Muylaert et al., 1996; Pryor et al., 1998; Somnuk et al., 2011; Whiteman et al., 2010, 2011). Though some attenuating mutations have conserved functions in multiple flaviviruses, differences amongst members of the flavivirus genus must be considered during WNV vaccine development as some mutations, including E-E138K, may not have conserved attenuating properties, regardless of genomic sequence homology.

Analysis of multigenic mutants, in which more than one viral gene was targeted for mutagenesis, is considered an important property for safety of a candidate WNV live, attenuated vaccine, as the attenuated phenotype should ideally not be based on mutations in only one viral gene. Each of the multigenic mutants included the NS1_{mut} as the backbone, as the NS1 glycosylation site mutations conferred strong mouse attenuation,

protective immunity, and decreased mosquito competence, making them excellent candidates for inclusion in a WNV vaccine. It was unexpected that the three mutations combined with the NS1_{mut} (NS4B-C102S, NS4B-W103Y, or E-E138K) would not independently attenuate WNV using doses of 500 PFU. A clone for a NS1_{mut}+NS4B-P38G mutant was also prepared, however, this mutant was not rescued after many attempts. Since the NS4B-P38G mutant has not been recovered without the NS4B-T116I compensatory mutation, site-directed mutagenesis of NS4B-T116I in the clone of the NS1_{mut}+NS4B-P38G mutant may be required for viability of this multigenic mutant.

Regardless of the lack of an “optimal” multigenic mutant vaccine candidate where each of the mutations was independently attenuating, investigation of the available mutants provided key insight into continued use of the NS1_{mut} as a WNV vaccine backbone. For example, combining NS4B mutations into the NS1_{mut} backbone was well tolerated, and the resulting multigenic mutants retained strong mouse attenuation. The NS1_{mut}+NS4B-W103Y mutant had enhanced attenuating properties compared to the NS1_{mut}, suggesting that the NS4B-W103Y mutation may mildly attenuate WNV and/or the synergistic effects of these NS1+NS4B mutations increased attenuation. Though attenuated, this multigenic mutant had an increase in viral population diversity compared to the single gene mutants. While the increased diversity was not associated with mouse virulence, high quasispecies diversity is not an ideal vaccine characteristic as the virus could potentially acquire additional mutations that could change the virulence phenotype. For the YFV 17D live, attenuated vaccine, low quasispecies diversity is associated with attenuation, as the parental, virulent Asibi strain of YFV had high diversity in comparison to 17D (Beck et al., 2014). It is not known if low quasispecies diversity will correlate with attenuation for

WNV as it does for YFV. Specifically, the NY99ic had low genotypic diversity compared to most of the attenuated and virulent mutants investigated in these studies, demonstrating a difference between the NY99ic and Asibi IC. Although a WNV vaccine may not have the same quasispecies differences from its parent strain as those that are observed between YFV 17D and Asibi, significant high peaks of quasispecies diversity, such as that observed in the NS1_{mut}+NS4B-W103Y mutant, indicates genotypic instability, which is an undesirable feature for any live, attenuated vaccine.

Important insights about the NS1_{mut} stability were also gained from NGS investigation of a NS1_{mut}+E-E138K mutant. Mutation of E-E138K not only induced reversion in the E protein, but it also induced reversion of the NS1 glycosylation site mutations. It was significant how rapidly WNV selected for specific mutations that could restore the WT genotype, as this multigenic mutant had SNVs encoding reversion in both E and NS1 proteins in the unpassaged P0 virus stock. While it is not known why E-E138K mutation caused such rapid reversion, the results indicate that addition of structural protein mutations into the NS1_{mut} backbone must be done with great care since the functions of interactions between NS1 and the E protein are not fully understood (Scaturro et al., 2015). Importantly, the glycosylation site mutation that had three amino acid substitutions (NS1-NNT130QQA) did not revert, but the two glycosylation sites with only one amino acid substitution (NXT→AXT) reverted to WT. This was surprising based on the stability of the NS1 glycosylation site mutations in the other multigenic mutants and in previous studies (Whiteman et al., 2011). Therefore, further stabilization of the NS1_{mut} is needed to increase the safety of this mutant for vaccine development. Future studies should characterize a NS1 mutant with glutamine substitution at all three glycosylation motifs

(NS1-NNT130QQA/NTT175QQA/NDT207QQA) to see if the resulting mutant is viable, attenuated, and stable, as hypothesized.

7.5 PHENOTYPIC COMPARISON OF ATTENUATED MUTANTS IN DIFFERENT VIRAL GENES

Though this dissertation investigated mutants across diverse regions of the WNV genome, only three stood out for their strong attenuation. The NS1_{mut}, NS4B-P54G, and NS5-K61A mutants each had notable attenuation and stability, albeit, the NS1_{mut} should be further stabilized since evidence of reversion was detected from one of the multigenic mutants. In studies of each set of mutants, TS assays, multiplication kinetics, and cytokine production were assessed to determine if there was an *in vitro* phenotype that was specific to WNV attenuated mutants. *In vitro* trends associated with WNV attenuation would be useful in future studies to identify optimal candidate mutations prior to *in vivo* evaluation, however, there was no *in vitro* phenotype that was conserved amongst attenuated mutants in different viral genes. For instance, the NS1_{mut} was strongly TS and had significant reductions in multiplication kinetics in A549 cells, but neither the NS4B-P54G nor NS5-K61A mutants had this phenotype. Additionally, there was no specific cytokine that acted as a biomarker for attenuation, but instead, different patterns were observed in each set of mutants. Specifically, the NS4B mutants had two distinct patterns associated with attenuation: strong pro-inflammatory cytokines (P38G) or relatively low pro-inflammatory cytokines (P54A/P54G). There was a trend toward low IFN- β production from all the attenuated NS4B mutants, and the attenuated multigenic mutants exhibited a similar trend, although it was not statistically significant. While low IFN- β production at certain timepoints could be associated with attenuation for NS4B and NS1 mutants, the attenuated

NS5 mutants induced IFN- β levels that were very similar to NY99ic. The attenuated multigenic mutants induced strong IFN- γ production, however, the same was not true for attenuated NS4B and NS5 mutants. Furthermore, the NS5-K61A and NS5-E218A mutants had distinct patterns of cytokine induction even though these mutants attenuate WNV by the same mechanism. The *in vitro* results indicate the unique functions that each viral protein has in viral replication and innate immune induction, and demonstrate that *in vitro* phenotype is not always predictive of *in vivo* attenuation for attenuated mutants in different viral genes.

7.6 FUTURE DIRECTIONS

In sum, an optimal WNV live, attenuated vaccine that is based on the full-length WNV genome has not yet been generated. There is a strong foundation of work on how to proceed with generation of a candidate WNV vaccine. Specifically, the NS1_{mut} backbone should be stabilized with glutamine substitution at all three glycosylation motifs. NS4B-P54G and NS5-K61A mutations are excellent candidates for investigation with the NS1_{mut}, as each attenuated the virus by distinct mechanisms. If a candidate vaccine is made that is strongly attenuated and protective in animal models and genotypically stable, it must also be tested for reduced vector competence prior to consideration of clinical evaluation. If the proposed mutations do not sufficiently attenuate WNV, or alternatively, lead to over-attenuation, there are mutations in other viral genes (summarized in **Table 1.2**) that have been investigated in previous studies that could also be utilized to make multigenic mutants. While empirical design was used to generate the YFV 17D and JEV SA14-14-2 vaccines, empirical vaccine development leaves many unanswered questions in regard to

vaccine mechanism of attenuation, quality of immune response generated, and stability of the resulting vaccine. Rational vaccine design is preferable to develop optimal vaccine candidates and to better understand the properties of vaccine attenuation and immunogenicity. In the flavivirus field, there is a strong body of work demonstrating the feasibility of WNV rational vaccine development, and with continued efforts, an optimal candidate can likely be developed.

Table 7.1: Overview of *in vitro* and *in vivo* characteristics of WNV mutants

Mutant	Additional consensus mutations	Vero cell passage number	Plaque morphology	TS (Δ titer 41° vs 37°)	Survived 500 PFU (%)	$^{\circ}$ AST	Survived 10,000 PFU challenge	High dose (PFU)	Survived high dose (%)	Evidence of reversion
NY99ic	-	1	large	0.1	0/10 (0)	9.0 \pm 1.3	n.d.	n.d.	n.d.	-
E-E138K	C1077U (nc)	1	large	0.1	0/5 (0)	9.4 \pm 1.3	n.d.	8.2x10 ⁷	0/5 (0)	Yes
NS5-K61A	-	1	small	0.2	5/5 (100)	>35	5/5	2.9x10 ⁵	5/5	No
NS5-E218A	-	1	medium	0.4	5/5 (100)	>35	5/5	3.8x10 ⁵	5/5	Yes
NS5-K61A/E218A	-	1	mixed	1.1	3/10 (30)	11.1 \pm 1.7	2/2	4.2x10 ⁷	3/5	Yes
NS4B-P38G	NS4B-T116I	1	medium	0.7	4/5 (80)	13.0 \pm 0.0	4/4	1.3 x 10 ⁷	4/5 (80)	No
NS4B-P38G	NS3-N480H NS4B-T116I	4	medium	1.2	5/5 (100)	>35	5/5	1.2 x 10 ⁶	5/5 (100)	⁺ Yes
NS4B-P54A	-	1	medium	1.0	5/5 (100)	>35	5/5	3.5 x 10 ⁵ 5.4 x 10 ⁷	5/5 (100) 5/5 (100)	Yes
NS4B-P54G	-	1	medium	0.2	5/5 (100)	>35	5/5	5.2 x 10 ⁵ 1.5 x 10 ⁷	5/5 (100) 5/10 (50)	No
NS4B-L56A	-	0	large	n.d.	0/5 (0)	9.6 \pm 2.6	n.d.	n.d.	n.d.	No
NS4B-L56A	NS1-T108S	1	large	0.2	0/5 (0)	11.6 \pm 2.4	n.d.	n.d.	n.d.	No
NS4B-C102S	-	1	medium	0.0	0/15 (0)	8.5 \pm 3.1	n.d.	n.d.	n.d.	No
NS4B-C102S	E-D114A E-V139M	2	medium	[#] > 6.1	5/5 (100)	>35	5/5	1.3 x 10 ⁶	5/5 (100)	⁺ Yes
NS4B-W103Y	-	1	medium	0.3	0/5 (0)	9.8 \pm 2.4	n.d.	n.d.	n.d.	No
NS4B-C102S/W103Y	-	1	medium	0.1	0/5 (0)	9.4 \pm 2.1	n.d.	n.d.	n.d.	No
NS1-NNT130QQA/N175A/N207A (NS1 _{mut})	-	1	small	2.7	5/5 (100)	>35	5/5 (100)	1.4 x10 ⁷	4/5 (80)	No
NS1 _{mut} +NS4B-C102S	-	1	small	2.7	5/5 (100)	>35	5/5 (100)	1.3 x10 ⁷	4/5 (80)	No
NS1 _{mut} +NS4B-W103Y	-	1	small	2.3	5/5 (100)	>35	5/5 (100)	1.1 x10 ⁷	15/15 (100)	No
NS1 _{mut} +E-E138K	-	1	mixed	0.3	0/5 (0)	11.6 \pm 1.5	n.d.	1.7 x10 ⁷	1/5 (20)	Yes

The statistics for TS and AST can be found in previous chapters. TS is listed as log₁₀ PFU/mL. All mouse inoculations were done by the intraperitoneal (i.p.) route. n.d. = not done. AST=average survival time. TS=temperature sensitivity. nc=non-coding. [#]41°C titer was below limit of detection (LOD<1.7 log₁₀ PFU/mL). [°]AST was calculated for mice that died from the 500 PFU dose. ⁺Reversion was evident in previous studies, but not in this dissertation.

References

- Aerssens, A., Cochez, C., Niedrig, M., Heyman, P., Kühlmann-Rabens, I., and Soentjens, P. (2016). Analysis of delayed TBE-vaccine booster after primary vaccination. *J. Travel Med.* 23, tav020. doi:10.1093/jtm/tav020.
- Akey, D. L., Brown, W. C., Dutta, S., Konwerski, J., Jose, J., Jurkiw, T. J., et al. (2015a). Flavivirus NS1 Crystal Structures Reveal a Surface for Membrane Association and Regions of Interaction With the Immune System. *Science* (80-.). 343, 881–885. doi:10.1126/science.1247749.Flavivirus.
- Akey, D. L., Brown, W. C., Jose, J., Kuhn, R. J., Smith, J. L., Arbor, A., et al. (2015b). Structure-guided insights on the role of NS1 in flavivirus infection. *Bioessays* 37, 489–494. doi:10.1002/bies.201400182.Structure-.
- Aliota, M. T., Jones, S. A., Dupuis, A. P., Ciota, A. T., Hubalek, Z., and Kramer, L. D. (2012). Characterization of Rabensburg virus, a Flavivirus closely related to West Nile virus of the Japanese encephalitis antigenic group. *PLoS One* 7, 3–8. doi:10.1371/journal.pone.0039387.
- Alkharsah, K. R. (2018). VEGF upregulation in viral infections and its possible therapeutic implications. *Int. J. Mol. Sci.* 19. doi:10.3390/ijms19061642.
- Amanna, I. J. (2013). Balancing the Efficacy and Safety of Vaccines in the Elderly. *Open Longev Sci* 6, 64–72. doi:10.2174/1876326X01206010064.
- American Veterinary Medical Association (2010). Intervet/Schering-Plough recalls PreveNile vaccine. *Am. Vet. Med. Assoc.* Available at: <https://www.avma.org/News/JAVMANews/Pages/100615k.aspx> [Accessed July 5, 2019].
- Angenvoort, J., Brault, A. C., Bowen, R. A., and Groschup, M. H. (2013). West Nile viral infection of equids. *Vet. Microbiol.* 167, 168–180.
- Annamalai, A. S., Pattnaik, A., Sahoo, B. R., Guinn, Z. P., Bullard, B. L., Weaver, E. A., et al. (2019). An Attenuated Zika Virus Encoding Non-Glycosylated Envelope (E) and Non-Structural Protein 1 (NS1) Confers Complete Protection against Lethal Challenge in a Mouse Model. *Vaccines* 7, 112. doi:10.3390/vaccines7030112.
- Arroyo, J., Miller, C., Catalan, J., Myers, G. A., Ratterree, M. S., Trent, D. W., et al. (2004). ChimeriVax-West Nile Virus Live-Attenuated Vaccine: Preclinical Evaluation of Safety, Immunogenicity, and Efficacy. *J. Virol.* 78, 12497–12507. doi:10.1128/jvi.78.22.12497-12507.2004.
- Austgen, L. E., Bowen, R. A., Bunning, M. L., Davis, B. S., Mitchell, C. J., and Chang, G. J. J. (2004). Experimental Infection of Cats and Dogs with West Nile Virus. *Emerg. Infect. Dis.* 10, 82–86.
- Barrett, A. (2018). West Nile in Europe: An increasing public health problem. *J. Travel Med.* 25.
- Barrett, P. N., Terpening, S. J., Snow, D., Cobb, R. R., and Kistner, O. (2017). Vero cell technology for rapid development of inactivated whole virus vaccines for emerging viral diseases. *Expert Rev. Vaccines* 16, 883–894. doi:10.1080/14760584.2017.1357471.

- Batista, W. C., Bifano, S., Vieira, D. S., Honda, E. R., Pereira, S. S., and Tada, M. S. (2011). Notification of the first isolation of Cacipacore virus in a human in the State of Rondônia, Brazil. *Rev. Soc. Bras. Med. Trop.* 44, 528–530.
- Beasley, D. W. C., Whiteman, M. C., Zhang, S., Huang, C. Y., Schneider, B. S., Smith, D. R., et al. (2005). Envelope Protein Glycosylation Status Influences Mouse Neuroinvasion Phenotype of Genetic Lineage 1 West Nile Virus Strains Envelope Protein Glycosylation Status Influences Mouse Neuroinvasion Phenotype of Genetic Lineage 1 West Nile Virus Strains. *J. Virol.* 79, 8339–8347. doi:10.1128/JVI.79.13.8339.
- Beck, A. S., and Barrett, A. D. T. (2015). Current status and future prospects of yellow fever vaccines. *Expert Rev. Vaccines* 14, 1479–92. doi:10.1586/14760584.2015.1083430.
- Beck, A., Tesh, R. B., Wood, T. G., Widen, S. G., Ryman, K. D., and Barrett, A. D. T. (2014). Comparison of the live attenuated yellow fever vaccine 17D-204 strain to its virulent parental strain asibi by deep sequencing. *J. Infect. Dis.* 209, 334–344. doi:10.1093/infdis/jit546.
- Best, S. M. (2017). The many faces of the flavivirus NS5 protein in antagonism of type I interferon signaling. *J. Virol.* 91. doi:10.1128/JVI.01970-16.
- Beth, D. K., Anna, P. D., Kristen, K. P., Marya, P. C., Cecilia, M. T., Palmtama, L. G., et al. (2015). Robust and Balanced Immune Responses to All 4 Dengue Virus Serotypes Following Administration of a Single Dose of a Live Attenuated Tetravalent Dengue Vaccine to Healthy, Flavivirus-Naive Adults. *J. Infect. Dis.* 212, 702–710.
- Bhatt, T. R., Crabtree, M. B., Guirakhoo, F., Monath, T. P., and Miller, B. R. (2000). Growth Characteristics of the Chimeric Japanese Encephalitis Virus Vaccine Candidate, ChimeriVax-JE (YF/JE SA14-14-2), in *Culex Tritaeniorhynchus*, *Aedes Albopictus*, and *Aedes Aegypti* Mosquitoes. *Am. J. Trop. Med. Hyg.* 62, 480–484.
- Biedenbender, R., Bevilacqua, J., Gregg, A. M., Watson, M., and Dayan, G. (2011). Phase II, randomized, double-blind, placebo-controlled, multicenter study to investigate the immunogenicity and safety of a West Nile virus vaccine in healthy adults. *J. Infect. Dis.* 203, 75–84. doi:10.1093/infdis/jiq003.
- Bigham, A. W., Buckingham, K. J., Husain, S., Emond, M. J., Bofferd, K. M., Gildersleeve, H., et al. (2011). Host genetic risk factors for West Nile virus infection and disease progression. *PLoS One* 6, 1–11. doi:10.1371/journal.pone.0024745.
- Blitvich, B. J. (2008). Transmission dynamics and changing epidemiology of West Nile virus. *Anim. Heal. Res. Rev.* 9, 71–86.
- Bolger, A. M., Lohse, M., and Usadel, B. (2014). Genome analysis Trimmomatic : a flexible trimmer for Illumina sequence data. *Bioinformatics* 30, 2114–2120. doi:10.1093/bioinformatics/btu170.
- Brandler, S., and Tangy, F. (2013). Vaccines in Development against West Nile Virus. *Viruses*, 2384–2409. doi:10.3390/v5102384.
- Brault, A. C., Langevin, S. A., Ramey, W. N., Fang, Y., Beasley, D. W. C., Barker, C. M., et al. (2011). Reduced Avian Virulence and Viremia of West Nile Virus Isolates from Mexico and Texas. 85, 758–767. doi:10.4269/ajtmh.2011.10-0439.
- Brien, J. D., Uhrlaub, J. L., Hirsh, A., Wiley, C. A., and Nikolich-Zugich, J. (2009). Key role of T cell defects in age-related vulnerability to West Nile virus. *J. Exp. Med.*

- 206, 2735–2745.
- Brien, J. D., Uhrlaub, J. L., and Nikolich-Zugich, J. (2007). Protective capacity and epitope specificity of CD8⁺ T cells responding to lethal West Nile virus infection. *Eur. J. Immunol.* 37, 1855–1863. doi:10.1002/eji.200737196.
- Brinton, M. A. (2013). Replication cycle and molecular biology of the west nile virus. *Viruses* 6, 13–53. doi:10.3390/v6010013.
- Brown, H. E., Childs, J. E., Diuk-Wasser, M. A., and Fish, D. (2008). Ecologic Factors Associated with West Nile Virus Transmission, Northeastern United States. *Emerg. Infect. Dis.* 14.
- Byrne, S. N., Halliday, G. M., Johnston, L. J., and King, N. J. C. (2001). Interleukin-1 β but not tumor necrosis factor is involved in West Nile virus-induced Langerhans cell migration from the skin in C57BL/6 mice. *J. Invest. Dermatol.* 117, 702–709. doi:10.1046/j.0022-202x.2001.01454.x.
- Calvert, A. E., Huang, C. Y.-H., Blair, C. D., and Roehrig, J. T. (2012). Mutations in the West Nile prM protein affect VLP and virion secretion in vitro. *Virology* 433, 35–44.
- Campbell, G., Lanciotti, R., Bernard, B., and Lu, H. (2002). Laboratory-acquired West Nile virus infections - United States, 2002. *Morb. Mortal. Wkly. Rep.* 51, 1133–1135.
- CDC (2016). Mosquito species in which West Nile virus has been detected, United States, 1999-2016. *ArboNET*, 1. Available at: <https://www.cdc.gov/westnile/resources/pdfs/MosquitoSpecies1999-2016.pdf>.
- CDC (2018a). West Nile Virus- Symptoms, Diagnosis, & Treatment. *Centers Dis. Control Prev.* Available at: <https://www.cdc.gov/westnile/symptoms/index.html> [Accessed July 5, 2019].
- CDC (2018b). West Nile Virus. *Centers Dis. Control Prev.* Available at: <https://www.cdc.gov/westnile/index.html> [Accessed July 5, 2019].
- CDC (2018c). West Nile Virus & Dead Birds. *Centers Dis. Control Prev.* Available at: <https://www.cdc.gov/westnile/dead-birds/index.html>.
- CDC (2019a). Saint Louis Encephalitis- Statistics and Maps. *Centers Dis. Control Prev.* Available at: <https://www.cdc.gov/sle/technical/epi.html>.
- CDC (2019b). West Nile Virus- Statistics and Maps. *Centers Dis. Control Prev.* Available at: <https://www.cdc.gov/westnile/statsmaps/index.html> [Accessed July 5, 2019].
- CDC (2019c). Yellow Fever Vaccine. *Centers Dis. Control Prev.* Available at: <https://www.cdc.gov/yellowfever/vaccine/index.html> [Accessed July 5, 2019].
- Chancey, C., Grinev, A., Volkova, E., and Rios, M. (2015). The global ecology and epidemiology of west nile virus. *Biomed Res. Int.*, 1–20. doi:10.1155/2015/376230.
- Chappell, K. J., Stoermer, M. J., Fairlie, D. P., and Young, P. R. (2008). Mutagenesis of the West Nile virus NS2B cofactor domain reveals two regions essential for protease activity. *J. Gen. Virol.* 89, 1010–1014. doi:10.1099/vir.0.83447-0.
- Chen, H. L., Chang, J. K., and Tang, R. Bin (2015). Current recommendations for the Japanese encephalitis vaccine. *J. Chinese Med. Assoc.* 78, 271–275. doi:10.1016/j.jcma.2014.12.009.
- Chokephaibulkit, K., Houillon, G., Feroldi, E., and Bouckennooghe, A. (2016). Safety and immunogenicity of a live attenuated Japanese encephalitis chimeric virus vaccine

- (IMOJEV®) in children. *Expert Rev. Vaccines* 15, 153–166. doi:10.1586/14760584.2016.1123097.
- Clapham, H. E., and Wills, B. A. (2018). Implementing a dengue vaccination programme—who, where and how? *Trans. R. Soc. Trop. Med. Hyg.* 112, 367–368. doi:10.1093/trstmh/try070.
- Clé, M., Beck, C., Salinas, S., Lecollinet, S., Gutierrez, S., Van de Perre, P., et al. (2019). Usutu virus: A new threat? *Epidemiol. Infect.* 147. doi:10.1017/s0950268819001213.
- Coller, I. B., Pai, V., Weeks-levy, C. L., and Ogata, S. A. Recombinant subunit West Nile virus vaccine for protection of human subjects. United States Patent Application US 2017 / 0165349 A1. 1.
- Collins, N. D., Beck, A. S., Widen, S. G., Wood, T. G., Higgs, S., and Barrett, D. T. (2018). Structural and Nonstructural Genes Contribute to the Genetic Diversity of RNA Viruses. *MBio* 9, 1–13.
- Colpitts, T. M., Rodenhuis-Zybert, I., Moesker, B., Wang, P., Fikrig, E., and Smit, J. M. (2011). PrM-antibody renders immature West Nile virus infectious in vivo. *J. Gen. Virol.* 92, 2281–2285. doi:10.1099/vir.0.031427-0.
- Conde, J. N., Silva, E. M., Barbosa, A. S., and Mohana-Borges, R. (2017). The Complement System in Flavivirus Infections. *Front. Microbiol.* 8, 1–7. doi:10.3389/fmicb.2017.00213.
- Daffis, S., Szretter, K. J., Schriewer, J., Li, J., Youn, S., Errett, J., et al. (2011). 2'-O methylation of the viral mRNA cap evades host restriction by IFIT family members. *Nature* 468, 452–456. doi:10.1038/nature09489.2.
- Danet, L., Beauclair, G., Berthet, M., Moratorio, G., Gracias, S., Tangy, F., et al. (2019). Midgut barriers prevent the replication and dissemination of the yellow fever vaccine in *Aedes aegypti*. *PLoS Negl. Trop. Dis.*, 1–18. doi:https://doi.org/10.1371/journal.pntd.0007299.
- Davis, A., Bunning, M., Gordy, P., Panella, N., Blitvich, B., and Bowen, R. (2005). Experimental and natural infection of North American bats with West Nile virus. *Am. J. Trop. Med. Hyg.* 73, 467–469.
- Davis, C. T., Beasley, D. W. C., Guzman, H., Siirin, M., Parsons, R. E., Tesh, R. B., et al. (2004). Emergence of attenuated West Nile virus variants in Texas, 2003. *Virology* 330, 342–350. doi:10.1016/j.virol.2004.09.016.
- Davis, C. T., Galbraith, S. E., Zhang, S., Whiteman, M. C., Li, L., Kinney, R. M., et al. (2007). A combination of naturally occurring mutations in North American West Nile virus nonstructural protein genes and in the 3' untranslated region alters virus phenotype. *J. Virol.* 81, 6111–6. doi:10.1128/JVI.02387-06.
- Dayan, G. H., Bevilacqua, J., Coleman, D., Buldo, A., and Risi, G. (2012). Phase II , dose ranging study of the safety and immunogenicity of single dose West Nile vaccine in healthy adults ≥ 50 years of age. *Vaccine* 30, 6656–6664. doi:10.1016/j.vaccine.2012.08.063.
- de Figueiredo, M. L. G., Amarilla, A. A., De Figueiredo, G. G., Alfonso, H. L., Lippi, V., Maia, F. G. M., et al. (2017). Cacipacore virus as an emergent mosquito-borne flavivirus. *Rev. Soc. Bras. Med. Trop.* 50, 539–542. doi:10.1590/0037-8682-0485-2016.
- Diamond, M. S., Shrestha, B., Marri, A., Mahan, D., and Engle, M. (2003a). B Cells and

- Antibody Play Critical Roles in the Immediate Defense of Disseminated Infection by West Nile Encephalitis Virus. *J. Virol.* 77, 2578–2586. doi:10.1128/jvi.77.4.2578-2586.2003.
- Diamond, M. S., Sitati, E. M., Friend, L. D., Higgs, S., Shrestha, B., and Engle, M. (2003b). A Critical Role for Induced IgM in the Protection against West Nile Virus Infection. *J. Exp. Med.* 198, 1853–1862. doi:10.1084/jem.20031223.
- Dubischar-Kastner, K., Eder, S., Buerger, V., Gartner-Woelfl, G., Kaltenboeck, A., Schuller, E., et al. (2010). Long-term immunity and immune response to a booster dose following vaccination with the inactivated Japanese encephalitis vaccine IXIARO®, IC51. *Vaccine* 28, 5197–5202. doi:10.1016/j.vaccine.2010.05.069.
- Dunster, L. M., Wang, H., Ryman, K. D., Miller, B. R., Watowich, S. J., Minor, P. D., et al. (1999). Molecular and Biological Changes Associated with HeLa Cell Attenuation of Wild-Type Yellow Fever Virus. 318, 309–318.
- Durbin, A. P., Wright, P. F., Cox, A., Kagucia, W., Elwood, D., Henderson, S., et al. (2013). The live attenuated chimeric vaccine rWN/DEN4 30 is well-tolerated and immunogenic in healthy flavivirus-naïve adult volunteers. *Vaccine* 31, 5772–5777. doi:10.1016/j.vaccine.2013.07.064.
- Ebel, G. D., Fitzpatrick, K. A., Lim, P. Y., Bennett, C. J., Deardorff, E. R., Jerzak, G. V., et al. (2011). Nonconsensus West Nile virus genomes arising during mosquito infection suppress pathogenesis and modulate virus fitness in vivo. *J Virol* 85, 12605–12613. doi:10.1128/JVI.05637-11.
- ECDC (2019). Weekly updates: 2019 West Nile virus transmission season. Available at: <https://www.ecdc.europa.eu/en/west-nile-fever/surveillance-and-disease-data/disease-data-ecdc> [Accessed November 18, 2019].
- Egloff, M. P., Benarroch, D., Selisko, B., Romette, J. L., and Canard, B. (2002). An RNA cap (nucleoside-2'-O-)-methyltransferase in the flavivirus RNA polymerase NS5: Crystal structure and functional characterization. *EMBO J.* 21, 2757–2768. doi:10.1093/emboj/21.11.2757.
- El Garch, H., Minke, J. M., Rehder, J., Richard, S., Edlund Toulemonde, C., Dinic, S., et al. (2008). A West Nile virus (WNV) recombinant canarypox virus vaccine elicits WNV-specific neutralizing antibodies and cell-mediated immune responses in the horse. *Vet. Immunol. Immunopathol.* 123, 230–239. doi:10.1016/j.vetimm.2008.02.002.
- Engle, M. J., and Diamond, M. S. (2003). Antibody prophylaxis and therapy against West Nile virus infection in wild-type and immunodeficient mice. *J. Virol.* 77, 12941–12949.
- Falconar, A. K. I. (1997). The dengue virus nonstructural-1 protein (NS1) generates antibodies to common epitopes on human blood clotting, integrin/adhesin proteins and binds to human endothelial cells: potential implications in haemorrhagic fever pathogenesis. *Arch. Virol.* 142, 897–916.
- Fall, G., Diallo, M., Loucoubar, C., Faye, O., and Sall, A. A. (2014). Vector competence of *Culex neavei* and *Culex quinquefasciatus* (Diptera: Culicidae) from Senegal for lineages 1, 2, Koutango and a putative new lineage of West Nile virus. *Am. J. Trop. Med. Hyg.* 90, 747–754. doi:10.4269/ajtmh.13-0405.
- Fall, G., Paola, N. Di, Faye, M., Dia, M., Ce, C., Freire, M., et al. (2017). Biological and phylogenetic characteristics of West African lineages of West Nile virus. *PLoS*

- Negl. Trop. Dis.*, 1–23.
- Fink, K., Shi, P.-Y., and Qin, C. F. (2014). Novel attenuated dengue virus strains for vaccine application. WO 2014/04.
- Fredericksen, B. L. (2014). The neuroimmune response to West Nile virus. *J. Neurovirol.* 20, 113–121. doi:10.1007/s13365-013-0180-z.
- Fredericksen, B. L., and Gale, M. (2006). West Nile Virus Evades Activation of Interferon Regulatory Factor 3 through RIG-I-Dependent and -Independent Pathways without Antagonizing Host Defense Signaling. *J. Virol.* 80, 2913–2923. doi:10.1128/jvi.80.6.2913-2923.2006.
- Fredericksen, B. L., Keller, B. C., Fornek, J., Katze, M. G., and Gale, M. (2008). Establishment and Maintenance of the Innate Antiviral Response to West Nile Virus Involves both RIG-I and MDA5 Signaling. *J. Virol.* 82, 609–616. doi:10.1128/JVI.01305-07.
- Fredericksen, B. L., Smith, M., Katze, M. G., Shi, P.-Y., and Gale, M. (2004). The Host Response to West Nile Virus Infection Limits Viral Spread through the Activation of the Interferon Regulatory Factor 3 Pathway. *J. Virol.* 78, 7737–7747. doi:10.1128/JVI.78.14.7737.
- Garcia, M. N., Hasbun, R., and Murray, K. O. (2015). Persistence of West Nile virus. *Microbes Infect.* 17, 163–168. doi:10.1016/j.micinf.2014.12.003.
- Gardner, I., Wong, S., Ferraro, G., Balasuriya, U., Hullinger, P., Wilson, W., et al. (2007). Incidence and effects of West Nile virus infection in vaccinated and unvaccinated horses in California. *Vet. Res.* 38, 109–116.
- Getts, D. R., Terry, R. L., Getts, M. T., Müller, M., Rana, S., Deffrasnes, C., et al. (2012). Targeted blockade in lethal West Nile virus encephalitis indicates a crucial role for very late antigen (VLA)-4-dependent recruitment of nitric oxide-producing macrophages. *J. Neuroinflammation* 9, 2–9. doi:10.1186/1742-2094-9-246.
- Ginsburg, A. S., Meghani, A., Halstead, S. B., Yaich, M., Sarah, A., Meghani, A., et al. (2017). Use of the live attenuated Japanese Encephalitis vaccine SA14-14-2 in children: A review of safety and tolerability studies. *Hum. Vaccines Immunother.* 13, 2222–2231. doi:10.1080/21645515.2017.1356496.
- Glass, W. G., Lim, J. K., Cholera, R., Pletnev, A. G., Gao, J., and Murphy, P. M. (2005). Chemokine receptor CCR5 promotes leukocyte trafficking to the brain and survival in West Nile virus infection. *J. Exp. Med.* 202, 1087–1098. doi:10.1084/jem.20042530.
- Glass, W. G., Mcdermott, D. H., Lim, J. K., Lekhong, S., Yu, S. F., Frank, W. A., et al. (2006). CCR5 deficiency increases risk of symptomatic West Nile virus infection. *J. Exp. Med.* 203, 35–40. doi:10.1084/jem.20051970.
- Goo, L., Vanblargan, L. A., Dowd, K. A., Diamond, M. S., and Pierson, C. (2017). A single mutation in the envelope protein modulates flavivirus antigenicity, stability, and pathogenesis. *Plos Pathog.*, 1–32. doi:10.1371/journal.ppat.1006178.
- Goswami, R., and Kaplan, M. H. (2011). A brief history of IL-9. *J. Immunol.* 186, 3283–3288.
- Graham, J. B., Swarts, J. L., Thomas, S., Voss, K. M., Sekine, A., Green, R., et al. (2019). Immune Correlates of Protection From West Nile Virus Neuroinvasion and Disease. *J. Infect. Dis.* 219, 1162–1171. doi:10.1093/infdis/jiy623.
- Grant, D., Tan, G. K., Qing, M., Ng, J. K. W., Yip, A., Zou, G., et al. (2011). A single

- amino acid in nonstructural protein NS4B confers virulence to dengue virus in AG129 mice through enhancement of viral RNA synthesis. *J. Virol.* 85, 7775–7787. doi:10.1128/JVI.00665-11.
- Gromowski, G. D., Firestone, C., and Whitehead, S. S. (2015). Genetic Determinants of Japanese Encephalitis Virus Vaccine Strain SA14-14-2 That Govern Attenuation of Virulence in Mice. *J. Virol.* 89, 6328–6337. doi:10.1128/JVI.00219-15.
- Guirakhoo, F., Pugachev, K., Zhang, Z., Myers, G., Levenbook, I., Draper, K., et al. (2004). Safety and Efficacy of Chimeric Yellow Fever-Dengue Virus Tetravalent Vaccine Formulations in Nonhuman Primates. *J. Virol.* 78, 4761–4775. doi:10.1128/jvi.78.9.4761-4775.2004.
- Gutsche, I., Coulibaly, F., Voss, J. E., Salmon, J., D’Alayer, J., Ermonval, M., et al. (2011). Secreted dengue virus nonstructural protein NS1 is an atypical barrel-shaped high-density lipoprotein. *Proc. Natl. Acad. Sci. U. S. A.* 108, 8003–8008. doi:10.1073/pnas.1017338108.
- Hahn, C. S., Dalrymple, J. M., Strauss, J. H., and Rice, C. M. (1987). Comparison of the virulent Asibi strain of yellow fever virus with the 17D vaccine strain derived from it. *Proc. Natl. Acad. Sci. U. S. A.* 84, 2019–23. doi:10.1073/pnas.84.7.2019.
- Hall, R. A., Scherret, J. H., and Mackenzie, J. S. (2001). Kunjin Virus: An Australian Variant of West Nile? *Ann. N. Y. Acad. Sci.* 951, 153–160.
- Halstead, S. B. (2018). Which dengue vaccine approach is the most promising, and should we be concerned about enhanced disease after vaccination? There is only one true winner. *Cold Spring Harb. Perspect. Biol.* 10.
- Hanna, S. L., Pierson, T. C., Sanchez, M. D., Ahmed, A. A., Murtadha, M. M., and Doms, R. W. (2005). N-Linked Glycosylation of West Nile Virus Envelope Proteins Influences Particle Assembly and Infectivity. 79, 13262–13274. doi:10.1128/JVI.79.21.13262.
- Health, I. A. (2019). Prestige WNV. *Intervet/Merck Anim. Heal.* Available at: <https://merckusa.cvpservice.com/product/basic/view/1047544> [Accessed July 16, 2019].
- Hess, A., Davis, J. K., and Wimberly, M. C. (2018). Identifying Environmental Risk Factors and Mapping the Distribution of West Nile Virus in an Endemic Region of North America. *GeoHealth* 2, 395–409.
- Hombach, J., Solomon, T., Kurane, I., Jacobson, J., and Wood, D. (2005). Report on a WHO consultation on immunological endpoints for evaluation of new Japanese encephalitis vaccines, WHO, Geneva, 2-3 September, 2004. *Vaccine* 23, 5205–5211. doi:10.1016/j.vaccine.2005.07.002.
- Jacobson, E. R., Ginn, P. E., Troutman, J. M., Farina, L., Stark, L., Klenk, K., et al. (2005). West Nile virus infection in farmed American alligators (*Alligator mississippiensis*) in Florida. *J. Wildl. Dis.* 41, 96–106. doi:10.7589/0090-3558-41.1.96.
- Kakumani, P. K., Ponia, S. S., S, R. K., Sood, V., Chinnappan, M., Banerjea, A. C., et al. (2013). Role of RNA Interference (RNAi) in Dengue Virus Replication and Identification of NS4B as an RNAi Suppressor. *J. Virol.* 87, 8870–8883. doi:10.1128/jvi.02774-12.
- Kanai, R., Kar, K., Anthony, K., Gould, L. H., Ledizet, M., Fikrig, E., et al. (2006). Crystal Structure of West Nile Virus Envelope Glycoprotein Reveals Viral Surface

- Epitopes. *J. Virol.* 80, 11000–11008. doi:10.1128/JVI.01735-06.
- Kaufusi, P. H., Kelley, J. F., Yanagihara, R., and Nerurkar, V. R. (2014). Induction of endoplasmic reticulum-derived replication-competent membrane structures by West Nile virus non-structural protein 4B. *PLoS One* 9, e84040. doi:10.1371/journal.pone.0084040.
- Kim, M. K., and Kang, Y. K. (1999). Positional preference of proline in α -helices. *Protein Sci.* 8, 1492–1499. doi:10.1110/ps.8.7.1492.
- Klee, A. L., Maidin, B., Edwin, B., Poshni, I., Mostashari, F., Fine, A., et al. (2004). Long-term prognosis for clinical West Nile virus infection. *Emerg. Infect. Dis.* 10, 1405–11. doi:10.3201/eid1008.030879.
- Klein, R. S., Lin, E., Zhang, B., Luster, A. D., Tollett, J., Samuel, M. A., et al. (2005). Neuronal CXCL10 Directs CD8 γ T-Cell Recruitment and Control of West Nile Virus Encephalitis. 79, 11457–11466. doi:10.1128/JVI.79.17.11457.
- Klema, V. J., Padmanabhan, R., and Choi, K. H. (2015). Flaviviral Replication Complex: Coordination between RNA Synthesis and 5'-RNA Capping. *Viruses* 7, 4640–4656. doi:10.3390/v7082837.
- Knox, J., Cowan, R. U., Doyle, J. S., Ligtermoet, M. K., Archer, J. S., Burrow, J. N. C., et al. (2012). Murray valley encephalitis: A review of clinical features, diagnosis and treatment. *Med. J. Aust.* 196, 322–326. doi:10.5694/mja11.11026.
- Kumar, M., Verma, S., and Nerurkar, V. R. (2010). Pro-inflammatory cytokines derived from West Nile virus (WNV)-infected SK-N-SH cells mediate neuroinflammatory markers and neuronal death. *J. Neuroinflammation* 7, 73. doi:10.1186/1742-2094-7-73.
- Kumeta, M., Konishi, H. A., Zhang, W., Sakagami, S., and Yoshimura, S. H. (2017). Prolines in the α -helix confer the structural flexibility and functional integrity of importin- β . *J. Cell Sci.* 131. doi:10.1242/jcs.206326.
- Kummerer, B. M., and Rice, C. M. (2002). Mutations in the Yellow Fever Virus Nonstructural Protein NS2A Selectively Block Production of Infectious Particles. *J. Virol.* 76, 4773–4784. doi:10.1128/jvi.76.10.4773-4784.2002.
- Kuno, G., Chang, G. J., Tsuchiya, K. R., Karabatsos, N., and Cropp, C. B. (1998). Phylogeny of the Genus Flavivirus. *J. Virol.* 72, 73–83.
- Lanciotti, R. S., Ebel, G. D., Deubel, V., Kerst, A. J., Murri, S., Meyer, R., et al. (2002). Complete genome sequences and phylogenetic analysis of West Nile virus strains isolated from the United States, Europe, and the Middle East. *Virology* 298, 96–105. doi:10.1006/viro.2002.1449.
- Lanciotti, R. S., Roehrig, J. T., Deubel, V., Smith, J., Parker, M., Steele, K., et al. (1999). Origin of the West Nile Virus Responsible for an Outbreak of Encephalitis in the Northeastern United States. *Science* (80-.). 286, 2333–2337.
- Lanteri, M. C., Heitman, J. W., Owen, R. E., Busch, T., Geffer, N., Kiely, N., et al. (2008). Comprehensive Analysis of West Nile Virus-Specific T Cell Responses in Humans. *J. Infect. Dis.* 197, 1296–1306. doi:10.1086/586898.
- Laurent-rolle, M., Boer, E. F., Lubick, K. J., Wolfinbarger, J. B., Carmody, A. B., Rockx, B., et al. (2010). The NS5 Protein of the Virulent West Nile Virus NY99 Strain Is a Potent Antagonist of Type I Interferon-Mediated. *J. Virol.* 84, 3503–3515. doi:10.1128/JVI.01161-09.
- Ledgerwood, J. E., Pierson, T. C., Hubka, S. A., Desai, N., Rucker, S., Gordon, I. J., et al.

- (2011). A West Nile Virus DNA Vaccine Utilizing a Modified Promoter Induces Neutralizing Antibody in Younger and Older Healthy Adults in a Phase I Clinical Trial. *J. Infect. Dis.* 203, 1396–1404. doi:10.1093/infdis/jir054.
- Lee, E., Hall, R. A., and Lobigs, M. (2004). Common E Protein Determinants for Attenuation of Glycosaminoglycan-Binding Variants of Japanese Encephalitis and West Nile Viruses. *J. Virol.* 78, 8271–8280. doi:10.1128/JVI.78.15.8271.
- Lee, E., and Lobigs, M. (2008). E Protein Domain III Determinants of Yellow Fever Virus 17D Vaccine Strain Enhance Binding to Glycosaminoglycans, Impede Virus Spread, and Attenuate Virulence. *J. Virol.* 82, 6024–6033. doi:10.1128/jvi.02509-07.
- Li, S.-H., Dong, H., Li, X.-F., Xie, X., Zhao, H., Deng, Y.-Q., et al. (2013). Rational design of a flavivirus vaccine by abolishing viral RNA 2'-O methylation. *J. Virol.* 87, 5812–9. doi:10.1128/JVI.02806-12.
- Li, Y., Mee, Y., Zou, J., Wang, Q., Gayen, S., Lei, Y., et al. (2015). Secondary structure and membrane topology of dengue virus NS4B N-terminal 125 amino acids. *BBA - Biomembr.* 1848, 3150–3157. doi:10.1016/j.bbamem.2015.09.016.
- Li, Y., Wong, Y. L., Lee, M. Y., Li, Q., Wang, Q. Y., Lescar, J., et al. (2016). Secondary Structure and Membrane Topology of the Full-Length Dengue Virus NS4B in Micelles. *Angew. Chemie - Int. Ed.* 55, 12068–12072. doi:10.1002/anie.201606609.
- Liang, J. J., Liao, C. L., Liao, J. T., Lee, Y. L., and Lin, Y. L. (2009). A Japanese encephalitis virus vaccine candidate strain is attenuated by decreasing its interferon antagonistic ability. *Vaccine* 27, 2746–2754. doi:10.1016/j.vaccine.2009.03.007.
- Lim, J. K., Louie, C. Y., Glaser, C., Jean, C., Johnson, B., Johnson, H., et al. (2008). Genetic Deficiency of Chemokine Receptor CCR5 Is a Strong Risk Factor for Symptomatic West Nile Virus Infection : A Meta-Analysis of 4 Cohorts in the US Epidemic. *J. Infect. Chemother.* 197, 262–265. doi:10.1086/524691.
- Lim, J. K., Obara, C. J., Rivollier, A., Pletnev, A. G., Kelsall, B. L., and Murphy, P. M. (2011). Chemokine Receptor CCR2 is Critical for Monocyte Accumulation and Survival in West Nile Virus Encephalitis. *J. Immunol.* 186, 471–478. doi:10.4049/jimmunol.1003003.
- Lindenbach, B. D., and Rice, C. M. (1999). Genetic interaction of flavivirus nonstructural proteins NS1 and NS4A as a determinant of replicase function. *J. Virol.* 73, 4611–21. Available at: <http://www.ncbi.nlm.nih.gov/pubmed/10233920> <http://www.pubmedcentral.nih.gov/articlerender.fcgi?artid=PMC112502>.
- Lindenbach, B. D., Thiel, H.-J., and Rice, C. M. (2007). *Fields Virology, 5th Edition*. 5th ed., eds. D. M. Knipe and P. M. Howley Philadelphia: Lippincott-Raven Publishers.
- Liu, W. J., Wang, X. J., Clark, D. C., Lobigs, M., Hall, R. a, and Khromykh, A. a (2006). A Single Amino Acid Substitution in the West Nile Virus Nonstructural Protein NS2A Disables Its Ability To Inhibit Alpha / Beta Interferon Induction and Attenuates Virus Virulence in Mice A Single Amino Acid Substitution in the West Nile Virus Nonstructur. *J. Virol.* 80, 2396–2404. doi:10.1128/JVI.80.5.2396.
- Liu, X., Jia, L., Nie, K., Zhao, D., Na, R., Xu, H., et al. (2019). Evaluation of environment safety of a Japanese encephalitis live attenuated vaccine. *Biologicals* 60, 36–41. doi:10.1016/j.biologicals.2019.06.001.
- Liu, X., Zhao, D., Jia, L., Xu, H., Na, R., Ge, Y., et al. (2018). Genetic and

- neuroattenuation phenotypic characteristics and their stabilities of SA14-14-2 vaccine seed virus. *Vaccine* 36, 4650–4656. doi:10.1016/j.vaccine.2018.06.040.
- Malet, H., Egloff, M., Selisko, B., Butcher, R. E., Wright, P. J., Roberts, M., et al. (2007). Crystal Structure of the RNA Polymerase Domain of the West Nile Virus Non-structural Protein 5. *J. Biol. Chem.* 282, 10678–10689. doi:10.1074/jbc.M607273200.
- Mann, B. R., McMullen, A. R., Swetnam, D. M., and Barrett, A. D. T. (2013). Molecular epidemiology and evolution of West Nile virus in North America. *Int. J. Environ. Res. Public Health* 10, 5111–5129. doi:10.3390/ijerph10105111.
- Marcantonio, M., Rizzoli, A., Metz, M., Rosa, R., Marini, G., Chadwick, E., et al. (2015). Identifying the Environmental Conditions Favouring West Nile Virus Outbreaks in Europe. *PLoS One* 10.
- Markoff, L. (2000). Points to consider in the development of a surrogate for efficacy of novel Japanese encephalitis virus vaccines. *Vaccine* 18, 26–32. doi:10.1016/S0264-410X(00)00038-4.
- Martin, J. E., Pierson, T. C., Hubka, S., Rucker, S., Gordon, I. J., Enama, M. E., et al. (2007). A West Nile virus DNA vaccine induces neutralizing antibody in healthy adults during a phase 1 clinical trial. *J. Infect. Dis.* 196, 1732–1740. doi:10.1086/523650.A.
- Martins, R. D. M., Leal, M. D. L. F., and Homma, A. (2015). Serious adverse events associated with yellow fever vaccine. *Hum. Vaccines Immunother.* 11, 2183–2187. doi:10.1080/21645515.2015.1022700.
- May, F. J., Davis, C. T., Tesh, R. B., and Barrett, A. D. T. (2011). Phylogeography of West Nile Virus: from the Cradle of Evolution in Africa to Eurasia, Australia, and the Americas. *J. Virol.* 85, 2964–2974. doi:10.1128/jvi.01963-10.
- May, F. J., Li, L., Davis, C. T., Galbraith, S. E., and Barrett, A. D. T. (2010). Multiple pathways to the attenuation of West Nile virus in South-East Texas in 2003. *Virology* 405, 8–14. doi:10.1016/j.virol.2010.04.022.
- McMurtrey, C. P., Lelic, A., Piazza, P., Chakrabarti, A. K., Yablonsky, E. J., Wahl, A., et al. (2008). Epitope discovery in West Nile virus infection: Identification and immune recognition of viral epitopes. *Proc. Natl. Acad. Sci. U. S. A.* 105, 2981–2986. doi:10.1073/pnas.0711874105.
- Melian, E. B., Edmonds, J. H., Nagasaki, T. K., Hinzman, E., Floden, N., and Khromykh, A. A. (2013). West Nile virus NS2A protein facilitates virus-induced apoptosis independently of interferon response. *J. Gen. Virol.* 94, 308–313. doi:10.1099/vir.0.047076-0.
- Monath, T. P., Liu, J., Kanesa-athan, N., Myers, G. A., Ni, R., Deary, A., et al. (2006). A live, attenuated recombinant West Nile virus vaccine. *PNAS* 103.
- Mun, J. L., Ashok, M., Lipkin, W. I., and Garci, A. (2005). Inhibition of Alpha / Beta Interferon Signaling by the NS4B Protein of Flaviviruses. 79, 8004–8013. doi:10.1128/JVI.79.13.8004.
- Muylaert, I. R., Chambers, T. J., Galler, R., and Rice, C. M. (1996). Mutagenesis of the N-linked glycosylation sites of the yellow fever virus NS1 protein: Effects on virus replication and mouse neurovirulence. *Virology* 222, 159–168. doi:10.1006/viro.1996.0406.
- Nash, D., Mostashari, F., Fine, A., Miller, J., O’Leary, D., Murray, K., et al. (2001). The

- Outbreak of West Nile Virus Infection in the New York City Area in 1999. *N. Engl. J. Med.* 344, 1807–1814.
- NCBI (2019). IL5 interleukin 5. *NCBI Natl. Institutes Heal.* Available at: <https://www.ncbi.nlm.nih.gov/gene/3567> [Accessed July 12, 2019].
- Ng, T., Hathaway, D., Jennings, N., Champ, D., Chiang, Y. W., and Chu, H. J. (2003). Equine vaccine for West Nile virus. *Dev. Biol. (Basel)*. 114, 221–227.
- Ni, H., Burns, N. J., Chang, G.-J. J., Zhang, M.-J., Wills, M. R., Trent, D. W., et al. (1994). Comparison of nucleotide and deduced amino acid sequence of the 5' non-coding region and structural protein genes of the wild-type Japanese encephalitis virus strain SA14 and its attenuated vaccine derivatives. *J. Gen. Virol.* 75, 1505–1510.
- Ni, H. L., Chang, G. J. J., Xie, H., Trent, D. W., and Barrett, A. D. T. (1995). Molecular basis of attenuation of neurovirulence of wild- type Japanese encephalitis virus strain SA14. *J. Gen. Virol.* 76, 409–413.
- Nishijima, N., Marusawa, H., Ueda, Y., Takahashi, K., and Nasu, A. (2012). Dynamics of Hepatitis B Virus Quasispecies in Association with Nucleos(t)ide Analogue Treatment Determined by Ultra-Deep Sequencing. *PLoS One* 7, 1–10. doi:10.1371/journal.pone.0035052.
- Nybakken, G. E., Nelson, C. A., Chen, B. R., Diamond, M. S., and Fremont, D. H. (2006). Crystal Structure of the West Nile Virus Envelope Glycoprotein. *J. Virol.* 80, 11467–11474. doi:10.1128/JVI.01125-06.
- Orozco, S., Schmid, M. A., Parameswaran, P., Lachica, R., Henn, M. R., Beatty, R., et al. (2012). Characterization of a model of lethal dengue virus 2 infection in C57BL/6 mice deficient in the alpha/beta interferon receptor. *J. Gen. Virol.* 93, 2152–2157. doi:10.1099/vir.0.045088-0.
- Pachler, K., Lebl, K., Berer, D., Rudolf, I., Hubalek, Z., and Nowotny, N. (2014). Putative new west nile virus lineage in *Uranotaenia unguiculata* mosquitoes, Austria, 2013. *Emerg. Infect. Dis.* 20, 2119–2122. doi:10.3201/eid2012.140921.
- Padgett, K. A., Reisen, W. K., Kahl-purcell, N., Fang, Y., Cahoon-young, B., Carney, R., et al. (2007). West Nile Virus Infection In Tree Squirrels (Rodentia: Sciuridae) In California, 2004-2005. *Am J Trop Med Hyg* 76, 810–813.
- Paz, S., and Semenza, J. C. (2013). Environmental Drivers of West Nile Fever Epidemiology in Europe and Western Asia —A Review. *Int. J. Environ. Res. Public Health* 10, 3543–3562.
- Pérez-Ramírez, E., Llorente, F., Del Amo, J., Fall, G., Sall, A. A., Lubisi, A., et al. (2017). Pathogenicity evaluation of twelve west nile virus strains belonging to four lineages from five continents in a mouse model: Discrimination between three pathogenicity categories. *J. Gen. Virol.* 98, 662–670. doi:10.1099/jgv.0.000743.
- Petersen, L. R., Brault, A. C., and Nasci, R. S. (2013). West Nile virus: review of the literature. *Jama* 310, 308–15. doi:10.1001/jama.2013.8042.
- Pierce, K. K., Whitehead, S. S., Kirkpatrick, B. D., and Grier, P. L. (2017). A Live Attenuated Chimeric West Nile Virus Vaccine, rWN/DEN4Δ30, Is Well Tolerated and Immunogenic in Flavivirus-Naive Older Adult Volunteers. *J. Infect. Dis.* 215, 52–55. doi:10.1093/infdis/jiw501.
- Platt, K. B., Tucker, B. J., Halbur, P. G., Tiawsirisup, S., Blitvich, B. J., Fabiosa, F. G., et al. (2007). West Nile virus viremia in eastern chipmunks (*Tamias striatus*) sufficient

- for infecting different mosquitoes. *Emerg. Infect. Dis.* 13, 831–837. doi:10.3201/eid1306.061008.
- Pletnev, A. G., Putnak, R., Speicher, J., Wagar, E. J., and Vaughn, D. W. (2002). West Nile virus/dengue type 4 virus chimeras that are reduced in neurovirulence and peripheral virulence without loss of immunogenicity or protective efficacy. *Proc. Natl. Acad. Sci.* 99, 3036–3041. doi:10.1073/pnas.022652799.
- Pletnev, A. G., Swayne, D. E., Speicher, J., Rumyantsev, A. A., and Murphy, B. R. (2006). Chimeric West Nile/dengue virus vaccine candidate: Preclinical evaluation in mice, geese and monkeys for safety and immunogenicity. *Vaccine* 24, 6392–6404. doi:10.1016/j.vaccine.2006.06.008.
- Plotkin, S. A., Cadoz, M., Meignier, B., Meric, C., Leroy, O., Excler, J. L., et al. (1995). The safety and use of canarypox vectored vaccines. *Dev. Biol. Stand.* 84, 165–170.
- Prow, N. A., Setoh, Y. X., Biron, R. M., Sester, D. P., Kim, K. S., Hobson-Peters, J., et al. (2014). The West Nile Virus-Like Flavivirus Koutango Is Highly Virulent in Mice due to Delayed Viral Clearance and the Induction of a Poor Neutralizing Antibody Response. *J. Virol.* 88, 9947–9962. doi:10.1128/jvi.01304-14.
- Pryor, M. J., Gualano, R. C., Lin, B., Davidson, A. D., and Wright, P. J. (1998). Growth restriction of dengue virus type 2 by site-specific mutagenesis of virus-encoded glycoproteins. *J. Gen. Virol.* 79, 2631–2639. doi:10.1099/0022-1317-79-11-2631.
- Puig-Basagoiti, F., Tilgner, M., Bennett, C. J., Zhou, Y., Muñoz-Jordán, J. L., García-Sastre, A., et al. (2007). A mouse cell-adapted NS4B mutation attenuates West Nile virus RNA synthesis. *Virology* 361, 229–241. doi:10.1016/j.virol.2006.11.012.
- Purtha, W. E., Myers, N., Mitaksov, V., Sitati, E., Connolly, J., Fremont, D. H., et al. (2007). Antigen-specific cytotoxic T lymphocytes protect against lethal West Nile virus encephalitis. *Eur. J. Immunol.* 37, 1845–1854. doi:10.1002/eji.200737192.
- Qian, F., Goel, G., Meng, H., Wang, X., You, F., Devine, L., et al. (2015). Systems Immunology Reveals Markers of Susceptibility to West Nile Virus Infection. *Clin. Vaccine Immunol.* 22, 6–16. doi:10.1128/CVI.00508-14.
- Rastogi, M., Sharma, N., and Singh, S. K. (2016). Flavivirus NS1: A multifaceted enigmatic viral protein. *Virol. J.* 13, 1–10. doi:10.1186/s12985-016-0590-7.
- Ray, D., Shah, A., Tilgner, M., Guo, Y., Zhao, Y., Dong, H., et al. (2006). West Nile Virus 5'-Cap Structure Is Formed by Sequential Guanine N-7 and Ribose 2'-O Methylations by Nonstructural Protein 5. *J. Virol.* 80, 8362–8370. doi:10.1128/JVI.00814-06.
- Roehrig, J. T. (2013). West Nile virus in the United States - A historical perspective. *Viruses* 5, 3088–3108. doi:10.3390/v5123088.
- Roehrig, J. T., Staudinger, L. A., Hunt, A. R., Mathews, J. H., and Blair, C. D. (2006). Antibody prophylaxis and therapy for flavivirus encephalitis infections. *Ann. N. Y. Acad. Sci.* 951, 286–297.
- Roesch, F., Fajardo, A., Moratorio, G., and Vignuzzi, M. (2019). Usutu Virus: An Arbovirus on the Rise. *Viruses* 11, 1–14. doi:10.3390/v11070640.
- Rosenberg, R., Lindsey, N. P., Fischer, M., Gregory, C. J., Hinckley, A. F., Mead, P. S., et al. (2018). Vital signs: Trends in reported vectorborne disease cases — United States and Territories, 2004–2016. *Morb. Mortal. Wkly. Rep.* 67, 496–501.
- Rossi, S. L., Fayzulin, R., Dewsbury, N., Bourne, N., and Mason, P. W. (2007). Mutations in West Nile virus nonstructural proteins that facilitate replicon

- persistence in vitro attenuate virus replication in vitro and in vivo. *Virology* 364, 184–195. doi:10.1016/j.virol.2007.02.009.
- Ryman, K. D., Ledger, T. N., Campbell, G. A., Watowich, S. J., and Barrett, A. D. T. (1998). Mutation in a 17D-204 vaccine substrain-specific envelope protein epitope alters the pathogenesis of yellow fever virus in mice. *Virology* 244, 59–65. doi:10.1006/viro.1998.9057.
- Samuel, M. A., and Diamond, M. S. (2005). Alpha/Beta Interferon Protects against Lethal West Nile Virus Infection by Restricting Cellular Tropism and Enhancing Neuronal Survival. *J. Virol.* 79, 13350–13361. doi:10.1128/jvi.79.21.13350-13361.2005.
- Samuel, M. A., and Diamond, M. S. (2006). Pathogenesis of West Nile Virus Infection: a Balance between Virulence, Innate and Adaptive Immunity, and Viral Evasion. *J. Virol.* 80, 9349–9360. doi:10.1128/JVI.01122-06.
- Scaturro, P., Cortese, M., Chatel-Chaix, L., Fischl, W., and Bartenschlager, R. (2015). Dengue Virus Non-structural Protein 1 Modulates Infectious Particle Production via Interaction with the Structural Proteins. *PLoS Pathog.* 11, 1–32. doi:10.1371/journal.ppat.1005277.
- Schneider, A., Krüger, C., Steigleder, T., Weber, D., Pitzer, C., Laage, R., et al. (2005). The hematopoietic factor G-CSF is a neuronal ligand that counteracts programmed cell death and drives neurogenesis. *J. Clin. Invest.* 115, 2083–2098. doi:10.1172/JCI23559.or.
- Schuler, L., Khaitisa, M., Dyer, N., and Stoltenow, C. (2004). Evaluation of an outbreak of West Nile virus infection in horses: 569 cases (2002). *J Am Vet Med Assoc* 225, 1084–9.
- Schweitzer, B. K., Chapman, N. M., and Iwen, P. C. (2009). Overview of the *Flaviviridae* With an Emphasis on the Japanese Encephalitis Group Viruses. *Lab. Med.* 40, 493–499. doi:10.1309/LM5YWS85NJPCWESW.
- Scott, K. A., Alonso, D. O. V., Sato, S., Fersht, A. R., and Daggett, V. (2007). Conformational entropy of alanine versus glycine in protein denatured states. *Proc. Natl. Acad. Sci. U. S. A.* 104, 2661–2666. doi:10.1073/pnas.0611182104.
- Shankar, M. B., Staples, J. E., Meltzer, M. I., and Fischer, M. (2017). Cost effectiveness of a targeted age-based West Nile virus vaccination program. *Vaccine* 35, 3143–3151. doi:10.1016/j.vaccine.2016.11.078.
- Shi, P., Tilgner, M., Lo, M. K., Kent, K. A., and Bernard, K. A. (2002). Infectious cDNA Clone of the Epidemic West Nile Virus from New York City. *J. Virol.* 76, 5847–56. doi:10.1128/JVI.76.12.5847.
- Shiryaev, S. A., Chernov, A. V., Aleshin, A. E., Shiryaeva, T. N., and Strongin, A. Y. (2009). NS4A regulates the ATPase activity of the NS3 helicase: A novel cofactor role of the non-structural protein NS4A from West Nile virus. *J. Gen. Virol.* 90, 2081–2085. doi:10.1099/vir.0.012864-0.
- Shrestha, B., and Diamond, M. S. (2004). Role of CD8⁺ T cells in control of West Nile virus infection. *J. Virol.* 78, 8312–8321.
- Shrestha, B., Ng, T., Chu, H., Noll, M., and Diamond, M. (2008). The relative contribution of antibody and CD8⁺ T cells to vaccine immunity against West Nile encephalitis virus. *Vaccine* 26, 2020–33.
- Shrestha, B., Samuel, M. A., and Diamond, M. S. (2006a). CD8⁺ T Cells Require

- Perforin To Clear West Nile Virus from Infected Neurons. *J. Virol.* 80, 119–129. doi:10.1128/jvi.80.1.119-129.2006.
- Shrestha, B., Wang, T., Samuel, M. A., Whitby, K., Craft, J., Fikrig, E., et al. (2006b). Gamma Interferon Plays a Crucial Early Antiviral Role in Protection against West Nile Virus Infection. *J. Virol.* 80, 5338–5348. doi:10.1128/jvi.00274-06.
- Sitati, E. M., and Diamond, M. S. (2006). CD4+ T-Cell Responses Are Required for Clearance of West Nile Virus from the Central Nervous System. *J. Virol.* 80, 12060–12069. doi:10.1128/jvi.01650-06.
- Smith, H. L., Monath, T. P., Pazoles, P., Rothman, A. L., Casey, D. M., Terajima, M., et al. (2011). Development of antigen-specific memory CD8+ T cells following live-attenuated chimeric West Nile virus vaccination. *J. Infect. Dis.* 203, 513–522. doi:10.1093/infdis/jiq074.
- Smithburn, K. C., Hughes, T. P., Burke, A. W., and Paul, J. H. (1940). A neurotropic virus isolated from the blood of a native of uganda. *Am. J. Trop. Med. Hyg.* 20, 471–492.
- Sohn, Y. M., Tandan, J. B., Yoksan, S., Ji, M., and Ohrr, H. (2008). A 5-year follow-up of antibody response in children vaccinated with single dose of live attenuated SA14-14-2 Japanese encephalitis vaccine: Immunogenicity and anamnestic responses. *Vaccine* 26, 1638–1643. doi:10.1016/j.vaccine.2008.01.021.
- Somnuk, P., Hauhart, R. E., Atkinson, J. P., Diamond, M. S., and Avirutnan, P. (2011). N-linked glycosylation of dengue virus NS1 protein modulates secretion, cell-surface expression, hexamer stability, and interactions with human complement. *Virology* 413, 253–264. doi:10.1016/j.virol.2011.02.022.
- Staples, J. E., Shankar, M. B., Sejvar, J. J., Meltzer, M. I., and Fischer, M. (2014). Initial and Long-Term Costs of Patients Hospitalized with West Nile Virus Disease. *Am. J. Trop. Med. Hyg.* 90, 402–409. doi:10.4269/ajtmh.13-0206.
- Suthar, M. S., Ma, D. Y., Thomas, S., Lund, J. M., Zhang, N., Daffis, S., et al. (2010). IPS-1 Is Essential for the Control of West Nile Virus Infection and Immunity. 6. doi:10.1371/journal.ppat.1000757.
- Tanaka, M., Haishi, S., Aira, Y., Kurihara, S., Morita, K., and Igarashi, A. (1991). Homology among Eleven Flavivirus by Comparative Nucleotide Sequence of Geomic RNAs and Deduced Amino Acid Sequences of Viral Proteins. *Trop. Med.* 33, 23–33.
- Tsai, T. F., Popovici, F., Cernescu, C., Campbell, G. L., Nedelcu, N. I., and Team, I. (1998). West Nile encephalitis epidemic in southeastern Romania. *Lancet* 352, 1–5.
- Uhrlaub, J. L., Brien, J. D., Widman, D. G., Mason, P. W., and Nikolich-zugich, J. (2011). Repeated in vivo stimulation of T and B cell responses in old mice generates protective immunity against lethal West Nile virus encephalitis. *J. Immunol.* 186, 3882–3891.
- Umareddy, I., Chao, A., Sampath, A., Gu, F., and Vasudevan, S. G. (2006). Dengue virus NS4B interacts with NS3 and dissociates it from single-stranded RNA. *J. Gen. Virol.* 87, 2605–2614. doi:10.1099/vir.0.81844-0.
- Van Slyke, G. A., Jia, Y., Whiteman, M. C., Wicker, J. A., Barrett, A. D. T., and Kramer, L. D. (2013). Vertebrate attenuated West Nile virus mutants have differing effects on vector competence in *Culex tarsalis* mosquitoes. *J. Gen. Virol.* 94, 1069–1072. doi:10.1099/vir.0.049833-0.

- Vázquez, A., Sánchez-Seco, M. P., Ruiz, S., Molero, F., Hernández, L., Moreno, J., et al. (2010). Putative new lineage of West Nile virus, Spain. *Emerg. Infect. Dis.* 16, 549–552. doi:10.3201/eid1603.091033.
- Vetera WNV *Boehringer Ingelheim*. Available at: https://www.bi-vetmedica.com/species/equine/products/vetera_vaccines/Vetera_WNV.html [Accessed July 5, 2019].
- Wang, T., Scully, E., Yin, Z., Kim, J. H., Wang, S., Yan, J., et al. (2003a). IFN- γ -Producing $\gamma\delta$ T Cells Help Control Murine West Nile Virus Infection. *J. Immunol.* 171, 2524–2531. doi:10.4049/jimmunol.171.5.2524.
- Wang, T., Town, T., Alexopoulou, L., Anderson, J. F., Fikrig, E., Flavell, R. A., et al. (2004). Toll-like receptor 3 mediates West Nile virus entry into the brain causing lethal encephalitis. *Nat. Med.* 10, 1366–1373. doi:10.1038/nm1140.
- Wang, X., Li, S., Zhu, L., Nian, Q., Yuan, S., Gao, Q., et al. (2017). Near-atomic structure of Japanese encephalitis virus reveals critical determinants of virulence and stability. *Nat. Commun.* 8, 1–8. doi:10.1038/s41467-017-00024-6.
- Wang, X., Liu, W. J., Wang, X. J., Mokhonov, V. V., and Shi, P. (2005). Inhibition of Interferon Signaling by the New York 99 Strain and Kunjin Subtype of West Nile Virus Involves Blockage of ... Inhibition of Interferon Signaling by the New York 99 Strain and Kunjin Subtype of West Nile Virus Involves Blockage of STAT1 and S. *J. Virol.* 79, 1934–1942. doi:10.1128/JVI.79.3.1934.
- Wang, Y., Lobigs, M., Lee, E., and Mullbacher, A. (2003b). CD8+ T Cells Mediate Recovery and Immunopathology in West Nile Virus Encephalitis. *J. Virol.* 77, 13323–13334. doi:10.1128/jvi.77.24.13323-13334.2003.
- Weinberger, B. (2012). Vaccines for the elderly. *Clin. Microbiol. Infect.* 18, 100–108.
- Welte, T., Xie, G., Wicker, J. A., Whiteman, M. C., Li, L., Rachamalla, A., et al. (2011). Immune responses to an attenuated West Nile virus NS4B-P38G mutant strain. *Vaccine* 29, 4853–4861. doi:10.1016/j.vaccine.2011.04.057.
- Whiteman, M. C., Li, L., Wicker, J. A., Kinney, R. M., Huang, C., Beasley, D. W. C., et al. (2010). Development and characterization of non-glycosylated E and NS1 mutant viruses as a potential candidate vaccine for West Nile virus. *Vaccine* 28, 1075–1083. doi:10.1016/j.vaccine.2009.10.112.
- Whiteman, M. C., Popov, V., Sherman, M. B., Wen, J., and Barrett, A. D. T. (2015). Attenuated West Nile Virus Mutant NS1 130-132QQA/175A/207A Exhibits Virus-Induced Ultrastructural Changes and Accumulation of Protein in the Endoplasmic Reticulum. *J. Virol.* 89, 1474–1478. doi:10.1128/JVI.02215-14.
- Whiteman, M. C., Wicker, J. A., Kinney, R. M., Huang, C. Y. H., Solomon, T., and Barrett, A. D. T. (2011). Multiple amino acid changes at the first glycosylation motif in NS1 protein of West Nile virus are necessary for complete attenuation for mouse neuroinvasiveness. *Vaccine* 29, 9702–9710. doi:10.1016/j.vaccine.2011.09.036.
- WHO Japanese encephalitis virus- vaccines. *World Heal. Organ.* Available at: https://www.who.int/ith/vaccines/japanese_encephalitis/en/ [Accessed July 5, 2017].
- WHO (2013). Correlates of vaccine-induced protection: methods and implications. *World Heal. Organ. Initiat. Vaccine Res.* Available at: https://apps.who.int/iris/bitstream/handle/10665/84288/WHO_IVB_13.01_eng.pdf;sequence=1 [Accessed August 15, 2019].
- WHO (2019). Japanese encephalitis. *World Heal. Organ.* Available at:

- <https://www.who.int/news-room/fact-sheets/detail/japanese-encephalitis>.
- Wicker, J. A., Whiteman, M. C., Beasley, D. W. C., Davis, C. T., McGee, C. E., Lee, J. C., et al. (2012). Mutational analysis of the West Nile virus NS4B protein. *Virology* 426, 22–33. doi:10.1016/j.virol.2011.11.022.
- Wicker, J. A., Whiteman, M. C., Beasley, D. W. C., Davis, C. T., Zhang, S., Schneider, B. S., et al. (2006). A single amino acid substitution in the central portion of the West Nile virus NS4B protein confers a highly attenuated phenotype in mice. *Virology* 349, 245–253. doi:10.1016/j.virol.2006.03.007.
- Williams, R. A. J., Vazquea, A., IAsante, I., Bonney, K., Odoom, S., Puplampu, N., et al. (2012). Yaoundé-like virus in resident wild bird, Ghana. *African J. Microbiol. Res.* 6, 1966–1969. doi:10.5897/ajmr11.479.
- Wilm, A., Aw, P. P. K., Bertrand, D., Yeo, G. H. T., Ong, S. H., Wong, C. H., et al. (2012). LoFreq: A sequence-quality aware, ultra-sensitive variant caller for uncovering cell-population heterogeneity from high-throughput sequencing datasets. *Nucleic Acids Res.* 40, 11189–11201. doi:10.1093/nar/gks918.
- Wilson, J. R., de Sessions, P. F., Leon, M. A., and Scholle, F. (2008). West Nile virus nonstructural protein 1 inhibits TLR3 signal transduction. *J. Virol.* 82, 8262–71. doi:10.1128/JVI.00226-08.
- Woods, C. W., Sanchez, A. M., Swamy, G. K., McClain, M. T., Harrington, L., Freeman, D., et al. (2019). An observer blinded, randomized, placebo-controlled, phase I dose escalation trial to evaluate the safety and immunogenicity of an inactivated West Nile virus Vaccine, HydroVax-001, in healthy adults. *Vaccine* 37, 4222–4230. doi:10.1016/j.vaccine.2018.12.026.
- Xie, G., Luo, H., Tian, B., Mann, B., Bao, X., McBride, J., et al. (2015). A West Nile virus NS4B-P38G mutant strain induces cell intrinsic innate cytokine responses in human monocytic and macrophage cells. *Vaccine* 33, 869–878. doi:10.1021/ja303183z.Aqueous.
- Xie, X., Zou, J., Wang, Q., Noble, C. G., Lescar, J., and Shi, P. (2014). Generation and characterization of mouse monoclonal antibodies against NS4B protein of dengue virus. *Virology* 450–451, 250–257. doi:10.1016/j.virol.2013.12.025.
- Yakub, I., Lillibridge, K. M., Moran, A., Gonzalez, O. Y., Belmont, J., Gibbs, R. A., et al. (2005). Single Nucleotide Polymorphisms in Genes for 2'-5'-Oligoadenylate Synthetase and RNase L in Patients Hospitalized with West Nile Virus Infection. *J. Infect. Dis.* 192, 1741–1748. doi:10.1086/497340.
- Yamshchikov, V., Manuvakhova, M., and Rodriguez, E. (2016). Development of a human live attenuated West Nile infectious DNA vaccine : Suitability of attenuating mutations found in SA14-14-2 for WN vaccine design. *Virology* 487, 198–206. doi:10.1016/j.virol.2015.10.015.
- Yamshchikov, V., Manuvakhova, M., Rodriguez, E., and Hébert, C. (2017). Development of a human live attenuated West Nile infectious DNA vaccine: Identification of a minimal mutation set conferring the attenuation level acceptable for a human vaccine. *Virology* 500, 122–129. doi:10.1016/j.virol.2016.10.012.
- Yang, D., Li, X. F., Ye, Q., Wang, H. J., Deng, Y. Q., Zhu, S. Y., et al. (2014). Characterization of live-attenuated Japanese encephalitis vaccine virus SA14-14-2. *Vaccine* 32, 2675–2681. doi:10.1016/j.vaccine.2014.03.074.
- Yang, J., Yang, H., Li, Z., Wang, W., Lin, H., Liu, L., et al. (2017). Envelope protein

- mutations L107F and E138K are important for neurovirulence attenuation for Japanese encephalitis virus SA14-14-2 strain. *Viruses* 9. doi:10.3390/v9010020.
- Youn, S., Li, T., McCune, B. T., Edeling, M. A., Fremont, D. H., Cristea, I. M., et al. (2012). Evidence for a genetic and physical interaction between nonstructural proteins NS1 and NS4B that modulates replication of West Nile virus. *J. Virol.* 86, 7360–71. doi:10.1128/JVI.00157-12.
- Yu, L., Takeda, K., and Markoff, L. (2013). Protein-protein interactions among West Nile non-structural proteins and transmembrane complex formation in mammalian cells. *Virology* 446, 365–377. doi:10.1016/j.virol.2013.08.006.
- Yu, Y. (2010). Phenotypic and genotypic characteristics of Japanese encephalitis attenuated live vaccine virus SA14-14-2 and their stabilities. *Vaccine* 28, 3635–3641. doi:10.1016/j.vaccine.2010.02.105.
- Zhang, B., Chan, Y. K., Lu, B., Diamond, M. S., Klein, R. S., Zhang, B., et al. (2008). CXCR3 Mediates Region-Specific Antiviral T Cell Trafficking within the Central Nervous System during West Nile Virus. *J. Immunol.* 180, 2641–2649. doi:10.4049/jimmunol.180.4.2641.
- Zhang, H., Ye, H., Liu, S., Deng, C., Li, X., Shi, P., et al. (2017). West Nile Virus NS1 Antagonizes interferon beta production by targeting RIG-I and MDA5. *J. Virol.* 91, 1–17.
- Zhang, S., Li, L., Woodson, S. E., Huang, C. Y., Kinney, R. M., Barrett, A. D. T., et al. (2006). A mutation in the envelope protein fusion loop attenuates mouse neuroinvasiveness of the NY99 strain of West Nile virus. *Virology* 353, 35–40. doi:10.1016/j.virol.2006.05.025.
- Zhao, Z., Date, T., Li, Y., Kato, T., Miyamoto, M., Yasui, K., et al. (2005). Characterization of the E-138 (Glu/Lys) mutation in Japanese encephalitis virus by using a stable, full-length, infectious cDNA clone. *J. Gen. Virol.* 86, 2209–2220. doi:10.1099/vir.0.80638-0.
- Zhou, Y., Ray, D., Zhao, Y., Dong, H., Ren, S., Li, Z., et al. (2007). Structure and Function of Flavivirus NS5 Methyltransferase. *J. Virol.* 81, 3891–3903. doi:10.1128/JVI.02704-06.
- Zmurko, J., Neyts, J., and Dallmeier, K. (2015). Flaviviral NS4b, chameleon and jack-in-the-box roles in viral replication and pathogenesis, and a molecular target for antiviral intervention. *Rev. Med. Virol.* 25, 205–223. doi:10.1002/rmv.1835.
- Zou, J., Lee, L. T., Wang, Q. Y., Xie, X., Lu, S., Yau, Y. H., et al. (2015a). Mapping the Interactions between the NS4B and NS3 Proteins of Dengue virus. 89, 3471–3483. doi:10.1128/JVI.03454-14.
- Zou, J., Xie, X., Lee, L. T., Chandrasekaran, R., Reynaud, A., Yap, L., et al. (2014). Dimerization of flavivirus NS4B protein. *J. Virol.* 88, 3379–91. doi:10.1128/JVI.02782-13.
- Zou, J., Xie, X., Wang, Q.-Y., Dong, H., Lee, M. Y., Kang, C., et al. (2015b). Characterization of Dengue Virus NS4A and NS4B Protein Interaction. *J. Virol.* 89, 3455–3470. doi:10.1128/JVI.03453-14.
- Zust, R., Dong, H., Li, X., Chang, D. C., Zhang, B., Zu, R., et al. (2013). Rational Design of a Live Attenuated Dengue Vaccine : 2'-O-Methyltransferase Mutants Are Highly Attenuated and Immunogenic in Mice and Macaques. *Plos Pathog.* 9. doi:10.1371/journal.ppat.1003521.

Züst, R., Li, S. H., Xie, X., Velumani, S., Chng, M., Toh, Y. X., et al. (2017). Characterization of a candidate tetravalent vaccine based on 2'-O-methyltransferase mutants. *PLoS One* 13, 1–19. doi:10.1371/journal.pone.0189262.

Curriculum Vitae

NAME: Jaclyn Kaiser

DATE: Nov. 19, 2019

PRESENT POSITION AND ADDRESS:

Pre-doctoral Research Fellow
Microbiology and Immunology Graduate Program
University of Texas Medical Branch at Galveston
301 University Blvd.
Galveston, TX 77555-0609

Phone: 409-772-2547

Email: jakaiser@utmb.edu

BIOGRAPHICAL:

Date of birth: January 14, 1991
Birthplace: Ranson, WV
Citizenship: USA
Contact information: 543 Morison Street
Charles Town, WV 25414
304-268-4847
jblanc91@gmail.com

EDUCATION:

Aug. 2014 to present: Doctor of Philosophy
Microbiology & Immunology
The University of Texas Medical Branch, Galveston, TX
Expected completion: 2019

Aug. 2009 – May 2013: Bachelor of Science in Biology
Shepherd University, Shepherdstown, WV

CERTIFICATIONS:

2015: Approved to work at biosafety level 3 (BSL-3)
2012: CDC select agent clearance
2012: Approved to work at biosafety level 2 (BSL-2)

PROFESSIONAL EXPERIENCE:

Aug. 2014 to present: Pre-doctoral research fellow
Microbiology & Immunology Graduate Program
The University of Texas Medical Branch, Galveston, TX
Mentor: Alan Barrett, PhD

Project: Characterization of attenuating mutations in West Nile virus

July 2012- Aug. 2014: Biological Science Aid
United States Department of Agriculture
Frederick, MD
Mentor: William Schneider
Project: Genomic and proteomic analysis of *Rathayibacter toxicus*

Grant support:

May 2017- May 2019: NIH NIAID T32 Emerging and Tropical Infectious Diseases Training Program (2 T32 AI 7526-16).
Principal Investigator Dr. Lynn Soong.

MENTORING RESPONSIBILITIES:

University of Texas Medical Branch

Jan. 2019 – April 2019: Mentored two laboratory rotation students on projects generating West Nile virus mutants

Oct. 2017 - Dec. 2017: Mentored laboratory rotation student on a project investigating West Nile virus mutants for differential regulation of intracellular proteins

Nov. 2016: Lecture given to grant writing class to teach writing and oral presentation skills

United States Department of Agriculture

Aug 2013- Aug 2014: Mentored two new undergraduate interns in bacteriology and molecular biology technical skills

LEADERSHIP AND TEAMWORK:

University of Texas Medical Branch

Sep. 2018: Lead organizer of T32 training program student retreat. Responsibilities included inviting speakers and other attendees and organizing retreat agenda.

2017-2018: Admissions committee student officer for Microbiology & Immunology graduate program- meet with faculty to discuss which graduate school applicants to recruit for interviews and assist with recruitment events

- May 2017 and May 2018: Student marshal for 2017 UTMB Graduate School of Biomedical Sciences commencement ceremony- assisted with set up and organization of graduation ceremony
- Apr. 2015: Volunteered for UTMB United to Serve program and worked with a team to clean up trash around Galveston, TX

United States Department of Agriculture

- Oct. 2013 - Mar. 2014: Participated in National Cancer Institute's Elementary Outreach Program to do experiments at local schools
- July 2013: Extracted DNA with children for Ft. Detrick "Take Your Child To Work Day"

HONORS:

University of Texas Medical Branch

- Apr. 2018: Awarded \$500 travel award to from the American Society for Virology to attend 2018 ASV conference in College Park, MD
- Jan. 2018: Awarded travel funds from UTMB Sealy Institute for Vaccine Sciences to attend the 2018 National Foundation for Infectious Diseases Annual Conference for Vaccinology Research in Bethesda, MD
- Aug. 2017 - Dec. 2017: Awarded UTMB-World Health Organization Collaborating Center internship to complete a literature review of severe fever with thrombocytopenia syndrome virus to detail the progress toward vaccine development
- May 2017 - May 2019: Awarded NIAID T32 Training Grant in Emerging and Tropical Diseases
- Aug. 2014 - Aug. 2019: Awarded McLaughlin Scholarship, UTMB Graduate School of Biological Sciences

United States Department of Agriculture

- May 2014: Awarded Top Research Technician Presentation Award for the lecture "Genomic and Proteomic Characterization of *Rathayibacter toxicus*" at Ft. Detrick Spring Research Festival science symposium

PUBLISHED:

Kaiser, JA; Luo, H; Widen, SG; Wood, TG; Huang, C; Wang, T; Barrett, ADT. *Genotypic and phenotypic characterization of West Nile virus NS5 methyltransferase mutants*. Vaccine. Published online Oct. 2019.

Kaiser, JA; Barrett, ADT. *Twenty years of progress toward WNV vaccine development*. (Sep. 2019) Viruses 11(823):1-17.

Li, L; Collins, ND; Widen, SG; Davis, EH; **Kaiser, JA**; White, M; Greenberg, M; Barrett, ADT; Bourne, N; Sarathy, VV. *Attenuation of Zika virus by passage in human HeLa Cells*. (Aug. 2019) Vaccines 7 (3): 1-16.

Sarathy, VV; White, M; Li, L; **Kaiser, JA**; Campbell, GA; Milligan, GM; Bourne, N; Barrett, ADT. *Characterization of a murine model of non-lethal, symptomatic dengue virus infection*. (Mar. 2018) Scientific Reports 8(1):4900.

Fennessey, CM; McMahon, MB; Sechler, AJ; **Kaiser, JA**; Garrett, WN; Tancos, MA; Luster, DG; Rogers, EE; Schneider, WL. *Partial proteome of the Corynetoxin-producing gram-positive bacterium, Rathayibacter toxicus*. (Feb. 2018) Proteomics 18:3-4.

Kaiser, JA; Wang, T; Barrett, ADT. *Virulence determinants of West Nile virus: how can these be used for vaccine design?* (May 2017) Future Virology 12(5):283-295.

PUBLICATIONS – ACCEPTED:

Kaiser, JA; Luo, H; Widen, SG; Wood, TG; Huang, C; Wang, T; Barrett, ADT. *Japanese encephalitis vaccine-specific envelope protein E138K mutation does not attenuate virulence of West Nile virus*. (Sept. 2019) npj Vaccines.

PUBLICATIONS – SUBMITTED:

Bopp, NE; **Kaiser, JA**; Strother, AE; Barrett, ADT; Beasley, DWC; Benassi, V; Milligan, GN; Preziosi, M-P; Reece, LM. *Baseline mapping of severe fever with thrombocytopenia syndrome virology, epidemiology and vaccine research and development*. (Oct. 2019) npj Vaccines.

PUBLICATIONS - IN PREPARATION:

Kaiser, JA; Luo, H; Widen, SG; Wood, TG; Huang, C; Wang, T; Barrett, ADT. *Characterization of mutations in West Nile virus NS4B protein identifies proline residue 54 as a determinant of attenuation*.

ABSTRACTS:

Kaiser, JA; Luo, H; Widen, SG; Wood, TG; Huang, C; Wang, T; Barrett, ADT. *Genotypic and phenotypic characterization of West Nile virus NS5 methyltransferase mutants*. (March 2019) Poster. UTMB McLaughlin Colloquium. Galveston, TX.

Kaiser, JA; Luo, H; Huang, C-Y; Wang, T; Barrett, ADT. *Combination of independent attenuating mutations in West Nile virus non-structural proteins NS1 and NS4B.* (July 2018) Oral Presentation. American Society for Virology. College Park, MD.

Kaiser, JA; Luo, H; Huang, C-Y; Wang, T; Barrett, ADT. *Combination of independent attenuating mutations in West Nile virus non-structural proteins NS1 and NS4B.* (April 2018) Poster. National Foundation for Infectious Diseases, Annual Conference for Vaccinology Research. Bethesda, MD.

Kaiser, JA; Luo, H; Huang, CY; Wang, T; Barrett, ADT. *Characterization of attenuating mutations in West Nile virus nonstructural protein NS4B.* (March 2018) Poster. UTMB McLaughlin Colloquium. Galveston, TX.

Kaiser, JA; Luo, H; Huang, C-Y; Wang, T; Barrett, ADT. *Combination of independent attenuating mutations in West Nile virus non-structural proteins NS1 and NS4B.* (October 2017) Poster. International Society of Vaccines. Paris, France.

Kaiser, J; Luo, H; Wicker, J; Whiteman, M; Wang, T; Barrett, A. *Characterization of attenuating mutations in West Nile virus nonstructural proteins.* (March 2017) Poster. UTMB McLaughlin Colloquium. Galveston, TX.

This dissertation was typed by the author.